

Isoform Selective Inhibitors of Phosphatidylinositol 3-Kinase

Michelle Susan Miller

Hons. B.Pharm.Sci.

B.Sc. (Science Scholar)

Dip. Lang. (Mandarin)

A thesis submitted in fulfilment of the requirements for the degree of

Doctor of Philosophy

Department of Medicinal Chemistry

Faculty of Pharmacy and Pharmaceutical Sciences

Monash University

2013

Errata and Addendum

- p.3, line 18 Insert "(Figure 1.1)" after "Protein Kinase B)"
- p.4, line 6 Add the following sentences at the end of the paragraph:
"In particular, mTORC1 increases GLUT1 expression, and thus cellular glucose uptake.²⁹ The clinical effect of PI3K inhibition on blood glucose levels will therefore have to be closely monitored."
- p.8, line 7 Insert the following sentence at the end of the paragraph:
"As derivatives of the inhibitor ZSTK474 will be the main focus of this thesis, the subset of pan-PI3K inhibitors selected for discussion are those containing similar binding motifs, namely a dimorpholino moiety."
- p.19, line 17 Delete "This would result in the administration of a sub-optimal dose that could allow for the development of resistance." and replace with:
"There is also the possibility of acquired resistance through the upregulation of alternative growth pathways. Clinical trials combining PI3K inhibition with MEK/Erk pathway inhibitors are currently underway and these sorts of combination therapies may reduce resistance and prove more effective than single agent therapies."
- p.67, 3rd last line Replace "N2" with "N3"
- p. 76, line 6 Replace "N2" with "N3"
- p. 80, Figure 3.5 Insert the following after "ZSTK474 analogues."
"Compounds **25b-25f** previously described by Jo-Anne Pinson."
- p. 85, line 1 Insert the following paragraph at the beginning of the page:
"The level of isoform selectivity desirable in either a potential clinical candidate or chemical tool would be greater than 100-fold, which would allow inhibition of the desired isoform, without significantly affecting the others."
- p. 88, Scheme 3.3 Insert at the end of the caption: "Specific compounds and substituents are detailed in Table 3.6."
- p. 93, line 8 Replace "only set" with "only one set"
- p. 102, line 13 Replace "Whether this remains the case in the triazine substituted compounds is difficult to predict." with the following sentence:
"However, in the triazine conjugated piperazine, protonation of the nitrogen is unlikely, and therefore the zwitterionic stabilisation doubtful."
- p. 110, ref. 34 Replace "Mruphy" with "Murphy"
- p.128, ref. 8 Insert at the end of reference "55, 5887-5900."
- p. 132, line 20 Insert the following sentence after "the PI3K γ isoform." :
"Selectivity achieved for PI3K α against the PI3K γ is greater than the desired 100-fold in three of the compounds tested, **38a**, **38b** and **40a**, however, selectivity against PI3K β and PI3K δ , still require further optimisation."
- p. 141, line 2 Insert "All tested compounds had greater than 95% purity as determined by analytical HPLC." as a new paragraph.
- p. 155-157 For Compounds 25b-25f, include the reference:
Pinson, JA. PI3 Kinase and inhibitors: Targeting isoform selectivity. PhD Dissertation, Monash University, 2011.

Copyright Notices

Under the Copyright Act 1968, this thesis must be used only under the normal conditions of scholarly fair dealing. In particular no results or conclusions should be extracted from it, nor should it be copied or closely paraphrased in whole or in part without the written consent of the author. Proper written acknowledgement should be made for any assistance obtained from this thesis.

I certify that I have made all reasonable efforts to secure copyright permissions for third-party content included in this thesis and have not knowingly added copyright content to my work without the owner's permission.

Table of Contents

Statement of Originality	v
Part A: General Declaration	vi
Acknowledgements	viii
Abbreviations and Acronyms.....	x
Abstract.....	xvi
Chapter 1: Introduction	1
1.1 PI3K – an important target for the treatment of cancer	1
1.2 PI3K signalling.....	2
1.3 Involvement of PI3K in cancer	5
1.4 PI3K inhibitors	7
1.5 Structural insights into isoform selectivity.....	11
1.6 Isoform selective inhibitors in the clinic.....	19
1.7 Thesis aims.....	21
1.8 References.....	22
PART B: Declaration for Chapter 2	32
Chapter 2: Structural insights into the regulation and lipid binding of PI3Kα ...	36
2.1 Introduction.....	36
2.1.1 Aims	37
2.2 Structural insights into the regulation and lipid binding of PI3K α	37
2.3 Prepared manuscript.....	40
2.3.1 Abstract	42
2.3.2 Manuscript	42
2.3.3 Supplementary figures.....	55

2.4	Post-Script: Ongoing work and conclusions.....	56
2.5	References.....	59
PART B: Declaration for Chapter 3		63
Chapter 3: Structural modification of ZSTK474 to probe isoform selective		
interactions with PI3K.....		65
3.1	Introduction.....	65
3.1.1	Aims	69
3.2	Regioselective synthesis of 5- and 6-methoxybenzimidazole ZSTK474 derivatives.....	70
3.2.1	Post-script: Rationalising selectivity	75
3.3	Evaluation of a series of ZSTK474 analogues	77
3.3.1	Synthesis of ZSTK474 derivatives	81
3.3.2	Evaluation against Class I PI3K.....	83
3.4	Further derivatisation of ZSTK474 analogues	87
3.4.1	Synthesis.....	88
3.4.2	Evaluation of ZSTK474 derivatives	94
3.4.3	Docking investigation into compounds 37b , 38b and 41a-b	100
3.5	Conclusions.....	105
3.6	References.....	107
Chapter 4: Dipeptide analogues of ZSTK474 targeting non-conserved region 1		
residues		111
4.1	Introduction.....	111
4.1.1	Aims	114
4.2	Synthesis of dipeptide derivatives.....	114
4.3	Evaluation of ZSTK474 dipeptide analogues	119
4.4	Site-directed mutagenesis.....	123

4.5	Conclusions.....	125
4.6	References.....	128
Chapter 5:	Conclusions and future directions.....	129
5.1	References.....	134
Chapter 6:	Experimental.....	135
6.1	Chapter 2 experimental.....	135
6.1.1	PI3K protein expression.....	135
6.1.2	p85 α protein expression and purification	136
6.1.3	Crystallisation.....	136
6.1.4	Data collection.....	136
6.1.5	Structure determination	137
6.1.6	Preparation of BODIPY-FL-PIP ₂ vesicles.....	137
6.1.7	Fluorescence quenching experiments	137
6.2	Synthetic chemistry.....	138
6.2.1	General experimental	138
6.2.2	Regioselective synthesis of 5- and 6-methoxybenzimidazole-1,3,5-triazines as inhibitors of phosphoinositide 3-kinase (published paper)	141
6.2.3	Chapter 3 experimental.....	152
6.2.4	Chapter 4 experimental.....	168
6.3	Enzyme assays.....	175
6.4	Docking.....	176
6.5	References.....	177
Appendices	178
	Appendix 1: Assay results.....	179
	Appendix 2: Docking results for p110 γ	181

Appendix 3: Docking results for p110 δ	182
Appendix 4: Publication	183
Appendix 5: Publication	189

Statement of Originality

To the best of the author's knowledge and belief, this thesis contains no material which has been accepted for the award of any other degree or diploma in any University or other institutions, and contains no material previously published or written by another person except where due reference is made.

Michelle S. Miller

August 2013

Part A: General Declaration

Monash University. Declaration for thesis based or partially based on conjointly published or unpublished work

General Declaration

In accordance with Monash University Doctorate Regulation 17.2 Doctor of Philosophy and Research Master's regulations the following declarations are made:

I hereby declare that this thesis contains no material which has been accepted for the award of any other degree or diploma at any university or equivalent institution and that, to the best of my knowledge and belief, this thesis contains no material previously published or written by another person, except where due reference is made in the text of the thesis.

This thesis includes 1 original paper published in a peer reviewed journal and 1 unpublished manuscript. The core theme of the thesis is the synthesis and evaluation of novel PI3K inhibitors. The requirements to fulfil a 'thesis by publication' allows for chapters to be prepared as manuscripts for submission, as presented herein. Overall, the material presented equates to that which would otherwise be presented in the traditional thesis format. The ideas, development and writing up of all the papers in the thesis were the principal responsibility of myself, the candidate, working within the Department of Medicinal Chemistry under the supervision of Philip Thompson and in collaboration with Dr. Sandra Gabelli at Johns Hopkins University. The nature of assistance from co-authors has been reflected at the commencement of each chapter, referred to as 'Specific Declaration'. The inclusion of co-authors reflects the fact that the work came from active collaboration between researchers and acknowledges input into team-based research.

In the case of Chapter 2, my contribution to the work involved the following: refinement and analysis of the two crystal structures and co-authorship of the manuscript. The chapter has been prepared as a manuscript in preparation for submission to *Oncogene* as a full research article.

In the case of Chapter 3 my contribution to the work involved the following: design of experiments, synthesis of 7 of 9 final compounds and accompanying intermediates, testing of 8 of 9 compounds, all molecular docking experiments and co-authorship of manuscript.

Thesis chapter	Publication title	Publication status	Nature and extent of candidate's contribution
2	Structural insights into the regulation and lipid-binding of PI3K α	Unpublished	Candidate refined and analysed the two crystal structures and co-authored the manuscript. 50% contribution
3	Regioselective synthesis of 5- and 6-methoxybenzimidazole-1,3,5-triazines as inhibitors of phosphoinositide 3-kinase	Published	Candidate synthesised 7 compounds, tested 8 compounds, performed all docking experiments and co-authored manuscript. 80% contribution.

I have renumbered sections of the unpublished manuscript in Chapter 2 to generate a consistent presentation within the thesis. I have not renumbered sections of the published paper in Chapter 3.

Signed: _____

Date: _____

Acknowledgements

Firstly, I want to thank my main supervisor, Associate Professor Philip Thompson, for all his help, wisdom and guidance throughout the course of my honours and PhD. I learnt a lot from your endless optimism and ability to keep focused on the ‘big picture’.

Thank you to Dr. Ian Jennings for his input into the project and for teaching me all the assay basics.

Thank you to Professor Mario Amzel for hosting me to work in your lab at Johns Hopkins. I learnt so much while I was there and discovered a passion for crystallography.

To Dr. Sandra Gabelli, thank you so much for all your help throughout my time in Baltimore. I learnt so much in my time working with you. Your passion and dedication to research is truly inspiring.

To all the past and present members of the Thompson Group – Dr. Jo-Anne Pinson, Dr. Michelle Camerino, Dr. Jacob Nankervis, Dr. Timothy Blackmore, Dr. William Nguyen, Dr. Diana Neale, Dr. Susan Northfield, Dr. Brittany Howard, Syazwani Amran, Oscar Lui, Dr. Simon Mountford, Dr. Joyce Zheng, Dr. Kade Roberts, Krithika Sundaram – thank you for being such a great group of people to work with. Thank you for all the help, support and friendship over the past few years. Jo – thanks for all your encouragement and for all the groundwork you did in this project. A special thank you to Joyce for the many discussions on assays, for teaching me protein expression, and for your amazing support and friendship both in and out of the lab.

Thank you to all of the people in the Medicinal Chemistry department at MIPS, both past and present PhD students and post-docs, specifically – Jennifer La, Natalie Vinh, Dr. Bradley Doak, Dr. Chris Opie, Mansha Vazirani, Vladimir Moudretski, Dr. Joshua Gosling, Dr. Fiona McRobb, Lucy Ping, Dr. Sandeep Chhabra and Dr. Eleanor Leung. Thanks for making the PhD process that little bit less painful!

Thank you to Dr. Jason Dang for performing all HRMS, and for his assistance with LCMS and NMR.

Thank you to all the members of the Amzel group, who welcomed me and helped me adjust to working in a new lab, a new area and a new country – Srinivas, Anita, Saif, Mauricio, Daniele, David, Evan, Andres, Akunna, Kasia.

To all the members of our little Tuesday morning prayer group – Emmanuel Birru, Sam Robinson, Dr. Anna Cook, Dr. Martina Kocan, Christine Yeo and Dr. Phillip Bergen – thank you for all your prayer, support and encouragement throughout the past four years. Thank you for being a light in my life in a very difficult time.

To my close friends Amanda Cheong and Annie Kuo – thank you for pulling me up when I was down, for laughing with me, for praying with me, and for walking with me throughout all the ups and downs. I couldn't have done it without you two!

To my family – Mum, Dad and Andrew – thank you for your unconditional support, for your understanding, encouragement and love.

I want to dedicate this thesis to my Mum and her ongoing battle with cancer – I hope that this research, even if in just a small way, will contribute to the continued search for better treatment options.

Abbreviations and Acronyms

4EBP	4E-binding protein
Å	Angstrom
ABD	Adaptor binding domain
Ac	Acetyl
AML	Acute myeloid leukaemia
aq	Aqueous
ATP	Adenosine triphosphate
ax	Axial
BAD	Bcl-2 associated death promoter
Bcl-2	B-cell lymphoma 2
BH	Bcl-2 homology domain
BODIPY-FL	3-(5,5-difluoro-7,9-dimethyl-5 <i>H</i> -4λ ⁴ ,5λ ⁴ -dipyrrolo[1,2- <i>c</i> :2',1'- <i>f</i>][1,3,2]diazaborinin-3-yl)propanoic acid
BODIPY-TMR	3-(5,5-difluoro-7-(4-methoxyphenyl)-1,3-dimethyl-5 <i>H</i> -4λ ⁴ ,5λ ⁴ -dipyrrolo[1,2- <i>c</i> :2',1'- <i>f</i>][1,3,2]diazaborinin-2-yl)propanoic acid
br	Broad
C	Celcius
calc'd	Calculated
CK	Casein kinase
cSH2	C-terminal Src homology domain 2
d	doublet
dd	doublet of doublets
ddd	doublet of doublet of doublets
DIPEA	N,N-diisopropylethylamine

DMF	Dimethylformamide
DMSO	Dimethylsulfoxide
DNA-PK	Deoxyribonucleic acid-dependent protein kinase
DTT	Dithiothreitol
EDTA	Ethylenediaminetetraacetic acid
eq	Equatorial
ESI	Electrospray ionisation
F	Structure factor
Fmoc	Fluorenylmethyloxycarbonyl chloride
FOXO	Forkhead box family of transcription factors
g	Gram
GAB	GRB2-associated-binding protein
GPCR	G protein coupled receptor
GRB2	Growth factor receptor-bound protein 2
GSK	Glycogen synthase kinase
GST	Glutathione S-transferase
GTPase	Guanine triphosphatase
HBTU	O-Benzotriazole-N,N,N',N'-tetramethyluronium hexafluorophosphate
HCTU	O-(1H-6-Chlorobenzotriazole-1-yl)-1,1,3,3-tetramethyluronium hexafluorophosphate
HEPES	4-(2-hydroxyethyl)-1-piperazineethanesulfonic acid
HPLC	High-performance liquid chromatography
HRMS	High resolution mass spectrometry
HSQC	Heteronuclear single quantum coherence
Hz	Hertz
I	Measured intensities of diffraction pattern

σI	Standard uncertainty in the measured intensities
IC ₅₀	Half maximal inhibitory concentration
ID	Identification code
IPTG	Isopropyl β -D-1-thiogalactopyranoside
iSH2	inter Src homology 2 domain
J	Coupling constant
kDa	Kilodalton
L	Litre
LB	Lysogeny broth
LCMS	Liquid chromatography-mass spectrometry
LHS	Left-hand side substituent
[MH] ⁺	Singly protonated molecular ion
m	Multiplet
M	Molar
m/z	mass-to-charge ratio
MARCKS	Myristoylated alanine-rich C-kinase substrate
MBP	Maltose-binding protein
MDM2	Mouse double minute 2 homologue
mg	Milligram
MHz	Megahertz
MIPs	Molecularly imprinted polymers
mL	Millilitre
μ L	Microlitre
μ M	Micromolar
μ m	Micrometre
mm	Millimetre

mM	Millimolar
mmol	Millimole
MS	Mass-spectrometry
MW	Microwave
mTOR(C)	Mammalian target of rapamycin (complex)
NAP-22	Neuronal tissue-enriched acidic membrane protein-22
nm	Nanometre
NMR	Nuclear Magnetic Resonance
nSH2	N-terminal Src homology 2 domain
NSLS	National Synchrotron Light Source
PBS	Phosphate buffered saline
PC	Phosphatidylcholine
PCy ₃	Tricyclohexylphosphine
PDB	Protein Data Bank
PDK	3-Phosphoinositide-dependent protein kinase
PE	Phosphatidylethanolamine
pH	Decimal cologarithm of the concentration of hydrogen ions
PH	Pleckstrin homology domain
PI	Phosphatidylinositol
PI3K	Phosphatidylinositol 3-kinase
PI(3,4)P ₂	Phosphatidylinositol 3,4-bisphosphate
PIP	Phosphatidylinositol 4-phosphate
PIP ₂	Phosphatidylinositol 4,5-bisphosphate
PIP ₃	Phosphatidylinositol 3,4,5-trisphosphate
PISA	Proteins, Interfaces, Structures and Assemblies
PLC	Phospholipase C

ppm	Parts per million
PS	Phosphatidylserine
psi	Pounds per square inch
PTEN	Phosphatase and tensin homologue
q	Quartet
R	R-factor
Raf	Rapidly accelerated fibrosarcoma
RalGDS	Ral guanine nucleotide dissociation stimulator
Ras	Rat sarcoma
RBD	Ras binding domain
R_{free}	Free R-factor
Rheb	Ras homologue enriched in brain
RhoGAP	Rho-like small guanine triphosphatase activating protein
RHS	Right-hand side substituents
R.M.S	Root mean square
RMSD	Root mean square deviation
RP	Reverse phase
R_{sym}	Linear merging R-value
RTK	Receptor tyrosine kinase
s	Singlet
S6K	S6 kinase
s.e.	Standard error
SAR	Structure-activity relationship
SDS-PAGE	Sodium dodecylsulfate polyacrylamide gel electrophoresis
SF9/21	Spodoptera frugiperda cell lines 9 or 21
SH2/3	Src homology domain 2/3

SHIP	SH2 domain containing inositol 5-phosphatase
t	Triplet
TBAB	Tetra N-butylammonium bromide
TEV	Tobacco etch virus
TFA	Trifluoroacetic acid
TIC	Total ion chromatogram
TLC	Thin layer chromatography
TOF	Time of flight
Tris	Tris(hydroxymethyl)aminomethane
TSC	Tuberous sclerosis protein
UHPLC	Ultra high-performance liquid chromatography
V	Volt
WT	Wild-type

Amino acids are referred to by their standard one or three letter codes, unless otherwise stated.

Abstract

Inhibitors of the phosphatidylinositol 3-kinase (PI3K) pathway are at the forefront of the search for novel cancer treatments, as aberrations in the pathway are found in up to 50% of human cancers. Class I PI3K consists of four isoforms, PI3K α , PI3K β , PI3K γ and PI3K δ , which phosphorylate phosphatidylinositol 4,5-bisphosphate to form the second messenger, phosphatidylinositol 3,4,5-trisphosphate. This second messenger signals downstream to regulate cell metabolism, growth and proliferation. Oncogenic mutations in PI3K α occur in approximately 30% of colorectal cancers and 25-40% of breast cancers. The work in this thesis has sought to add to the understanding of isoform selectivity in PI3K inhibitors, which will hopefully contribute to the successful treatment of human cancers. This has been conducted in two parts: (i) the structural investigation of wild-type PI3K α , examining the differences in regulation compared with the oncogenic mutant, p110 α His1047Arg, and the characterisation of the lipid-binding site; (ii) the design, synthesis and testing of novel PI3K inhibitors designed to explore the determinants of isoform selectivity.

Two wild-type X-ray crystal structures of PI3K α , one in complex with the lipid substrate di-C₄-phosphatidylinositol 4,5-bisphosphate, have been determined. The apo structure was refined to 2.96 Å (R/R_{free} 0.19/0.27), and the lipid structure refined to 3.37 Å (R/R_{free} 0.24/0.34). Comparison of these structures with that of the oncogenic mutant, p110 α His1047Arg (PDB ID: 3HHM) has revealed important differences in the nSH2 domain regulation. Increased buried surface area and unique salt-bridges in the wild-type structure are suggestive of tighter regulation. Two lipid-binding sites have been identified in p110 α , and the presence of multiple binding sites confirmed by fluorescence quenching experiments.

Chapters 3 and 4 have described the synthesis and testing of 38 analogues of the pan PI3K inhibitor, ZSTK474. In Chapter 3, an efficient, regioselective synthetic method was developed for the synthesis of 5- and 6-substituted benzimidazole derivatives of ZSTK474. Methoxy substitutions at these positions resulted in a decrease in potency at PI3K α . A more dramatic impact on PI3K γ potency was observed, suggesting alternative substitutions at this position may be a suitable method to dial out PI3K γ inhibition. Two hydroxyphenyl substituents were investigated as alternatives to the 2-difluoromethylbenzimidazole substituent of ZSTK474. The 3-hydroxyphenyl substituted compounds (**37-42**) had a greater preference for the PI3K α isoform than the equivalent 2-difluoromethylbenzimidazole compounds (**25a-f**), despite a decrease in potency. The 3-hydroxyphenyl substituted compounds also showed significantly greater selectivity against PI3K γ , suggesting it may be a better affinity pocket binding moiety for the development of PI3K α selective inhibitors. More work is required to optimise the other binding moiety, replacing a morpholine group of ZSTK474, to improve potency and PI3K α selectivity.

In Chapter 4, a series of inhibitors targeting a specific non-conserved residue in PI3K α , p110 α Gln859, was designed, synthesised and tested. Compounds showed a general trend of improved selectivity towards PI3K δ , due to the presence of a similar residue at the analogous position, p110 δ Asn836. Compound **46** was the most PI3K δ selective compound, showing a selectivity of 6-35-fold. Compound **50** displayed the greatest selectivity for PI3K δ against PI3K β of 21-fold. Site-directed mutagenesis assay results of compound **50** are consistent with interactions at the residue p110 α Gln859.

The work in thesis has investigated the design of novel PI3K α inhibitors. The identification of key differences in interaction and regulation between wild-type PI3K α and the oncogenic mutant, p110 α His1047Arg has the potential to inform the design of novel, oncogenic mutant

specific inhibitors. The characterisation of the PI3K α lipid-binding site can aid in the structure-based drug design of lipid-competitive inhibitors, potentially providing increased selectivity over related protein kinases. We have demonstrated the applicability of targeting specific non-conserved residues in the PI3K binding site for the rational design of isoform selective inhibitors, and the importance of the affinity pocket binding portion of the inhibitor for dialling out PI3K γ inhibition.

Chapter 1: Introduction

1.1 PI3K – an important target for the treatment of cancer

In recent years there has been a dramatic increase in the understanding of the molecular mechanisms that drive the pathogenesis of human cancers. This has fuelled the pursuit and discovery of new therapies, with most of the effort focused on the development of novel chemotherapy candidates targeting cancer-specific processes.¹ The phosphatidylinositol 3-kinase (PI3K) pathway is at the forefront of this approach. Aberrations in PI3K signalling occur in up to 50% of human cancers, making the pathway an exciting target for the treatment of cancer.² The PI3K signalling pathway plays a vital role in cell metabolism, growth and proliferation. Under normal circumstances, signalling responses are tightly regulated. If this control is lost, constitutive activation of the pathway can result in tumorigenesis, tumour growth and metastasis.³⁻⁶

In this thesis, attention is drawn to PI3K as a target in anti-cancer drug discovery, focusing particularly on the PI3K α isoform and the features that distinguish the wild-type from the oncogenic mutant forms and the three other PI3K family members. Gaining an understanding of the differences between these enzymes has the potential to lead to the development of new drugs for the treatment of cancer.

1.2 PI3K signalling

PI3Ks are a family of lipid kinases that phosphorylate the 3'-hydroxyl position of phosphoinositides to form intracellular signalling molecules, which modulate the activity of various downstream effectors. PI3Ks have been divided into three classes based on their sequence homology and substrate specificity. Class I PI3K, of which there are four isoforms, preferentially phosphorylates phosphatidylinositol 4,5-bisphosphate (PIP₂) *in vivo* to form the second messenger, phosphatidylinositol 3,4,5-trisphosphate (PIP₃). Class I PI3K can also phosphorylate phosphatidylinositol (PI) and phosphatidylinositol 4-phosphate (PIP) *in vitro*. The substrate for Class II PI3K is PIP, while Class III PI3K phosphorylates PI.⁷⁻⁹

Class I PI3Ks are the most researched of the three classes and are the focus of this thesis. Each of the four isoforms, designated PI3K α , PI3K β , PI3K γ and PI3K δ , consist of a 110 kDa catalytic subunit, known as p110, and a regulatory subunit. They can be further categorised into two subclasses, Class IA and IB, based on the identity of the regulatory binding partner. Class IA (PI3K α , PI3K β and PI3K δ) form obligate heterodimers with any member of the family of regulatory subunits collectively known as p85.¹⁰ These regulatory subunits act both to stabilise and inhibit p110.¹¹ Keeping p110 in a basally repressed state is important for the tight regulation of signalling by the cell, and loss of this regulation can result in tumorigenesis. A number of different regulatory subunits have been identified, p85 α , p85 β and p55 γ .¹²⁻¹⁴ Different splice variants of p85 α also exist, giving rise to the proteins p55 α and p50 α .^{15,16} Class

IB consists of a single member, PI3K γ , which binds either a p84 (also known as p87) or p101 regulatory subunit.^{17–20}

Receptor binding activates PI3K in a twofold manner, firstly via the release of regulatory subunit mediated inhibition, and secondly via the recruitment of the complex to the membrane, increasing substrate accessibility. Class I PI3Ks can be activated via four distinct mechanisms. Firstly, upon activation and auto-phosphorylation of receptor tyrosine kinases (RTKs), the Src homology 2 (SH2) domains of p85 can bind directly to the phosphorylated tyrosine residues, relieving p85 mediated inhibition.^{21,22} Secondly, the adaptor protein GRB2 can also bind to phosphorylated tyrosine motifs on RTKs. GRB2 binds GAB, which then interacts with p85 and activates p110.²³ These two mechanisms serve exclusively to activate Class IA PI3Ks. The activation of the GTPase, Ras, either through RTK or G protein coupled receptor (GPCR) related pathways, can also activate PI3K activity. Ras binds to the p110 subunit and activates p110 activity independently of the regulatory subunit.^{23,24} Finally, the catalytic subunit of PI3K β and the regulatory subunits of PI3K γ are activated upon binding G $\beta\gamma$ proteins downstream of GPCRs.^{17–19,25,26}

The PIP₃ generated upon activation can recruit and activate plekstrin homology (PH) domain containing proteins such as 3-phosphoinositide-dependent protein kinase 1 (PDK1) and Akt (also known as Protein Kinase B)(Figure 1.1). Activated PDK1 then phosphorylates Akt at Thr308. For full activation, Akt also requires phosphorylation by mammalian target of rapamycin complex 2 (mTORC2) or DNA-dependent protein kinase (DNA-PK) at Ser473.²⁸ The downstream effects of Akt activation are mediated by its kinase activity, with more than 50 substrates identified.²⁹ The regulation and activation of these substrates is complex, with many having multiple functions and multiple activators. Only a subset is summarised here from a number of recent reviews.^{28–30} Phosphorylation of glycogen synthase kinase 3 (GSK3) by Akt inhibits its activity, increasing the stability of cyclin D1 and stimulating cell cycle progression.

Reduced GSK3 activity also results in increased glycogen synthase activity and glycogen synthesis. Cell survival signals include the inhibition of the ubiquitin E3 ligase MDM2, the proapoptotic factor BAD and Caspase-9. Promotion of growth and metabolism is mediated via inhibition of the Forkhead box (FOXO) family of transcription factors. Activation of tuberous sclerosis proteins 1 and 2 (TSC1 and 2) relieves their inhibition of the GTPase Rheb and activates mTORC1, which promotes protein synthesis.^{28–30} In particular, mTORC1 increases GLUT1 expression, and thus cellular glucose uptake.²⁹ The clinical effect of PI3K inhibition on blood glucose levels will therefore have to be closely monitored.

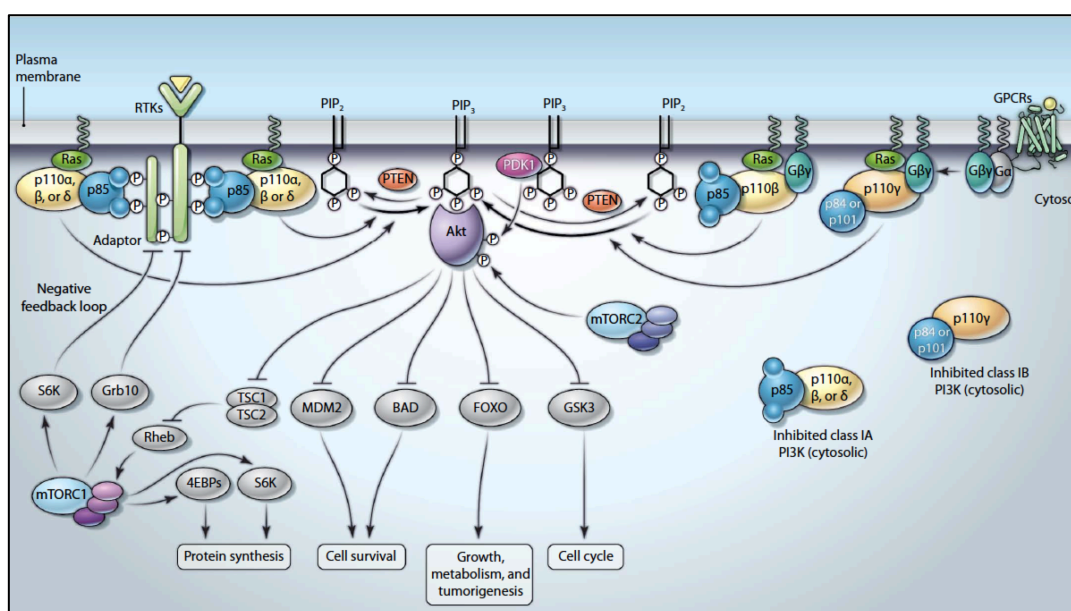


Figure 1.1: PI3K signalling pathway showing the cellular responses. Diagram taken from Vadas *et al. Sci. Signaling* 2011, 4, re227

PI3K signalling is directly antagonised through 3'-hydroxyl dephosphorylation of PIP₃ by phosphatase and tensin homologue (PTEN).^{31,32} With its pivotal role in attenuating PI3K signalling, the elucidation of PTEN as a tumour suppressor gene is not surprising. Deactivating mutations in PTEN are common both in sporadic cancers and hereditary cancer predisposition syndromes.³³ Alternatively to dephosphorylation by PTEN, PIP₃ can be processed by the 5-phosphatases, SH2 domain containing inositol 5-phosphatase 1 and 2 (SHIP1 and 2), generating

the phospholipid messenger, phosphatidylinositol 3-4-bisphosphate (PI(3,4)P₂).³³ PI(3,4)P₂ can also be involved in the activation of Akt, thus serving to propagate PIP₃ signalling.³⁴ However, other downstream effectors have different functions that can result in termination of the signal. 5-Phosphatases, therefore, can have cell specific effects that either propagate or terminate PIP₃ signalling. In line with this, SHIP1 has been shown to have tumour suppressor properties, while SHIP2 appears to play an oncogenic role.³³

1.3 Involvement of PI3K in cancer

The PI3K pathway has long been known to be involved in cancer. With the availability of high throughput sequencing technology, it became possible to determine if oncogenic somatic mutations were present in any of the PI3K genes. In 2004, Samuels *et al.* sequenced the PI3K genes in 35 colorectal cancer biopsy samples.³⁵ *PIK3CA*, the gene encoding the p110 α catalytic subunit, was the only PI3K gene of any class found to contain oncogenic mutations. A more detailed study of a total of 234 colorectal cancer samples revealed mutations in 74 tumours, an occurrence of 32%.³⁵ In the same study, oncogenic mutations in *PIK3CA* were also identified in glioblastoma, gastric, lung and breast cancers, but absent in a small sample of pancreatic cancers and medulloblastomas.³⁵ This initial study fuelled efforts to further characterise the role of oncogenic mutations in *PIK3CA* in various cancers. It is now generally accepted that these mutations occur in 25-40% of all breast cancers.³⁶ A high frequency of *PIK3CA* mutations has also been found in endometrial cancers.³⁷⁻³⁹ Follow up studies have confirmed the initial identification of mutations in glioblastoma in a larger number of samples, suggesting a frequency of about 5%.⁴⁰⁻⁴³ A similar frequency of mutations has been found in follow up studies of gastric cancer and lung cancer.³⁶

Somatic, missense mutations have been identified throughout the sequence of p110 α . Interestingly, however, about 80% of *PIK3CA* mutations are concentrated at 3 'hotspots',

Glu542Lys, Glu545Lys and His1047Arg.^{35,36} These mutations and the mechanisms by which they cause constitutive activation, will be discussed in more detail in Chapter 2.

Although not as well established as PI3K α , a role for the other isoforms in cancer is emerging. Cancers deficient in the phosphatase PTEN have been linked with increased PI3K β expression and activity. Studies in PTEN-deficient cell lines, as well as conditional knock-out mice have shown that PI3K β inactivation blocks prostate cancer development.^{44–46}

PI3K δ , which is highly enriched in haematopoietic cells, has consistently high levels of expression in acute myeloid leukaemia (AML).^{47–49} It was found that a PI3K δ selective inhibitor reduced AML cell proliferation without affecting normal haematopoietic progenitor cells.⁴⁷ This discovery is particularly promising for the treatment of AML. PI3K δ has also been proposed as a target in B-cell malignancies and multiple myeloma.^{50,51} It plays an important role in the immune system, and, along with PI3K γ has been proposed as a novel target for the treatment of immune and inflammatory conditions.⁵²

The most recent reports have identified a role for PI3K γ expression and activity in the proliferation of cells derived from hepatocellular carcinomas, pancreatic ductal adenocarcinoma and medullablastoma.^{53–55} Xie *et al.* have demonstrated PI3K γ expression in metastatic breast cancer cells, but not in non-metastatic or normal breast tissue, suggesting a role for PI3K γ inhibition in preventing metastasis.⁵⁶ Brazzati *et al.* have also revealed a role for PI3K γ in the proliferation of certain breast cancer cell lines.⁵⁷

It is clear from these data that the PI3K pathway plays a prominent role in the development of cancer. As PIP₃ is a major regulator of cell growth and proliferation, tumour cells will acquire genetic and molecular changes in a variety of ways to increase levels of this vital signalling molecule.

1.4 PI3K inhibitors

The gradual elucidation of the role of PI3K in cancer has been aided by a concomitant development of both class and isoform specific inhibitors. These inhibitors have been used as pharmacological tools, providing a deepening understanding of both general and isoform specific PI3K signalling. Numerous candidates are now also entering the clinic at a rapid rate, predominantly for the treatment of cancer, but also for inflammatory and immune conditions.

Wortmannin **1a** (Figure 1.2), isolated in 1957 from *Penicillium wortmanni*, was the first PI3K inhibitor to be identified.⁵⁸ It potently and irreversibly inhibits each of the PI3K isoforms with an IC_{50} in the low nanomolar range.⁵⁸ However, it cross-reacts with a number of other kinases, including mTOR and DNA-PK, limiting its use as a research tool.^{59,60} Wortmannin's therapeutic utility is restricted by poor solubility and high toxicity.⁶¹ A semi-synthetic derivative, PX-866 **1b**, has been developed with improved solubility and reduced toxicity. Having displayed promising results in a Phase I dose-escalation study, it is currently entering Phase I/II trials for the treatment of solid tumours.^{62,63}

The first synthetic PI3K inhibitor, LY294002 **2** (Figure 1.2), was described in 1994, elaborated from the naturally occurring flavonoid, quercetin.⁶⁴ It inhibits all Class I PI3K isoforms with an IC_{50} in the low micromolar range. While initially LY294002 was thought to be selective for Class I PI3K, more recent studies have shown LY294002 also inhibits a host of other proteins including casein kinase 2 (CK2), Class II and III PI3Ks, mTOR and DNA-PK.^{59,60,64–68} This discovery limits the utility of LY294002 as a research tool and hinders therapeutic application. By conjugating LY294002 to a short peptide sequence (Arg-Gly-Asp-Ser) designed to target specific integrins expressed on the surface of cancer cells, SF1126 has been developed with increased solubility and better pharmacokinetic properties.⁶⁹ SF1126 has shown good tumour distribution, anti-angiogenic effect and antitumour efficacy. It is currently undergoing Phase I trials for cancer treatment.⁶⁹

Since the early generations of PI3K inhibitors, significant effort has been invested into improving the potency, selectivity profile and pharmacokinetic properties of PI3K inhibitors. A wide range of chemical scaffolds has been developed for PI3K inhibition, and at the time of writing there are 32 PI3K inhibitors in clinical trials. Most of these are pan-PI3K or PI3K/mTOR dual inhibitors, but a number of isoform selective inhibitors are now also starting to enter clinical trials. These have been extensively reviewed, so only a subset will be discussed here.^{61,70-72} As derivatives of the inhibitor ZSTK474 will be the main focus of this thesis, the subset of pan-PI3K inhibitors selected for discussion are those containing similar binding motifs, namely a dimorpholino moiety.

ZSTK474 **3** (Figure 1.2) was first reported as a PI3K inhibitor in 2006 by Yaguchi *et al.*⁷³ It was discovered in a functional screening campaign investigating *s*-triazine compounds for anti-proliferative activity.⁷⁴ Subsequent tests identified it as a potent, selective inhibitor for Class I PI3K, with reported IC₅₀ values of 16, 44, 49 and 4.6 nM against PI3K α , β , γ and δ , respectively, and no significant inhibition of mTOR or a panel of 139 protein kinases.^{73,75} Having shown promising antitumour activity *in vivo*, ZSTK474 is currently in Phase I clinical trials for patients with advanced solid malignancies.⁷⁶⁻⁷⁸

The dimorpholino moiety attached to a central six-membered heterocycle found in ZSTK474 is a common PI3K binding motif, and is also found in two other PI3K inhibitors in clinical trials. BKM120 **4** (Figure 1.2), a dimorpholinopyrimidine, is the focus of 58 clinical trials ranging from Phase I to Phase III.^{79,80} It is the first pan-PI3K inhibitor to progress to Phase III trials. Published results from a Phase I dose-escalation study report that treatment was well tolerated.⁸¹ The main toxicities identified were rash, hyperglycaemia and mood alterations, which are most likely associated with on-target effects. One patient demonstrated a partial response, and seven patients showed stable disease for more than 8 months. Five of the patients with stable disease had either PTEN loss or a mutation in *PIK3CA*.^{81,82}

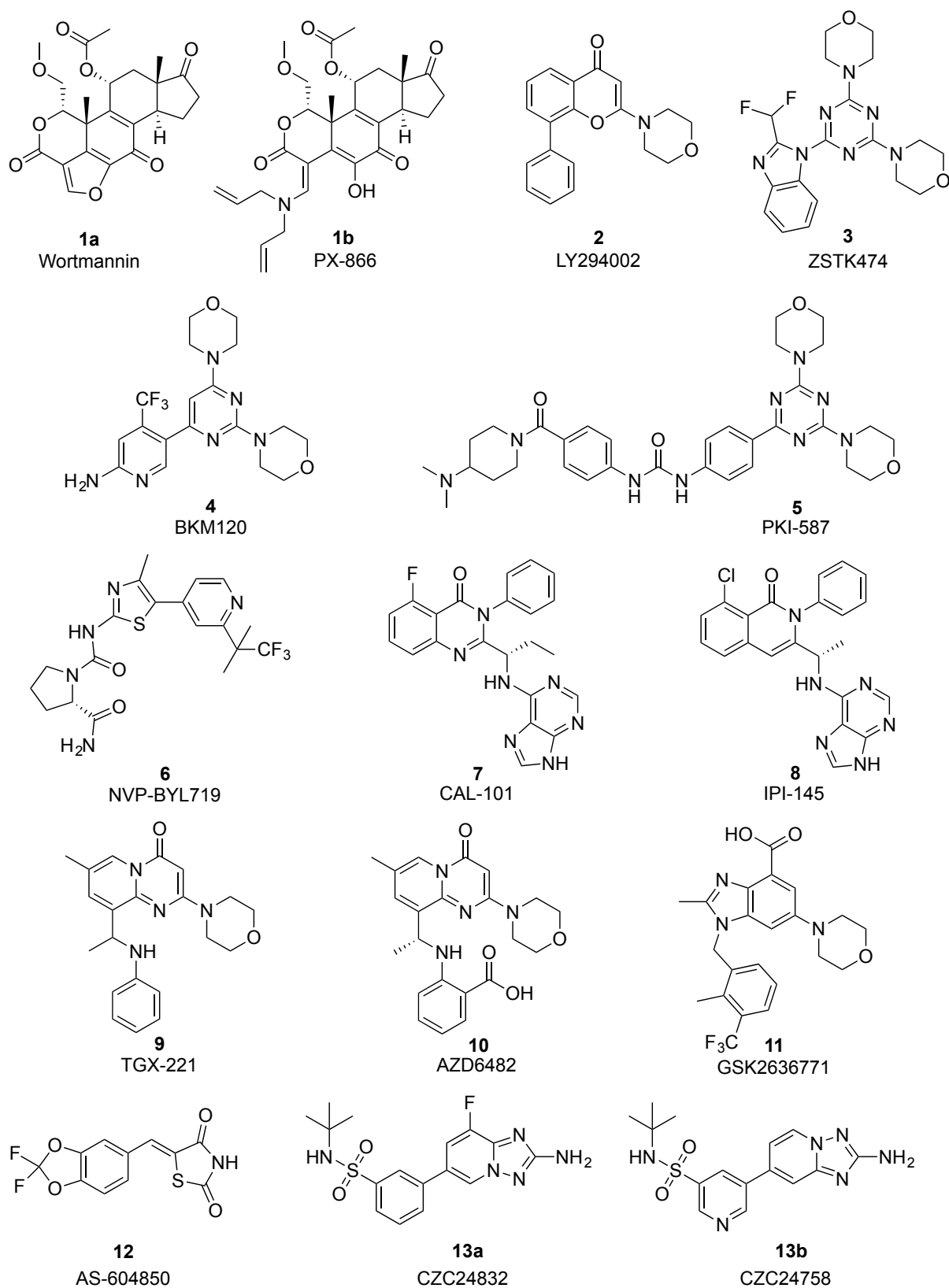


Figure 1.2: Structures of PI3K inhibitors.

PKI-587 **5** (Figure 1.2), is another dimorpholino-triazine and inhibits both PI3K and mTOR.^{83,84} It inhibits PI3K α with an IC₅₀ of 0.4 nM and mTOR at 1.6 nM.⁸³ *In vitro* cell-growth inhibition of 50 human cancer cell lines, with good *in vivo* efficacy in xenograft models and good pharmacokinetic profile recommended PKI-587 for entering Phase I clinical trials.⁸⁴

Despite the similarities in the ATP-binding site between the four isoforms, significant progress has been made in the development of isoform selective inhibitors. PI3K α selective inhibitors have aided in the elucidation of the role of PI3K α in glucose regulation and insulin signalling.⁸⁵ NVP-BYL719 **6** (Figure 1.2) is the first PI3K α selective inhibitor to enter clinical trials. It inhibits PI3K α with an IC₅₀ of 5 nM and has 50-240-fold selectivity against the other Class I isoforms.⁸⁶ Preliminary Phase I results have been promising, with one confirmed partial response and tumour shrinkage in 8 out of 17 patients.⁸⁷ Side-effects are mostly in-line with expected on-target effects, such as hyperglycaemia.⁸⁷ INK1117 has greater than 100-fold selectivity for PI3K α and has just entered dose-escalating Phase I trials.^{88,89} A dual PI3K α /mTOR inhibitor, PWT33597, has also recently entered clinical trials, and is the first inhibitor possessing this selectivity profile.⁷⁰

Three PI3K δ selective inhibitors are currently in clinical evaluation for the treatment of haematological malignancies, CAL-101 (GS-1101) **7** (Figure 1.2), AMG 319 and GS-9820. CAL-101 is the most advanced of these, and has shown promising patient responses in Phase I trials.^{51,90} GSK2269557 is in trials for the treatment of inflammatory airway diseases and CAL-263 for allergic rhinitis. IPI-145 **8** (Figure 1.2) is a dual-selective PI3K γ and δ inhibitor currently in trials for the treatment of haematological malignancies, rheumatoid arthritis and asthma.

PI3K β selective inhibitors have proven useful in elucidating isoform specific functions. The first to be discovered was TGX-221 **9** (Figure 1.2).⁹¹ This aided in the discovery of the role of PI3K β in platelet aggregation, and proposed PI3K β as a novel target for the treatment of

thrombosis.⁹¹ The first clinical studies of AZD6482 (KIN-193) **10** (Figure 1.2), a PI3K β selective inhibitor developed from TGX-221, have recently been reported. This study is the first demonstration of an anti-platelet effect in humans.⁹² It has also shown anti-proliferative effects in PTEN-deficient cancer cell lines.⁹³ GSK2636771 **11** (Figure 1.2) and SAR260301 have both recently entered Phase I clinical trials for treatment of patients with solid tumours showing PTEN loss.^{94,95}

There are no PI3K γ selective inhibitors currently in the clinic. Serono have developed AS-604850 **12** (Figure 1.2), which has greater than 100-fold selectivity against PI3K β and PI3K δ , and 18-fold selectivity against PI3K α .⁹⁶ More recently, CZC24832 **13a** (Figure 1.2) has been reported as the first PI3K γ selective inhibitor with efficacy in models of inflammation.⁹⁷ Further development of this compound has led to CZC24758 **13b**, which is a potent, orally bioavailable and selective PI3K γ inhibitor.⁹⁸

1.5 Structural insights into isoform selectivity

A detailed understanding of ligand binding has made a significant contribution to the design of potent, selective inhibitors as pharmacological tools and therapeutic agents. The involvement of X-ray crystallography has been indispensable for the structure-based drug design and optimisation of many PI3K inhibitors.

The Class IB PI3K, p110 γ was the first member of the family to be crystallised (Figure 1.3A).^{99,100} Unlike members of Class IA, which require the regulatory subunit for stabilisation, p110 γ can be stably expressed as a monomer. All four p110 subunits contain an adaptor-binding domain (ABD), Ras binding domain (RBD), C2 domain, helical domain and kinase domain. For crystallisation, p110 γ was expressed with an N-terminal truncation removing the ABD. The p110 γ crystal structures revealed each of the domains had folds similar to homologous domains in known protein structures. The RBD in p110 γ (residues 220-311) contains a five-stranded β -

sheet flanked by two α -helices, a similar fold to the RBD of two other well-known Ras effectors, Raf and RalGDS.^{99,101,102} The crystal structure indicates the RBD is situated in close proximity to the kinase domain, suggesting that Ras may activate p110 γ via an allosteric mechanism. Conformational changes in the RBD upon Ras binding could be communicated to the kinase domain resulting in activation.⁹⁹ The fold of the C2 domain of p110 γ (residues 357-522) is analogous to that of PLC δ 1, containing an eight-stranded antiparallel β -sandwich.^{99,103} The C2 domain is postulated to be involved in membrane binding.⁹⁹ The helical domain (residues 545-725) consists of five pairs of antiparallel α -helices. The precise function of this domain is unknown. The fold of the kinase or catalytic domain (residues 726-1092) has a high level of similarity to that observed in protein kinases.^{99,100} It is a two-lobed structure, with ATP-binding at the hinge region between these two-lobes.

These initial structures revealed a number of important features of the ATP-binding site, which is of particular interest to the development of inhibitors (Figure 1.4). In a similar fashion to that observed in protein kinases, N1 and N6 of the adenine ring system form complementary hydrogen bonding interactions with the amide backbone of Ile881 at the hinge region between the N- and C-lobes of the kinase domain. The presence of this 'hinge' interaction is preserved in all inhibitor-bound structures determined to date. The adenine ring moiety is sandwiched between hydrophobic residues (Ile831, Ile879, Phe961 and Ile963) at the base and roof of the binding site. The ribose ring projects towards the solvent exposed region, but doesn't make any specific interactions with the protein. The phosphate tail of ATP interacts with a loop designated the P-loop (p110 γ residues 803-811), analogous to that in protein kinases. The α -phosphate interacts with Lys833, the β -phosphate with Ser806 and the γ -phosphate with Asn951. Since the first structures of PI3K γ , there have been more than 70 inhibitor-bound structures deposited in the Protein Data Bank (PDB). Its relative ease of expression and crystallisation has made it the mainstay of PI3K structural studies of inhibitor binding.

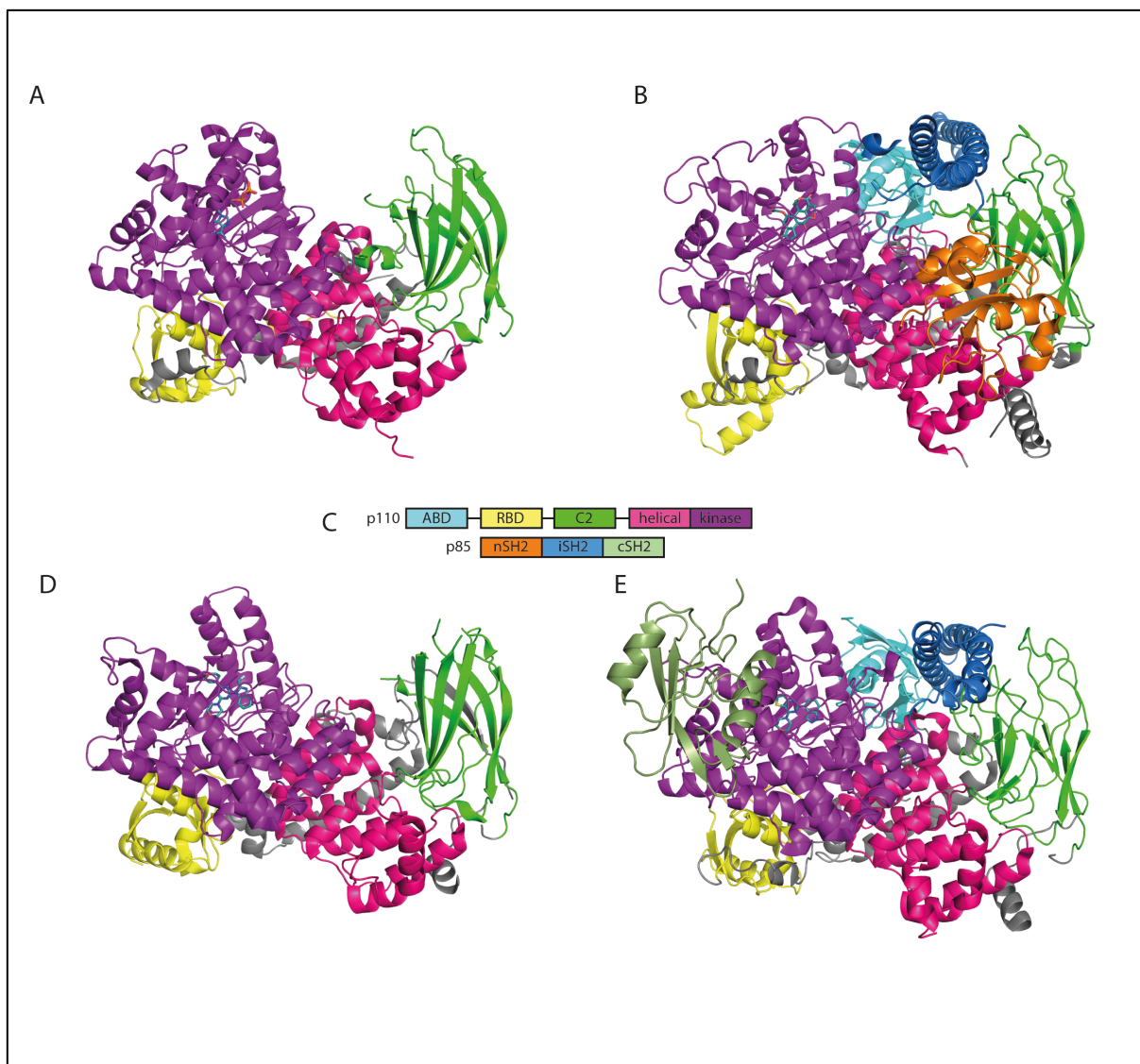


Figure 1.3: Ribbon representation of PI3K isoform crystal structures highlighting the domain structures (ABD – cyan, RBD – yellow, C2 – green, helical – pink, kinase – purple, nSH2 – orange, iSH2 – blue, cSH2 – pale green). A) p110 γ structure co-crystallised with ATP (PDB ID: 1E8X)¹⁰⁰; B) His1047Arg p110 α /niSH2 p85 α crystal structure co-crystallised with wortmannin (PDB ID: 3HHM)¹⁰⁴; C) domain structures of p110 and p85; D) p110 δ co-crystallised with ZSTK474 (PDB ID: 2WXL)¹⁰⁵; E) p110 β /icSH2 p85 β co-crystallised with GDC-0941 (PDB ID: 2Y3A).¹⁰⁶

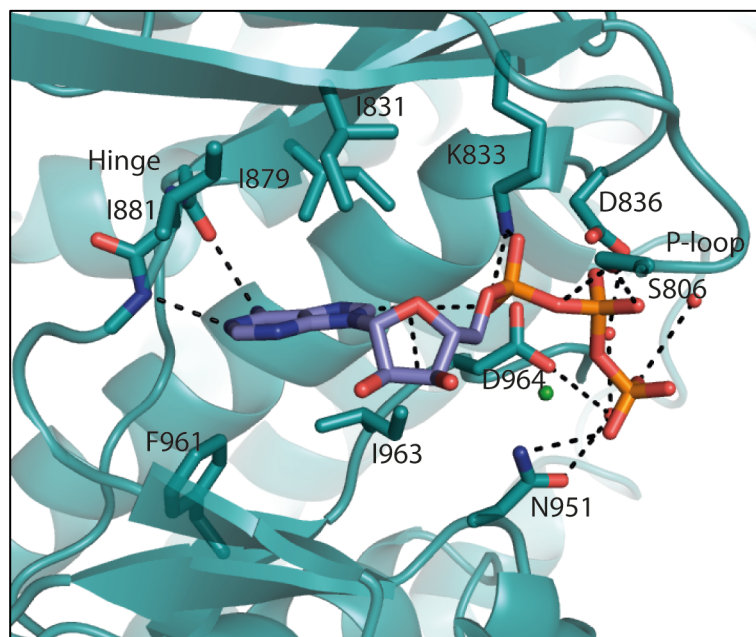


Figure 1.4: Ribbon representation of the p110 γ ATP-binding site (PDB ID: 1E8X) revealing key features of ATP binding. Key binding residues are shown in stick representation. ATP is shown in purple. Water molecules are shown as red spheres, lutetium ions are shown as green spheres. Hydrogen bonds have been represented as black dashed lines.

It took another seven years before the crystal structure of a Class IA PI3K was published. One of the major complicating factors in the crystallisation of the Class IA PI3K isoforms is the requirement to co-express with p85 for stability. Full-length p85 has an SH3 domain, Bcl-2 homology (BH) domain and two SH2 domains, connected by the inter-SH2 (iSH2) domain. The minimum construct of p85 α required for stable expression of p110 α is the N-terminal SH2 (nSH2) and the iSH2 domains.¹⁰⁷ In 2007, Huang *et al.* published the wild-type structure of p110 α in complex with this truncated construct of p85 α .¹⁰⁸ Despite only 35% sequence identity, the overall fold of p110 α displays a high degree of similarity to p110 γ .¹⁰⁸ The iSH2 domain is an extended coiled-coil which interacts with p110 α via the ABD and C2 domains. The electron density for the nSH2 domain of p85 α was disordered, and the structure not able to be traced.

This PI3K α structure provided some important insights into mechanisms of activation of some of the oncogenic mutants, which will be discussed in more detail in Chapter 2. However, its

use for structure-based drug design was limited, as the soaking of substrate or inhibitors was precluded by the binding of the RBD of a symmetry-related molecule in the ATP-binding site.¹⁰⁸ In 2009, the structure of the kinase domain oncogenic mutant, p110 α His1047Arg, was determined (Figure 1.3B).¹⁰⁴ Unlike the wild-type structure, the structure of the nSH2 domain was ordered and able to be determined. Both wortmannin-bound and holo-enzyme structures were reported. The binding mode of wortmannin shows no significant differences from that reported with p110 γ .¹⁰⁰ There have only been two further PI3K α wild-type structures published, one with the reversible dual-selective PI3K β and δ inhibitor, PIK-108, and the other with a novel covalent PI3K α inhibitor.^{109,110}

Crystal structures of p110 δ followed in early 2010 (Figure 1.3D).¹⁰⁵ A tobacco etch virus (TEV) protease cleavage site was introduced between the ABD and the RBD. A complex containing p110 δ and iSH2 of p85 α was expressed, and then the ABD cleaved with TEV protease, leaving just the N-terminally truncated p110 δ . A total of 14 structures were determined, including the holo-enzyme and the enzyme in complex with a range of pan-PI3K and PI3K δ selective inhibitors.¹⁰⁵

The final isoform to be crystallised was PI3K β (Figure 1.3E).¹⁰⁶ Unlike p110 α , it was found that the C-terminal SH2 domain (cSH2) of p85 was more important than the nSH2 for stabilisation and inhibition of p110 β . For crystallisation, therefore, p110 β was expressed in complex with the iSH2 and cSH2 domains of p85 β . No structure of the holo-enzyme was reported, only that in complex with the pan-PI3K inhibitor, GDC-0941 **14** (Figure 1.5).¹⁰⁶

As a prelude to the rational design of isoform selective PI3K α inhibitors it is important to understand the determinants of isoform selectivity in a highly conserved ATP-binding site. Structural information gained from X-ray crystallography can work in tandem with kinetic, mutagenesis and computational modelling data to provide insights into the structural basis of

isoform selectivity. Two regions of non-conserved residues have been identified around the perimeter of the ATP-binding site, designated Regions 1 and 2 (Figure 1.6).^{111,112} There have been several reports from our lab regarding the role of these residues in shaping selectivity of isoform selective inhibitors. The PI3K α selectivity of A-66 **15** (Figure 1.5) was shown by site-directed mutagenesis and molecular modelling to make a specific interaction with non-conserved p110 α Gln859 in Region 1.^{113,114} This compound is closely related to the clinical candidate NVP-BYL719 **6** from Novartis.⁸⁶ A novel PI3K β selective ZSTK474 derivative JP9-114 **16** (Figure 1.5) developed in our lab was shown by mutagenesis and modelling to rely on a key interaction at the corresponding residue p110 β Asp862.¹¹⁵

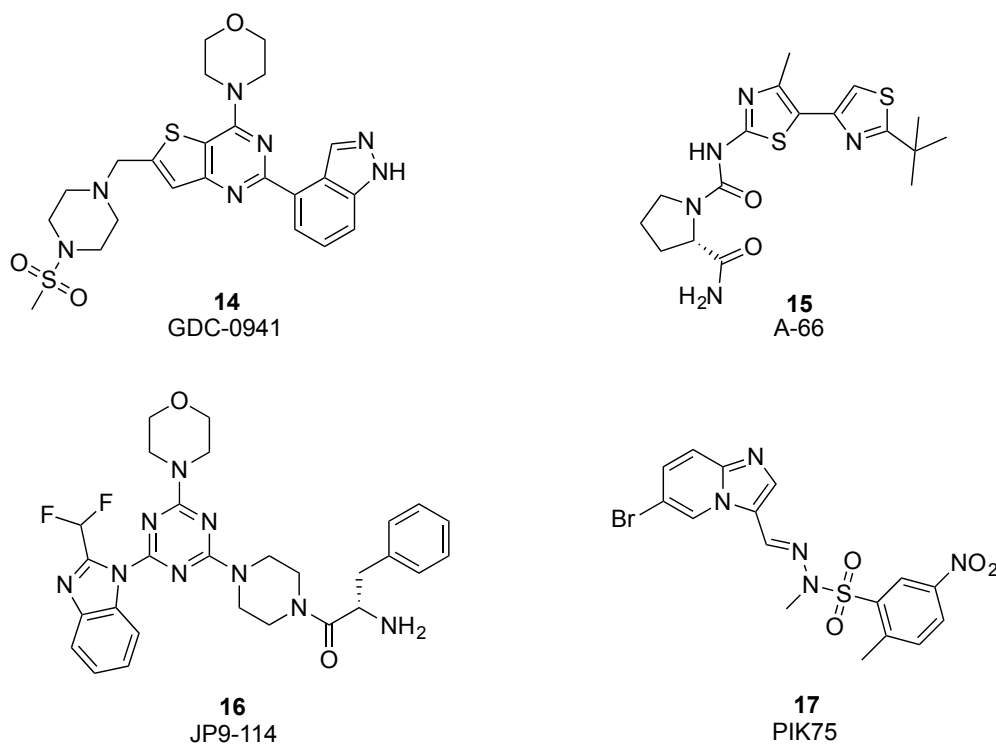


Figure 1.5: Structures of PI3K inhibitors.

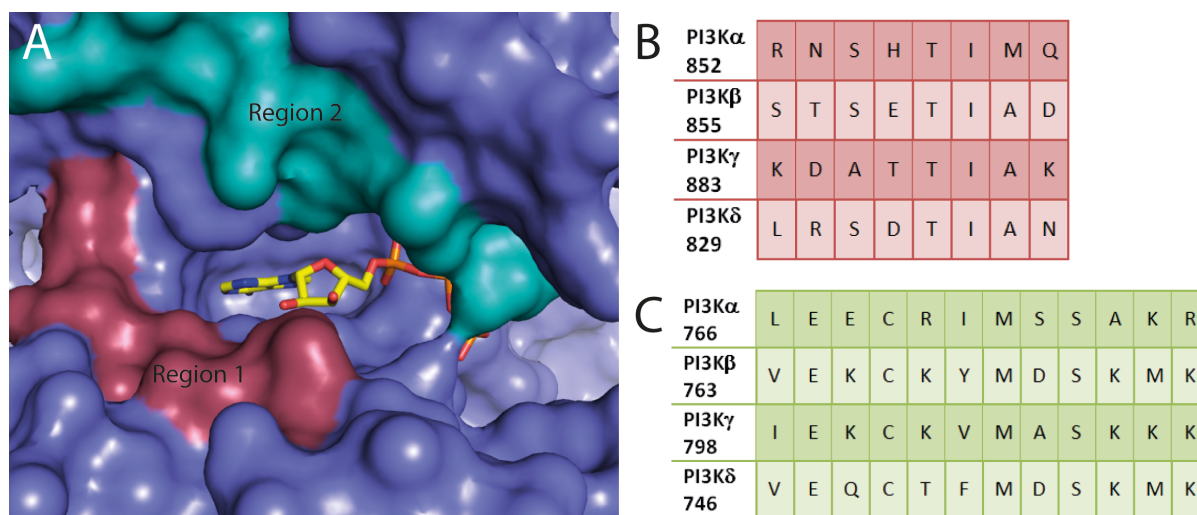


Figure 1.6: Regions of Selectivity. A) p110 γ structure shown in surface representation. Bound ATP is shown in yellow (PDB ID: 1E8X). Region 1 is highlighted in red in the diagram, with the residues for each isoform shown in table B. Region 2 is highlighted in green with the residues for each isoform shown in table C.

Residues from Region 2, which comprise the P-loop, can also influence isoform selectivity.^{112,113} This can be through isoform specific interactions, as in the case of the PI3K α selective inhibitor, PIK-75 **17** (Figure 1.5), which interacts with p110 α Ser773.¹¹² Alternatively, the formation of an induced specificity pocket through the movement of the conserved p110 α Met772 (and the analogous residues in the other isoforms) has been demonstrated to convey PI3K β and δ selectivity (Figure 1.7).^{85,105} Formation of the specificity pocket has been demonstrated crystallographically in PI3K α , γ and δ , but it appears to be more easily formed in PI3K β and δ .^{85,105,109} Recent mutagenesis studies have implicated another residue located on the P-loop, p110 β Tyr778, in affecting the loop's conformational flexibility.¹¹⁶ The residue in this position is aliphatic in PI3K α and γ (isoleucine and valine, respectively), but aromatic in PI3K β and δ (tyrosine and phenylalanine, respectively). Reciprocal mutations (p110 α Ile771Tyr and p110 β Tyr778Ile) at this position between PI3K α and β revealed an important role for this residue in the PI3K β -selectivity of four PI3K β selective inhibitors (note that the candidate performed the modelling associated with the published mutagenesis studies that do not form part of this thesis).¹¹⁶

Berndt *et al.* reported that the formation of the specificity pocket in p110 δ is accompanied by a local change in the P-loop, whereas in p110 γ , it requires a conformational change involving a much larger movement of the N- and C-lobes of the kinase domain with respect to each other.¹⁰⁵ This is thought to be caused by the presence of a longer loop sitting above the P-loop in p110 γ (residues 752-760) compared with p110 δ , possibly serving to rigidify the P-loop in p110 γ (Figure 1.7).¹⁰⁵ These two mechanisms may influence the flexibility of the P-loop in different isoforms.¹¹⁶

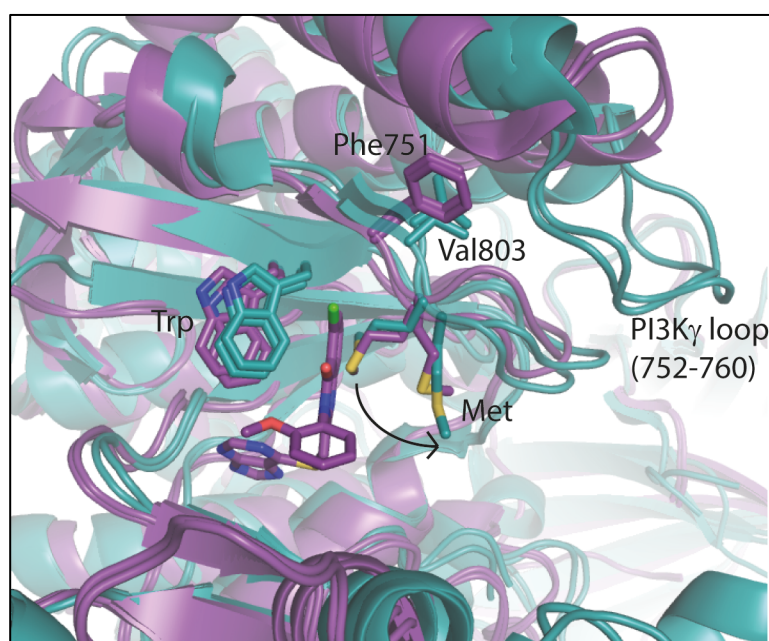


Figure 1.7: Specificity pocket. p110 γ structures (teal) with the specificity pocket ‘closed’ (PDB ID: 1E8X) and ‘open’ (PDB ID: 2CHW) overlaid with p110 δ structures (purple) with the specificity pocket ‘closed’ (PDB ID: 2WXL) and ‘open’ (PDB ID: 2WXF). PIK39 from 2WXF is shown in the binding site. The long p110 γ loop (residues 752-760) is highlighted, with the equivalent p110 δ loop much shorter. The equivalent residues to p110 β Tyr778, which has been shown to influence specificity pocket formation, are also shown (p110 γ Val803, p110 δ Phe751).

Significant progress has been made in understanding the basis for inhibitor isoform selectivity in the examples discussed above. There remains, however, a number of inhibitors for which the selectivity cannot be explained. This is especially clear in the example of PI3K γ selective inhibitors that only interact with conserved residues within the binding site.⁹⁶ While

rational design of isoform selective inhibitors is currently possible under some circumstances, a deeper understanding of the mechanisms of PI3K isoform selectivity is still required.

1.6 Isoform selective inhibitors in the clinic

While a structural understanding of the determinants of isoform selectivity is important for the design of isoform selective inhibitors, the ideal selectivity profile for therapeutic action against cancer is still unknown. In principle, the ideal PI3K inhibitors would be specific for oncogenic mutant PI3K α and spare wild-type PI3K so that only cancer cells would be targeted. To date, inhibitors of this type remain elusive, although some preliminary selectivity has been observed.^{117,118} Structural studies allow us to start to understand how these oncogenic mutations affect the kinetics and regulation of these enzymes, and may further the quest for oncogene-specific PI3K inhibitors. In the meantime, as has been described in this chapter, there are currently a selection of both pan and isoform selective PI3K inhibitors under clinical evaluation. As this new generation of inhibitors progresses through the clinic, the influence of isoform selectivity on therapeutic efficacy and patient tolerance should become apparent. Theoretically, pan-PI3K inhibition should reduce the occurrence of acquired resistance through up-regulation of the other PI3K isoforms. However, the inhibition of all isoforms of such an integral signalling enzyme risks a more severe side-effect profile. There is also the possibility of acquired resistance through the upregulation of alternative growth pathways. Clinical trials combining PI3K inhibition with MEK/Erk pathway inhibitors are currently underway and these sorts of combination therapies may reduce resistance and prove more effective than single agent therapies. Clinical results available to date, however, indicate that the pan-PI3K inhibitors are well tolerated. Further clinical results will reveal whether this approach and the tolerated doses indeed provide efficacious therapy. The alternative clinical strategy is the use of isoform selective inhibitors. Theoretically, these inhibitors should result in significantly reduced side effects and potentially reduced resistance. In the case of PI3K α selective inhibitors, the specific

targeting of PI3K α should allow for higher doses, which could induce complete apoptosis before there is a chance for resistance to develop. Certainly, early trials of the PI3K α selective inhibitor NVP-BYL719 have shown promising results.⁸⁷ As the clinical trials of this and other PI3K α selective inhibitors progress, the efficacy of this approach as compared with pan-PI3K inhibition will become apparent. There is also a likelihood of combining PI3K inhibition with inhibition of other pathways for maximum efficacy.

There remains a need for a thorough understanding of the determinants of inhibitor selectivity to design isoform selective inhibitors of novel chemical classes, and ultimately inhibitors specific for oncogenic mutants. This thesis has therefore sought to contribute to this search by investigating structural differences between wild-type PI3K α and the oncogenic mutant p110 α His1047Arg, and developing novel inhibitors probing the influence of various binding regions on selectivity.

1.7 Thesis aims

The overall aim of this work is to investigate the design and synthesis of PI3K α isoform selective inhibitors. This will be done in two sections:

1. **To examine the structure and regulation of PI3K α .** Structure-based insights into the regulation of PI3K α activity, alongside how this regulation is altered with oncogenic mutations, have been explored. The understanding gained can further the search for PI3K α specific inhibitors, and potentially lead to the design of PI3K α oncogenic mutant specific inhibitors.
2. **To investigate structural changes that can influence inhibitor selectivity.** Using the pan-PI3K inhibitor ZSTK474 as a starting point, structure-based design principles were applied to identify opportunities for building isoform selectivity in novel compounds. This work has demanded the establishment of new synthetic routes to target compounds and the evaluation of inhibitory activity of synthesised molecules.

Taken together the work that follows seeks to generate new understanding of the ways in which PI3K can be inhibited in cancer patients, and hopefully contribute to the successful treatment of human cancers.

1.8 References

- (1) Cao, Y.; DePinho, R. A.; Ernst, M.; Vousden, K. Cancer research: past, present and future. *Nat. Rev. Cancer* **2011**, *11*, 749–754.
- (2) Fyffe, C.; Buus, R.; Falasca, M. Genetic and Epigenetic Regulation of Phosphoinositide 3-kinase Isoforms. *Curr. Pharm. Des.* **2013**, *19*, 680–686.
- (3) Engelman, J. A. Targeting PI3K signalling in cancer: opportunities, challenges and limitations. *Nat. Rev. Cancer* **2009**, *9*, 550–562.
- (4) Vanhaesebroeck, B.; Guillermet-Guibert, J.; Graupera, M.; Bilanges, B. The emerging mechanisms of isoform-specific PI3K signalling. *Nat. Rev. Mol. Cell Biol.* **2010**, *11*, 329–341.
- (5) Vanhaesebroeck, B.; Stephens, L.; Hawkins, P. PI3K signalling: the path to discovery and understanding. *Nat. Rev. Mol. Cell Biol.* **2012**, *13*, 195–203.
- (6) Liu, P.; Cheng, H.; Roberts, T. M.; Zhao, J. J. Targeting the phosphoinositide 3-kinase pathway in cancer. *Nat. Rev. Drug Disc.* **2009**, *8*, 627–644.
- (7) Cantley, L. C. The Phosphoinositide 3-Kinase Pathway. *Science* **2002**, *296*, 1655–1657.
- (8) Jia, S.; Roberts, T. M.; Zhao, J. J. Should individual PI3 kinase isoforms be targeted in cancer? *Curr. Opin. Cell Biol.* **2009**, *21*, 199–208.
- (9) Ihle, N. T.; Powis, G. Take your PIK: phosphatidylinositol 3-kinase inhibitors race through the clinic and toward cancer therapy. *Mol. Cancer Ther.* **2009**, *8*, 1–9.
- (10) Geering, B.; Cutillas, P. R.; Nock, G.; Gharbi, S. I.; Vanhaesebroeck, B. Class IA phosphoinositide 3-kinases are obligate p85-p110 heterodimers. *Proc. Natl. Acad. Sci. U.S.A.* **2007**, *104*, 7809–7814.
- (11) Yu, J.; Zhang, Y.; McIlroy, J.; Rordorf-Nikolic, T.; Orr, G. A.; Backer, J. M. Regulation of the P85/P110 Phosphatidylinositol 3'-Kinase: Stabilization and Inhibition of the p110 α Catalytic Subunit by the p85 Regulatory Subunit. *Mol. Cell. Biol.* **1998**, *18*, 1379–1387.
- (12) Escobedo, J. A.; Navankasattusas, S.; Kavanaugh, W. M.; Milfay, D.; Fried, V. A.; Williams, L. T. cDNA cloning of a Novel 85 kd protein that has SH2 domains and regulates binding of PI3-kinase to the PDGF β -receptor. *Cell* **1991**, *65*, 75–82.
- (13) Otsu, M.; Hiles, I.; Gout, I.; Fry, M. J.; Ruiz-Larrea, F.; Panayotou, G.; Thompson, A.; Dhand, R.; Hsuan, J.; Totty, N.; Smith, A. D.; Morgan, S. J.; Courtneidge, S. A.; Parker, P. J.; Waterfield, M. D. Characterization of two 85 kd proteins that associate with receptor tyrosine kinases, middle-T/pp60c-src complexes, and PI3-kinase. *Cell* **1991**, *65*, 91–104.
- (14) Pons, S.; Asano, T.; Glasheen, E.; Miralpeix, M.; Zhang, Y.; Fisher, T. L.; Myers, M. G.; Sun, X. J.; White, M. F. The structure and function of p55PIK reveal a new regulatory subunit for phosphatidylinositol 3-kinase. *Mol. Cell. Biol.* **1995**, *15*, 4453–4465.
- (15) Inukai, K.; Anai, M.; Breda, E. V.; Hosaka, T.; Katagiri, H.; Funaki, M.; Fukushima, Y.; Ogihara, T.; Yazaki, Y.; Kikuchi, M.; Oka, Y.; Asano, T. A Novel 55-kDa Regulatory Subunit

- for Phosphatidylinositol 3-Kinase Structurally Similar to p55PIK Is Generated by Alternative Splicing of the p85 Gene. *J. Biol. Chem.* **1996**, *271*, 5317–5320.
- (16) Inukai, K.; Funaki, M.; Ogihara, T.; Katagiri, H.; Kanda, A.; Anai, M.; Fukushima, Y.; Hosaka, T.; Suzuki, M.; Shin, B.-C.; Takata, K.; Yazaki, Y.; Kikuchi, M.; Oka, Y.; Asano, T. p85 α Gene Generates Three Isoforms of Regulatory Subunit for Phosphatidylinositol 3-Kinase (PI 3-Kinase), p50 α , p55 α , and p85 α , with Different PI 3-Kinase Activity Elevating Responses to Insulin. *J. Biol. Chem.* **1997**, *272*, 7873–7882.
 - (17) Suire, S.; Coadwell, J.; Ferguson, G. J.; Davidson, K.; Hawkins, P.; Stephens, L. p84, a New G $\beta\gamma$ -Activated Regulatory Subunit of the Type IB Phosphoinositide 3-Kinase p110 γ . *Curr. Biol.* **2005**, *15*, 566–570.
 - (18) Stephens, L.; Hawkins, P. T.; Eguinoa, A.; Cooke, F.; Saklatvala, J.; Rozengurt, E.; Karin, M. A Heterotrimeric GTPase-Regulated Isoform of PI3K and the Regulation of its Potential Effectors [and Discussion]. *Phil. Trans. R. Soc. Lond. B* **1996**, *351*, 211–215.
 - (19) Stephens, L. ; Eguinoa, A.; Erdjument-Bromage, H.; Lui, M.; Cooke, F.; Coadwell, J.; Smrcka, A. ; Thelen, M.; Cadwallader, K.; Tempst, P.; Hawkins, P. . The G $\beta\gamma$ Sensitivity of a PI3K Is Dependent upon a Tightly Associated Adaptor, p101. *Cell* **1997**, *89*, 105–114.
 - (20) Voigt, P.; Dorner, M. B.; Schaefer, M. Characterization of p87PIKAP, a Novel Regulatory Subunit of Phosphoinositide 3-Kinase γ That Is Highly Expressed in Heart and Interacts with PDE3B. *J. Biol. Chem.* **2006**, *281*, 9977–9986.
 - (21) Carpenter, C. L.; Auger, K. R.; Chanudhuri, M.; Yoakim, M.; Schaffhausen, B.; Shoelson, S.; Cantley, L. C. Phosphoinositide 3-kinase is activated by phosphopeptides that bind to the SH2 domains of the 85-kDa subunit. *J. Biol. Chem.* **1993**, *268*, 9478–9483.
 - (22) Rordorf-Nikolic, T.; Horn, D. J. V.; Chen, D.; White, M. F.; Backer, J. M. Regulation of Phosphatidylinositol 3'-Kinase by Tyrosyl Phosphoproteins: Full activation requires occupancy of both SH2 domains in the 85-kDa regulatory subunit. *J. Biol. Chem.* **1995**, *270*, 3662–3666.
 - (23) Ong, S. H.; Hadari, Y. R.; Gotoh, N.; Guy, G. R.; Schlessinger, J.; Lax, I. Stimulation of phosphatidylinositol 3-kinase by fibroblast growth factor receptors is mediated by coordinated recruitment of multiple docking proteins. *Proc. Natl. Acad. Sci. U.S.A.* **2001**, *98*, 6074–6079.
 - (24) Kurig, B.; Shymanets, A.; Bohnacker, T.; Prajwal; Brock, C.; Ahmadian, M. R.; Schaefer, M.; Gohla, A.; Harteneck, C.; Wymann, M. P.; Jeanclos, E.; Nürnberg, B. Ras is an indispensable coregulator of the class IB phosphoinositide 3-kinase p87/p110 γ . *Proc. Natl. Acad. Sci. U.S.A.* **2009**, *106*, 20312–20317.
 - (25) Guillermet-Guibert, J.; Bjorklof, K.; Salpekar, A.; Gonella, C.; Ramadani, F.; Bilancio, A.; Meek, S.; Smith, A. J. H.; Okkenhaug, K.; Vanhaesebroeck, B. The p110 β isoform of phosphoinositide 3-kinase signals downstream of G protein-coupled receptors and is functionally redundant with p110 γ . *Proc. Natl. Acad. Sci. U.S.A.* **2008**, *105*, 8292–8297.
 - (26) Dbouk, H. A.; Vadas, O.; Shymanets, A.; Burke, J. E.; Salamon, R. S.; Khalil, B. D.; Barrett, M. O.; Waldo, G. L.; Surve, C.; Hsueh, C.; Perisic, O.; Harteneck, C.; Shepherd, P. R.; Harden, T. K.; Smrcka, A. V.; Taussig, R.; Bresnick, A. R.; Nurnberg, B.; Williams, R. L.; Backer, J. M. G

- Protein-Coupled Receptor-Mediated Activation of p110 β by G $\beta\gamma$ Is Required for Cellular Transformation and Invasiveness. *Sci. Signaling* **2012**, 5, ra89.
- (27) Vadas, O.; Burke, J. E.; Zhang, X.; Berndt, A.; Williams, R. L. Structural basis for activation and inhibition of class I phosphoinositide 3-kinases. *Sci. Signaling* **2011**, 4, re2.
 - (28) Fayard, E.; Xue, G.; Parcellier, A.; Bozulic, L.; Hemmings, B. A. Protein Kinase B (PKB/Akt), a Key Mediator of the PI3K Signaling Pathway. *Curr. Top. Microbiol. Immunol.* **2011**, 346, 31–56.
 - (29) Manning, B. D.; Cantley, L. C. AKT/PKB Signaling: Navigating Downstream. *Cell* **2007**, 129, 1261–1274.
 - (30) Fayard, E.; Tintignac, L. A.; Baudry, A.; Hemmings, B. A. Protein kinase B/Akt at a glance. *J. Cell Sci.* **2005**, 118, 5675–5678.
 - (31) Maehama, T.; Dixon, J. E. The Tumor Suppressor, PTEN/MMAC1, Dephosphorylates the Lipid Second Messenger, Phosphatidylinositol 3,4,5-Trisphosphate. *J. Biol. Chem.* **1998**, 273, 13375–13378.
 - (32) Myers, M. P.; Pass, I.; Batty, I. H.; Kaay, J. V. der; Stolarov, J. P.; Hemmings, B. A.; Wigler, M. H.; Downes, C. P.; Tonks, N. K. The lipid phosphatase activity of PTEN is critical for its tumor suppressor function. *Proc. Natl. Acad. Sci. U.S.A.* **1998**, 95, 13513–13518.
 - (33) Bunney, T. D.; Katan, M. Phosphoinositide signalling in cancer: beyond PI3K and PTEN. *Nat. Rev. Cancer* **2010**, 10, 342–352.
 - (34) Franke, T. F.; Kaplan, D. R.; Cantley, L. C.; Toker, A. Direct Regulation of the Akt Proto-Oncogene Product by Phosphatidylinositol-3,4-bisphosphate. *Science* **1997**, 275, 665–668.
 - (35) Samuels, Y.; Wang, Z.; Bardelli, A.; Silliman, N.; Ptak, J.; Szabo, S.; Yan, H.; Gazdar, A.; Powell, S. M.; Riggins, G. J.; Willson, J. K. V.; Markowitz, S.; Kinzler, K. W.; Vogelstein, B.; Velculescu, V. E. High frequency of mutations of the PIK3CA gene in human cancers. *Science* **2004**, 304, 554.
 - (36) Samuels, Y.; Waldman, T. Oncogenic Mutations of PIK3CA in Human Cancers. *Curr. Top. Microbiol. Immunol.* **2011**, 347, 21–41.
 - (37) Kang, S.; Seo, S. S.; Chang, H. J.; Yoo, C. W.; Park, S. Y.; Dong, S. M. Mutual exclusiveness between PIK3CA and KRAS mutations in endometrial carcinoma. *Int. J. Gynecol. Cancer* **2008**, 18, 1339–1343.
 - (38) Hayes, M. P.; Wang, H.; Espinal-Witter, R.; Douglas, W.; Solomon, G. J.; Baker, S. J.; Ellenson, L. H. PIK3CA and PTEN Mutations in Uterine Endometrioid Carcinoma and Complex Atypical Hyperplasia. *Clin. Cancer Res.* **2006**, 12, 5932–5935.
 - (39) Oda, K.; Stokoe, D.; Taketani, Y.; McCormick, F. High Frequency of Coexistent Mutations of PIK3CA and PTEN Genes in Endometrial Carcinoma. *Cancer Res.* **2005**, 65, 10669–10673.
 - (40) Broderick, D. K.; Di, C.; Parrett, T. J.; Samuels, Y. R.; Cummins, J. M.; McLendon, R. E.; Fults, D. W.; Velculescu, V. E.; Bigner, D. D.; Yan, H. Mutations of PIK3CA in Anaplastic

- Oligodendrogliomas, High-Grade Astrocytomas, and Medulloblastomas. *Cancer Res.* **2004**, *64*, 5048–5050.
- (41) Kita, D.; Yonekawa, Y.; Weller, M.; Ohgaki, H. PIK3CA alterations in primary (de novo) and secondary glioblastomas. *Acta Neuropathol.* **2007**, *113*, 295–302.
 - (42) Knobbe, C. B.; Trampe-Kieslich, A.; Reifemberger, G. Genetic alteration and expression of the phosphoinositol-3-kinase/Akt pathway genes PIK3CA and PIKE in human glioblastomas. *Neuropath. App. Neurobiol.* **2005**, *31*, 486–490.
 - (43) Hartmann, C.; Bartels, G.; Gehlhaar, C.; Holtkamp, N.; von Deimling, A. PIK3CA mutations in glioblastoma multiforme. *Acta Neuropathol.* **2005**, *109*, 639–642.
 - (44) Berenjano, I. M.; Guillermet-Guibert, J.; Pearce, W.; Gray, A.; Fleming, S.; Vanhaesebroeck, B. Both p110 α and p110 β isoforms of PI3K can modulate the impact of loss-of-function of the PTEN tumour suppressor. *Biochem. J.* **2012**, *442*, 151–159.
 - (45) Wee, S.; Wiederschain, D.; Maira, S.-M.; Loo, A.; Miller, C.; deBeaumont, R.; Stegmeier, F.; Yao, Y.-M.; Lengauer, C. PTEN-deficient cancers depend on PIK3CB. *Proc. Natl. Acad. Sci. U.S.A.* **2008**, *105*, 13057–13062.
 - (46) Dbouk, H. A.; Pang, H.; Fiser, A.; Backer, J. M. A biochemical mechanism for the oncogenic potential of the p110 β catalytic subunit of phosphoinositide 3-kinase. *Proc. Natl. Acad. Sci. U.S.A.* **2010**, *107*, 19897–19902.
 - (47) Sujobert, P.; Bardet, V.; Cornillet-Lefebvre, P.; Hayflick, J. S.; Prie, N.; Verdier, F.; Vanhaesebroeck, B.; Muller, O.; Pesce, F.; Ifrah, N.; Hunault-Berger, M.; Berthou, C.; Villemagne, B.; Jourdan, E.; Audhuy, B.; Solary, E.; Witz, B.; Harousseau, J. L.; Himberlin, C.; Lamy, T.; Lioure, B.; Cahn, J. Y.; Dreyfus, F.; Mayeux, P.; Lacombe, C.; Bouscary, D. Essential role for the p110 δ isoform in phosphoinositide 3-kinase activation and cell proliferation in acute myeloid leukemia. *Blood* **2005**, *106*, 1063–1066.
 - (48) Billottet, C.; Grandage, V.; Gale, R.; Quattropiani, A.; Rommel, C.; Vanhaesebroeck, B.; Khwaja, A. A selective inhibitor of the p110 δ isoform of PI 3-kinase inhibits AML cell proliferation and survival and increases the cytotoxic effects of VP16. *Oncogene* **2006**, *25*, 6648–6659.
 - (49) Kok, K.; Geering, B.; Vanhaesebroeck, B. Regulation of phosphoinositide 3-kinase expression in health and disease. *Trends Biochem. Sci.* **2009**, *34*, 115–127.
 - (50) Ikeda, H.; Hideshima, T.; Fulciniti, M.; Perrone, G.; Miura, N.; Yasui, H.; Okawa, Y.; Kiziltepe, T.; Santo, L.; Vallet, S.; Cristea, D.; Calabrese, E.; Gorgun, G.; Raje, N. S.; Richardson, P.; Munshi, N. C.; Lannutti, B. J.; Puri, K. D.; Giese, N. A.; Anderson, K. C. PI3K/p110 δ is a novel therapeutic target in multiple myeloma. *Blood* **2010**, *116*, 1460–1468.
 - (51) Lannutti, B. J.; Meadows, S. A.; Herman, S. E. M.; Kashishian, A.; Steiner, B.; Johnson, A. J.; Byrd, J. C.; Tyner, J. W.; Loriaux, M. M.; Deininger, M.; Druker, B. J.; Puri, K. D.; Ulrich, R. G.; Giese, N. A. CAL-101, a p110 δ selective phosphatidylinositol-3-kinase inhibitor for the treatment of B-cell malignancies, inhibits PI3K signaling and cellular viability. *Blood* **2010**, *117*, 591–594.

-
- (52) Ghigo, A.; Damilano, F.; Braccini, L.; Hirsch, E. PI3K inhibition in inflammation: Toward tailored therapies for specific diseases. *BioEssays* **2010**, *32*, 185–196.
- (53) Dituri, F.; Mazzocca, A.; Lupo, L.; Edling, C. E.; Azzariti, A.; Antonaci, S.; Falasca, M.; Giannelli, G. PI3K class IB controls the cell cycle checkpoint promoting cell proliferation in hepatocellular carcinoma. *Int. J. Cancer* **2012**, *130*, 2505–2513.
- (54) Edling, C. E.; Selvaggi, F.; Buus, R.; Maffucci, T.; Sebastiano, P. D.; Friess, H.; Innocenti, P.; Kocher, H. M.; Falasca, M. Key Role of Phosphoinositide 3-Kinase Class IB in Pancreatic Cancer. *Clin. Cancer Res.* **2010**, *16*, 4928–4937.
- (55) Guerreiro, A. S.; Fattet, S.; Kulesza, D. W.; Atamer, A.; Elsing, A. N.; Shalaby, T.; Jackson, S. P.; Schoenwaelder, S. M.; Grotzer, M. A.; Delattre, O.; Arcaro, A. A Sensitized RNA Interference Screen Identifies a Novel Role for the PI3K p110 γ Isoform in Medulloblastoma Cell Proliferation and Chemoresistance. *Mol. Cancer Res.* **2011**, *9*, 925–935.
- (56) Xie, Y.; Abel, P. W.; Kirui, J. K.; Deng, C.; Sharma, P.; Wolff, D. W.; Toews, M. L.; Tu, Y. Identification of upregulated phosphoinositide 3-kinase γ as a target to suppress breast cancer cell migration and invasion. *Biochem. Pharmacol.* **2013**, *85*, 1454–1462.
- (57) Brazzatti, J. A.; Klingler-Hoffmann, M.; Haylock-Jacobs, S.; Harata-Lee, Y.; Niu, M.; Higgins, M. D.; Kochetkova, M.; Hoffmann, P.; McColl, S. R. Differential roles for the p101 and p84 regulatory subunits of PI3K γ in tumor growth and metastasis. *Oncogene* **2012**, *31*, 2350–2361.
- (58) Arcaro, A.; Wymann, M. P. Wortmannin is a potent phosphatidylinositol 3-kinase inhibitor: the role of phosphatidylinositol 3,4,5-trisphosphate in neutrophil responses. *Biochem. J.* **1993**, *296*, 297–301.
- (59) Brunn, G. J.; Williams, J.; Sabers, C.; Wiederrecht, G.; Lawrence, J. C.; Abraham, R. T. Direct inhibition of the signaling functions of the mammalian target of rapamycin by the phosphoinositide 3-kinase inhibitors, wortmannin and LY294002. *EMBO J.* **1996**, *15*, 5256–5267.
- (60) Davies, S. P.; Reddy, H.; Caivano, M.; Cohen, P. Specificity and mechanism of action of some commonly used protein kinase inhibitors. *Biochem. J.* **2000**, *351*, 95–105.
- (61) Marone, R.; Cmiljanovic, V.; Giese, B.; Wymann, M. P. Targeting phosphoinositide 3-kinase—Moving towards therapy. *Biochim. Biophys. Acta* **2008**, *1784*, 159–185.
- (62) Hong, D. S.; Bowles, D. W.; Falchook, G. S.; Messersmith, W. A.; George, G. C.; O'Bryant, C. L.; Vo, A. C. H.; Klucher, K.; Herbst, R. S.; Eckhardt, S. G.; Peterson, S.; Hausman, D. F.; Kurzrock, R.; Jimeno, A. A Multicenter Phase I Trial of PX-866, an Oral Irreversible Phosphatidylinositol 3-Kinase Inhibitor, in Patients with Advanced Solid Tumors. *Clin. Cancer Res.* **2012**, *18*, 4173–4182.
- (63) Ihle, N. T.; Williams, R.; Chow, S.; Chew, W.; Berggren, M. I.; Paine-Murrieta, G.; Minion, D. J.; Halter, R. J.; Wipf, P.; Abraham, R.; Kirkpatrick, L.; Powis, G. Molecular pharmacology and antitumor activity of PX-866, a novel inhibitor of phosphoinositide-3-kinase signaling. *Mol. Cancer Ther.* **2004**, *3*, 763–772.

-
- (64) Vlahos, C. J.; Matter, W. F.; Hui, K. Y.; Brown, R. F. A specific inhibitor of Phosphatidylinositol 3-kinase, 2-(4-morpholinyl)-8-phenyl-4H-1-benzopyran-4-one (LY294002). *J. Biol. Chem.* **1994**, *269*, 5241–5248.
- (65) Gharbi, S. I.; Zvelebil, M. J.; Shuttleworth, S. J.; Hancox, T. C.; Saghir, N.; Timms, J. F.; Waterfield, M. D. Exploring the specificity of the PI3K family inhibitor LY294002. *Biochem. J.* **2007**, *404*, 15–21.
- (66) Jacobs, M. D.; Black, J.; Futer, O.; Swenson, L.; Hare, B.; Fleming, M.; Saxena, K. Pim-1 ligand-bound structures reveal the mechanism of serine/threonine kinase inhibition by LY294002. *J. Biol. Chem.* **2005**, *280*, 13728–13734.
- (67) Yamaguchi, K.; Lee, S.-H.; Kim, J.-S.; Wimalasena, J.; Kitajima, S.; Baek, S. J. Activating transcription factor 3 and early growth response 1 are the novel targets of LY294002 in a phosphatidylinositol 3-kinase-independent pathway. *Cancer Res.* **2006**, *66*, 2376–2384.
- (68) Abbott, B. M.; Thompson, P. E. PDE2 inhibition by the PI3 kinase inhibitor LY294002 and analogues. *Bioorg. Med. Chem. Lett.* **2004**, *14*, 2847–2851.
- (69) Garlich, J. R.; De, P.; Dey, N.; Su, J. D.; Peng, X.; Miller, A.; Murali, R.; Lu, Y.; Mills, G. B.; Kundra, V.; Shu, H. K.; Peng, Q.; Durden, D. L. A vascular targeted pan phosphoinositide 3-kinase inhibitor prodrug, SF1126, with antitumour and antiangiogenic activity. *Cancer Res.* **2008**, *68*, 206–215.
- (70) Markman, B.; J. Tao, J.; Scaltriti, M. PI3K Pathway Inhibitors: Better Not Left Alone. *Curr. Pharm. Des.* **2013**, *19*, 895–906.
- (71) Kong, D.; Yamori, T. Advances in development of phosphatidylinositol 3-kinase inhibitors. *Curr. Med. Chem.* **2009**, *16*, 2839–2854.
- (72) Wu, P.; Liu, T.; Hu, Y. PI3K inhibitors for cancer therapy: what has been achieved so far? *Curr. Med. Chem.* **2009**, *16*, 916–930.
- (73) Yaguchi, S.; Fukui, Y.; Koshimizu, I.; Yoshimi, H.; Matsuno, T.; Gouda, H.; Hirono, S.; Yamazaki, K.; Yamori, T. Antitumor activity of ZSTK474, a new phosphatidylinositol 3-kinase inhibitor. *J. Natl. Cancer Inst.* **2006**, *98*, 545–556.
- (74) Matsuno, T.; Kato, M.; Sasahara, H.; Watanabe, T.; Inaba, M.; Takahashi, M.; Yaguchi, S.; Yoshioka, K.; Sakato, M.; Kawashima, S. Synthesis and Antitumor Activity of Benzimidazolyl-1, 3, 5-triazine and Benzimidazolylpyrimidine Derivatives. *Chem. Pharm. Bull.* **2000**, *48*, 1778–1781.
- (75) Kong, D.; Yamori, T. ZSTK474 is an ATP-competitive inhibitor of class I phosphatidylinositol 3 kinase isoforms. *Cancer Sci.* **2007**, *98*, 1638–1642.
- (76) A Safety Study of Oral ZSTK474 in Patients With Cancer
<http://clinicaltrials.gov/show/NCT01280487> (accessed Apr 11, 2013).
- (77) A Study of ZSTK474 in Japanese Patients With Advanced Solid Malignancies
<http://clinicaltrials.gov/ct2/show/NCT01682473> (accessed Apr 11, 2013).
- (78) Kong, D.; Okamura, M.; Yoshimi, H.; Yamori, T. Antiangiogenic effect of ZSTK474, a novel phosphatidylinositol 3-kinase inhibitor. *Eur. J. Cancer* **2009**, *45*, 857–865.

-
- (79) Maira, S.-M.; Pecchi, S.; Huang, A.; Burger, M.; Knapp, M.; Sterker, D.; Schnell, C.; Guthy, D.; Nagel, T.; Wiesmann, M.; Brachmann, S.; Fritsch, C.; Dorsch, M.; Chène, P.; Shoemaker, K.; Pover, A. D.; Menezes, D.; Martiny-Baron, G.; Fabbro, D.; Wilson, C. J.; Schlegel, R.; Hofmann, F.; García-Echeverría, C.; Sellers, W. R.; Voliva, C. F. Identification and Characterization of NVP-BKM120, an Orally Available Pan-Class I PI3-Kinase Inhibitor. *Mol. Cancer Ther.* **2012**, *11*, 317–328.
- (80) Burger, M. T.; Pecchi, S.; Wagman, A.; Ni, Z.-J.; Knapp, M.; Hendrickson, T.; Atallah, G.; Pfister, K.; Zhang, Y.; Bartulis, S.; Frazier, K.; Ng, S.; Smith, A.; Verhagen, J.; Haznedar, J.; Huh, K.; Iwanowicz, E.; Xin, X.; Menezes, D.; Merritt, H.; Lee, I.; Wiesmann, M.; Kaufman, S.; Crawford, K.; Chin, M.; Bussiere, D.; Shoemaker, K.; Zaror, I.; Maira, S.-M.; Voliva, C. F. Identification of NVP-BKM120 as a Potent, Selective, Orally Bioavailable Class I PI3 Kinase Inhibitor for Treating Cancer. *ACS Med. Chem. Lett.* **2011**, *2*, 774–779.
- (81) Bendell, J. C.; Rodon, J.; Burris, H. A.; Jonge, M. de; Verweij, J.; Birle, D.; Demanse, D.; Buck, S. S. D.; Ru, Q. C.; Peters, M.; Goldbrunner, M.; Baselga, J. Phase I, Dose-Escalation Study of BKM120, an Oral Pan-Class I PI3K Inhibitor, in Patients With Advanced Solid Tumors. *J. Clin. Oncol.* **2012**, *30*, 282–290.
- (82) Clarke, P. A.; Workman, P. Phosphatidylinositol-3-Kinase Inhibitors: Addressing Questions of Isoform Selectivity and Pharmacodynamic/Predictive Biomarkers in Early Clinical Trials. *J. Clin. Oncol.* **2012**, *30*, 331–333.
- (83) Venkatesan, A. M.; Dehnhardt, C. M.; Delos Santos, E.; Chen, Z.; Dos Santos, O.; Ayrál-Kaloustian, S.; Khafizova, G.; Brooijmans, N.; Mallon, R.; Hollander, I.; Feldberg, L.; Lucas, J.; Yu, K.; Gibbons, J.; Abraham, R. T.; Chaudhary, I.; Mansour, T. S. Bis(morpholino-1,3,5-triazine) Derivatives: Potent Adenosine 5'-Triphosphate Competitive Phosphatidylinositol-3-kinase/Mammalian Target of Rapamycin Inhibitors: Discovery of Compound 26 (PKI-587), a Highly Efficacious Dual Inhibitor. *J. Med. Chem.* **2010**, *53*, 2636–2645.
- (84) Mallon, R.; Feldberg, L. R.; Lucas, J.; Chaudhary, I.; Dehnhardt, C.; Santos, E. D.; Chen, Z.; Santos, O. dos; Ayrál-Kaloustian, S.; Venkatesan, A.; Hollander, I. Antitumor Efficacy of PKI-587, a Highly Potent Dual PI3K/mTOR Kinase Inhibitor. *Clin. Cancer Res.* **2011**, *17*, 3193–3203.
- (85) Knight, Z. A.; Gonzalez, B.; Feldman, M. E.; Zunder, E. R.; Goldenberg, D. D.; Williams, O.; Loewith, R.; Stokoe, D.; Balla, A.; Toth, B.; Balla, T.; Weiss, W. A.; Williams, R. L.; Shokat, K. M. A Pharmacological Map of the PI3-K Family Defines a Role for p110 α in Insulin Signaling. *Cell* **2006**, *125*, 733–747.
- (86) Furet, P.; Guagnano, V.; Fairhurst, R. A.; Imbach-Weese, P.; Bruce, I.; Knapp, M.; Fritsch, C.; Blasco, F.; Blanz, J.; Aichholz, R.; Hamon, J.; Fabbro, D.; Caravatti, G. Discovery of NVP-BYL719 a potent and selective phosphatidylinositol-3 kinase α inhibitor selected for clinical evaluation. *Bioorg. Med. Chem. Lett.* **2013**, *23*, 3741–3748.
- (87) Juric, D.; Rodon, J.; Gonzalez-Angulo, A. M.; Burris, H. A.; Bendell, J.; Berlin, J. D.; Middleton, M. R.; Bootle, D.; Boehm, M.; Schmitt, A.; Rouyrre, N.; Quadts, C.; Baselga, J. Abstract CT-01: BYL719, a next generation PI3K α specific inhibitor: Preliminary safety, PK, and efficacy results from the first-in-human study. *Cancer Res.* **2012**, *72*, CT-01.

-
- (88) Jessen, K.; Kessler, L.; Kucharski, J.; Guo, X.; Staunton, J.; Janes, M.; Elia, M.; Banerjee, U.; Lan, L.; Wang, S.; Stewart, J.; Luzader, A.; Darjania, L.; Li, L.; Chan, K.; Martin, M.; Ren, P.; Rommel, C.; Liu, Y. Abstract A171: A potent and selective PI3K inhibitor, INK1117, targets human cancers harboring oncogenic PIK3CA mutations. *Mol. Cancer Ther.* **2011**, *10*, A171.
- (89) So, L.; Yea, S. S.; Oak, J. S.; Lu, M.; Manmadhan, A.; Ke, Q. H.; Janes, M. R.; Kessler, L. V.; Kucharski, J. M.; Li, L.-S.; Martin, M. B.; Ren, P.; Jessen, K. A.; Liu, Y.; Rommel, C.; Fruman, D. A. Selective Inhibition of Phosphoinositide 3-Kinase p110 α Preserves Lymphocyte Function. *J. Biol. Chem.* **2013**, *288*, 5718–5731.
- (90) Furman, R. R.; Byrd, J. C.; Flinn, I. W.; Coutre, S. E.; Benson Jr, D. M.; Brown, J. R.; Kahl, B. S.; Wagner-Johnston, N. D.; Giese, N. A.; Yu, A. S. Interim results from a phase I study of CAL-101, a selective oral in phosphatidylinositol 3-kinase p110 δ isoform, in patients with relapsed or refractory hematologic malignancies. *J. Clin. Oncol.* **2010**, *28*, 3032.
- (91) Jackson, S. P.; Schoenwaelder, S. M.; Goncalves, I.; Nesbitt, W. S.; Yap, C. L.; Wright, C. E.; Kenche, V.; Anderson, K. E.; Dopheide, S. M.; Yuan, Y.; Sturgeon, S. A.; Prabakaran, H.; Thompson, P. E.; Smith, G. D.; Shepherd, P. R.; Daniele, N.; Kulkarni, S.; Abbott, B.; Saylik, D.; Jones, C.; Lu, L.; Giuliano, S.; Hughan, S. C.; Angus, J. A.; Robertson, A. D.; Salem, H. H. PI 3-kinase p110 β : a new target for antithrombotic therapy. *Nat. Med.* **2005**, *11*, 507–514.
- (92) Nylander, S.; Kull, B.; Björkman, J. A.; Ulvinge, J. C.; Oakes, N.; Emanuelsson, B. M.; Andersson, M.; Skärby, T.; Inghardt, T.; Fjellström, O.; Gustafsson, D. Human target validation of phosphoinositide 3-kinase (PI3K) β : effects on platelets and insulin sensitivity, using AZD6482 a novel PI3K β inhibitor. *J. Thromb. Haemostasis* **2012**, *10*, 2127–2136.
- (93) Ni, J.; Liu, Q.; Xie, S.; Carlson, C.; Von, T.; Vogel, K.; Riddle, S.; Benes, C.; Eck, M.; Roberts, T.; Gray, N.; Zhao, J. Functional Characterization of an Isoform-Selective Inhibitor of PI3K-p110 β as a Potential Anticancer Agent. *Cancer Discov.* **2012**, *2*, 425–433.
- (94) Rivero, R. A.; Hardwicke, M. A. Abstract 2913: Identification of GSK2636771, a potent and selective, orally bioavailable inhibitor of phosphatidylinositol 3-kinase-beta (PI3K β) for the treatment of PTEN deficient tumors. *Cancer Res.* **2012**, *72*, 2913.
- (95) Brana, I.; Siu, L. L. Clinical development of phosphatidylinositol 3-kinase inhibitors for cancer treatment. *BMC Med.* **2012**, *10*, 161–175.
- (96) Camps, M.; Rückle, T.; Ji, H.; Ardisson, V.; Rintelen, F.; Shaw, J.; Ferrandi, C.; Chabert, C.; Gillieron, C.; Françon, B.; Martin, T.; Gretener, D.; Perrin, D.; Leroy, D.; Vitte, P.-A.; Hirsch, E.; Wymann, M. P.; Cirillo, R.; Schwarz, M. K.; Rommel, C. Blockade of PI3K γ suppresses joint inflammation and damage in mouse models of rheumatoid arthritis. *Nat. Med.* **2005**, *11*, 936–943.
- (97) Bergamini, G.; Bell, K.; Shimamura, S.; Werner, T.; Cansfield, A.; Müller, K.; Perrin, J.; Rau, C.; Ellard, K.; Hopf, C.; Doce, C.; Leggate, D.; Mangano, R.; Mathieson, T.; O'Mahony, A.; Plavec, I.; Rharbaoui, F.; Reinhard, F.; Savitski, M. M.; Ramsden, N.; Hirsch, E.; Drewes, G.; Rausch, O.; Bantscheff, M.; Neubauer, G. A selective inhibitor reveals PI3K γ dependence of TH17 cell differentiation. *Nat. Chem. Biol.* **2012**, *8*, 576–582.
- (98) Sunose, M.; Bell, K.; Ellard, K.; Bergamini, G.; Neubauer, G.; Werner, T.; Ramsden, N. Discovery of 5-(2-amino-[1,2,4]triazolo[1,5-a]pyridin-7-yl)-N-(tert-butyl)pyridine-3-

- sulfonamide (CZC24758), as a potent, orally bioavailable and selective inhibitor of PI3K for the treatment of inflammatory disease. *Bioorg. Med. Chem. Lett.* **2012**, *22*, 4613–4618.
- (99) Walker, E. H.; Perisic, O.; Ried, C.; Stephens, L.; Williams, R. L. Structural insights into phosphoinositide 3-kinase catalysis and signalling. *Nature* **1999**, *402*, 313–320.
- (100) Walker, E.; Pacold, M. E.; Perisic, O.; Stephens, L.; Hawkins, P. T.; Wymann, M. P.; Williams, R. L. Structural determinants of phosphoinositide 3-kinase inhibition by wortmannin, LY294002, Quercetin, Myricetin, and Staurosporine. *Mol. Cell* **2000**, *6*, 909–919.
- (101) Nassar, N.; Horn, G.; Herrmann, C. A.; Scherer, A.; McCormick, F.; Wittinghofer, A. The 2.2 Å crystal structure of the Ras-binding domain of the serine/threonine kinase c-Raf1 in complex with Rap1A and a GTP analogue. *Nature* **1995**, *375*, 554–560.
- (102) Huang, L.; Hofer, F.; Martin, G. S.; Kim, S.-H. Structural basis for the interaction of Ras with RalGDS. *Nat. Struct. Mol. Biol.* **1998**, *5*, 422–426.
- (103) Essen, L.-O.; Perisic, O.; Lynch, D. E.; Katan, M.; Williams, R. L. A Ternary Metal Binding Site in the C2 Domain of Phosphoinositide-Specific Phospholipase C- δ 1. *Biochemistry* **1997**, *36*, 2753–2762.
- (104) Mandelker, D.; Gabelli, S. B.; Schmidt-Kittler, O.; Zhu, J.; Cheong, I.; Huang, C. H.; Kinzler, K. W.; Vogelstein, B.; Amzel, L. M. A frequent kinase domain mutation that changes the interaction between PI3K α and the membrane. *Proc. Natl. Acad. Sci. U.S.A.* **2009**, *106*, 16996–17001.
- (105) Berndt, A.; Miller, S.; Williams, O.; Le, D. D.; Houseman, B. T.; Pacold, J. I.; Gorrec, F.; Hon, W.-C.; Liu, Y.; Rommel, C.; Gaillard, P.; Rückle, T.; Schwarz, M. K.; Shokat, K. M.; Shaw, J. P.; Williams, R. L. The p110 δ structure: mechanisms for selectivity and potency of new PI(3)K inhibitors. *Nat. Chem. Biol.* **2010**, *6*, 117–124.
- (106) Zhang, X.; Vadas, O.; Perisic, O.; Anderson, K. E.; Clark, J.; Hawkins, P. T.; Stephens, L. R.; Williams, R. L. Structure of Lipid Kinase p110 β /p85 β Elucidates an Unusual SH2-Domain-Mediated Inhibitory Mechanism. *Mol. Cell* **2011**, *41*, 567–578.
- (107) Yu, J.; Wjasow, C.; Backer, J. M. Regulation of the P85/P110 α Phosphatidylinositol 3'-Kinase: Distinct roles for the N-terminal and C-terminal SH2 domains. *J. Biol. Chem.* **1998**, *273*, 30199–30203.
- (108) Huang, C. H.; Mandelker, D.; Schmidt-Kittler, O.; Samuels, Y.; Velculescu, V. E.; Kinzler, K. W.; Vogelstein, B.; Gabelli, S. B.; Amzel, L. M. The structure of a human p110 α /p85 α complex elucidates the effects of oncogenic PI3K α mutations. *Science* **2007**, *318*, 1744–1748.
- (109) Hon, W.-C.; Berndt, A.; Williams, R. L. Regulation of lipid binding underlies the activation mechanism of class IA PI3-kinases. *Oncogene* **2012**, *31*, 3655–3666.
- (110) Nacht, M.; Qiao, L.; Sheets, M. P.; St. Martin, T.; Labenski, M.; Mazdiyasni, H.; Karp, R.; Zhu, Z.; Chaturvedi, P.; Bhavsar, D.; Niu, D.; Westlin, W.; Petter, R. C.; Medikonda, A. P.; Singh, J. Discovery of a Potent and Isoform-Selective Targeted Covalent Inhibitor of the Lipid Kinase PI3K α . *J. Med. Chem.* **2013**, *56*, 712–721.

-
- (111) Frazzetto, M.; Suphioglu, C.; Zhu, J.; Schmidt-Kittler, O.; Jennings, I. G.; Cranmer, S. L.; Jackson, S. P.; Kinzler, K. W.; Vogelstein, B.; Thompson, P. E. Dissecting Isoform Selectivity of PI3 Kinase Inhibitors. The Role of Non-conserved Residues in the Catalytic Pocket. *Biochem. J.* **2008**, *414*, 383–390.
- (112) Zheng, Z.; Amran, S. I.; Thompson, P. E.; Jennings, I. G. Isoform-Selective Inhibition of Phosphoinositide 3-Kinase: Identification of a New Region of Nonconserved Amino Acids Critical for p110 α Inhibition. *Mol. Pharmacol.* **2011**, *80*, 657–664.
- (113) Zheng, Z.; Amran, S. I.; Zhu, J.; Schmidt-Kittler, O.; Kinzler, K. W.; Vogelstein, B.; Shepherd, P. R.; Thompson, P. E.; Jennings, I. G. Definition of the binding mode of a new class of phosphoinositide 3-kinase α -selective inhibitors using in vitro mutagenesis of non-conserved amino acids and kinetic analysis. *Biochem. J.* **2012**, *444*, 529–535.
- (114) Jamieson, S.; Flanagan, J. U.; Kolekar, S.; Buchanan, C.; Kendall, J. D.; Lee, W.; Rewcastle, G. W.; Denny, W. A.; Singh, R.; Dickson, J.; Baguley, B. C.; Shepherd, P. R. A drug targeting only p110 α can block phosphoinositide 3-kinase signalling and tumour growth in certain cell types. *Biochem. J.* **2011**, *438*, 53–62.
- (115) Pinson, J.-A.; Zheng, Z.; Miller, M. S.; Chalmers, D. K.; Jennings, I. G.; Thompson, P. E. L-Aminoacyl-triazine Derivatives Are Isoform-Selective PI3K β Inhibitors That Target Nonconserved Asp862 of PI3K β . *ACS Med. Chem. Lett.* **2013**, *4*, 206–210.
- (116) Zheng, Z.; Miller, M. S.; Jennings, I. G.; Thompson, P. E. Mechanisms of PI3K β -Selective Inhibition Revealed by Reciprocal Mutagenesis. *ACS Chem. Biol.* **2013**, *8*, 679–683.
- (117) Sabbah, D. A.; Simms, N. A.; Brattain, M. G.; Vennerstrom, J. L.; Zhong, H. Biological evaluation and docking studies of recently identified inhibitors of phosphoinositide-3-kinases. *Bioorg. Med. Chem. Lett.* **2012**, *22*, 876–880.
- (118) Sabbah, D. A.; Simms, N. A.; Wang, W.; Dong, Y.; Ezell, E. L.; Brattain, M. G.; Vennerstrom, J. L.; Zhong, H. A. N-Phenyl-4-hydroxy-2-quinolone-3-carboxamides as selective inhibitors of mutant H1047R phosphoinositide-3-kinase (PI3K α). *Bioorg. Med. Chem.* **2012**, *20*, 7175–7183.

PART B: Declaration for Chapter 2

Monash University

Declaration for Thesis Chapter 2

Declaration by candidate

In the case of Chapter 2, the nature and extent of my contribution to the work was the following:

Nature of contribution	Extent of contribution (%)
Refinement of crystal structures, data analysis, co-authorship of manuscript	50%

The following co-authors contributed to the work. If co-authors are students at Monash University, the extent of their contribution in percentage terms must be stated:

Name	Nature of contribution	Extent of contribution (%)*
Oleg Schmidt-Kittler	Expression and purification of PI3K α (p110 α /niSH2), performed research	
David Bolduc	Designed and performed the fluorescence quenching assay	
Evan Brower	Designed fluorescence quenching assay; expression and purification of p85 α .	
Daniele Chaves-Moreira	Expression and purification of PI3K α (p110 α /p85 α), oncogenic mutants (E545K p110 α /niSH2, H1047R p110 α /niSH2)	
Mark Allaire	Data collection at Brookhaven National lab	
Kenneth Kinzler	Designed and analysed data	
Ian Jennings	Analysed data	

Philip Thompson	Analysed data and co-authorship of manuscript
Philip Cole	Analysed data
L. Mario Amzel	Analysed data and co-authorship of manuscript
Bert Vogelstein	Designed research, analysed data and co-authorship of manuscript
Sandra Gabelli	Designed and executed research, analysed data and co-authorship of manuscript

**Shown for Monash University students only*

The undersigned hereby certify that the above declaration correctly reflects the nature and extent of the candidate's and co-authors' contributions to this work.

Candidate's Signature		Date
Main Supervisor's Signature		Date

Declaration by co-authors

The undersigned hereby certify that:

- (1) the above declaration correctly reflects the nature and extent of the candidate's contribution to this work, and the nature of the contribution of each of the co-authors;
- (2) they meet the criteria for authorship in that they have participated in the conception, execution, or interpretation, of at least that part of the publication in their field of expertise;
- (3) they take public responsibility for their part of the publication, except for the responsible author who accepts overall responsibility for the publication;
- (4) there are no other authors of the publication according to these criteria;

(5) potential conflicts of interest have been disclosed to (a) granting bodies, (b) the editor or publisher of journals or other publications, and (c) the head of the responsible academic unit; and

(6) the original data are stored at the following location(s) and will be held for at least five years from the date indicated below:

Locations:

Department of Medicinal Chemistry, Monash Institute of Pharmaceutical Sciences, 381 Royal Pde, Parkville VIC 3052, Australia

Ludwig Center for Cancer Genetics and Therapeutics and Howard Hughes Medical Institutions, Johns Hopkins University School of Medicine, Baltimore, Maryland 21205, USA

Departments of Pharmacology and Molecular Sciences, Biophysics and Biophysical Chemistry, Medicine and Oncology, Johns Hopkins University School of Medicine, Baltimore, Maryland 21205, USA

Biology Department, Brookhaven National Laboratory, Upton, NY 11973-5000, USA

Signatures:

Signed: _____ Date: 25/07/2013

Signed: _____ Date: 26/07/2013


Signed: _____ Date: 26/07/2013

Signed: _____ Date: 26/07/2013

Signed: _____ Date: 26/07/2013

Signed: _____ Date: 30/07/2013

Signed: _____ Date: _____

Signed:	<hr/>	Date:	
Signed:		Date:	26/07/2013
Signed:		Date:	26/07/2013
Signed:		Date:	30/07/2013
Signed:		Date:	30/07/2013

Chapter 2: Structural insights into the regulation and lipid binding of PI3K α

2.1 Introduction

Rational drug discovery is underpinned by a comprehensive knowledge of the structural biology of the target protein. In the development of enzyme inhibitors, X-ray crystallography can work in conjunction with biochemical studies to provide a detailed structural understanding of enzymatic regulation and catalysis, leading to new avenues for inhibitor design. In the particular case of PI3K and its role in cancer, X-ray crystallography can reveal specific mechanisms by which common oncogenic mutations are constitutively activated. This may uncover details to lead to the future design of oncogenic mutant-specific inhibitors. Inhibitors of this type would greatly reduce the associated side-effects experienced with general inhibition of PI3K.

2.1.1 Aims

In this chapter, work performed principally at Johns Hopkins University under the supervision of Dr. Sandra Gabelli is described. The aim of this work was to use X-ray crystallography to investigate the structure and regulation of wild-type PI3K α and had four facets: (i) the determination of new wild-type PI3K α crystal structures at improved resolution to allow comparison of wild-type PI3K α with that of the His1047Arg oncogenic mutant; (ii) the characterisation of the lipid-binding site of PI3K α ; (iii) the development of new techniques to enable crystallisation of full length PI3K α and (iv) the attempted co-crystallisation of PI3K α with inhibitors prepared as described in Chapter 3. The first two of these endeavours were successful and are the focus of data presented as a prepared manuscript. Two new X-ray crystal structures of p110 α in complex with nSH2 and iSH2 of p85 α were solved. One structure presents the first look at the nSH2 domain in complex with wild-type p110 α , allowing a detailed comparison of the structures of wild-type and oncogenic mutant enzymes. The second structure is in complex with the substrate, diC4-PIP₂, the first PI3K isoform structure to be determined with a lipid substrate bound.

2.2 Structural insights into the regulation and lipid binding of PI3K α

As discussed in Chapter 1, the first X-ray crystal structure of wild-type p110 α in complex with iSH2 was published in 2007 (PDB ID: 2RD0), followed by the structure of the His1047Arg oncogenic mutant in 2009 (PDB ID: 3HHM).^{1,2} The successful crystallisation of the Class IA PI3K isoforms was a major challenge and demanded the development of a crystallisable fragment of p85 α containing the nSH2 and iSH2 domains co-expressed with p110 α , hereafter referred to as p110 α /niSH2.^{1,3}

The SH2 domains of p85 are important to the regulation of catalysis. They inhibit p110 activity until activation by binding of phosphorylated tyrosine motifs on receptor tyrosine

kinases.^{4,5} The nSH2 domain appears most important for the regulation of p110 α , whereas for p110 β and p110 δ , the cSH2 appears to play a more important role.^{3,6,7} Of all the available p110 α /niSH2 structures, only the oncogenic mutant structure had clear, traceable electron density for the nSH2 domain, preventing a direct comparison which might identify important differences between wild-type and oncogenic forms.^{1,2,8}

Another key structural feature of PI3K α that is yet to be fully investigated is the lipid-binding site. Although the location of the ATP-binding site was established with the co-crystal structure of p110 γ and ATP, a crystal structure containing the lipid substrate is yet to be determined.⁹ Modelling studies of lipid-binding to p110 γ place the phospholipid headgroup between the P-loop (p110 α residues 772-778) and the activation loop (p110 α residues 935-958), with the 3'-hydroxyl group positioned near the γ -phosphate of ATP.⁹ Sequence alignment and biochemical mutagenesis data have also postulated a role for the activation loop in lipid substrate specificity and binding.¹⁰ Computational studies suggest a role for the P-loop residue p110 α Lys776 in facilitating lipid substrate binding.^{10,11}

The p110 α /niSH2 construct was expressed using the baculovirus expression system in SF9 insect cells by Dr. Oleg Schmidt-Kittler as previously described.^{1,2} After purification, the protein was concentrated to 10-15 mg/mL. Needle crystals were obtained in 1.4 M sodium formate and 100 mM HEPES at pH 7.0 that could be used in repeated rounds of macroseeding until diffraction quality crystals were obtained. Diffraction data were collected using 1 oscillation frames for 180° at beamlines X6A and X25 of NSLS at Brookhaven National Laboratory. Data processing (integration, indexing and scaling) was performed with HKL2000.¹² The X-ray diffraction images must be indexed, integrated and scaled. Indexing identifies the individual reflections in each image and allows determination of the unit cell dimensions and symmetry of the crystal. The space group, which describes the symmetry of the protein crystal, was determined to be P2₁2₁2₁.¹³ The unit cell is a box containing the smallest group of atoms that has

the overall symmetry of the crystal, and from which the entire crystal can be built. The dimensions of the unit cell were determined to be 114.7 x 116.2 x 149.1 Å for the free enzyme structure. Once this information is obtained, the intensities of each reflection in each image are determined in the integration process. The integrated data for each image is then scaled and combined into one set of structure factors. The structure factor (F) is a mathematical representation of the diffracted X-ray path to produce each reflection. It is a Fourier sum that incorporates the contribution of the electrons of each atom within the protein to the overall diffraction pattern. In order to convert the structure factor equation into an electron density map, three pieces of information are required – the amplitude, frequencies and phases of the reflections. The intensity and position of each of the reflections give the amplitude and frequency. However, the phases cannot be measured.

The structure of the free enzyme was determined by Fourier synthesis using the coordinates of the previously determined wild-type p110 α /nSH2 (PDB ID: 2RD0) as a model.¹ This allows an initial estimation of the phases, which can subsequently be refined. An initial round of rigid body refinement using REFMAC 5.0, allows calculation of an electron density map from the structure factors and estimated phases.¹⁴ The program Coot was used to visualise the electron density map and allows manual manipulation of the model to fit the map.¹⁵ Iterative rounds of refinement were conducted with REFMAC 5.0.¹⁴ Each round of refinement uses the improved model to re-estimate the phases and compute an improved electron density map.

Initial refinement revealed that, distinct from the model protein (PDB ID: 2RD0), the nSH2 domain of p85 α was present and ordered in the structure. To fit the additional electron density in this region, the nSH2 domain of His1047Arg p110 α /nSH2 structure (PDB ID: 3HHM) and the isolated p85 α nSH2 crystal structure (PDB ID: 2IUG) were used as a guide.^{2,16} The free wild-type structure was refined to 2.96 Å (R/R_{free} 0.19/0.27). The residual index, or R-factor, ($R = \sum | |F_{\text{obs}}| - |F_{\text{calc}}| | / \sum |F_{\text{obs}}|$) is a measure of how well the observed reflection intensities

correspond to the calculated intensities from the current model. The lower the value, the better the model reflects the collected data. The free R-factor, R_{free} , is a method of cross-validation, which measures how well the current model predicts a small set of measured intensities (generally 5-10%) that were excluded from the refinement process. Ideally, the value of R_{free} will be close to the R-factor.

In the case of the lipid bound structure, the crystals were soaked with a 1 mM solution of the truncated soluble substrate, di-C₄-phosphatidylinositol-4,5-bisphosphate (diC4-PIP₂) for 1 hour before cryoprotection and data collection. In this case, the refined coordinates of the free wild-type structure determined above were used as an initial model for the determination of the structure. By comparison, two additional patches of electron density were revealed after initial rounds of refinement, attributed to the lipid substrate, which was successfully modelled into the density map. The overall structure was refined to 3.37 Å (R/R_{free} 0.24/0.34). This latter result also prompted an investigation of lipid binding to PI3K α by fluorescence quenching experiments. Performed by David Bolduc and Dr. Gabelli, this data supported some of the structural features suggested by the crystallographic data. The full details and conclusions of this study of PI3K α structure follows.

2.3 Prepared manuscript

Structural Insights into the Regulation and Lipid-binding of PI3K α

Michelle S. Miller^a, Oleg Schmidt-Kittler^b, David M. Bolduc^c, Evan T. Brower^b, Danielle Chaves-Moreira^d, Mark Allaire^g, Kenneth W. Kinzler^b, Ian G. Jennings^a, Philip E. Thompson^a, Philip Cole^c, L. Mario Amzel^d, Bert Vogelstein^b, Sandra B. Gabelli^{d,e,f}

^a *Medicinal Chemistry, Monash Institute of Pharmaceutical Sciences, 381 Royal Parade, Parkville, Victoria 3052, Australia*

^b *Ludwig Center for Cancer Genetics and Therapeutics, and Howard Hughes Medical Institutions, Johns Hopkins University School of Medicine, Baltimore, Maryland 21205, USA*

^c *Department of Pharmacology and Molecular Sciences, ^d Department of Biophysics and Biophysical Chemistry, ^e Departments of Medicine and ^f Oncology, Johns Hopkins University School of Medicine, Baltimore, Maryland 21205, USA*

^g *Biology Department, Brookhaven National Laboratory, Upton, NY 11973-5000, USA*

Keywords: *PIK3R1*, p85, *PIK3CA*, PI3K, somatic mutation, PIP₂, PIP₃

To whom correspondence should be addressed: E-mail: [REDACTED] (S.B.G.);

[REDACTED] (L.M.A.); [REDACTED] (B.V.)

2.3.1 Abstract

The phosphatidylinositol 3-kinase (PI3K)/Akt pathway is a key regulator of cell growth, proliferation and cell cycle progression. The PI3K α isoform is frequently mutated in breast, colon and endometrial cancers. We report two crystal structures of wild-type p110 α /nSH2, the free enzyme structure and that in complex with the lipid substrate, diC4-PIP₂, refined to 2.96 Å and 3.37 Å, respectively. The free enzyme structure reveals the first X-ray structure of the nSH2 domain in complex with wild-type p110 α , allowing identification of key differences in the binding of the nSH2 domain between wild-type and the oncogenic mutant, p110 α His1047Arg. Increased buried surface area and two unique salt-bridges in the wild-type structure are suggestive of tighter regulatory control in the wild-type PI3K α compared with the oncogenic mutant. In addition to previously identified differences in membrane binding, this provides new insight into the increased basal lipid kinase activity of the oncogenic mutant. The first PI3K isoform lipid-bound structure reveals two lipid-binding sites in PI3K α , confirmed by fluorescence quenching experiments.

2.3.2 Manuscript

The phosphatidylinositol 3-kinase (PI3K)/Akt pathway is a key regulator of cell growth, proliferation and cell cycle progression.^{17–20} Aberrations in pathway signaling are estimated to occur in up to 50% of human cancers, presenting this pathway as an exciting target for the treatment of cancer.¹⁷ Upon activation by receptor tyrosine kinases, PI3K phosphorylates phosphatidylinositol 4,5-bisphosphate (PIP₂) to form the second messenger phosphatidylinositol 3,4,5-trisphosphate (PIP₃). PIP₃ signals through pleckstrin homology domain-containing enzymes such as Akt/Protein Kinase B to activate signaling cascades resulting in increased cell growth, metabolism and proliferation.^{17–20} One key modulator of this pathway, the PI3K α isoform, is mutated in a high percentage of breast, colon and endometrial cancers.^{21–25} About 80% of these mutations are concentrated in three hotspots occurring in the

helical and kinase domains of the protein.²⁶ The most common is the kinase domain oncogenic mutation, p110 α His1047Arg. Key features of this mutant include increased basal lipid kinase activity in vitro and sensitivity to activation by receptor tyrosine kinases. It has been postulated to function via increased membrane binding, which in turn increases substrate accessibility.^{2,8,27,28}

PI3K α is a heterodimeric enzyme consisting of a 110 kDa catalytic subunit (p110 α) and one of five regulatory subunits (most frequently, the 85 kDa protein, p85 α).²⁹ Structures of wild-type PI3K α , as both the free enzyme and in complex with inhibitors have previously been reported.^{1,8,30} The p110 α subunit composes an N-terminal adaptor-binding domain (ABD), responsible for binding to p85, Ras-binding domain (RBD), C2 domain, helical domain and kinase domain.¹ The full-length p85 α subunit contains an SH3 domain, RhoGAP domain and two phosphotyrosine residue binding SH2 domains, connected by a coiled-coil region termed the inter-SH2 domain (iSH2). The most common heterodimer construct used for crystallography is full length p110 α with a truncated p85 α consisting of the N-terminal SH2 domain (nSH2) and the iSH2 domain (residues 322-600), hereafter referred to as p110 α /niSH2.^{1,8} The published structures reveal the overall structure of p110 α in complex with the iSH2 domain of p85 α . However, there remain key structural features that require investigation. For example, none of the published wild-type structures have had traceable electron density for the nSH2 domain, presumably due to its inherent flexibility.^{1,8} The structure of the nSH2 domain alone, and in complex with the His1047Arg mutant p110 α , is known.^{2,16} However, there may be unique features of the nSH2 domain interactions with wild-type p110 α that are yet to be explored. The activation loop (p110 α residues 935-958) has only been shown in one structure, where the conformation has been modified to accommodate the binding of the inhibitor PIK-108 in a non-catalytic site (PDB ID: 4A55).⁸

The Protein Data Bank (PDB) contains over 80 crystal structures of the four Class I PI3K isoforms, however, the lipid-binding site is yet to be explicitly identified. A survey of available PIP₂ containing structures in the PDB reveals binding is predominantly mediated by positively charged lysine and arginine residues.³¹⁻³⁶ Modeling studies of p110 γ have placed the phospholipid headgroup between the positively charged residues of the P-loop (p110 α residues 772-778) and the activation loop (p110 α residues 935-958), with the 3'-hydroxyl group positioned near the γ -phosphate of ATP.¹¹ In line with this, biochemical data points to an important role for the positively charged residues of the activation loop in determining substrate specificity and lipid kinase activity.¹⁰ Replacement of the activation loop in PI3K α with that of Class II or III PI3K, which do not phosphorylate PIP₂, renders PI3K α inactive towards PIP₂. Despite the lack of lipid kinase activity, however, lipid binding appeared to be unaffected, as pre-incubation of these hybrids with PIP₂ prevented binding of the covalent inhibitor, wortmannin.¹⁰ Further computational studies have also postulated a role for Lys776 on the P-loop in substrate specificity, as Class II and III PI3Ks do not have analogous positively charged residues in this region.¹⁰

Herein we report two structures of p110 α /nSH2. The first has interpretable electron density for the nSH2 domain, refined to 2.96 Å (R/R_{free} 0.19/0.27, Table 2.1). The second is a structure in complex with the truncated soluble substrate, di-C₄-phosphatidylinositol 4,5-bisphosphate (diC₄-PIP₂), refined to 3.37 Å (R/R_{free} 0.24/0.34, Table 2.1). The structures show no significant differences when aligned with previously published wild-type structures (Table 2.2).^{1,8}

Table 2.1: Data collection and refinement statistics

	p110 α /niSH2	p110 α /niSH2 with diC4-PIP ₂
Data collection		
Space group	p2 ₁ 2 ₁ 2 ₁	p2 ₁ 2 ₁ 2 ₁
Cell dimensions		
<i>a</i> , <i>b</i> , <i>c</i> (Å)	114.7, 116.2, 149.1	114.3, 116.1, 148.7
Resolution (Å)	50.00-2.96(3.01-2.96)	50.00-3.36(3.42-3.36)
<i>R</i> _{sym}	0.068 (0.69)	0.103 (0.71)
<i>I</i> / σI	36.9 (3.2)	35.7 (4.4)
Completeness (%)	99.6 (100)	99.9 (100)
Redundancy	7.2 (7.1)	9.0 (9.2)
Unique reflections	41,914	28,636
Total reflections	300,309	256,465
X-ray Source	1.1000 Å	1.1000 Å
wavelength		
Refinement		
Resolution (Å)	37.79-2.96	37.45-3.37
No. reflections	39,719	27,082
<i>R</i> _{work} / <i>R</i> _{free}	0.191/0.271	0.238/0.341
No. atoms		
Protein	10,830	10,584
Ligand	-	83
Water	18	5
<i>B</i> -factors		
Protein	53.82	65.81
Ligand	-	90.00
Water	21.22	78.00
R.m.s. deviations		
Bond lengths (Å)	0.011	0.013
Bond angles (°)	1.689	1.794

Table 2.2: RMSD of apo p110 α /niSH2 compared with available p110 α /niSH2 crystal structures, aligned by p110 α C α atoms

PI3K α structure	RMSD (Å)
p110 α /niSH2 p85 α (PDB ID: 2RD0)	1.46
p110 α /niSH2 p85 α (PDB ID: 4A55)	1.57
H1047R p110 α /niSH2 p85 α (PDB ID: 3HHM)	1.94

Structural alignment with the oncogenic mutant p110 α -His1047Arg structure (PDB ID: 3HHM) reveals some interesting differences. Some differences observed are consistent with those reported in Mandelker *et al.* and will not be further discussed here.² The major differences observed are in the nSH2 and iSH2 domains of p85 α and their interactions with p110. The new variations observed provide some key insights into distinctions in the regulation of the two enzymes (Figure 2.1A).²

The first significant difference is found in the iSH2 helices, which play an important role in modulating binding with the cell membrane (Figure 2.1B, S1). The N-terminal helix of the iSH2 domain (p85 α residues 443-475) bends towards the proposed membrane to a lesser degree in the wild-type structure. There is a shift in the position of C α atoms of up to 5.5 Å (measured at p85 α 450). The change is less pronounced in the second helix, with an average movement of 2.5 Å (measured at p85 α residues 565-579, maximum distance is 3.9 Å at p85 α 577, Figure 2.1B). This conformational change in the iSH2 domain may reflect the increased membrane binding of the oncogenic mutant.^{2,8} Mandelker *et al.*² identified a key C-terminal loop which was ordered in the mutant structure, and proposed this as a key structural change responsible for increased membrane binding. In addition to this, we have identified a shift in the iSH2 helices that position the mutant to maximize interactions with the cell membrane.⁸

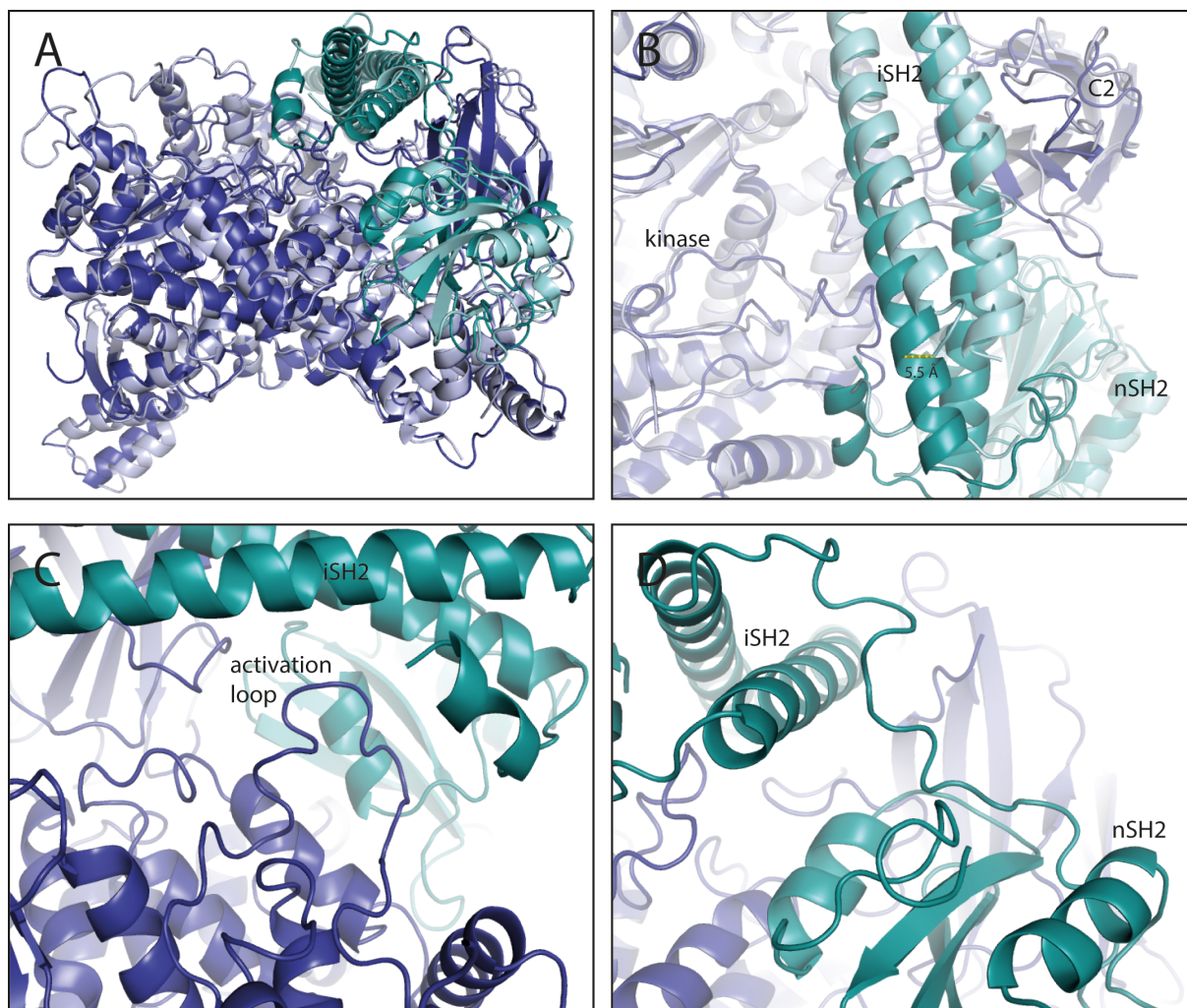


Figure 2.1: Structural alignment of the wild-type crystal structure with the His1047Arg oncogenic mutant (PDB ID: 3HHM), aligned via p110. Wild type is shown in dark blue (p110) and teal (p85); mutant structure is shown in light blue (p110) and cyan (p85). a) the whole protein; b) the iSH2 domain. The largest movement is highlighted with a yellow dotted line, measured between the C α atoms of p85 α 450 of each structure; c) The terminal residues of iSH2 (p85 α residues 587-598) form a short helix in close proximity to the activation loop d) the connection between the iSH2 domain and nSH2.

A clearly defined third helix is present (p85 α residues 587-598) at the C-terminal end of the iSH2 domain, sitting adjacent to the activation loop (Figure 2.1C). This helix may aid in the regulation of kinase activity by keeping the activation loop in an inactive conformation. Deletions (Δ 583-602) or truncations (p85-572^{STOP}) of this section of the iSH2 domain are oncogenic.³⁷ The oncogenic iSH2 deletions and truncations could activate the enzyme via loss of these inhibitory contacts with the activation loop. Previous studies have shown that these iSH2

mutations act via a similar mechanism to site-directed mutants where the iSH2-C2 interface has been disrupted.³⁷ As the activation loop is positioned near this iSH2-C2 interface, disruptions in this interface may also affect the conformation of the activation loop. This structure provides insight into a potential mechanism of activation for these iSH2 oncogenic mutations.

Unlike most of the previous p110 α structures, there is density for the activation loop (p110 α residues 935-958, Figure 2.3A). The activation loop is nestled near the iSH2 and nSH2 domains of p85. The conformation of the loop is different from that observed in the structure reported by Hon *et al* (PDB ID: 4A55).⁸ In that structure, the conformation of the loop is influenced by the binding of a PIK-108 molecule in a non-catalytic binding site.⁸ The activation loop is positioned to allow communication between p85 and the kinase domain of p110. The interactions with nSH2 and iSH2 may alter the conformation of the activation loop, leading to increased or decreased kinase activity.

The structure of the connection between the nSH2 and iSH2 domains (p85 α residues 426-443, Figure 2.1D) has not previously been shown. It is revealed in this crystal structure as a long, unstructured region. The nSH2 domain, vital for the regulation of kinase activity, is believed to disengage from p110 α upon binding of phosphorylated tyrosine motifs on activated receptor tyrosine kinases. This long unstructured connection supports this hypothesis that the domain is flexible and able to disengage from p110 α .

Furthermore, significant differences are observed in the interaction of the nSH2 domain with p110. In the oncogenic mutant crystal structure, the nSH2 domain was shown to interact with the C2, helical and kinase domains of p110 α , communicating regulatory state via conformational changes in these adjacent domains.^{2,38} The structure of the nSH2 domain in the wild-type and His1047Arg mutant structures have a similar overall secondary structure.² The position of the domain with respect to p110, however, is altered (Figure 2.2A). In the wild-type structure, the

nSH2 domain is rotated relative to that in the His1047Arg mutant. The nSH2 rotates 14° towards the kinase and C2 domains (around an axis that passes through (113.8, 154.2, 80.8)). This results in an increased buried surface area between the nSH2 domain and p110α in the wild-type protein, 1083 Å², compared with 820 Å² for the gain of function His1047Arg mutant (calculated with PISA, considering only the residues present in both structures).^{39,40} This suggests the regulatory control of the nSH2 domain in the oncogenic mutant may be only partially maintained with respect to the wild-type. Each of the interacting p110 domains shows differences in the interactions with the nSH2 domain between the two structures, with the wild-type structure showing extra interactions agreeing with a tighter contact and inhibition of activity. In the helical domain, an extra charge-assisted hydrogen bond is present between p110α Lys573 and p85α Asn417 in the wild-type structure (Figure 2.2B). In the His1047Arg mutant, p85α Asn417 instead interacts with the backbone of p110α Gly512. A greater difference is observed at the interface between the C2 domain and nSH2, where a number of unique hydrogen bonds are made in each structure (Figure 2.2C). The wild-type nSH2 domain makes three unique hydrogen bonds with the C2 domain, while the oncogenic mutant has five unique hydrogen bonds between these domains, reflecting the shift in nSH2 conformation. Perhaps most strikingly, there are two salt bridges between the kinase domain (Arg1023 and Asp1029) and nSH2 (Glu341 and Arg340, respectively) that are uniquely observed in the wild-type (Figure 2.2D). This salt-bridge may contribute to the inhibition of p110 and therefore the reduced kinase activity observed in the wild-type p110α. Taken together, these results suggest that in addition to altered membrane binding, the His1047Arg oncogenic mutant is only under partial nSH2 inhibitory control. This is in agreement with biochemical data that show increased basal lipid kinase activity in the oncogenic mutant.

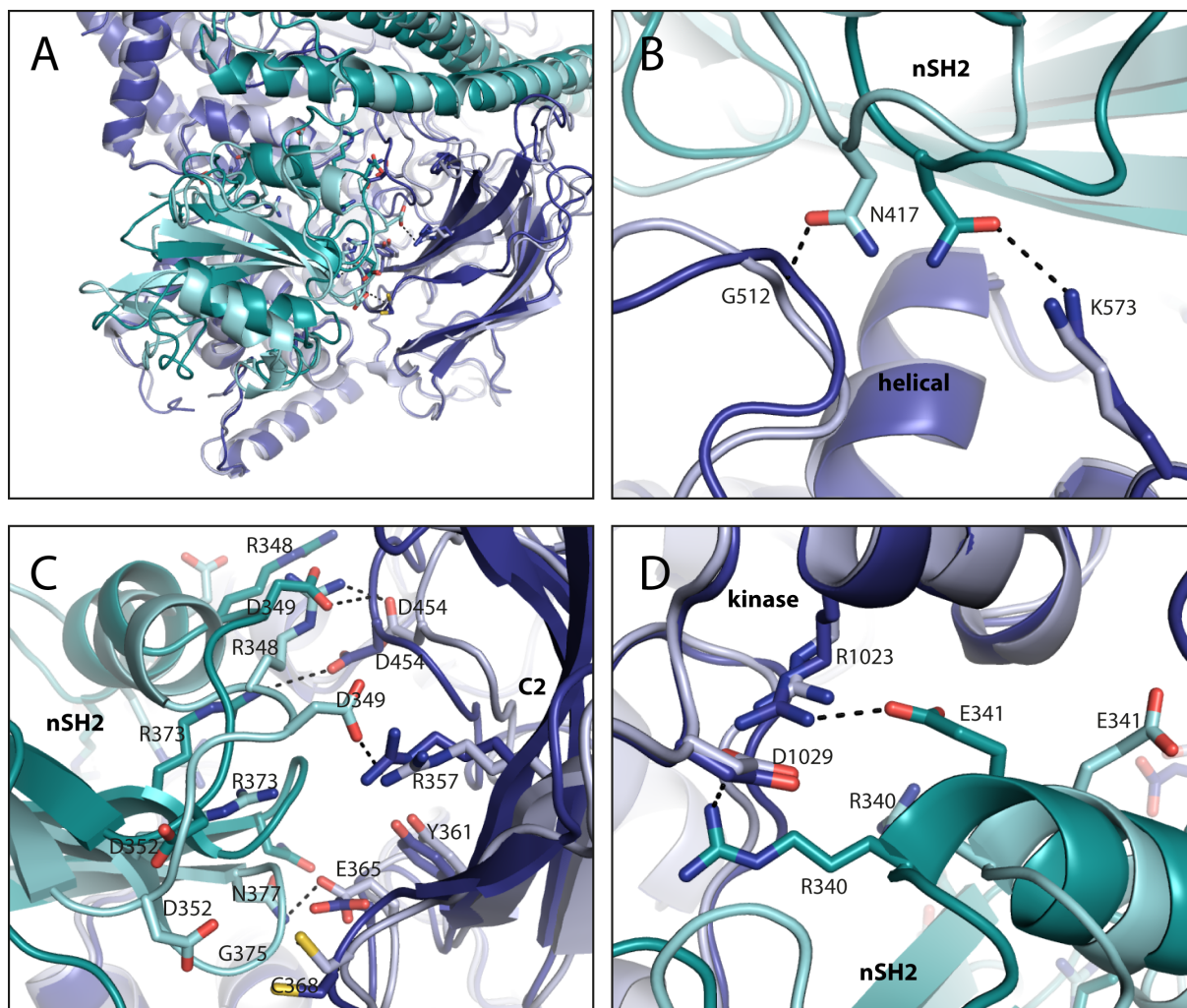


Figure 2.2: Structural overlay of nSH2 domain and differences in p110 interactions. Wild type is shown in dark blue (p110) and teal (p85); mutant structure (PDB ID: 3HHM) is shown in light blue (p110) and cyan (p85). a) the nSH2 domain; b) differences in interactions between the helical and nSH2 domains; c) differences in interactions between the C2 and nSH2 domains; d) two key salt-bridges between the kinase domain and nSH2 are present in the wild-type but absent in the oncogenic mutant structure.

The complex structure of PI3K α bound to PIP₂ was determined to 3.3 Å. There are two bound molecules of PIP₂ present in the structure (Figure 2.3B). The first sits adjacent to the ATP binding site, and we will refer to it as catalytic PIP₂. The catalytic PIP₂ binds in a groove delimited by two loops (p110 α residues 721-731 and 772-778) of the kinase domain, the iSH2 helix (p85 α residues 457-465) and the activation loop (p110 α residues 935-958) (Figure 2.3C). This is in line with biochemical data implicating the activation loop and Lys776 in lipid binding.¹⁰ The ester linkage on one of the tails forms a hydrogen bond to Lys941 of the

activation loop. Both of the truncated hydrophobic tails are positioned such that it would allow for the membrane binding of full-length PIP₂. The 3'-hydroxyl group is positioned within 4 Å of the ATP γ -phosphate when the structure is aligned with the p110 γ /ATP co-crystal structure (PDB ID: 1E8X, Figure ZB).⁹ This would allow for phosphate transfer ATP to PIP₂, using the catalytic Lys802 and the conserved Asp933 as the base.^{41,42}

The second PIP₂ molecule binds in a groove between the ABD, kinase and iSH2 domains (Figure 2.3D). One of the 4-phosphate oxygens is within hydrogen bonding distance of the backbone of Gly12. Glu722 forms a hydrogen bond with 2'-hydroxyl. As for the first PIP₂ molecule, the truncated C4-hydrophobic tails are positioned for membrane binding. A comparison of the free and bound structures of PI3K α reveals that the binding of PIP₂ at this position is accompanied by very little conformational rearrangement of the protein structure.

To determine if PI3K α could bind to multiple PIP₂ molecules within the lipid bilayer of a phospholipid membrane, we tested its ability to bind and cluster BODIPY-FL-PIP₂ embedded within vesicles. Gambhir *et al.* report that at a concentration of 0.1% PIP₂ in vesicles, the distance between PIP₂ molecules is ~ 300 Å.⁴³ Self-quenching of the BODIPY fluorescence occurs when PIP₂ molecules are brought within 50-60 Å.⁴⁴ Therefore if PI3K binds to and clusters two or more molecules of BODIPY-FL-PIP₂, fluorescence quenching should be observed. A similar approach has been used to demonstrate clustering of BODIPY-FL-PIP₂ by MARCKS, NAP-22 and myelin basic protein (MBP) and clustering of BODIPY-TMR-PIP₂ by dynamin.^{43,45-47}

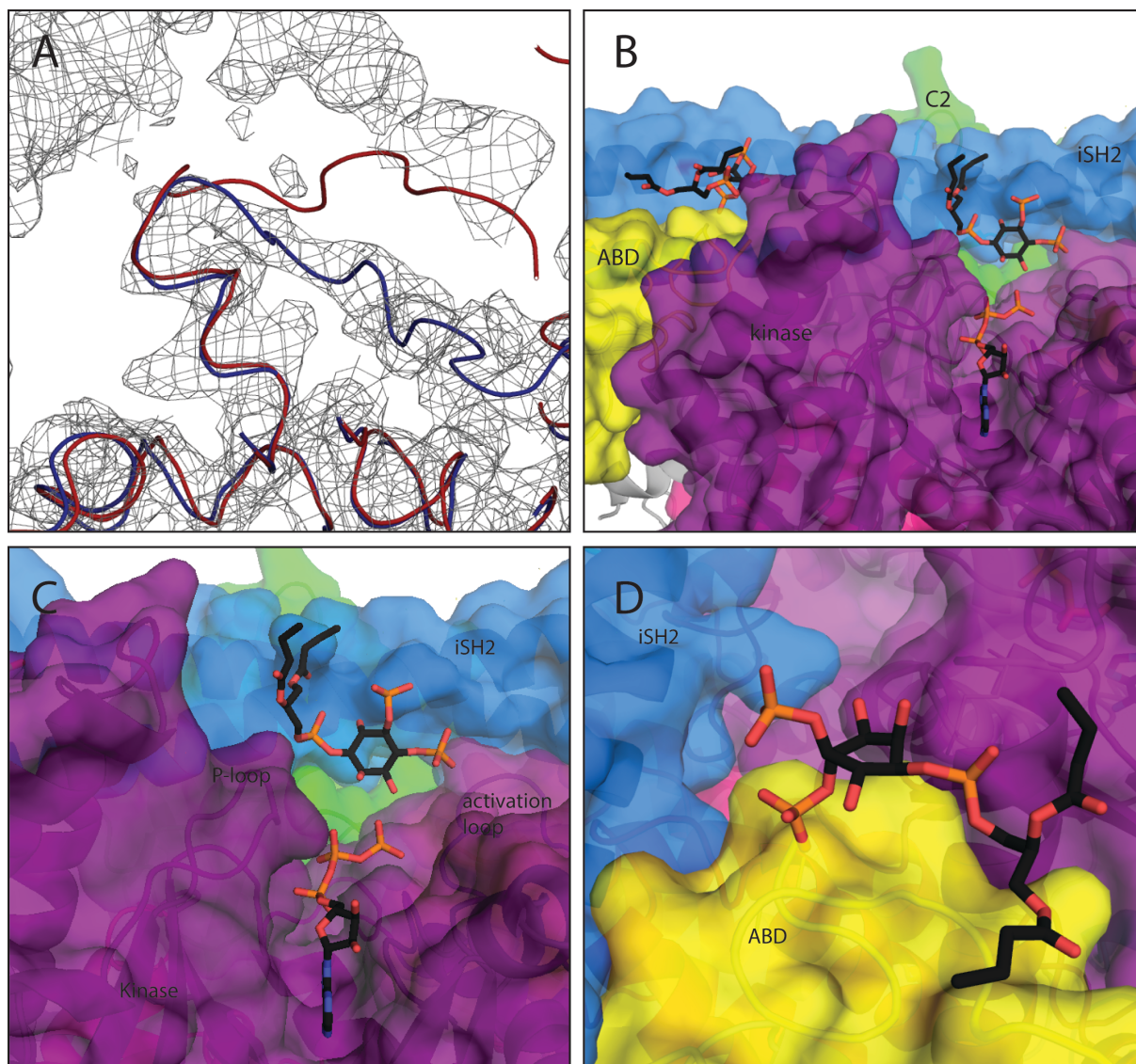


Figure 2.3: a) The electron density for the activation loop. The new structure is shown in dark blue. The activation loop from 4A55 is shown in red, highlighting the shifted conformation of the activation loop due to the binding of a PIK-108 molecule; b) Two PIP₂ molecules bound to p110 α /iSH2; ATP molecule from p110 γ (PDB ID: 1E8X) is overlaid to show the proximity of the catalytic PIP₂; c) the catalytic PIP₂ binds in a groove between the P-loop, activation loop and iSH2 domain; d) a second molecule of PIP₂ bound at the interface between the ABD and kinase domains.

We measured PIP₂ fluorescence quenching using unilamellar vesicles with a diameter of 100 nm generated by extrusion of lipids through a polycarbonate membrane. Vesicles were made using a membrane composition optimal for PI3K binding (PC/PE/PS/BODIPY-FL-PIP₂/cholesterol with a molar ratio of 54.9/25/5/0.1/15). The addition of wild-type full length PI3K (p110 α /p85 α) to vesicles with BODIPY-FL-PIP₂ resulted in the quenching of the

fluorescent signal in a dose dependent manner suggesting PI3K α can bind to and cluster two or more molecules of PIP₂ (Figure 2.4A). Titration of vesicles with p110 α /niSH2, which has deletions of the RhoGap, SH3 and cSH2 domains of p85 α , also demonstrated fluorescence quenching to the same level as p110 α /p85 α (Figure 2.4B). Additionally, p85 α alone could cause a very small amount of quenching of the signal compared to p110 α /niSH2 (Figure 2.4C). Taken together, this suggests that there are binding sites for PIP₂ on p110 α or at the interface of the p110 α and p85 α subunits, but not just at p85 α .

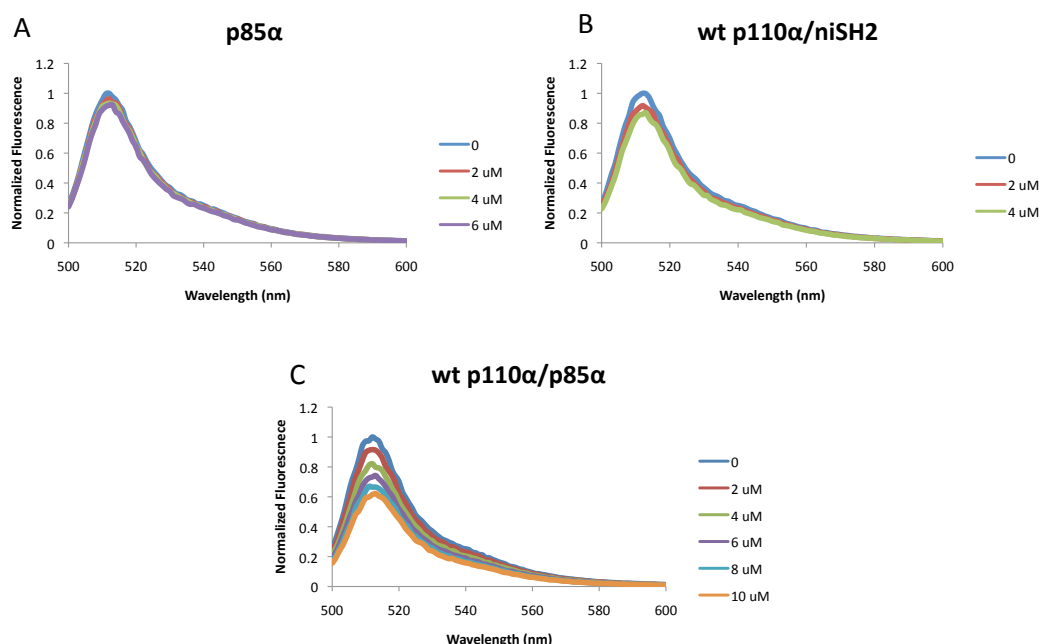


Figure 2.4: Fluorescence quenching experiments. A) p85 α shows negligible quenching of BODIPY-FL-PIP₂ fluorescence; B) and C) wild-type full length p110 α /p85 α and p110 α /niSH2 show similar levels of fluorescence quenching.

We also examined any effects that two mutations at the membrane binding surface of PI3K may have on its ability to sequester PIP₂. Glu545Lys-p110 α /niSH2 demonstrated similar quenching characteristics to wild-type p110 α /niSH2, suggesting that this mutation does not affect membrane or PIP₂ binding, as previously shown.^{8,27} His1047Arg-p110 α /niSH2, however, demonstrated greatly increased potency compared to wild-type p110 α /niSH2 (Figure 2.5).

Given that this mutant is about 10-fold more potent compared to wild-type it seems likely the effect is due to increased membrane binding affinity. However, we cannot rule out that this mutation results in the creation of an additional binding site for a molecule of PIP₂.

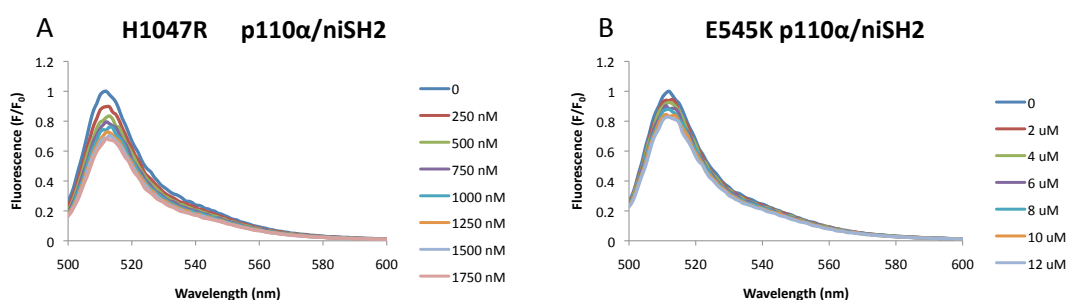


Figure 2.5: Oncogenic mutant fluorescence quenching experiments. A) The kinase domain mutant His1047Arg-p110 α /niSH2 shows 10-fold greater levels of fluorescence quenching compared to wild-type; B) the quenching observed for the helical domain mutant, Glu545Lys p110 α /niSH2 shows similar levels of quenching to wild-type.

In conclusion, we have presented the first X-ray crystal structure of the nSH2 domain in complex with wild-type p110 α , which reveals key differences in the interaction between the nSH2 and wild-type PI3K α compared with the His1047Arg oncogenic mutant, suggesting a tighter regulatory control in the wild-type protein. We have also presented the first X-ray crystal structure of PI3K α in complex with a lipid substrate, identifying multiple lipid binding sites and confirming biochemical data that implicate a role for the activation loop and P-loop residues in lipid-binding.

2.3.3 Supplementary figures

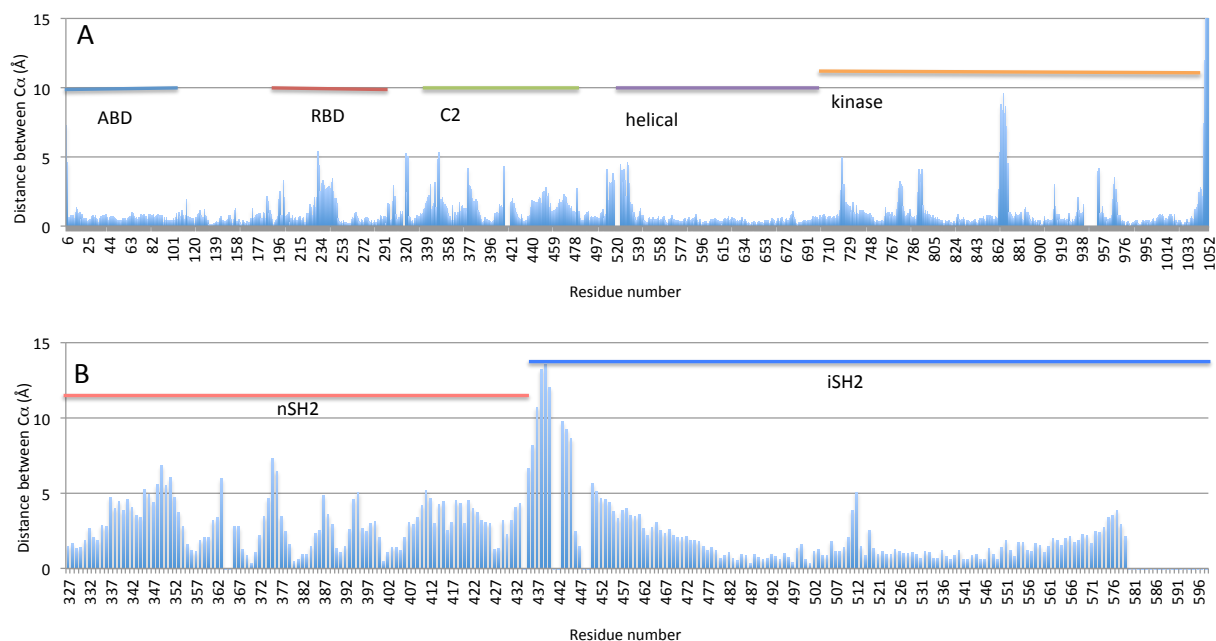


Figure S1: Distance plots of the distance between C α atoms of wild-type apo p110 α /niSH2 and p110 α -His1047Arg/niSH2 (PDB ID: 3HHM) aligned by C α atoms of p110 α . Approximate positions of domains are shown. A) p110 α ; B) p85 α

2.4 Post-Script: Ongoing work and conclusions

In the preceding manuscript, two new p110 α /niSH2 structures were described. These yielded vital insights into the regulation of PI3K α , and particularly suggest an additional structural basis for the increased activity of the oncogenic mutant, His1047Arg. Two lipid-binding sites have also been described, a first for any of the PI3K isoforms.

A streamlined approach to inhibitor-bound crystal structures of each of the isoforms would greatly aid the rational design of isoform selective inhibitors. Currently, as discussed in Chapter 1, PI3K γ is the mainstay of PI3K crystallography and structural studies of inhibitor binding. PI3K α has proven significantly more difficult to crystallise. The p110 α /niSH2 construct generally yields crystals of low resolution and with the ATP-binding site occluded by a symmetry-related molecule.¹ Co-crystallisation with inhibitors is theoretically possible, as the presence of the inhibitor can exert a positive influence on crystal formation. An example of this is the structure published by Hon *et al.*⁸ Co-crystallisation with the PI3K β and δ dual-selective inhibitor, PIK-108, yielded diffracting crystals, albeit of fairly low resolution (3.5 Å). There has been one further PI3K α structure published with a covalent inhibitor, but details of crystallisation are missing from the report.³⁰ We sought to co-crystallise two inhibitors (compounds **39b** and **42b**, which will be introduced in Chapter 3) with PI3K α . Trials were performed in parallel with apo-crystallisation experiments, but no crystals were observed.

Using molecularly imprinted polymers (MIPs) as a novel aid in protein crystallisation was proposed in 2011.⁴⁸ This involved forming the polymer, polyacrylamide, in the presence of protein. This leaves a polymer imprinted with the shape of the protein in question. The polymer was then passed through a sieve to create smaller particles suitable for addition to crystallisation drops to act like a nucleant. Saridakis *et al.* describe that the incorporation of

MIPs yielded crystals at metastable conditions for seven proteins. In screening experiments, a hit rate of 8-10% was observed in the presence of MIPs.⁴⁸

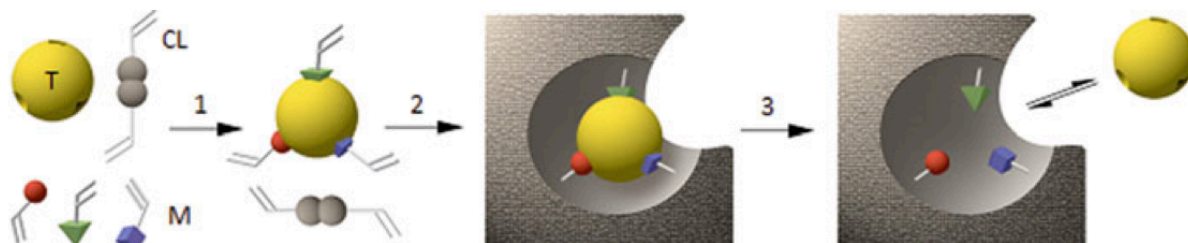


Figure 2.6: The process for making molecularly imprinted polymers. The template protein (represented by the yellow sphere) is mixed with acrylamide and bisacrylamide and polymerisation initiated by addition of N,N,N',N'-tetramethylethylenediamine and ammonium persulfate. The template protein can then be removed by washing with acetic acid and water, leaving the polymer imprinted with the shape of the protein. Image used with kind permission from Springer Science and Business Media.⁴⁶

This promising report led us to investigate the use of MIPs in the crystallisation of PI3K α . MIPs were prepared using methods adapted from those described in the published paper.⁴⁸ The MIPs were made in the presence of wild-type p110 α /niSH2, and the protein removed by washing with acetic acid and water. The polymer was then crushed through a sieve and the polymer added to drops of protein and set up in hanging drop crystallisation trays using the published crystallisation conditions for p110 α /niSH2 (Figure 2.7). No crystals were observed. However, some micro-crystals appeared to form like hairs on the polymer, suggesting that further optimisation of conditions may yield crystals of suitable size either for seeding or X-ray diffraction directly. Optimisation of these conditions is ongoing. Additionally, MIPs were made in the presence of wild-type full length p110 α /p85 α and crystallisation trials set up in an attempt to identify appropriate conditions. Unfortunately, no crystals were observed.

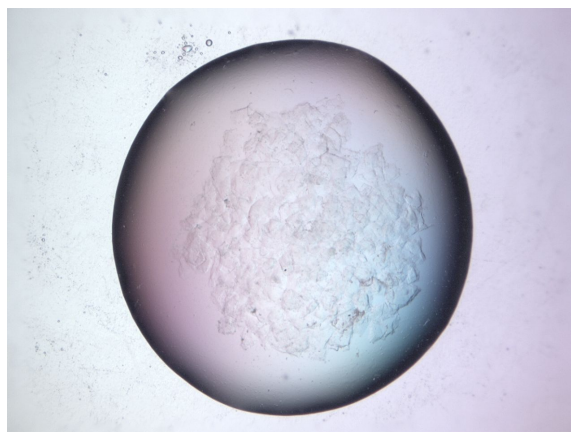


Figure 2.7: Crystallisation drop set with MIPs and p110 α /niSH2.

The work in this chapter has highlighted some key differences in the regulation of wild-type PI3K α when compared with that of the oncogenic mutant, His1047Arg. These differences could potentially be exploited in the design of novel non ATP-competitive oncogenic mutant specific inhibitors. Alternatively, the identification of two lipid-binding sites in PI3K α could inform the design of lipid-competitive inhibitors, providing a novel mechanism for achieving selectivity over related protein kinases.

2.5 References

- (1) Huang, C. H.; Mandelker, D.; Schmidt-Kittler, O.; Samuels, Y.; Velculescu, V. E.; Kinzler, K. W.; Vogelstein, B.; Gabelli, S. B.; Amzel, L. M. The structure of a human p110 α /p85 α complex elucidates the effects of oncogenic PI3K α mutations. *Science* **2007**, *318*, 1744–1748.
- (2) Mandelker, D.; Gabelli, S. B.; Schmidt-Kittler, O.; Zhu, J.; Cheong, I.; Huang, C. H.; Kinzler, K. W.; Vogelstein, B.; Amzel, L. M. A frequent kinase domain mutation that changes the interaction between PI3K α and the membrane. *Proc. Natl. Acad. Sci. U.S.A.* **2009**, *106*, 16996–17001.
- (3) Yu, J.; Wjasow, C.; Backer, J. M. Regulation of the P85/P110 α Phosphatidylinositol 3'-Kinase: Distinct roles for the N-terminal and C-terminal SH2 domains. *J. Biol. Chem.* **1998**, *273*, 30199–30203.
- (4) Carpenter, C. L.; Auger, K. R.; Chanudhuri, M.; Yoakim, M.; Schaffhausen, B.; Shoelson, S.; Cantley, L. C. Phosphoinositide 3-kinase is activated by phosphopeptides that bind to the SH2 domains of the 85-kDa subunit. *J. Biol. Chem.* **1993**, *268*, 9478–9483.
- (5) Rordorf-Nikolic, T.; Horn, D. J. V.; Chen, D.; White, M. F.; Backer, J. M. Regulation of Phosphatidylinositol 3'-Kinase by Tyrosyl Phosphoproteins: Full activation requires occupancy of both SH2 domains in the 85-kDa regulatory subunit. *J. Biol. Chem.* **1995**, *270*, 3662–3666.
- (6) Zhang, X.; Vadas, O.; Perisic, O.; Anderson, K. E.; Clark, J.; Hawkins, P. T.; Stephens, L. R.; Williams, R. L. Structure of Lipid Kinase p110 β /p85 β Elucidates an Unusual SH2-Domain-Mediated Inhibitory Mechanism. *Mol. Cell* **2011**, *41*, 567–578.
- (7) Burke, J. E.; Vadas, O.; Berndt, A.; Finegan, T.; Perisic, O.; Williams, R. L. Dynamics of the Phosphoinositide 3-Kinase p110 δ Interaction with p85 α and Membranes Reveals Aspects of Regulation Distinct from p110 α . *Structure* **2011**, *19*, 1127–1137.
- (8) Hon, W.-C.; Berndt, A.; Williams, R. L. Regulation of lipid binding underlies the activation mechanism of class IA PI3-kinases. *Oncogene* **2012**, *31*, 3655–3666.
- (9) Walker, E.; Pacold, M. E.; Perisic, O.; Stephens, L.; Hawkins, P. T.; Wymann, M. P.; Williams, R. L. Structural determinants of phosphoinositide 3-kinase inhibition by wortmannin, LY294002, Quercetin, Myricetin, and Staurosporine. *Mol. Cell* **2000**, *6*, 909–919.
- (10) Pirola, L.; Zvelebil, M. J.; Bulgarelli-Leva, G.; Van Obberghen, E.; Waterfield, M. D.; Wymann, M. P. Activation Loop Sequences Confer Substrate Specificity to Phosphoinositide 3-Kinase α (PI3K α): Functions of lipid kinase-deficient PI3K α in signaling. *J. Biol. Chem.* **2001**, *276*, 21544–21554.
- (11) Walker, E. H.; Perisic, O.; Ried, C.; Stephens, L.; Williams, R. L. Structural insights into phosphoinositide 3-kinase catalysis and signalling. *Nature* **1999**, *402*, 313–320.
- (12) Otwinowski, Z.; Minor, W. Processing of X-ray diffraction data collected in oscillation mode. *Methods Enzymol.* **1997**, *276*, 307–326.

-
- (13) Steinfink, H.; Peterca, M. Symmetry in Crystallography. *Characterization of Materials* **2012**, 1–14.
- (14) Vagin, A. A.; Steiner, R. A.; Lebedev, A. A.; Potterton, L.; McNicholas, S.; Long, F.; Murshudov, G. N. REFMAC5 dictionary: organization of prior chemical knowledge and guidelines for its use. *Acta Crystallogr. D Biol. Crystallogr.* **2004**, *60*, 2184–2195.
- (15) Emsley, P.; Cowtan, K. Coot: model-building tools for molecular graphics. *Acta Crystallogr. D Biol. Crystallogr.* **2004**, *60*, 2126–2132.
- (16) Nolte, R. T.; Eck, M. J.; Schlessinger, J.; Shoelson, S. E.; Harrison, S. C. Crystal structure of the PI 3-kinase p85 amino-terminal SH2 domain and its phosphopeptide complexes. *Nat. Struct. Biol.* **1996**, *3*, 364–374.
- (17) Fyffe, C.; Buus, R.; Falasca, M. Genetic and Epigenetic Regulation of Phosphoinositide 3-kinase Isoforms. *Curr. Pharm. Des.* **2013**, *19*, 680–686.
- (18) Markman, B.; J. Tao, J.; Scaltriti, M. PI3K Pathway Inhibitors: Better Not Left Alone. *Curr. Pharm. Des.* **2013**, *19*, 895–906.
- (19) W. Grunt, T.; L. Mariani, G. Novel Approaches for Molecular Targeted Therapy of Breast Cancer: Interfering with PI3K/AKT/mTOR Signaling. *Curr. Cancer Drug Targ.* **2013**, *13*, 188–204.
- (20) Rodon, J.; Dienstmann, R.; Serra, V.; Tabernero, J. Development of PI3K inhibitors: lessons learned from early clinical trials. *Nat. Rev. Clin. Oncol.* **2013**, *10*, 143–153.
- (21) Broderick, D. K.; Di, C.; Parrett, T. J.; Samuels, Y. R.; Cummins, J. M.; McLendon, R. E.; Fults, D. W.; Velculescu, V. E.; Bigner, D. D.; Yan, H. Mutations of PIK3CA in Anaplastic Oligodendrogliomas, High-Grade Astrocytomas, and Medulloblastomas. *Cancer Res.* **2004**, *64*, 5048–5050.
- (22) Campbell, I. G.; Russell, S. E.; Choong, D. Y. H.; Montgomery, K. G.; Ciavarella, M. L.; Hooi, C. S. F.; Cristiano, B. E.; Pearson, R. B.; Phillips, W. A. Mutation of the PIK3CA gene in ovarian and breast cancer. *Cancer Res.* **2004**, *64*, 7678–7681.
- (23) Levine, D. A.; Bogomolny, F.; Yee, C. J.; Lash, A.; Barakat, R. R.; Borgen, P. I.; Boyd, J. Frequent mutation of the PIK3CA gene in ovarian and breast cancers. *Clin. Cancer Res.* **2005**, *11*, 2875–2878.
- (24) Bachman, K. E.; Argani, P.; Samuels, Y.; Silliman, N.; Ptak, J.; Szabo, S.; Konishi, H.; Karakas, B.; Blair, B. G.; Lin, C.; Peters, B. A.; Velculescu, V. E.; Park, B. H. The PIK3CA gene is mutated with high frequency in human breast cancers. *Cancer Biol. Ther.* **2004**, *3*, 772–775.
- (25) Pedrero, J. M. G.; Carracedo, D. G.; Pinto, C. M.; Zapatero, A. H.; Rodrigo, J. P.; Nieto, C. S.; Gonzalez, M. V. Frequent genetic and biochemical alterations of the PI 3-K/AKT/PTEN pathway in head and neck squamous cell carcinoma. *Int. J. Cancer* **2005**, *114*, 242–248.
- (26) Samuels, Y.; Waldman, T. Oncogenic Mutations of PIK3CA in Human Cancers. *Curr. Top. Microbiol. Immunol.* **2011**, *347*, 21–41.

-
- (27) Burke, J. E.; Perisic, O.; Masson, G. R.; Vadas, O.; Williams, R. L. Oncogenic mutations mimic and enhance dynamic events in the natural activation of phosphoinositide 3-kinase p110 α (PIK3CA). *Proc. Natl. Acad. Sci. U.S.A.* **2012**, *109*, 15259–15264.
- (28) Carson, J. D.; Van Aller, G.; Lehr, R.; Sinnamon, R. H.; Kirkpatrick, R. B.; Auger, K. R.; Dhanak, D.; Copeland, R. A.; Gontarek, R. R.; Tummino, P. J.; Luo, L. Effects of oncogenic p110 α subunit mutations on the lipid kinase activity of phosphoinositide 3-kinase. *Biochem. J.* **2008**, *409*, 519–524.
- (29) Geering, B.; Cutillas, P. R.; Nock, G.; Gharbi, S. I.; Vanhaesebroeck, B. Class IA phosphoinositide 3-kinases are obligate p85-p110 heterodimers. *Proc. Natl. Acad. Sci. U.S.A.* **2007**, *104*, 7809–7814.
- (30) Nacht, M.; Qiao, L.; Sheets, M. P.; St. Martin, T.; Labenski, M.; Mazdiyasni, H.; Karp, R.; Zhu, Z.; Chaturvedi, P.; Bhavsar, D.; Niu, D.; Westlin, W.; Petter, R. C.; Medikonda, A. P.; Singh, J. Discovery of a Potent and Isoform-Selective Targeted Covalent Inhibitor of the Lipid Kinase PI3K α . *J. Med. Chem.* **2013**, *56*, 712–721.
- (31) Guerrero-Valero, M.; Ferrer-Orta, C.; Querol-Audi, J.; Marin-Vicente, C.; Fita, I.; Gomez-Fernandez, J. C.; Verdaguer, N.; Corbalan-Garcia, S. Structural and mechanistic insights into the association of PKC -C2 domain to PtdIns(4,5)P₂. *Proc. Natl. Acad. Sci. U.S.A.* **2009**, *106*, 6603–6607.
- (32) Ford, M. G. J.; Pearce, B. M. F.; Higgins, M. K.; Vallis, Y.; Owen, D. J.; Gibson, A.; Hopkins, C. R.; Evans, P. R.; McMahon, H. T. Simultaneous Binding of PtdIns(4,5)P₂ and Clathrin by AP180 in the Nucleation of Clathrin Lattices on Membranes. *Science* **2001**, *291*, 1051–1055.
- (33) Saad, J. S.; Miller, J.; Tai, J.; Kim, A.; Ghanam, R. H.; Summers, M. F. Structural basis for targeting HIV-1 Gag proteins to the plasma membrane for virus assembly. *Proc. Natl. Acad. Sci. U.S.A.* **2006**, *103*, 11364–11369.
- (34) Hansen, S. B.; Tao, X.; MacKinnon, R. Structural basis of PIP₂ activation of the classical inward rectifier K⁺ channel Kir2.2. *Nature* **2011**, *477*, 495–498.
- (35) Stolt, P. C.; Jeon, H.; Song, H. K.; Herz, J.; Eck, M. J.; Blacklow, S. C. Origins of peptide selectivity and phosphoinositide binding revealed by structures of disabled-1 PTB domain complexes. *Structure* **2003**, *11*, 569–579.
- (36) Rosenhouse-Dantsker, A.; Logothetis, D. E. Molecular characteristics of phosphoinositide binding. *Pflugers Arch - Eur J Physiol* **2007**, *455*, 45–53.
- (37) Wu, H.; Shekar, S. C.; Flinn, R. J.; El-Sibai, M.; Jaiswal, B. S.; Sen, K. I.; Janakiraman, V.; Seshagiri, S.; Gerfen, G. J.; Girvin, M. E.; Backer, J. M. Regulation of Class IA PI 3-kinases: C2 domain-iSH2 domain contacts inhibit p85/p110 α and are disrupted in oncogenic p85 mutants. *Proc. Natl. Acad. Sci. U.S.A.* **2009**, *106*, 20258–20263.
- (38) Miled, N.; Yan, Y.; Hon, W.-C.; Perisic, O.; Zvelebil, M. J.; Inbar, Y.; Schneidman-Duhovny, D.; Wolfson, H. J.; Backer, J. M.; Williams, R. L. Mechanism of two classes of cancer mutations in the phosphoinositide 3-kinase catalytic subunit. *Science* **2007**, *317*, 239–242.
- (39) http://www.ebi.ac.uk/pdbe/prot_int/pistart.html.

-
- (40) Krissinel, E.; Henrick, K. Inference of Macromolecular Assemblies from Crystalline State. *J. Mol. Biol.* **2007**, *372*, 774–797.
- (41) Okkenhaug, K.; Bilancio, A.; Farjot, G.; Priddle, H.; Sancho, S.; Peskett, E.; Pearce, W.; Meek, S. E.; Salpekar, A.; Waterfield, M. D.; Smith, A. J. H.; Vanhaesebroeck, B. Impaired B and T Cell Antigen Receptor Signaling in p110 δ PI 3-Kinase Mutant Mice. *Science* **2002**, *297*, 1031–1034.
- (42) Wymann, M. P.; Bulgarelli-Leva, G.; Zvelebil, M. J.; Pirola, L.; Vanhaesebroeck, B.; Waterfield, M. D.; Panayotou, G. Wortmannin inactivates phosphoinositide 3-kinase by covalent modification of Lys-802, a residue involved in the phosphate transfer reaction. *Mol. Cell. Biol.* **1996**, *16*, 1722–1733.
- (43) Gambhir, A.; Hangyás-Mihályné, G.; Zaitseva, I.; Cafiso, D. S.; Wang, J.; Murray, D.; Pentylä, S. N.; Smith, S. O.; McLaughlin, S. Electrostatic sequestration of PIP2 on phospholipid membranes by basic/aromatic regions of proteins. *Biophys. J.* **2004**, *86*, 2188–2207.
- (44) Karolin, J.; Johansson, L. B.-A.; Strandberg, L.; Ny, T. Fluorescence and Absorption Spectroscopic Properties of Dipyrrometheneboron Difluoride (BODIPY) Derivatives in Liquids, Lipid Membranes, and Proteins. *J. Am. Chem. Soc.* **1994**, *116*, 7801–7806.
- (45) Epand, R. M.; Vuong, P.; Yip, C. M.; Maekawa, S.; Epand, R. F. Cholesterol-dependent partitioning of PtdIns(4,5)P2 into membrane domains by the N-terminal fragment of NAP-22 (neuronal axonal myristoylated membrane protein of 22 kDa). *Biochem. J.* **2004**, *379*, 527–532.
- (46) Musse, A. A.; Gao, W.; Homchaudhuri, L.; Boggs, J. M.; Harauz, G. Myelin basic protein as a “PI(4,5)P2-modulin”: a new biological function for a major central nervous system protein. *Biochemistry* **2008**, *47*, 10372–10382.
- (47) Bethoney, K. A.; King, M. C.; Hinshaw, J. E.; Ostap, E. M.; Lemmon, M. A. A possible effector role for the pleckstrin homology (PH) domain of dynamin. *Proc. Natl. Acad. Sci. U.S.A.* **2009**, *106*, 13359–13364.
- (48) Saridakis, E.; Khurshid, S.; Govada, L.; Phan, Q.; Hawkins, D.; Crichlow, G. V.; Lolis, E.; Reddy, S. M.; Chayen, N. E. Protein Crystallization Facilitated by Molecularly Imprinted Polymers. *Proc. Natl. Acad. Sci. U.S.A.* **2011**, *108*, 11081–11086.
- (49) Haupt, K.; Linares, A. V.; Bompert, M.; Bui, B. T. S. Molecularly imprinted polymers. *Top. Curr. Chem.* **2012**, *325*, 1–28.

PART B: Declaration for Chapter 3

Monash University

Declaration for Thesis Chapter 3

Declaration by candidate

In the case of Chapter 3, the nature and extent of my contribution to the work was the following:

Nature of contribution	Extent of contribution (%)
Design of experiments, synthesis of all compounds except 4a and 4b , assays of all compounds except for 4a , docking, co-authorship of manuscript	80%

The following co-authors contributed to the work. If co-authors are students at Monash University, the extent of their contribution in percentage terms must be stated:

Name	Nature of contribution	Extent of contribution (%)*
Zhaohua Zheng	Protein expression and purification, assay for 4a	
Jo-Anne Pinson	Synthesis of compounds 4a and 4b .	5%
Ian Jennings	Co-authorship of manuscript	
Philip Thompson	Co-authorship of manuscript	

** Shown for Monash University students only*

The undersigned hereby certify that the above declaration correctly reflects the nature and extent of the candidate's and co-authors' contributions to this work.

Candidate's Signature		Date
Main Supervisor's Signature		Date

Declaration by co-authors

The undersigned hereby certify that:

- (1) the above declaration correctly reflects the nature and extent of the candidate's contribution to this work, and the nature of the contribution of each of the co-authors;
- (2) they meet the criteria for authorship in that they have participated in the conception, execution, or interpretation, of at least that part of the publication in their field of expertise;
- (3) they take public responsibility for their part of the publication, except for the responsible author who accepts overall responsibility for the publication;
- (4) there are no other authors of the publication according to these criteria;
- (5) potential conflicts of interest have been disclosed to (a) granting bodies, (b) the editor or publisher of journals or other publications, and (c) the head of the responsible academic unit; and
- (6) the original data are stored at the following location(s) and will be held for at least five years from the date indicated below:

Locations:

Department of Medicinal Chemistry, Monash Institute of Pharmaceutical Sciences, 381 Royal Pde, Parkville VIC 3052, Australia

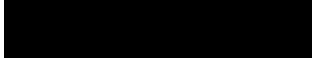
Signatures:

Signed:



Date: 02/08/2013

Signed:



Date: 30/07/2013

Signed: _____

Date:

Signed: _____

Date:

Chapter 3: Structural modification of ZSTK474 to probe isoform selective interactions with PI3K

3.1 Introduction

While Chapter 2 identified differences in regulation between wild-type PI3K α and the kinase domain oncogenic mutant, p110 α His1047Arg and characterised the lipid-binding site of PI3K α , this structural understanding ultimately illustrates how challenging the development of oncogenic mutant specific PI3K inhibitors will be. Indeed the development of PI3K α selective inhibitors has been challenging enough, such that very few have been identified in over a decade of effort. The following two chapters describe attempts to exploit our developing understanding of the structural determinants that dictate PI3K inhibitor selectivity to develop novel isoform selective inhibitors of PI3K generally and more particularly, PI3K α .

In order to probe isoform specific interactions, we first required a suitable starting point for inhibitor synthesis. Numerous methods for “hit” identification exist, most often via high-

throughput screening campaigns, ranging from *in vitro* to *in silico* methods, and from screening for “lead-like” compounds to fragment leads. Once a hit is identified, various parameters are optimised to develop a suitable inhibitor.¹⁻³ As a starting point for PI3K isoform selective inhibitors, lead molecules can be selected that are either potent but non selective, or selective, but not potent. An example of the former is a recent report from Novartis.⁴ A non selective hit, **18a**, from a high-throughput screening campaign was developed into three distinct isoform selective inhibitors targeting either PI3K α , PI3K δ or PI3K γ (Figure 3.1).⁴ As an example of the latter, Certal *et al.* have published their efforts in optimising potency and drug-like properties of a hit identified through high-throughput screening that displayed PI3K β selectivity.^{5,6} We decided to start from a non selective, potent PI3K inhibitor and investigate substitutions that might influence isoform selectivity. As a starting point molecule, we were looking for something with strong potency and that is amenable to synthetic modification at key positions that provide access to the non-conserved regions of the binding site discussed in Chapter 1.⁷⁻⁹

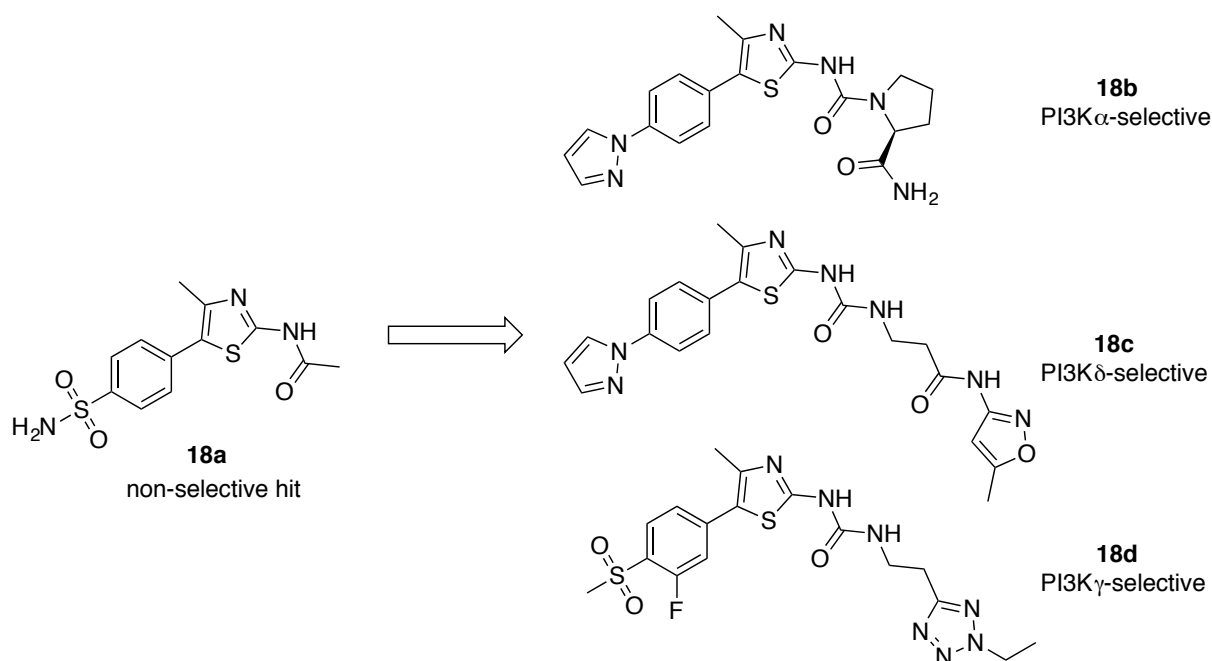
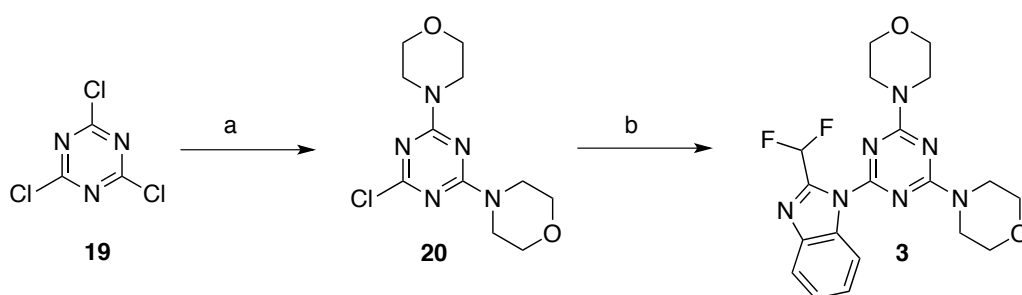


Figure 3.1: The development of isoform selective PI3K inhibitors from a non selective, potent hit molecule **18a**.⁴

We selected the potent, pan-PI3K inhibitor ZSTK474 **3** as the starting point for our analogue synthesis. The reported synthesis of ZSTK474 is simple, high-yielding and readily adapted.¹⁰ It proceeds via sequential substitution of cyanuric chloride **19** (Scheme 3.1). After each substitution, the remaining chloride groups become less reactive to substitution, allowing the variation of temperature to effectively control the selectivity of the reaction. Each step proceeds with high yield. The synthesis allows scope for derivatisation at any point by modification of the amine chosen for substitution. In addition to nucleophilic substitutions, other reactions of aryl halides can be used to introduce substituents, like Suzuki couplings for aromatic substitution.¹¹



Scheme 3.1: Synthesis of ZSTK474 **3**. Conditions: (a) morpholine, triethylamine, acetone, 0–22°C;¹² (b) 2-difluoromethylbenzimidazole, NaH or K₂CO₃, DMF or DMSO, 120°C.¹⁰

The crystal structure of ZSTK474 bound to p110δ was published in 2010 (Figure 3.2).¹³ In this structure, one of the morpholinyl oxygen atoms makes an interaction with the hinge region of the ATP binding site, forming a hydrogen bond with the amide backbone of Val828. As discussed in Chapter 1, the hinge interaction is considered essential for inhibitor binding. The second morpholinyl substituent projects towards non-conserved Region 1, a region of considerable heterogeneity between the different isoforms, presenting significant potential for derivatisation to engender isoform selectivity in analogues.^{7,9} The 2-difluoromethylbenzimidazole substituent binds in what has been described the affinity pocket, with the N3 atom forming a hydrogen bond with Lys779 of p110δ.^{14,15} The fused phenyl ring projects deep into the affinity pocket, with potential for substitution and interactions with Tyr813, Leu791 and Asp787.

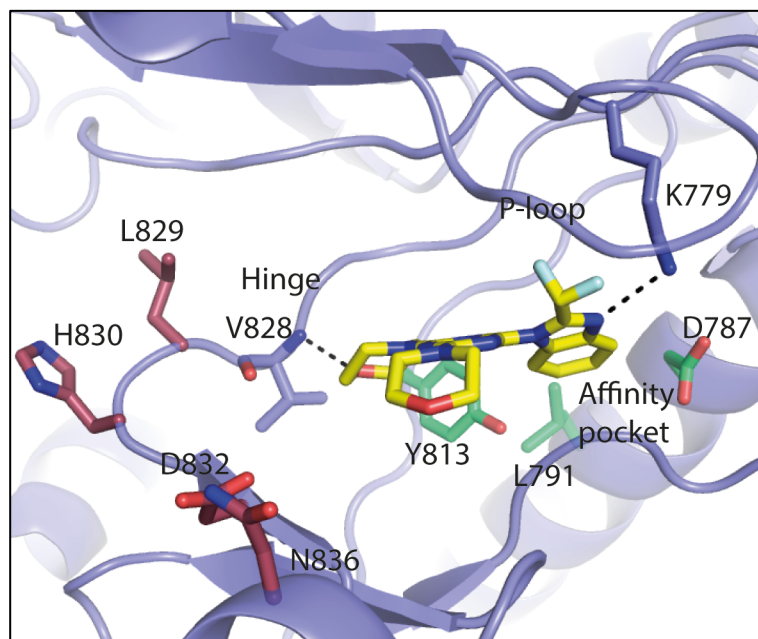
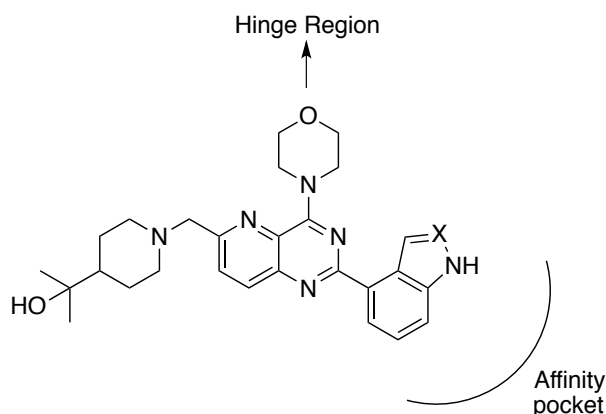


Figure 3.2: The binding mode of ZSTK474. The p110 δ crystal structure with ZSTK474 bound (PDB ID: 2WXL). Region 1 non-conserved amino acids are shown in dark red. The affinity pocket amino acids are highlighted in green.

Although the residues within the affinity pocket are largely conserved, interactions within this pocket have been shown to influence selectivity. An example of this is highlighted in a series of PI3K δ selective inhibitors developed by Genentech (Table 3.1).¹⁶ When an indole group is binding in the affinity pocket (**21a**), p110 δ selectivity is observed; but when replaced with an indazole moiety (**21b**), much of this selectivity is lost. The only difference is the presence of an extra, hydrogen bond-accepting nitrogen atom in the indazole. This allows a hydrogen bond to be formed between N2 of the indazole and Tyr813. In the indole inhibitors, this nitrogen is replaced by a C-H, which is unable to interact with Tyr813. It is postulated that this change results in a rearrangement of hydrogen bonding networks, which is most tolerated in p110 δ .¹⁶ This example demonstrates the potential for benzimidazole substitutions or aromatic replacements to influence isoform selectivity.

Table 3.1: Genentech's PI3K inhibitors.¹⁶

Compound	X	PI3K δ IC ₅₀ (nM)	Fold selectivity (α/δ)	Fold selectivity (β/δ)	Fold selectivity (γ/δ)
21a	C	2.8	370	210	610
21b	N	6.3	22	78	260

It can be seen, therefore, that the binding mode of ZSTK474 reveals substantial scope for modification towards an isoform selective inhibitor. The high-yielding synthesis also provides opportunity for derivatisation. We thus considered it a suitable starting point to investigate isoform selective interactions.

3.1.1 Aims

The aim for this part of the work was to investigate alterations in the aromatic portion of ZSTK474, to probe their effect on potency and selectivity. This work will be presented in three sections. The first section investigates the effect of 5- and 6-methoxybenzimidazole substitutions on isoform selectivity and necessitated the development of a regioselective synthetic route to access these molecules. It is included as the published article. The second section describes the evaluation of previously synthesised ZSTK474 analogues, and discusses the effect of various substitutions on both potency and selectivity. The third section builds on these ZSTK474

derivatives to develop a new series of analogues. The synthesis and activity profiles of this series are then discussed.

3.2 Regioselective synthesis of 5- and 6-methoxybenzimidazole ZSTK474 derivatives

Although ZSTK474 was first described in 2006, very little structure-activity data surrounding the structure has been published outside of the patent literature.^{10,17} Recent papers by Rewcastle *et al.* have reported significant gains in potency through inclusion of a 4-methoxy substituent to the 2-difluoromethylbenzimidazole group of ZSTK474, considered to be due to interactions with Lys779.^{10,18} We reasoned that 5- or 6-substitutions might be able to make isoform selective interactions with the binding site as seen with the Genentech inhibitors described above.¹⁶ We postulated, therefore, that these substitutions might result in improvements in potency and selectivity. In examining the target molecules, we found that the routine synthetic method for preparing ZSTK474 lacked regioselectivity when applied to 5- or 6-substituted benzimidazoles, giving rise to an inseparable mixture of both 5- and 6-substituted regioisomers. Furthermore, for this reason we found that in a range of medicinal chemistry studies, 5- and 6-benzimidazole substituted compounds have often been avoided, or accessed as mixtures and purified.¹⁹ The description of the development of a convenient regioselective synthetic method for accessing these molecules and the biochemical assessment of them is included as the published paper.



Contents lists available at SciVerse ScienceDirect

Bioorganic & Medicinal Chemistry Letters

journal homepage: www.elsevier.com/locate/bmcl

Regioselective synthesis of 5- and 6-methoxybenzimidazole-1,3,5-triazines as inhibitors of phosphoinositide 3-kinase

Michelle S. Miller, Jo-Anne Pinson, Zhaohua Zheng, Ian G. Jennings, Philip E. Thompson*

Medicinal Chemistry, Monash Institute of Pharmaceutical Sciences, 381 Royal Pde, Parkville, Victoria 3052, Australia

ARTICLE INFO

Article history:

Received 18 September 2012

Revised 19 November 2012

Accepted 20 November 2012

Available online 1 December 2012

Keywords:

Phosphoinositide 3-kinase inhibitors

ZSTK474

Regioselective synthesis

Benzimidazole derivatives

ABSTRACT

Phosphoinositide 3-kinases (PI3K) hold significant therapeutic potential as novel targets for the treatment of cancer. ZSTK474 (**4a**) is a potent, pan-PI3K inhibitor currently under clinical evaluation for the treatment of cancer. Structural studies have shown that derivatisation at the 5- or 6-position of the benzimidazole ring may influence potency and isoform selectivity. However, synthesis of these derivatives by the traditional route results in a mixture of the two regioisomers. We have developed a straightforward regioselective synthesis that gave convenient access to 5- and 6-methoxy substituted benzimidazole derivatives of ZSTK474. While 5-methoxy substitution abolished activity at all isoforms, the 6-methoxy substitution is consistently 10-fold more potent. This synthesis will allow convenient access to further 6-position derivatives, thus allowing the full scope of the structure–activity relationships of ZSTK474 to be probed.

© 2012 Elsevier Ltd. All rights reserved.

The phosphoinositide 3-kinase (PI3K) pathway is an important cellular signalling pathway that functions to elevate levels of cell growth and proliferation. It is one of the most frequently activated pathways in cancer.^{1,2} There are four highly homologous isoforms, designated PI3K α , PI3K β , PI3K γ and PI3K δ , each having a distinct array of physiological functions. Activating mutations in PI3K α have been found in about a quarter of breast and endometrial cancers, identifying PI3K as an important target for novel cancer therapeutics.³

Among a range of current clinical candidate drugs, ZSTK474 (**4a**) is a potent, pan-PI3K inhibitor that selectively inhibits PI3K over many other related kinases.⁴ It is currently in Phase I trials for the treatment of advanced solid malignancies.⁵ Like the majority of candidates it has comparable potency at the four Class I isoforms, which may lead to off-target effects that compromise therapeutic utility. Certainly, there is a need for more isoform-selective compounds to help delineate the roles played in cancer by individual isoforms.

The crystal structure of ZSTK474 bound to PI3K δ was released in 2010.⁶ Analysis of the binding mode of ZSTK474 to the p110 δ ATP binding site showed that the difluoromethylbenzimidazole ring projects into what has been described as an affinity pocket. It also appeared likely that substitution of the benzimidazole ring might lead to altered potency and selectivity. Indeed, a recent paper detailed a limited number of 4-substituted and 4,6-disubstituted analogues that were effective in improving both solubility and

potency.⁷ For example, 4-methoxy substitution alone results in a 3-fold increase in potency and a shift towards PI3K α -selectivity as compared to ZSTK474.

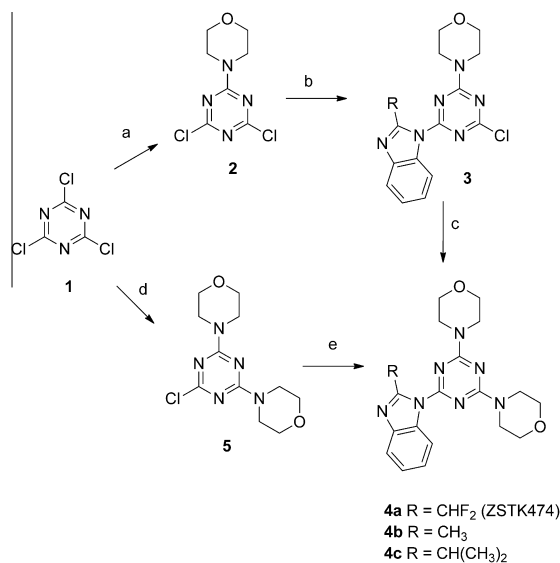
In a similar fashion, we were interested in investigating the influence of 5- and 6-methoxy substituents on potency and selectivity of ZSTK474 and analogues. The 2-difluoromethyl, 2-methyl and 2-isopropyl derivatives **4a–c** could be prepared readily through sequential substitution of cyanuric chloride as detailed in Scheme 1.⁷ However, this synthetic scheme was unsuitable for the synthesis of 5- or 6-methoxy substituted benzimidazole derivatives, as use of the 5-methoxybenzimidazoles as reagents resulted in inseparable mixtures of the 5- and 6-methoxy regioisomers due to tautomerism at the ring nitrogens.

This limitation has impeded others working on substituted benzimidazoles relative to other variations such that relatively few examples have been published. In certain cases it may be possible to separate the mixture of such 5- and 6-substituted regioisomers via chromatography as was shown in the case of triazine based MAP kinase inhibitors and in other examples in the patent literature.^{8–10} In our case, chromatographic separation couldn't be achieved readily, so a regioselective synthetic approach was necessary.

A recent review has identified a number of approaches to regioselective syntheses of N1-substituted benzimidazoles.¹¹ Palladium or copper catalysed reactions can be used in either intra- or intermolecular amination and cyclisation reactions using amidines or carbodiimides.^{12–16} More recently, Ma and Buchwald have reported the development of a metal-catalysed cascade aryl amination and condensation process.^{17–19} These reactions proceed via

* Corresponding author.

E-mail address: [redacted] (P.E. Thompson).



Scheme 1. Reagents and conditions: (a) morpholine, triethylamine, acetone, –20 °C; (b) 2-substituted benzimidazole, K₂CO₃, DMF, room temp; (c) morpholine, K₂CO₃, DMF, MW 140 °C; (d) morpholine, triethylamine, acetone, 0 °C to room temp; (e) 2-substituted benzimidazole, Pd(OAc)₂, Xantphos, Cs₂CO₃, 1,4-dioxane, MW 150 °C, 40 min.

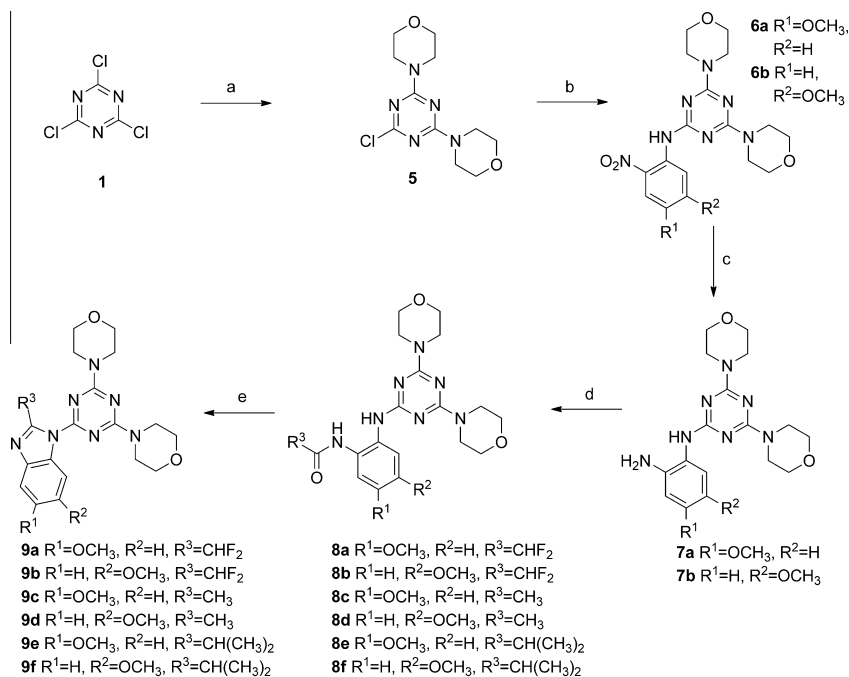
o-aminoanilides as intermediates, before a condensation reaction produces the desired benzimidazole product. Metal catalysts can also be used to amidate *o*-halonitroarenes, followed by a reductive

cyclisation process.^{20,21} Alternatively, an appropriate *o*-nitroaniline can be used, with the free amine group functionalised, followed by a reduction and cyclisation to form the benzimidazole.²² To our knowledge, there are no reports in the literature of these methods being applied to benzimidazole-substituted triazines.

We have developed a synthetic approach starting with appropriate 4- and 5-methoxy-2-nitroanilines for the synthesis of corresponding methoxy-substituted analogues of ZSTK474 derivatives. This efficient and general synthesis can be achieved under relatively mild conditions, provides regiospecific access to substituted benzimidazole-triazines and allows for further diversification through the 2-position of the benzimidazole (Scheme 2). It has allowed us to elucidate the specific influence of these substituents on P13K affinity and isoform selectivity.

The precursor 2-chloro-4,6-dimorpholino-1,3,5-triazine **5**⁷ was subjected to Buchwald–Hartwig amination conditions with 4-methoxy-2-nitroaniline or 5-methoxy-2-nitroaniline to yield the corresponding substituted triazines **6a** and **6b** in 85% and 77% yields, respectively. The nitro group was reduced with SnCl₂ under mild, non-acidic conditions.²³ Due to differences in solubility of the two precursors, the use of ethanol was preferable for the 4-methoxy-2-nitroaniline derivative, giving a yield of 91% of **7a** while ethyl acetate gave enhanced reaction time and yield of 83% for the 5-methoxy-2-nitroaniline derivative **7b**. SnCl₂ reduction under acidic conditions was trialled initially, but it was found that the morpholine group was labile.

Quite specific conditions were required to form the desired benzimidazole products, **9a–f**. In the first instance, where the phenylenediamine derivative **7a** was refluxed with difluoroacetic acid and a catalytic amount of polyphosphoric acid, a 60:40 mixture of the 6- and 5-methoxy derivatives **9a** and **9b** resulted, a consequence of acid-catalysed isomerisation of the diamine species. Alternatively, refluxing **7a** or **7b** under non-acidic conditions with



Scheme 2. Reagents and conditions: (a) morpholine, triethylamine, acetone, 0 °C to room temp; (b) 4- or 5-methoxy-2-nitroaniline, Pd(OAc)₂, Xantphos, Cs₂CO₃, 1,4-dioxane, MW 150 °C; (c) SnCl₂·2H₂O, ethanol or ethyl acetate, N₂, 70 °C; (d) acid chloride, DIPEA, DCM, room temp; (e) acetic acid, xylenes, 130 °C.

Table 1
Inhibition of PI3K isoforms

Compound	R	OCH ₃ position	IC ₅₀ (μM)			
			PI3Kα	PI3Kβ	PI3Kγ	PI3Kδ
4a	CHF ₂	—	0.006	0.006	0.038	0.003
9a	CHF ₂	5	>5	>10	>10	>1
9b	CHF ₂	6	0.375	0.214	>10	0.110
4b	CH ₃	—	0.290	0.523	1.86	0.187
9c	CH ₃	5	9.2	>10	>10	2.77
9d	CH ₃	6	0.823	1.79	>10	0.458
4c	CH(CH ₃) ₂	—	0.431	0.419	2.53	0.128
9e	CH(CH ₃) ₂	5	>10	>10	>10	1.12
9f	CH(CH ₃) ₂	6	1.05	0.726	>10	0.423

IC₅₀ values are the average of three independent experiments.

acetaldehyde in DMF in the presence of sodium metabisulfite did give the desired regioselective 2-methyl products **9c** and **d**.²⁴ However, a 2-desmethyl side-product was also present which made purification very difficult, resulting in low yields. It was thought to arise from thermal degradation or polymerisation of acetaldehyde during the reaction. Stirring **7a** and acetaldehyde at room temperature in the presence of sodium sulphate as a dehydrating agent gave no reaction after 48 h.²⁵

Finally, success was obtained using a two-step approach. Monoacylation of **7a** and **7b** with difluoroacetylchloride was high yielding and gave the regioisomerically pure acetamides **8a** and **8b**, respectively. Cyclisation was completed by refluxing overnight in a mixture of acetic acid and xylenes to give **9a** and **9b**. The corresponding 2-methyl (**9c, d**) and 2-isopropyl derivatives (**9e, f**) were also obtained using acetyl chloride and isobutyl chloride, respectively, illustrating the applicability of this method to the introduction of various substituents in the 2-position.

With the six methoxy-substituted derivatives **9a–f** and their unsubstituted counterparts **4a–c** in hand, they were then tested for activity against each of the four Class I PI3K isoforms. The results are summarized in Table 1.

The inclusion of a methoxy substituent at the 6- or 5-position of ZSTK474 results in analogues manyfold less potent than ZSTK474 (**4a**) itself. The 6-methoxy substituted analogue **9b** was at least 30-fold less potent against the PI3K isoforms and in fact activity was abolished against PI3Kγ. Substitution at the 5-position was even less favoured with compound **9a** unable to achieve 50% inhibition below 1 μM at any of the isoforms. This emphasizes the difference compared to the 4-methoxy substituted analogue reported by Rewcastle et al. which showed improved potency.⁷ It is also consistent with their results, which revealed that the 4,5-dimethoxy derivative was significantly less active than both the 4-methoxy and the 4,6-dimethoxy derivatives.⁷

Interestingly, the 2-position benzimidazole substituent influenced the magnitude of potency lost when 5- or 6-methoxy substituents were introduced. Both the 2-methyl and 2-isopropyl substituted analogues of ZSTK474 are themselves somewhat less active than ZSTK474, but in these cases the drop in potency upon addition of a 6-methoxy substituent as in **9d** and **9f** was more marginal at around 2- to 3-fold, except for PI3Kγ which again failed to be inhibited.

Molecular docking was used to study the binding of 5- and 6-methoxy derivatives compared to the crystallographically determined pose of ZSTK474 in PI3Kδ (PDB code 2WXL).⁶ In ZSTK474, one morpholinyl oxygen atom forms a hydrogen bond with the backbone amide of V828 in the hinge region of PI3K; the benzimidazole substituent extends into the affinity pocket and the second morpholine group faces the solvent exposed region. Docking suggests that the 6-methoxy substitution should not be as disfavoured as the biochemical data suggests, as compound **9b** is able to adopt

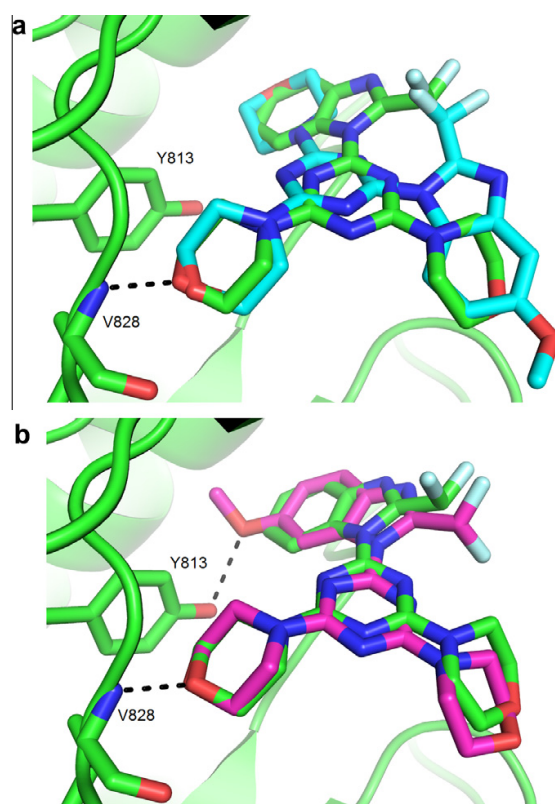


Figure 1. Compounds docked in the ATP-binding site of p110δ (2WXL PDB). (a) Comparison of the docked pose of **9a** (cyan) with the crystal structure binding mode of ZSTK474 (**4a**) (green); (b) comparison of the docked pose of **9b** (magenta) and ZSTK474 (**4a**) (green).

the expected pose (Fig. 1b). Compound **9a**, however, fails to assume the expected pose, instead the 5-methoxybenzimidazole group is facing the solvent exposed region, the second morpholine is in the affinity pocket and the triazine is rotated through the plane (Fig. 1a). The relative potency of the 6- and 5-methoxy substituents appears to be accounted for, however, as 6-methoxybenzimidazole derivatives can form a hydrogen bond with Y813 that the 5-methoxy derivatives cannot. The lost activity at PI3Kγ implies that this isoform is in some way more sensitive to substitution.

In conclusion, we have reported an efficient method for preparing 4,4'-(6-(5-methoxy-2-difluoromethyl-1*H*-benzo[d]imidazol-1-yl)-1,3,5-triazine-2,4-diyl)dimorpholine **9a**, its 6-methoxy regioisomer **9b**, and its 2-methyl **9c,d** and 2-isopropyl variants **9e,f**. Assay results indicate that 6-substituted benzimidazole rings were consistently more potent as PI3K inhibitors than the analogous 5-substituted benzimidazoles. These results illustrate both the synthetic accessibility of regioisomerically pure 6-substituted benzimidazole-1,3,5-triazines, and their utility as PI3K inhibitors.

Acknowledgments

This work was funded by a project Grant from the National Health and Medical Research Council (Grant no.: 545943). M.S. Miller was supported by an Australian Postgraduate Award scholarship and a Cooperative Research Centre for Cancer Therapeutics top-up scholarship.

Supplementary data

Supplementary data associated with this article can be found, in the online version, at <http://dx.doi.org/10.1016/j.bmcl.2012.11.076>.

References and notes

- Vanhaesebroeck, B.; Guillermet-Guibert, J.; Graupera, M.; Bilanges, B. *Nat. Rev. Mol. Cell Biol.* **2010**, *11*, 329.
- Engelman, J. A. *Nat. Rev. Cancer* **2009**, *9*, 550.
- Liu, P.; Cheng, H.; Roberts, T. M.; Zhao, J. J. *Nat. Rev. Drug Disc.* **2009**, *8*, 627.
- Yaguchi, S.; Fukui, Y.; Koshimizu, I.; Yoshimi, H.; Matsuno, T.; Gouda, H.; Hirono, S.; Yamazaki, K.; Yamori, T. *J. Natl. Cancer Inst.* **2006**, *98*, 545.
- Sugama, T.; Ishihara, K.; Tanaka, Y.; Takahashi, M.; Yaguchi, S.; Watanabe, T. WO2009066775, 2009.
- Berndt, A.; Miller, S.; Williams, O.; Le, D. D.; Houseman, B. T.; Pacold, J. I.; Gorrec, F.; Hon, W.-C.; Liu, Y.; Rommel, C.; Gaillard, P.; Rückle, T.; Schwarz, M. K.; Shokat, K. M.; Shaw, J. P.; Williams, R. L. *Nat. Chem. Biol.* **2010**, *6*, 117.
- Rewcastle, G. W.; Gamage, S. A.; Flanagan, J. U.; Frederick, R.; Denny, W. A.; Baguley, B. C.; Kestell, P.; Singh, R.; Kendall, J. D.; Marshall, E. S.; Lill, C. L.; Lee, W.-J.; Kolekar, S.; Buchanan, C. M.; Jamieson, S. M. F.; Shepherd, P. R. *J. Med. Chem.* **2011**, *54*, 7105.
- Clark, M. A.; Acharya, R. A.; Arico-Muendel, C. C.; Belyanskaya, S. L.; Benjamin, D. R.; Carlson, N. R.; Centrella, P. A.; Chiu, C. H.; Creaser, S. P.; Cuozzo, J. W.; Davie, C. P.; Ding, Y.; Franklin, G. J.; Franzen, K. D.; Geffer, M. L.; Hale, S. P.; Hansen, N. J. V.; Israel, D. I.; Jiang, J.; Kavarana, M. J.; Kelley, M. S.; Kollmann, C. S.; Li, F.; Lind, K.; Mataruse, S.; Medeiros, P. F.; Messer, J. A.; Myers, P.; O'Keefe, H.; Oliff, M. C.; Rise, C. E.; Satz, A. L.; Skinner, S. R.; Svendsen, J. L.; Tang, L.; van Vloten, K.; Wagner, R. W.; Yao, G.; Zhao, B.; Morgan, B. A. *Nat. Chem. Biol.* **2009**, *5*, 647.
- Andrews, I.; Cheung, M.; Davis-Ward, R.; Drewry, D.; Emmitte, K.; Hubbard, R.; Kuntz, K.; Linn, J.; Mook, R.; Smith, G.; Veal, J. WO2004014899, 2004.
- Armstrong, H.; Beres, R.; Goulet, J.; Holmes, M.; Hong, X.; Mills, S.; Parsons, W.; Sinclair, P.; Steiner, M.; Wong, F.; Zaller, D. WO0100213, 2001.
- Carvalho, L. C. R.; Fernandes, E.; Marques, M. M. B. *Chem. Eur. J.* **2011**, *17*, 12544.
- He, H.-F.; Wang, Z.-J.; Bao, W. *Adv. Synth. Catal.* **2010**, *352*, 2905.
- Brain, C. T.; Brunton, S. A. *Tetrahedron Lett.* **2002**, *43*, 1893.
- Brasche, G.; Buchwald, S. L. *Angew. Chem.* **2008**, *120*, 1958.
- Saha, P.; Ramana, T.; Purkait, N.; Ali, M. A.; Paul, R.; Punniyamurthy, T. *J. Org. Chem.* **2009**, *74*, 8719.
- Peng, J.; Ye, M.; Zong, C.; Hu, F.; Feng, L.; Wang, X.; Wang, Y.; Chen, C. *J. Org. Chem.* **2010**, *75*, 716.
- Zheng, N.; Buchwald, S. L. *Org. Lett.* **2007**, *9*, 4749.
- Zheng, N.; Anderson, K. W.; Huang, X.; Nguyen, H. N.; Buchwald, S. L. *Angew. Chem., Int. Ed.* **2007**, *46*, 7509.
- Zou, B.; Yuan, Q.; Ma, D. *Angew. Chem., Int. Ed.* **2007**, *46*, 2598.
- Hornberger, K. R.; Badiang, J. G.; Salovich, J. M.; Kuntz, K. W.; Emmitte, K. A.; Cheung, M. *Tetrahedron Lett.* **2008**, *49*, 6348.
- Skerlj, R. T.; Bastos, C. M.; Booker, M. L.; Kramer, M. L.; Barker, R. H.; Celatka, C. A.; O'Shea, T. J.; Munoz, B.; Sidhu, A. B.; Cortese, J. F.; Wittlin, S.; Papastogiannidis, P.; Angulo-Barturen, I.; Jimenez-Diaz, M. B.; Sybertz, E. *ACS Med. Chem. Lett.* **2011**, *2*, 708.
- Davies, D. J.; Crowe, M.; Lucas, N.; Quinn, J.; Miller, D. D.; Pritchard, S.; Grose, D.; Bettini, E.; Calcinaghi, N.; Virginio, C.; Abberley, L.; Goldsmith, P.; Michel, A. D.; Chessell, I. P.; Kew, J. N. C.; Miller, N. D.; Gunthorpe, M. J. *Bioorg. Med. Chem. Lett.* **2012**, *22*, 2620.
- Bellamy, F. D.; Ou, K. *Tetrahedron Lett.* **1984**, *25*, 839.
- Navarrete-Vázquez, G.; Hidalgo-Figueroa, S.; Torres-Piedra, M.; Vergara-Galicia, J.; Rivera-Leyva, J. C.; Estrada-Soto, S.; León-Rivera, I.; Aguilar-Guardarrama, B.; Ríos-Gómez, Y.; Villalobos-Molina, R.; Ibarra-Barajas, M. *Bioorg. Med. Chem.* **2010**, *18*, 3985.
- Kabir, M. S.; Namjoshi, O. A.; Verma, R.; Polanowski, R.; Krueger, S. M.; Sherman, D.; Rott, M. A.; Schwan, W. R.; Monte, A.; Cook, J. M. *Bioorg. Med. Chem.* **2010**, *18*, 4178.

3.2.1 Post-script: Rationalising selectivity

The preceding paper has described the synthesis of 5- and 6-methoxybenzimidazole substituted ZSTK474 derivatives. Despite the loss of potency compared with the parent molecule, significant selectivity against PI3K γ was achieved. This suggests that PI3K γ is more sensitive to substitutions within the affinity pocket than the other isoforms.

The rationale for this selectivity is not immediately apparent. As discussed in the introduction to this chapter, the binding residues in the affinity pocket are conserved between the four isoforms. Given that the docking results suggest the 6-methoxy substitution targets Tyr813, one potential explanation would be a similar rearrangement of hydrogen bonding networks as that proposed in the report of indole and indazole-based inhibitors by Genentech.¹⁶ However, if this was the case, a similar difference in PI3K δ selectivity would be expected between the unsubstituted and methoxy-substituted analogues and this is not apparent. Although this mechanism may influence potency and selectivity, it is not likely to be the sole explanation.

Another potential explanation for the dramatic loss of p110 γ potency may be the inability of this isoform to accommodate the extra bulk binding in the affinity pocket. The residues further removed from the affinity pocket are less conserved. Differences in the surrounding areas may affect the flexibility of the pocket, and thus its ability to accommodate substitutions like the methoxy group. For example, there is a tyrosine residue in p110 γ (Tyr787), which is a leucine in each of the other isoforms (Figure 3.3). The extra bulk of the tyrosine residue in p110 γ may influence the flexibility of the affinity pocket, and therefore sensitise the PI3K γ isoform to substitutions in this area.

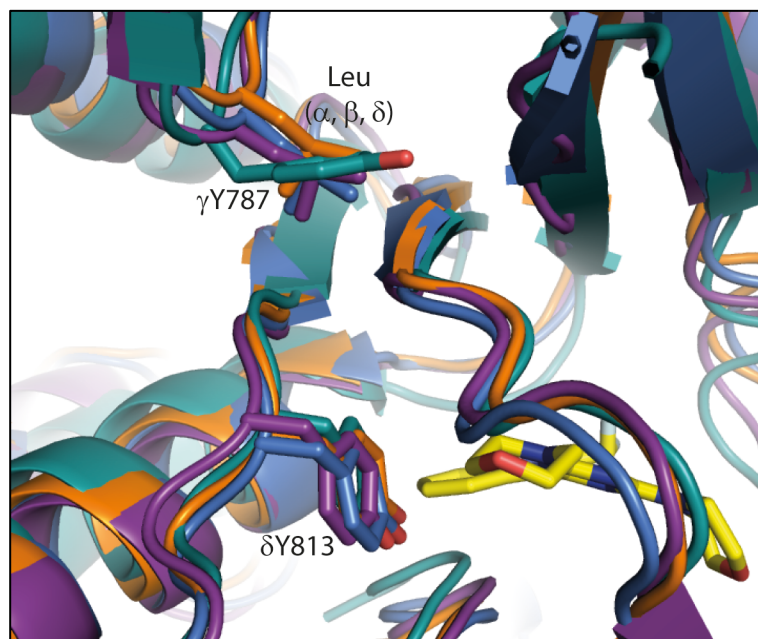


Figure 3.3: Structural alignment of p110 α (structure from Chapter 2, orange), p110 β (PDB ID: 2Y3A, blue), p110 γ (PDB ID: 1E8X, teal) and p110 δ (PDB ID: 2WXL, purple). ZSTK474 from p110 δ structure is shown in yellow. p110 γ Y787 is shown, with the leucine residue at the corresponding position in the other isoforms.

The paper reports the docking results into PI3K δ , which at first glance provide little explanation for the loss of potency in the 6-methoxy substituted analogue. A more detailed comparison of the crystal structure binding mode of ZSTK474 with the docked pose of the 6-methoxy substituted analogue reveals a shift in the placement of the benzimidazole moiety to accommodate the methoxy group. In the crystal structure, the distance from the benzimidazole N3 to Lys779 is 3.1 Å, whereas in the docking pose of the 6-methoxy analogue, this distance is increased to 3.3 Å. This hydrogen bond is one of only two hydrogen bonds that ZSTK474 makes with the enzyme, and therefore must be important for its potency. While this change in distance may not fully explain the loss in potency, it provides at least some rationale.

The synthetic method described in the paper now allows for the investigation of a wider range of 5- or 6-substitutions at the benzimidazole ring. This could include halogen substitutions, electron-withdrawing groups and hydrogen bond donors, to supplement the structure-activity relationship (SAR) data from the methoxy analogues. It is likely that smaller

substitutions will be more effective than larger ones at maintaining or improving the potency of ZSTK474.

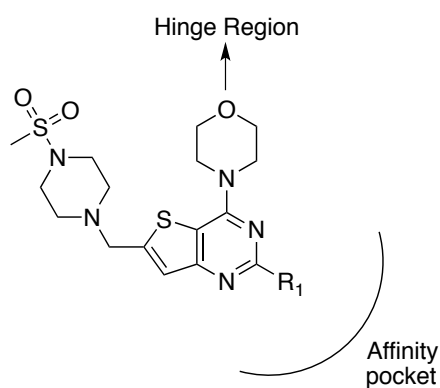
3.3 Evaluation of a series of ZSTK474 analogues

The methoxy substitutions described in Section 3.2 yielded some interesting insights into the effect of affinity pocket substitutions on selectivity against PI3K γ in particular. However, given that these substitutions were limited to abolishing PI3K γ inhibition, we decided to pursue replacements for the benzimidazole moiety that might display increased selectivity over the other isoforms via interactions within the affinity pocket. This also allows us to further investigate the effect of affinity pocket interactions on PI3K inhibitor selectivity.

A search of the literature surrounding PI3K inhibitors reveals a wealth of information on different affinity pocket binding motifs, which are generally aromatic in nature.^{20–22} Selectivity data on these motifs are more difficult to find, as the majority of papers report only PI3K α potency. There are isolated reports, however, that do highlight the ability of affinity pocket binding moieties to affect isoform selectivity in a variety of ways. In addition to the PI3K δ selective indole inhibitors discussed in Section 3.1, three further literature examples will be discussed here.

The first example from Sutherlin *et al.* reports selectivity data for nine different aromatic substitutions of the thienopyrimidine core of GDC0941 (**14**).²³ In this series of substitutions, the selectivity between PI3K α and δ is not substantially affected. Instead, the substitutions have a greater effect on the selectivity for PI3K α against PI3K β and γ . Variations in selectivity for PI3K α are observed from 1 to 20-fold, simply from changes in the affinity pocket binding group (Table 3.2).²³

Table 3.2: A summary of the inhibitors from Sutherlin *et al.*²³ highlighting the differences in selectivity observed between different affinity pocket binding moieties.



Compound	R ₁	PI3K α IC ₅₀ (nM)	Fold selectivity (β/α)	Fold selectivity (γ/α)
14		3.0	11	22
14a		1.6	7	13
14b		21	0.7	0.9
14c		2.0	19	4

A second example uses different affinity binding substitutions on a 5-morpholino-thienopyranone core to tune selectivity either towards PI3K α with a benzodioxine substituent (**22a**), or PI3K δ with a *para*-ethylbenzoate substituent (**22b**) (Figure 3.4).²⁴

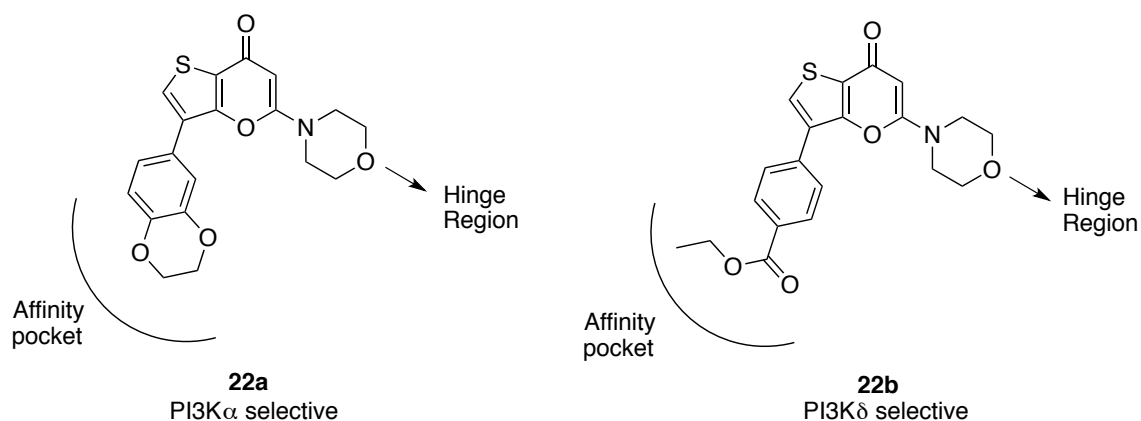
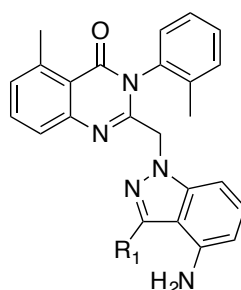


Figure 3.4: PI3K α and δ selective inhibitors from Morales *et al.* that differ only in the affinity pocket binding portion.²⁴

The third example uses a PI3K δ selective inhibitor as a starting point, and attaches an affinity pocket binding moiety to reintroduce PI3K γ inhibition and thus develop a dual PI3K γ and δ inhibitor (Table 3.3).¹⁴

Table 3.3: The introduction of an affinity pocket binding substituent increases potency for PI3K δ , and decreases selectivity against PI3K γ .¹⁴



Compound	R ₁	PI3K δ IC ₅₀ (nM)	Fold selectivity (δ/γ)
23a	H	237	42
23b	3-fluoro-4-hydroxyphenyl	9	2

These papers highlight the potential of different affinity pocket binders to influence isoform selectivity. The effect of a particular motif on selectivity can be combinatorial, depending also on the core and other binding motifs present. In light of this information, a large series of ZSTK474 analogues investigating aromatic replacements for the benzimidazole group has previously been synthesised by Jo-Anne Pinson in our laboratories.¹² The design of this series was based on common affinity binding pocket motifs found in literature. The compounds were assayed against each of the four isoforms to identify substituents that displayed either good potency or selectivity. Two benzimidazole replacements, the 3-hydroxyphenyl and 3-hydroxymethylphenyl, proved of particular interest (Compounds **24a** and **24b**, Figure 3.5). Substitutions at this position will hereafter be referred to as left-hand-side (LHS) substituents.

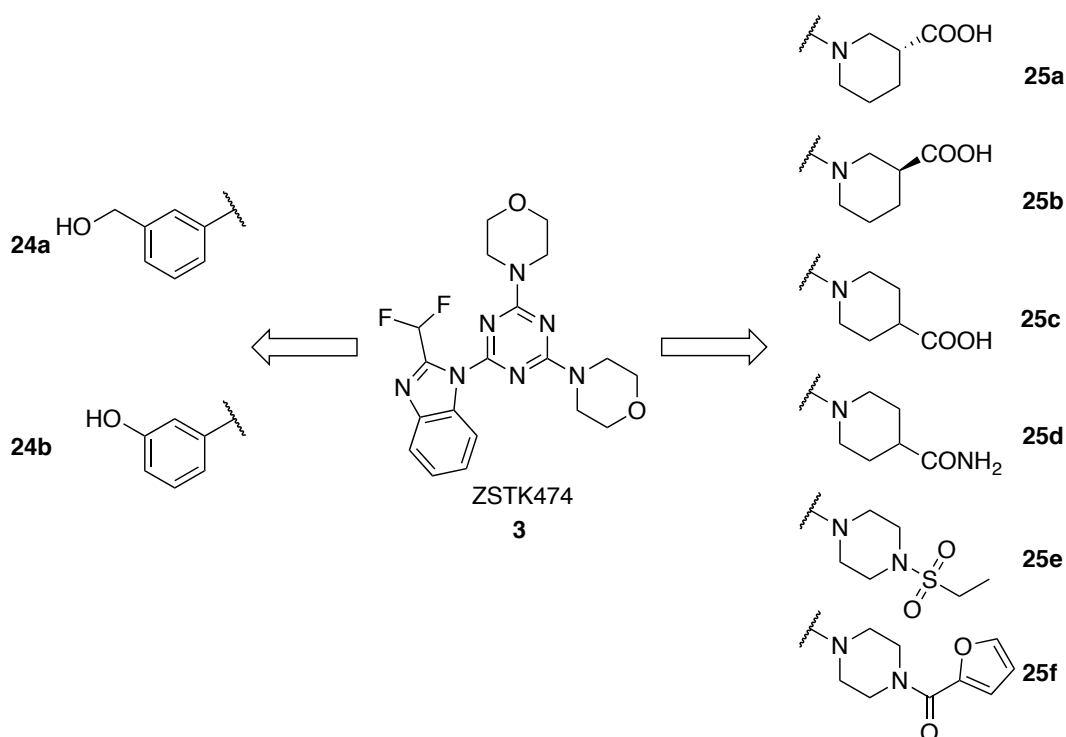


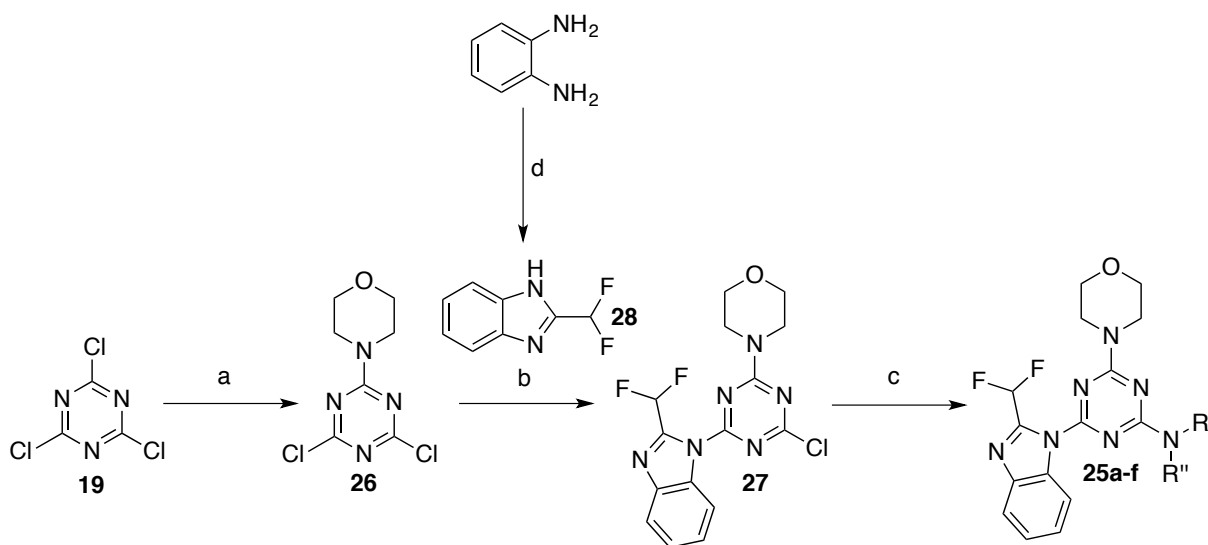
Figure 3.5: Promising ZSTK474 analogues (Compounds **25b-25f** previously described by Jo-Anne Pinson).¹²

As discussed in Section 3.1, the second morpholine ring points towards an area of significant isoform heterogeneity. We reasoned, therefore, that the introduction of different functionalities at this position (hereafter referred to as right-hand-side (RHS) substituents) could further

increase potency or selectivity. A number of substituted piperidine and piperazine derivatives were prepared and five of these were selected for follow up: 3-(S)-piperidinylcarboxyl (**25b**), 4-piperidinylcarboxyl (**25c**), 4-piperidinylcarboxamide (**25d**), 4-(ethylsulfonyl)piperazinyl (**25e**) and 4-(2-furoyl)piperazinyl (**25f**) (Figure 3.5).¹² Two of these derivatives, **25d** and **25f**, along with ZSTK474, were resynthesised to give sufficient material to test. The 3-(R)-piperidinylcarboxyl derivative, compound **25a**, was also synthesised as a point of comparison with **25b**, to investigate whether the configuration of the carboxyl group could influence selectivity. The evaluation of these eight inhibitors will be described in this section.

3.3.1 Synthesis of ZSTK474 derivatives

As described in Section 3.1, synthesis of 1,3,5-triazine derivatives proceeds by successive substitution reactions of cyanuric chloride (Scheme 3.2).²⁵



Scheme 3.2: Synthesis of ZSTK474 analogues. (a) morpholine, triethylamine, acetone, -20°C; (b) K₂CO₃, DMF, 25°C; (c) amine, K₂CO₃, DMF, 50°C; (d) difluoroacetic acid, 4 M HCl, reflux.

The key intermediate **27** was prepared according to literature reports (Scheme 3.2).^{10,12} The initial substitution of morpholine was performed by dropwise addition of a solution of morpholine and triethylamine in acetone to a solution of cyanuric chloride in acetone at -20°C.¹²

Using this method, **26** was obtained in 96% yield. 2-difluoromethylbenzimidazole **28** was then prepared by refluxing 1,2-phenylenediamine and difluoroacetic acid in 4 M hydrochloric acid for 3 hours.¹⁰ The product was precipitated upon neutralisation of the solution, and recovered in 90% yield. Finally, 2-difluoromethylbenzimidazole **28** was combined with **26** in the presence of potassium carbonate in DMF at room temperature to give 92% yield of **27**. All ¹H-NMR spectra corresponded with previous reports.^{10,12,26–28}

This key intermediate **27** was then treated with the various secondary amines at 50°C in DMF overnight. The products were obtained by addition of water to induce precipitation, followed by filtration and drying. For the nipecotic acid derivative **25a**, adjustment of the pH with 1 M hydrochloric acid to pH 4–5 was required to precipitate the product. All characterisation data was consistent with those previously described.^{10,12,29} Analysis by HPLC and NMR confirmed greater than 95% purity in the precipitated products without need for further purification.

The NMR spectra of compounds **25a** and **25b** showed some unusual features. While the chromatographic analysis (TLC, analytical HPLC) suggested a homogenous material of the expected mass (LCMS and High Resolution ESI-TOF-MS), the NMR data appeared to indicate the presence of two distinct but related species. ¹H-NMR (in *d*₆-DMSO) revealed two sets of resonances in approximately a 1:1 ratio. In **25a**, the characteristic CHF₂ triplet (*J* = 53 Hz) is present as two triplets at 7.75 and 7.72 ppm. The corresponding carbon is present as two triplets in the ¹³C-NMR spectrum at 108.6 and 108.5 ppm (*J* = 237 Hz), as determined by a ¹H-¹³C Heteronuclear Single Quantum Coherence (HSQC) experiment. A second proton signal in the aromatic region appears as doublets at 8.39 (*J* = 7.7 Hz) and 8.32 ppm (*J* = 8.2 Hz) rather than the expected doublet resonance, and corresponds to carbon signals at 115.9 and 115.7 ppm. Evidence of two distinct species is also present in the piperidinyl ¹H and ¹³C-NMR signals. Two multiplets are evident around 2.53 and 2.45 ppm, despite being partially obscured by the

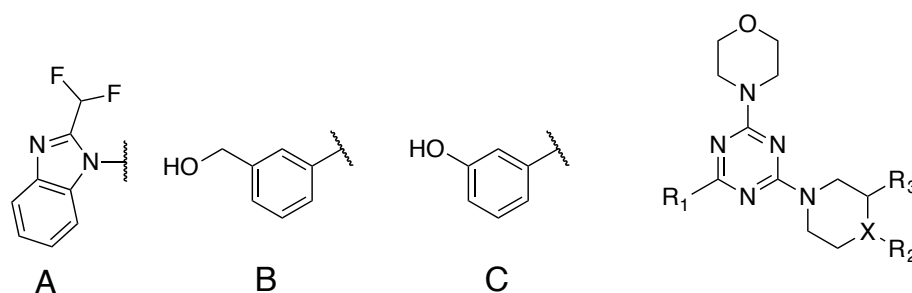
residual proteo-dimethylsulfoxide peak. This proton signal corresponds to the piperidinyl methine proton (H3), which would be expected to appear as a multiplet around 2.50 ppm. The corresponding carbon (C3) signals are at 40.6 and 40.5 ppm. The axial proton on C2 occurs as doublet of doublets at 4.63 ($J = 12.5, 2.5$ Hz) and 4.46 ($J = 12.8, 2.6$ Hz) ppm. The C2 carbon signals occur at 45.4 and 45.0 ppm. The axial proton on C6 occurs as multiplets at 4.42-4.34 and 4.30-4.21 ppm, corresponding to the signals in the ^{13}C -NMR spectrum at 43.6 and 43.5 ppm. The remaining piperidinyl proton signals are broad multiplets and are not clearly defined into two sets of signals. The characteristic morpholinyl proton signals at 3.83-3.75 and 3.72-3.65 ppm are multiplet signals, as expected, corresponding to the carbon signals at 65.9 and 43.6 ppm. Taken together, the ^1H and ^{13}C -NMR suggest the presence of two closely related species. The spectra of **25b** showed a similar phenomenon. This data would be consistent with two species in a 1:1 ratio possibly due to rotamers or different ionisation states. Compounds with the same nipecotic acid substituents described in Section 3.4.5 (compounds **37a-b** and **38a-b**) showed a single set of resonances, suggesting perhaps a conformational origin.

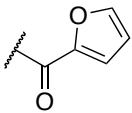
3.3.2 Evaluation against Class I PI3K

To evaluate their inhibitory potency, each of the eight compounds was then tested against the four Class I PI3K isoforms. The enzymes were produced in house by Zhaohua Zheng with recombinant expression using the baculovirus expression system in SF21 insect cells.^{8,9,30} We used the general kinase assay, Kinase-Glo®, available from Promega. In the Kinase-Glo® assay, the enzyme luciferase uses residual ATP to oxidise beetle luciferin, releasing energy as light. The intensity of this light signal is measurable and directly proportional to the concentration of ATP left in the reaction. As such, the assay measures ATP consumption by PI3K. Assays were performed by incubating PI3K enzyme with 10 μM ATP and 180 μM phosphatidylinositol in the presence of DMSO control or increasing concentrations of inhibitor for 60 minutes at room temperature. The reaction was quenched by addition of the Kinase-Glo® reagent, containing

luciferase and luciferin. The luminescent signal was then measured on a BMG FluoStar plate reader, allowing a dose-response curve to be plotted and the IC₅₀ values determined. Each inhibitor was tested in duplicate, and the results presented are the mean of at least three independent experiments. Standard errors are all within 20% of the mean (standard errors listed in Appendix 1). The assay results are presented in Table 3.4.

Table 3.4: Evaluation of ZSTK474 analogues. IC₅₀ values are the mean of at least 3 independent experiments. Standard errors are all within 20% of the mean.



Compound	R ₁	X	R ₂	R ₃	IC ₅₀ (nM)			
					PI3Kα	PI3Kβ	PI3Kγ	PI3Kδ
ZSTK474 3	A	O	H	H	35	39	166	17
24a	B	O	H	H	41	56	625	45
24b	C	O	H	H	59	124	1293	106
25a	A	C	H	COOH (R)	183	428	247	163
25b	A	C	H	COOH (S)	40	215	231	42
25c	A	C	COOH	H	76	217	64	38
25d	A	C	CONH ₂	H	65	165	304	35
25e	A	N	SO ₂ CH ₂ CH ₃	H	100	697	465	69
25f	A	N		H	112	134	626	33

The level of isoform selectivity desirable in either a potential clinical candidate or chemical tool would be greater than 100-fold, which would allow inhibition of the desired isoform, without significantly affecting the others.

As a control, the assay results for ZSTK474 were compared to published data.^{10,31} In line with published reports, ZSTK474 was most potent at the PI3K δ isoform, with an IC₅₀ of 17 nM. It is approximately 2-fold less potent at the PI3K α and β isoforms, with IC₅₀ values of 35 and 39 nM, respectively. ZSTK474 is least potent at the PI3K γ isoform, with an IC₅₀ value of 166 nM.

The two hydroxy substituted phenyl replacements for the benzimidazole group significantly altered the selectivity profile compared to ZSTK474. While ZSTK474 was most potent at the PI3K δ isoform, both compounds **24a** and **24b** are most potent at the PI3K α isoform. The 3-hydroxyphenyl LHS substituent in compound **24b** gives an inhibitor with PI3K α selectivity ranging from 2-22-fold. Potency at PI3K α is reduced slightly compared with ZSTK474, with an IC₅₀ of 59 nM. The potency loss at each of the other isoforms is greater, with a 3-fold loss at PI3K β , 6-fold at PI3K δ , and almost 8-fold at PI3K γ (IC₅₀ values of 124, 106 and 1293 nM, respectively). When the hydroxy group is extended out by the introduction of a methylene linker in compound **24a**, selectivity between the Class IA isoforms is lost, and the selectivity against PI3K γ is reduced from 22 to 15-fold. The potency at PI3K α is similar to that of ZSTK474, with an IC₅₀ of 41 nM. Similar potency was observed at the PI3K β and δ isoforms, a 2-fold improvement compared with compound **24b** (IC₅₀ values of 56 and 45 nM, respectively). Potency at PI3K γ also improves about 2-fold (IC₅₀ of 625 nM), giving compound **24a** 15-fold selectivity against PI3K γ .

Although these two compounds show only modest selectivity towards the PI3K α isoform, it is possible that if coupled with appropriate changes in the rest of the molecule, these two affinity pocket binding moieties may lead to the development of a PI3K α selective inhibitor. As with the

methoxy substitutions discussed in Section 3.2, PI3K γ is again the most affected by these affinity pocket binding changes.

When we evaluated the RHS modified compounds **25a-f**, these analogues showed fairly modest changes in potency compared with ZSTK474, but some interesting differences in selectivity. Compounds were generally most potent at PI3K δ , closely followed by PI3K α . Selectivity against PI3K β was most affected by these modifications.

Compound **25a**, with a 3-(R)-piperidinylcarboxyl RHS substituent, was essentially a pan-PI3K inhibitor with no greater than 2-fold selectivity between the isoforms. It showed a 5-fold loss of potency at PI3K α compared with ZSTK474, with an IC₅₀ of 183 nM. An even greater 10-fold potency loss was observed at PI3K β and δ , giving IC₅₀ values of 428 and 163 nM, respectively. The change in potency at PI3K γ was more modest, giving an IC₅₀ of 247 nM.

When the chirality of the carboxyl substituent at the 3-position of the piperidinyl ring is changed from R to S in compound **25b**, an overall increase in potency is observed, giving an inhibitor with dual selectivity for PI3K α and δ . At PI3K α , **25b** is approximately equipotent to ZSTK474 with an IC₅₀ of 40 nM. The potency is similar at PI3K δ , with an IC₅₀ value of 42 nM. Potency at PI3K β and γ is about 5-fold lower with IC₅₀ values of 215 and 231 nM, respectively. A comparison between the R and S carboxyl configuration reveals the S-configuration is favoured over the R at each of the Class I isoforms except PI3K γ , for which the stereoisomers show similar IC₅₀ values.

When the carboxyl group is moved from the 3-position to the 4-position of the piperidinyl ring in compound **25c**, an almost 4-fold increase in potency at PI3K γ is observed (IC₅₀ of 64 nM), while maintaining potency at PI3K α , β and δ , with IC₅₀ values of 76, 217 and 38 nM, respectively. This results in an inhibitor with 3-5-fold selectivity against PI3K β . When the 4-piperidinylcarboxyl is replaced with a 4-carboxamide in compound **25d**, PI3K γ is again most

affected, with a decrease in potency by about five-fold compared with **25c** (IC_{50} of 304 nM). The carboxyl to carboxamide substitution has little effect on potency at PI3K α , β and δ , with IC_{50} values of 65, 165 and 35 nM, respectively.

When an 1-(ethylsulfonyl)piperazinyl substituent was introduced in compound **25e**, selectivity over the PI3K β and PI3K γ isoforms was observed. Compound **25e** was most potent at PI3K δ (IC_{50} of 69 nM). Potency at PI3K α was similar with an IC_{50} of 100 nM, a decrease compared with ZSTK474 of almost 3-fold. It showed a 5-10-fold selectivity against PI3K β and γ (IC_{50} values of 697 and 465 nM, respectively). Compound **25f** bearing a 1-(2-furoyl)piperazinyl substituent, was the most potent and PI3K δ selective compound tested with an IC_{50} of 33 nM, showing 3-fold selectivity over PI3K α and PI3K β , and almost 20-fold selectivity against PI3K γ .

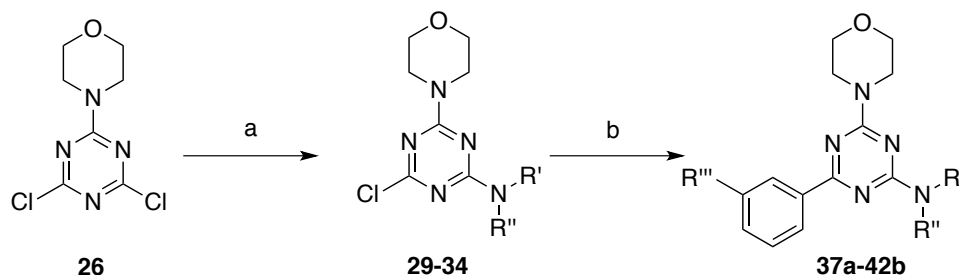
This series of RHS substitutions has displayed interesting selectivity, particularly against the PI3K β and γ isoforms. PI3K β was most affected by the introduction of a 1-(ethylsulfonyl)piperazinyl substituent (**25e**), showing an 18-fold reduction in potency compared with ZSTK474. PI3K γ showed almost a 3-fold increase in potency compared with ZSTK474 when a 4-piperidinylcarboxyl substituent was introduced (**25c**), and a 4-fold decrease in potency when this was switched for a 1-(2-furoyl)piperazinyl group (**25f**). These inhibitors were generally most potent at PI3K α and δ .

3.4 Further derivatisation of ZSTK474 analogues

Given the interesting selectivity profiles of the RHS derivatives **25a-f**, and particularly their selectivity against PI3K β , we hypothesised that the combination of these six RHS substituents with the phenolic and hydroxymethylphenyl LHS substituents might result in further increases in PI3K α selectivity.

3.4.1 Synthesis

The synthesis of these twelve new derivatives **37a-42b** began in a similar manner to the previous series of ZSTK474 analogues with a substitution of the morpholinyltriazine **26**. This was then followed by a Suzuki coupling reaction to install the aromatic moiety (Scheme 3.3).



Scheme 3.3: Synthesis of ZSTK474 analogues. (a) amine, K_2CO_3 , 25°C ; (b) boronic acid, $\text{Pd}(\text{OAc})_2$, TBAB, PCy_3 , Cs_2CO_3 , DMF, 150°C , MW, 30 minutes. Specific compounds and substituents are detailed in Table 3.6.

A series of key intermediates were synthesised by the amination of **26** at room temperature in DMF over 4 hours in the presence of potassium carbonate which afforded the diaminomonochloro-1,3,5-triazines (**29-34**) in yields from 76-96%. For compounds **32** and **33**, water was added to precipitate the desired pure product with no further purification required. For carboxylic acid containing intermediates **29-31**, this was varied by addition of hydrochloric acid to precipitate the desired product. The 1-(2-furoyl)piperazinyl derivative **34** did not precipitate, so the mixture was extracted with ethyl acetate, dried over sodium sulfate and evaporated under reduced pressure to give the pure desired product.

The correct parent ion for each of the intermediates was found by LCMS (Table 3.5). The ^1H -NMR spectra corresponded well to the expected products. The morpholinyl protons all appear as two multiplets around 3.80-3.60 ppm (for example in compound **29**: 3.82-3.76 and 3.74-3.68 ppm). The ^1H -NMR spectra for the piperidinyl compounds **29-32** are similar with the piperidinyl proton signals generally appearing as broadened multiplets between 4.50-1.50 ppm. The spectrum for **32** has two broad singlets at 5.44 and 5.29 ppm from the two amide protons. The

^1H -NMR signals for the piperazinyl protons overlap with the morpholinyl protons in **33** and **34**. Compound **33** shows characteristic ethyl quartet and triplet signals at 2.97 ($J = 7.4$ Hz) and 1.38 ppm ($J = 7.4$ Hz), respectively. The spectrum for **34** includes three aromatic proton resonances at 7.50, 7.07 and 6.51 ppm, corresponding to the furanyl protons.

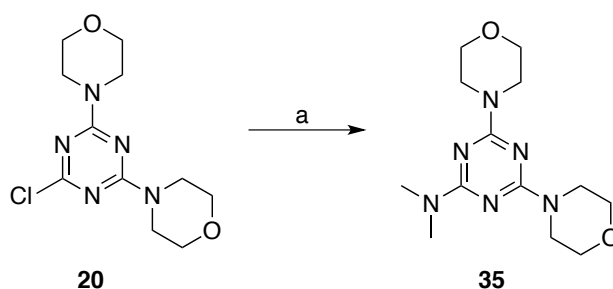
Table 3.5: Yields of key intermediates **29-34**

Compound	Amine	Yield	LCMS (m/z) [MH] ⁺
29	(R)-nipecotic acid	76%	328.1
30	(S)-nipecotic acid	99%	328.1
31	Isonipecotic acid	78%	328.2
32	Isonipecotamide	95%	327.2
33	1-(ethylsulfonyl)piperazine	78%	377.1
34	1-(2-furoyl)piperazine	96%	379.2

The final step was a Suzuki coupling reaction to install the aryl substituent (Scheme 3.3). Reactions were first performed using palladium (II) acetate, tetra-*n*-butylammonium bromide (TBAB) and tricyclohexylphosphine (PCy_3) for the catalyst, and caesium chloride as the base, in DMF under microwave heating at 150°C for 30 minutes. This method had been developed previously in our group with yields ranging from 24-88%.¹²

However, for this series of compounds, low yields were obtained under these conditions. This was due to significant formation (approximately 50%) of a side product that was difficult to resolve from the desired product by column chromatography. As a result, purification for derivatives **38b**, **39a-b**, **40b** and **42a-b** was achieved via reverse-phase semi-preparative HPLC. Analysis by LCMS revealed that the side product had a mass-to-charge ratio consistent with a

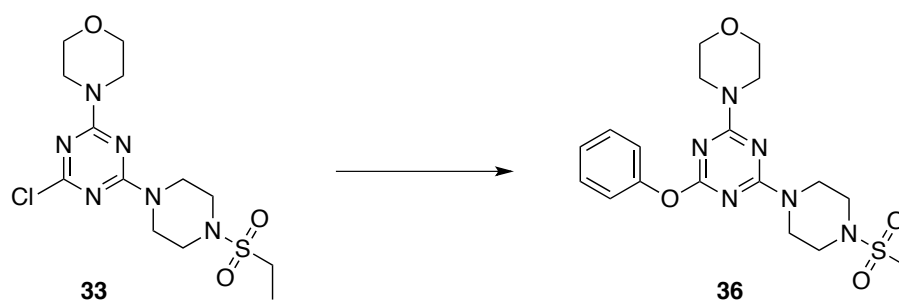
mass increase of 9 units compared with the relevant triazine intermediate (**30-32** or **34**). It was suspected that dimethylamine, a degradation product of DMF, was reacting at the 6-position of the triazine to form the dimethylamine substituted product. This reaction was competing with the Suzuki reaction. It was found that increasing the equivalents of boronic acid resulted in increased yields (compounds **38a** and **40a**), in agreement with the hypothesised side-reaction. To confirm the identity of the side product, 6-chloro-2,4-dimorpholino-1,3,5-triazine **20** was reacted under the same Suzuki reaction conditions in DMF without the boronic acid (Scheme 3.4). The isolated product **35** had a mass-to-charge ratio of 295, consistent with the dimethylamine substitution product ($[MH]^+$). The 1H -NMR revealed two multiplet resonances (3.77-3.74 and 3.72-3.68 ppm) indicative of the sixteen morpholinyl protons. A singlet at 3.09 ppm is consistent with the dimethylamine protons. The ^{13}C -NMR spectrum is also consistent with the product. Two resonances at 67.1 and 43.9 ppm are consistent with the morpholinyl carbons, and a signal at 36.2 ppm is consistent with the methyl carbons. To avoid formation of the side product, DMF was replaced by 1,4-dioxane, which resulted in greatly increased yields and simpler purification by column chromatography.³²



Scheme 3.4: Proposed side product. (a) $Pd(OAc)_2$, TBAB, PCy_3 , Cs_2CO_3 , DMF, $150^\circ C$, MW, 30 minutes

The use of 3-hydroxyphenylboronic acid posed another challenge. In the synthesis of compound **41b** in 1,4-dioxane, a different, also significant side-product was identified. This was isolated by column chromatography and is thought to be the aromatic ether, **36** (Scheme 3.5). The parent ion in the LCMS is 435, identical to that of the desired compound **41b**. The 1H -NMR

has two multiplet signals in the aromatic region at 7.38-7.33 and 7.22-7.14 ppm in a ratio of 2:3, respectively. These signals are consistent with the proposed structure of **36**. The signals for the morpholinyl, piperazinyl and ethylsulfonamide protons are similar to those observed in the spectrum of the desired product, compound **41b**. This ether was difficult to separate from the desired product and generally resulted in lower yields for these derivatives, even after the solvent was switched to 1,4-dioxane (**37b** and **41b**). For future analogues, protection of the hydroxyl group should result in increased yields and improved purification.



Scheme 3.5: Proposed side product formed in the reaction of **33** with 3-hydroxyphenylboronic acid.

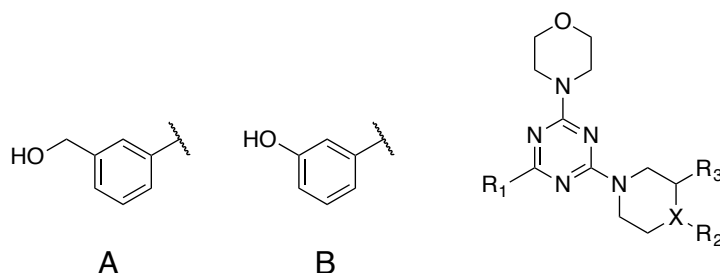
A total of twelve derivatives were synthesised by this method (Table 3.6). Characterisation was initially achieved by LCMS, with the correct parent ion identified for each of the compounds. HRMS provided further evidence of the desired product.

^1H -NMR and ^{13}C -NMR spectra were all consistent with the structures. As a representative example, the ^1H -NMR spectrum of compound **38a** reveals four aromatic proton resonances at 8.39, 8.29, 7.53-7.46 and 7.41 ppm from the four phenyl protons. The methylene protons next to the hydroxyl group appear as a singlet at 4.67 ppm. The morpholinyl protons appear as a broad singlet and multiplet at 3.91 and 3.79-3.68 ppm, respectively. The two axial piperidinyl protons on C2 and C6 appear as a multiplet at 5.20-4.87 ppm. The two equatorial protons ($\text{H}_{2\text{eq}}$ and $\text{H}_{6\text{eq}}$) appear at 3.01-2.91 and 2.85 ppm. The methine proton appears as a multiplet at 2.35-2.26 ppm. The remaining piperidinyl protons on C3 and C5 appear as four resonances at 2.14, 1.80

and 1.75-1.64 and 1.59-1.43 ppm. The ^{13}C -NMR spectrum contains the correct number of signals in line with the expected structure.

The aromatic region in the ^1H -NMR spectra of the other eleven compounds is very similar to that of compound **38a** with four aromatic proton resonances from the *meta*-substituted phenyl ring. The spectra for compounds **42a** and **42b** include signals for the three furanyl protons (**42a**: 7.54-7.51, 7.11 and 6.53 ppm; **42b**: 7.72, 7.10 and 6.61 ppm). The morpholinyl proton signals in each of the compounds appear in a similar fashion to that of compound **38a**. The piperidinyl proton signals for compounds **37a-b** and **38b** are similar to those observed in **38a**. In **37a** and **37b**, the signal for two of the piperidinyl protons was obscured by residual proteo-solvent peaks. Notably, there was only one set of signals for these derivatives, unlike the 2-difluoromethylbenzimidazole substituted derivatives **25a** and **25b**. For the four 4-substituted piperidinyl compounds, **39a-b** and **40a-b**, the piperidinyl proton signals are similar. As an example, the axial protons on C2 and C6 for compound **39b** appear as a doublet at 4.67 ppm ($J = 13.4$ Hz), while the two equatorial protons appear as a triplet 3.24 ppm ($J = 11.6$ Hz). The methine proton appears as a multiplet at 2.72-2.63 ppm. The remaining four protons appear as two multiplets, each representing two protons, 2.09-1.98 and 1.77-1.64 ppm. In compound **40a**, the amide protons appear as singlets at 7.31 and 6.80 ppm. The spectrum for **40b** was run in deuterated methanol, and so signals for the exchangeable amide protons are not evident. A quartet ($J = 7.4$ Hz) at 2.98 ppm and a triplet ($J = 7.4$ Hz) at 1.39 ppm, characteristic of the ethyl protons, were observed in the 1-(ethylsulfonyl)piperazinyl substituted compounds, **41a** and **41b**.

Table 3.6: Yields and characterisation of ZSTK474 analogues. Unless otherwise indicated, Suzuki conditions were 1.3 equivalents boronic acid, Pd(OAc)₂, TBAB, PCy₃, Cs₂CO₃ in DMF. *Compounds were synthesised with 1,4-dioxane as solvent; **2.6 equivalents boronic acid was used.



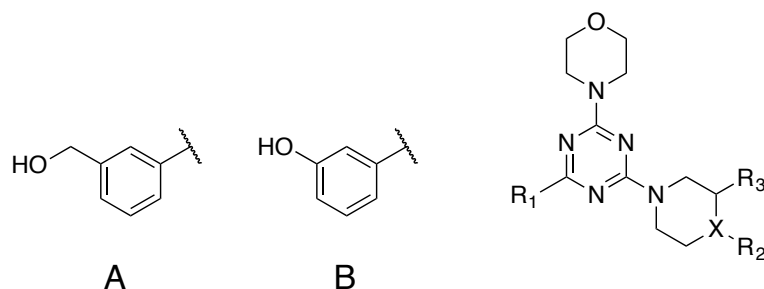
Compound	R ₁	X	R ₂	R ₃	Yield	LCMS (m/z) [MH] ⁺	HRMS (m/z) [MH] ⁺
37a	A	C	H	COOH (R)	72%*	400.1	Calc'd 400.1979 Found 400.1975
37b	B	C	H	COOH (R)	16%*	386.1	Calc'd 386.1823 Found 386.1832
38a	A	C	H	COOH (S)	70%**	400.2	Calc'd 400.1979 Found 400.1984
38b	B	C	H	COOH (S)	21%	386.2	Calc'd 386.1823 Found 386.1834
39a	A	C	COOH	H	9%	400.1	Calc'd 400.1979 Found 400.1983
39b	B	C	COOH	H	15%	386.1	Calc'd 386.1823 Found 386.1806
40a	A	C	CONH ₂	H	33%**	399.3	Calc'd 399.2139 Found 399.2129
40b	B	C	CONH ₂	H	12%	385.1	Calc'd 385.1983 Found 385.1979
41a	A	N	SO ₂ CH ₂ CH ₃	H	74%*	449.1	Calc'd 449.1966 Found 449.1977
41b	B	N	SO ₂ CH ₂ CH ₃	H	16%*	435.1	Calc'd 435.1809 Found 435.1830
42a	A	N		H	47%	451.2	Calc'd 451.2088 Found 451.2086
42b	B	N		H	5%	437.1	Calc'd 437.1932 Found 437.1942

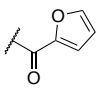
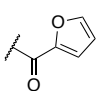
^{13}C -NMR spectra also showed appropriate resonances for each of the compounds. The low yields for compounds **38b**, **40b**, **41b** and **42b** meant that not all quaternary carbon signals were observed, despite increasing the number of scans. However, remaining signals were all consistent with the expected products, and coupled with ^1H -NMR and HRMS data, firmly support the identity of the synthesised products.

3.4.2 Evaluation of ZSTK474 derivatives

Each of the synthesised analogues was tested against the four Class I PI3K isoforms using the Kinase-Glo® assay described in Section 3.3.2. The results are shown in Table 3.7. A range of potencies and selectivity profiles were observed. Overall, the substitution of the 2-difluoromethylbenzimidazole for a hydroxy-substituted phenyl group resulted in a decrease in potency at PI3K α . The potency loss was generally greater at the other isoforms, and so these changes resulted in increased PI3K α selectivity for these compounds compared with ZSTK474.

When the 3-(R)-piperidinylcarboxyl substituent was combined with a 3-hydroxymethylphenyl substituent in compound **37a**, 3-6-fold selectivity for PI3K α and δ was observed. Unfortunately, this was coupled with more than 10-fold drop in potency at PI3K α compared (IC₅₀ of 411 nM) with ZSTK474. Potency at PI3K δ was similar with an IC₅₀ of 433 nM. When the same RHS substituent was combined with a 3-hydroxyphenyl LHS substituent in compound **37b**, there was an increase of selectivity for PI3K α , showing 2-9-fold selectivity against the other isoforms. This was accompanied with a further decrease in potency at PI3K α , with an IC₅₀ of 567 nM. This is a greater than 16-fold loss of potency compared with ZSTK474. Potency at PI3K β and γ dropped a further 2-fold compared with **37a**, giving IC₅₀ values of 2810 and 4950 nM, respectively.

Table 3.7: Evaluation of ZSTK474 analogues. All IC₅₀ values are the mean of at least three independent experiments.

Compound	R ₁	X	R ₂	R ₃	IC ₅₀ (nM)			
					PI3K α	PI3K β	PI3K γ	PI3K δ
37a	A	C	H	COOH (R)	411	1180	2460	433
37b	B	C	H	COOH (R)	567	2810	4950	1290
38a	A	C	H	COOH (S)	811	3050	>100,000	1820
38b	B	C	H	COOH (S)	477	1660	>50,000	800
39a	A	C	COOH	H	350	2020	>10,000	786
39b	B	C	COOH	H	614	6400	35,000	2410
40a	A	C	CONH ₂	H	249	939	>50,000	563
40b	B	C	CONH ₂	H	292	1220	>10,000	454
41a	A	N	SO ₂ CH ₂ CH ₃	H	128	552	1880	201
41b	B	N	SO ₂ CH ₂ CH ₃	H	252	1950	>10,000	566
42a	A	N		H	51	70	4920	32
42b	B	N		H	74	71	2880	80

Compound **38a**, which combined the 3-(S)-piperidinylcarboxyl group with a 3-hydroxymethylphenyl substituent, was most potent at the PI3K α isoform, and showed greater than 100-fold selectivity against PI3K γ . Unfortunately, a 23-fold loss of potency at PI3K α (IC₅₀ of

811 nM) compared with ZSTK474 was observed. This was coupled with even greater losses of potency at the other isoforms, with IC_{50} values of 3050 and 1820 nM for PI3K β and PI3K δ , respectively, and greater than 100,000 nM for PI3K γ . This same RHS substituent could be combined with a 3-hydroxyphenyl in compound **38b** to give a similar selectivity profile with an overall 2-fold increase in potency at Class IA isoforms (PI3K α IC_{50} of 477 nM). No significant inhibition of PI3K γ was observed at limits of solubility.

When the carboxyl group was moved around the piperidinyll ring to the 4-position and combined with a 3-hydroxymethylphenyl substituent as in compound **39a**, PI3K α selectivity of 2 to at least 30-fold was observed. A 10-fold loss in PI3K α potency compared with ZSTK474 was observed, giving an IC_{50} value of 350 nM. Potency at PI3K δ was 2-fold lower, with an IC_{50} of 786 nM. Compound **39a** shows about 6-fold selectivity for PI3K α over PI3K β , with an IC_{50} of 2020 nM. No PI3K γ inhibition was seen at concentrations up to 10,000 nM. The change to a 3-hydroxyphenyl LHS substituent in compound **39b** displayed increased PI3K α selectivity, but with an accompanying decrease in potency. PI3K α potency was decreased by about 2-fold, giving an IC_{50} of 614 nM. About 3-fold reduction in potency was observed against PI3K β and PI3K δ , giving IC_{50} values of 6400 and 2410 nM, respectively. PI3K γ had an IC_{50} of 35,000 nM. This results in PI3K α selectivity of 4-fold over PI3K δ , 10-fold over PI3K β and 57-fold over PI3K γ . Compound **39b** showed the best selectivity for PI3K α over both PI3K β and δ compared with other inhibitors in this series, whilst also maintaining good selectivity over PI3K γ .

When the 4-carboxyl was changed to a carboxamide, the compounds showed an increase in potency at each of the Class IA isoforms, with a loss of selectivity for PI3K α . PI3K γ inhibition could not be measured in either of the compounds. Compound **40a**, which combined the 4-piperidinylcarboxamide RHS substituent with a 3-hydroxymethylphenyl LHS substituent, showed a 7-fold decrease in potency compared with ZSTK474, with an IC_{50} of 249 nM. It was

almost 4-fold less potent at PI3K β , with an IC₅₀ value of 939 nM, and about 2-fold less potent at PI3K δ , with an IC₅₀ value of 563 nM. When the same RHS substituent was combined with the 3-hydroxyphenyl LHS substituent in compound **40b**, similar potency was observed at each of the four isoforms.

The piperazinyl RHS substituents were generally more potent at PI3K α than the piperidinyl ones. The compound **41a**, which combined a 1-(ethylsulfonamide)piperazinyl substituent with a 3-hydroxymethylphenyl substituent, had 4-15-fold selectivity for PI3K α and δ . It was most potent at PI3K α with an IC₅₀ value of 128 nM, which is only a 3.5-fold loss of potency compared with ZSTK474. Potency at PI3K δ was slightly less, with an IC₅₀ of 201 nM. Four-fold selectivity over PI3K β was observed, with an IC₅₀ of 552 nM. Compound **41a** was least potent at PI3K γ , with an IC₅₀ of 1880 nM. This gives almost 15-fold selectivity for PI3K α over PI3K γ . When the 3-hydroxyphenyl LHS substituent was introduced in compound **41b**, a general increase in selectivity but decrease in potency was observed. The potency loss was least at PI3K α , showing a 2-fold loss and IC₅₀ value of 252 nM. PI3K β and PI3K δ showed approximately 3-fold loss of potency, giving IC₅₀ values of 1950 and 566 nM, respectively. The IC₅₀ value PI3K γ was greater than 10,000 nM and unable to be determined. This gave a PI3K α inhibitor with approximately 8-fold selectivity of PI3K β , at least 40-fold over PI3K γ and 2-fold selectivity over PI3K δ .

The most potent PI3K α inhibitor of this series was compound **42a**, which combined a 1-(2-furoyl)piperazine substitution with a 3-hydroxymethylphenyl. It had 100-fold selectivity against PI3K γ (IC₅₀ of 4920 nM). The PI3K α IC₅₀ was 51 nM, similar in potency to ZSTK474. The IC₅₀ values at PI3K β and δ were also similar, 70 and 32 nM, respectively. When the LHS substituent was changed to a 3-hydroxyphenyl in compound **42b**, the PI3K α IC₅₀ was about 2-fold less than ZSTK474, at 74 nM. Similar potencies were seen at PI3K β and δ , with IC₅₀ values of 71 and 80 nM, respectively. Compound **42b** showed about 40-fold selectivity against PI3K γ .

The most significant feature of this series of compounds is the gain in selectivity against PI3K γ . In the original benzimidazole substituted series of compounds **25a-f**, the selectivity for PI3K α over γ ranged from 0.8-6-fold. The two phenyl substituted compounds, **24a** and **24b** showed a modest increase in selectivity for PI3K α over PI3K γ of 15-20-fold. However, when these RHS and LHS substitutions were combined in compounds **37-42**, PI3K α selectivity over PI3K γ ranged from 6 to more than 200-fold. Because many of the PI3K γ IC₅₀ values were too high to be measured, it is not possible to find a clear trend for which of the two LHS substituents is most disfavoured at PI3K γ . For the two 3-(R)-piperidinylcarboxyl compounds, **37a** and **37b**, only 2-fold difference in potency is seen at PI3K γ , with the 3-hydroxymethylphenyl compound showing superior potency. There is a significant difference, however, in the potency of the two ethylsulfonamide derivatives at PI3K γ . The IC₅₀ for the 3-hydroxymethylphenyl compound, **41a** is 1880 nM, while the IC₅₀ for the 3-hydroxyphenyl compound, **41b**, could not be measured at concentrations up to 10,000 nM.

A comparison of the 3-hydroxyphenyl with the 3-hydroxymethylphenyl sub-series of compounds reveals that the 3-hydroxyphenyl compounds have a generally higher selectivity for PI3K α over both PI3K β and δ . This trend is in line with the data from the parent compounds. Compound **24b**, the 3-hydroxyphenyl substituted compound, has a 2-fold selectivity for PI3K α over both PI3K β and δ ; whereas compound **24a**, which contains the 3-hydroxymethylphenyl, is essentially equipotent at the three isoforms.

The loss of inhibitory potency in this series was disappointing. At first glance, this could be interpreted as signifying the two substituted phenyl rings are not ideal LHS substituents. However, this disappointment is tempered when looking at the two 1-(2-furoyl)piperazine substituted compounds, **42a** and **42b**. The similar potency in these compounds to the parent piperazinyl compound, **25f**, suggests that the potency loss in this series is not a direct effect of the LHS phenyl substituents. The different affinity pocket binding moiety presumably alters the

binding conformation of the inhibitor within the ATP-binding site, causing some of the RHS substitutions to either pick up unfavourable interactions or lose favourable ones in the phenyl-substituted series of compounds.

Overall, these data suggest that the 3-hydroxyphenyl substituent is a reasonable choice for an affinity pocket binding moiety in the design of a PI3K α selective inhibitor. However, this substituent is likely to be a metabolic liability *in vivo*. Further improvements to potency and selectivity would require tuning of the RHS substituent to pick up appropriate PI3K α selective interactions with the non-conserved Region 1 amino acids.

When coupled with the 2-difluoromethylbenzimidazole, the S-configuration of the 3-piperidinylcarboxyl was favoured with higher potency at each of the four isoforms. Interestingly, the stereochemistry made little difference at the PI3K γ isoform in the benzimidazole compounds, **25a** and **25b**. In the phenyl series, the biggest difference is seen at the PI3K γ isoform. The R-configuration in compounds **37a** and **37b** gave IC₅₀ values of 2460 and 4950 nM, whereas the IC₅₀ values could not be measured in the two S-configuration compounds, **38a** and **38b** at concentrations up to 50,000 nM. An explanation for this is not immediately apparent. Insights from computational work and potential explanations for this observation will be discussed in the next section.

Both the ethylsulfonamide and 4-piperidinylcarboxyl moieties have good selectivity for PI3K α over PI3K β . Compound **41b** shows almost 8-fold selectivity for PI3K α over PI3K β , with PI3K α potency of 252 nM. This is concordant with the 7-fold selectivity for PI3K α over PI3K β observed in the parent compound **25e**. In this case, therefore, there has not been a significant increase in selectivity over PI3K β through the introduction of the 3-hydroxyphenyl RHS substituent. Compound **39b** has almost 10-fold selectivity for PI3K α over PI3K β , which is an improvement over that in the 4-piperidinylcarboxyl parent compound, **25c**, which only

displayed 3-fold selectivity. The 3-hydroxyphenyl RHS substituent seems to have the capacity to influence selectivity between PI3K α and β , however this is obviously greatly dependent on the nature of the LHS substituent.

PI3K α and δ have proven the most difficult isoforms to differentiate between in these series of compounds. In the initial series of benzimidazole-substituted analogues **25a-f**, compounds were generally 1-2-fold more potent at PI3K δ than PI3K α . This trend has been changed in the phenyl-substituted series, with compounds generally showing 2-4-fold higher potency at PI3K α compared with PI3K δ . Progress has been made that has increased the PI3K α selectivity of these compounds, although a lot of work needs to be done in order to increase this selectivity further.

Overall, these results show the complexities involved in achieving isoform selectivity. The LHS and RHS substituents work together to position the inhibitor within the binding site and influence the interactions it makes with each isoform. The changes made in this series have increased the overall PI3K α selectivity of the inhibitors, however, this has been at the cost of potency. Significant selectivity for PI3K α over PI3K γ has been achieved with quite simple changes. Greater selectivity for PI3K α over PI3K β has also been achieved, with compound **39b** showing almost 10-fold selectivity. Unfortunately, selectivity over PI3K δ was more difficult to obtain, so more work needs to be done on the differences between these isoforms to differentiate them structurally.

3.4.3 Docking investigation into compounds **37b**, **38b** and **41a-b**

In order to investigate at a structural level the differences in potency and selectivity observed in these inhibitors, each of the inhibitors was docked into the p110 γ (PDB ID: 3DBS) crystal structures using Glide from within the Maestro software suite by Schrödinger.³³⁻³⁵ The software samples a large number of inhibitor conformations within a static protein structure, evaluating each docked pose against a scoring function, which incorporates the effects of

hydrophobic interactions, hydrogen bonds and charge-charge interactions. The docked poses of the inhibitors are then ranked, and the best ones selected based on the scoring function.^{34,35} Docking has certainly played an important role in high throughput screening campaigns and the discovery of novel inhibitor scaffolds.^{36,37} However, it has a few limitations. The first limitation is the use of static protein structures, which maximises computational efficiency. Proteins are inherently flexible, and will make structural adjustments to accommodate inhibitor binding. Docking with static protein structures is unable to account for this flexibility. Although flexible protein docking algorithms do exist, these take significantly more computational time.^{38,39} Secondly, while reasonable binding modes can often be found using docking, the scoring functions struggle to accurately predict the ranked potency of the docked analogues.^{40,41} This was also true of this study (see Appendix 2-3). The results discussed in this section, therefore, are based upon the predicted binding mode of the inhibitors rather than the ranking based on scoring function. We have used docking to attempt to provide structural explanations for specific questions raised by the assay results.

The first question we sought to address with docking was the difference in potency at the PI3K γ isoform observed between the two 3-piperidinylcarboxyl substituted stereoisomers, compounds **37b** and **38b**. As discussed in the above section, the compound with the R-stereochemistry, **37b**, has an IC₅₀ value of 4950 nM at PI3K γ , while the compound with the S-stereochemistry, **38b** has no measurable inhibition of PI3K γ at concentrations up to 50,000 nM.

When docked into the p110 γ structure, compound **37b** binds with the morpholine oxygen making the expected hydrogen bond interaction with the backbone amide of Val882 (Figure 3.6). The 3-hydroxyphenyl ring binds in the affinity pocket, with the hydroxyl group making hydrogen bond interactions with Tyr867 and Asp841. This is the same binding mode predicted for compound **24b** (data not shown). The carboxyl group is in the axial position and is able to make an ionic interaction with Lys807 and a hydrogen bond interaction with Asn951. The

carboxyl group is positioned 3.6 and 3.9 Å away from the carboxyl groups of Asp950 and Asp964, respectively. If compound **37b** indeed binds in this mode, these close aspartate residues may result in some repulsive charge-charge interactions and contribute to the low potency, despite many favourable interactions.

Compound **38b** binds in a very similar pose, with the morpholine and 3-hydroxyphenyl rings making the same interactions with the protein. The position of the carboxyl group is different, now being positioned equatorially on the piperidine ring. It is still able to make an ionic interaction with Lys807. Due to the conformation of the carboxyl group, the hydrogen bond with Asn951 is now absent. The distances to the carboxyl groups on Asp950 and Asp964 are now 4.2 and 4.9 Å, lessening any charge-charge repulsion effects. The absence of the hydrogen bond to Asn951 certainly accounts for a lower potency of compound **38b**, but it fails to account for the complete lack of inhibition observed, given the compound is still predicted to make the ionic interaction with Lys807. The major difference between the two predicted binding modes is the axial or equatorial conformation of the carboxyl group on the piperidine ring. Predicting the stability of different conformations of these substituted piperidines is complex. Nipecotic acid prefers the carboxyl group in an axial position, as it is then able to make intra-molecular charge-charge zwitterionic interactions between the carboxyl and the piperidine nitrogen.⁴² However, in the triazine conjugated piperazine, protonation of the nitrogen is unlikely, and therefore the zwitterionic stabilisation doubtful. Neither of these docked poses position the carboxyl such that it can form these intramolecular interactions. It is possible that there is an energy barrier involved in the conversion between these two conformations, and the axial conformation of the S-stereoisomer may not be able to bind thus forcing the equatorial conformation. This provides some limited rationale for understanding the dramatic differences in potency observed at PI3K γ between the two stereoisomers. These binding modes would ultimately require confirmation

with X-ray crystal structures of the ligands bound to p110 γ , however, they provide some insight into how the conformation of binding groups can influence potency.

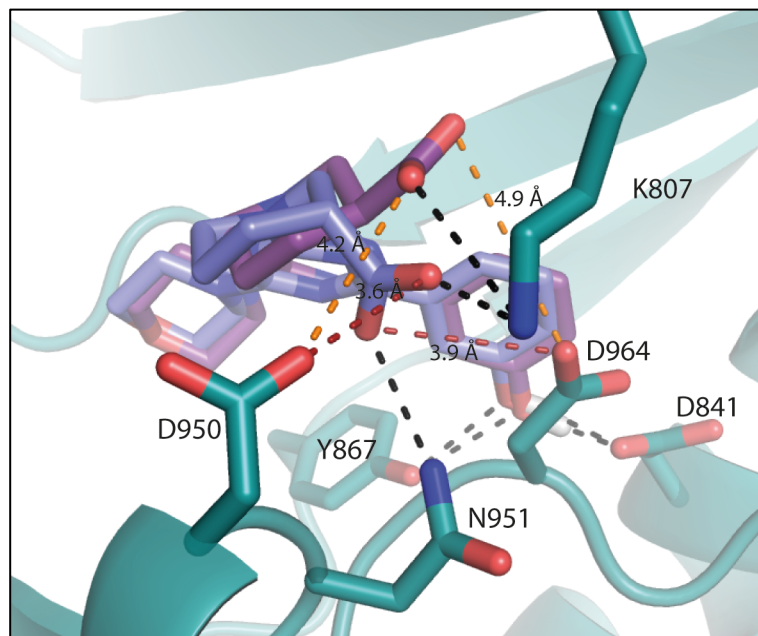


Figure 3.6: Compound **37b** (light purple) and compound **38b** (dark purple) docked into p110 γ (PDB ID: 3DBS). Hydrogen bonds are shown in black dashed lines. Specific distances discussed in the text are highlighted in red for compound **37b** and orange for compound **38b**.

The second question we attempted to answer with docking was the difference in PI3K γ potency between compounds **41a** and **41b**. Compound **41a** has 1-(ethylsulfonamide)piperidinyl substituent at the RHS, with a 3-hydroxyphenyl substituent at the LHS, and inhibits PI3K γ with an IC₅₀ of 1880 nM. Compound **41b** has the same ethylsulfonamide RHS substituent, but is instead coupled to a 3-hydroxymethylphenyl substituent at the LHS and fails to inhibit PI3K γ at concentrations up to 10,000 nM. We wished to investigate whether docking was able to provide insight into why the simple introduction of a methylene linker could so dramatically alter the potency at PI3K γ .

Docking compound **41a** in p110 γ predicts the morpholinyl oxygen will form a hydrogen bond at the hinge region with the backbone of Val882 (Figure 3.7). The substituted phenyl ring

binds in the affinity pocket, with the hydroxyl group predicted to form a hydrogen bond with Asp836. The sulfonyl group is positioned 3.1 Å from the carboxyl of Asp950, possibly resulting in a small degree of repulsion between the two electronegative atoms.

The core of compound **41b** binds in the same manner. The *meta*-hydroxy group is oriented within the affinity pocket to form hydrogen bonds with Tyr867 and Asp841, much in the same manner as compounds **37b** and **38b**. The sulfonyl group is positioned differently with the ethyl group oriented towards Ala805 on the P-loop, but the two oxygen atoms are not within interacting distance of any residues. It is not at all clear from these binding modes why compound **41b** would be so much less potent than compound **41a** at inhibiting PI3K γ . Unfortunately, in this case, docking has failed to provide reasonable structural explanations for how small changes in the inhibitor structure can result in such large differences in potency at PI3K γ .

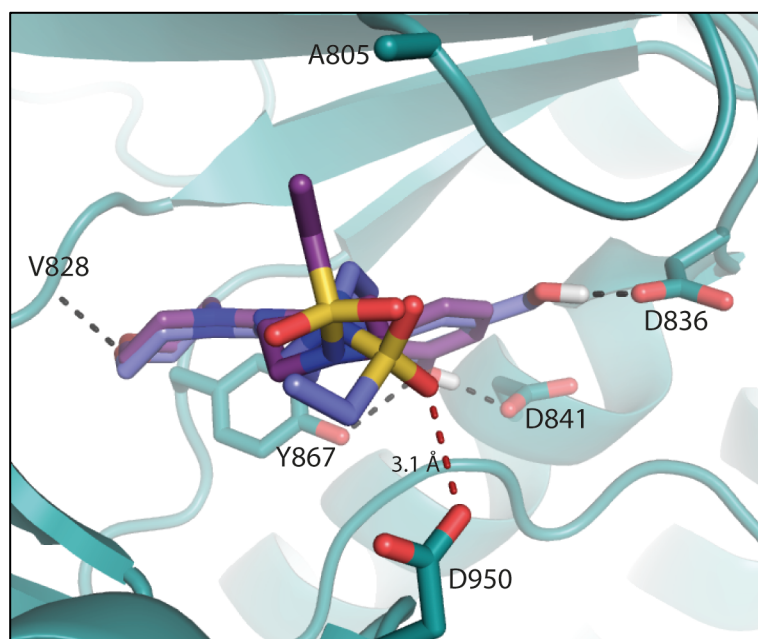


Figure 3.7: Compounds **41a** (light purple) and **41b** (dark purple) docked into p110 γ (PDB ID: 3DBS). Hydrogen bonds are represented as black dashed lines. Distances discussed in the text are highlighted in red.

3.5 Conclusions

This chapter has described the synthesis and biochemical evaluation of 28 analogues of ZSTK474 against the Class I PI3K isoforms to identify features that might influence isoform selectivity. More specifically compounds were assessed to probe the effect of interactions within the conserved affinity pocket. Substitutions at the benzimidazole group were made, or the group replaced by a substituted phenyl ring alone or in combination with replacements for one of the morpholinyl groups. The resultant effect on potency and selectivity for PI3K can be added to the SAR and selectivity studies of this type reported elsewhere.

In the first phase of the work, an efficient, regioselective synthetic method was developed which allows access to 5- and 6-substituted benzimidazole derivatives of ZSTK474, substitutions that had been neglected in other studies. These results add to the SAR of previously reported 4- and 4,6- benzimidazole substitutions.¹⁰ Although the methoxy substitutions used resulted in an overall decrease in potency at PI3K α , this synthetic method would now allow ready access to alternative 5- or 6-substitutions, like halogens or hydrogen bond donors, which may be able to pick up selective interactions in the affinity pocket. In particular, it was noted that the methoxy substitution had a dramatically negative impact on potency at the PI3K γ isoform. As such, substitutions at the 6-position may be a suitable method to dial out PI3K γ inhibition.

In the second phase of this work, alternatives to the benzimidazole substituent were investigated. The 3-hydroxyphenyl substituent was identified as a better affinity pocket binding moiety for the development of PI3K α selective inhibitors than the 2-difluoromethylbenzimidazole. Overall, the compounds with this substituent (**37-42**) showed a greater preference for the PI3K α isoform than those with the 2-difluoromethylbenzimidazole substituent (**25a-f**). Changes were particularly dramatic in the inhibitory potency at PI3K γ , where many of the phenyl-substituted compounds had little to no inhibition at concentrations

up to 10,000 nM. It appears that these selectivity effects are influenced by both LHS and RHS substituents. Our data emphasises the multi-faceted problem of designing an isoform selective inhibitor. Each aspect or binding moiety of the inhibitor must be optimised concurrently both with respect to potency and selectivity.

By combining a hydroxyphenyl substituent with a 4-piperidinylcarboxyl substituent, we were able to synthesise a novel inhibitor (**39b**) with 4-57-fold selectivity for the PI3K α isoform. Unfortunately, this selectivity was achieved at the expense of potency, with the inhibitor, compound **39b** showing an IC₅₀ of only 614 nM at PI3K α . A potent inhibitor, compound **42a** with similar potency to ZSTK474 at the three Class IA isoforms, but more than 70-fold selectivity against PI3K γ was also identified.

Taken together, the results from this chapter particularly highlight the sensitivity of PI3K γ to substitutions in the affinity pocket-binding region of the inhibitors. One possible structural explanation for this is the presence of a tyrosine residue (p110 γ Tyr787) situated behind the affinity pocket, where each of the other isoforms has a leucine residue. This significant difference in bulk surrounding the affinity pocket may affect its flexibility and ability to accommodate various substitutions. Just as the specificity pocket discussed in Chapter 1 confers selectivity for PI3K β and δ , so the affinity pocket appears to be an important consideration for the design of inhibitors with selectivity for or against PI3K γ .^{13,15,43}

3.6 References

- (1) Verdonk, M. L.; Hartshorn, M. J. Structure-guided fragment screening for lead discovery. *Curr. Opin. Drug Discov. Devel.* **2004**, *7*, 404–410.
- (2) Hughes, J.; Rees, S.; Kalindjian, S.; Philpott, K. Principles of early drug discovery. *Br. J. Pharmacol.* **2011**, *162*, 1239–1249.
- (3) McInnes, C. Virtual screening strategies in drug discovery. *Curr. Opin. Chem. Biol.* **2007**, *11*, 494–502.
- (4) Bruce, I.; Akhlaq, M.; Bloomfield, G. C.; Budd, E.; Cox, B.; Cuenoud, B.; Finan, P.; Gedeck, P.; Hatto, J.; Hayler, J. F.; Head, D.; Keller, T.; Kirman, L.; Leblanc, C.; Grand, D. L.; McCarthy, C.; O'Connor, D.; Owen, C.; Oza, M. S.; Pilgrim, G.; Press, N. E.; Sviridenko, L.; Whitehead, L. Development of isoform selective PI3-kinase inhibitors as pharmacological tools for elucidating the PI3K pathway. *Bioorg. Med. Chem. Lett.* **2012**, *22*, 5445–5450.
- (5) Certal, V.; Halley, F.; Virone-Oddos, A.; Thompson, F.; Filoche-Rommé, B.; El-Ahmad, Y.; Carry, J.-C.; Delorme, C.; Karlsson, A.; Abecassis, P.-Y.; Vincent, L.; Bonnevaux, H.; Nicolas, J.-P.; Morales, R.; Michot, N.; Vade, I.; Louboutin, A.; Perron, S.; Doerflinger, G.; Tric, B.; Monget, S.; Lengauer, C.; Schio, L. Preparation and optimization of new 4-(morpholin-4-yl)- (6-oxo-1,6-dihydropyrimidin-2-yl)amide derivatives as PI3K β inhibitors. *Bioorg. Med. Chem. Lett.* **2012**, *22*, 6381–6384.
- (6) Certal, V.; Halley, F.; Virone-Oddos, A.; Delorme, C.; Karlsson, A.; Rak, A.; Thompson, F.; Filoche-Rommé, B.; El-Ahmad, Y.; Carry, J.-C.; Abecassis, P.-Y.; Lejeune, P.; Vincent, L.; Bonnevaux, H.; Nicolas, J.-P.; Bertrand, T.; Marquette, J.-P.; Michot, N.; Benard, T.; Below, P.; Vade, I.; Chatreaux, F.; Lebourg, G.; Pilorge, F.; Angouillant-Boniface, O.; Louboutin, A.; Lengauer, C.; Schio, L. Discovery and Optimization of New Benzimidazole- and Benzoxazole-Pyrimidone Selective PI3K β Inhibitors for the Treatment of Phosphatase and TENsin homologue (PTEN)-Deficient Cancers. *J. Med. Chem.* **2012**, *55*, 4788–4805.
- (7) Frazzetto, M.; Suphioglu, C.; Zhu, J.; Schmidt-Kittler, O.; Jennings, I. G.; Cranmer, S. L.; Jackson, S. P.; Kinzler, K. W.; Vogelstein, B.; Thompson, P. E. Dissecting Isoform Selectivity of PI3 Kinase Inhibitors. The Role of Non-conserved Residues in the Catalytic Pocket. *Biochem. J.* **2008**, *414*, 383–390.
- (8) Zheng, Z.; Amran, S. I.; Thompson, P. E.; Jennings, I. G. Isoform-Selective Inhibition of Phosphoinositide 3-Kinase: Identification of a New Region of Nonconserved Amino Acids Critical for p110 α Inhibition. *Mol. Pharmacol.* **2011**, *80*, 657–664.
- (9) Zheng, Z.; Amran, S. I.; Zhu, J.; Schmidt-Kittler, O.; Kinzler, K. W.; Vogelstein, B.; Shepherd, P. R.; Thompson, P. E.; Jennings, I. G. Definition of the binding mode of a new class of phosphoinositide 3-kinase α -selective inhibitors using in vitro mutagenesis of non-conserved amino acids and kinetic analysis. *Biochem. J.* **2012**, *444*, 529–535.
- (10) Rewcastle, G. W.; Gamage, S. A.; Flanagan, J. U.; Frederick, R.; Denny, W. A.; Baguley, B. C.; Kestell, P.; Singh, R.; Kendall, J. D.; Marshall, E. S.; Lill, C. L.; Lee, W.-J.; Kolekar, S.; Buchanan, C. M.; Jamieson, S. M. F.; Shepherd, P. R. Synthesis and Biological Evaluation of Novel Analogues of the Pan Class I Phosphatidylinositol 3-Kinase (PI3K) Inhibitor 2-

- (Difluoromethyl)-1-[4,6-di(4-morpholinyl)-1,3,5-triazin-2-yl]-1H-benzimidazole (ZSTK474). *J. Med. Chem.* **2011**, *54*, 7105–7126.
- (11) Rossi, R.; Bellina, F.; Lessi, M. Selective Palladium-Catalyzed Suzuki–Miyaura Reactions of Polyhalogenated Heteroarenes. *Adv. Synth. Catal.* **2012**, *354*, 1181–1255.
- (12) Pinson, J.-A. PI3 Kinase and inhibitors: Targeting isoform selectivity. PhD Dissertation, Monash University, 2011.
- (13) Berndt, A.; Miller, S.; Williams, O.; Le, D. D.; Houseman, B. T.; Pacold, J. I.; Gorrec, F.; Hon, W.-C.; Liu, Y.; Rommel, C.; Gaillard, P.; Rückle, T.; Schwarz, M. K.; Shokat, K. M.; Shaw, J. P.; Williams, R. L. The p110 δ structure: mechanisms for selectivity and potency of new PI(3)K inhibitors. *Nat. Chem. Biol.* **2010**, *6*, 117–124.
- (14) Williams, O.; Houseman, B. T.; Kunkel, E. J.; Aizenstein, B.; Hoffman, R.; Knight, Z. A.; Shokat, K. M. Discovery of Dual Inhibitors of the Immune Cell PI3Ks p110 δ and p110 γ : a Prototype for New Anti-inflammatory Drugs. *Chem. Biol.* **2010**, *17*, 123–134.
- (15) Knight, Z. A.; Gonzalez, B.; Feldman, M. E.; Zunder, E. R.; Goldenberg, D. D.; Williams, O.; Loewith, R.; Stokoe, D.; Balla, A.; Toth, B.; Balla, T.; Weiss, W. A.; Williams, R. L.; Shokat, K. M. A Pharmacological Map of the PI3-K Family Defines a Role for p110 α in Insulin Signaling. *Cell* **2006**, *125*, 733–747.
- (16) Sutherlin, D. P.; Baker, S.; Bisconte, A.; Blaney, P. M.; Brown, A.; Chan, B. K.; Chantry, D.; Castanedo, G.; DePledge, P.; Goldsmith, P.; Goldstein, D. M.; Hancox, T.; Kaur, J.; Knowles, D.; Kondru, R.; Lesnick, J.; Lucas, M. C.; Lewis, C.; Murray, J.; Nadin, A. J.; Nonomiya, J.; Pang, J.; Pegg, N.; Price, S.; Reif, K.; Safina, B. S.; Salphati, L.; Staben, S.; Seward, E. M.; Shuttleworth, S.; Sohal, S.; Sweeney, Z. K.; Ultsch, M.; Waszkowycz, B.; Wei, B. Potent and selective inhibitors of PI3K δ : Obtaining isoform selectivity from the affinity pocket and tryptophan shelf. *Bioorg. Med. Chem. Lett.* **2012**, *22*, 4296–4302.
- (17) Matsuno, T.; Kato, M.; Sasahara, H.; Watanabe, T.; Inaba, M.; Takahashi, M.; Yaguchi, S.; Yoshioka, K.; Sakato, M.; Kawashima, S. Synthesis and Antitumor Activity of Benzimidazolyl-1, 3, 5-triazine and Benzimidazolylpyrimidine Derivatives. *Chem. Pharm. Bull.* **2000**, *48*, 1778–1781.
- (18) Rewcastle, G. W.; Gamage, S. A.; Flanagan, J. U.; Kendall, J. D.; Denny, W. A.; Baguley, B. C.; Buchanan, C. M.; Chao, M.; Kestell, P.; Kolekar, S.; Lee, W.-J.; Lill, C. L.; Malik, A.; Singh, R.; Jamieson, S. M. F.; Shepherd, P. R. Synthesis and biological evaluation of novel phosphatidylinositol 3-kinase inhibitors: Solubilized 4-substituted benzimidazole analogs of 2-(difluoromethyl)-1-[4,6-di(4-morpholinyl)-1,3,5-triazin-2-yl]-1H-benzimidazole (ZSTK474). *Eur. J. Med. Chem.* **2013**, *64*, 137–147.
- (19) Clark, M. A.; Acharya, R. A.; Arico-Muendel, C. C.; Belyanskaya, S. L.; Benjamin, D. R.; Carlson, N. R.; Centrella, P. A.; Chiu, C. H.; Creaser, S. P.; Cuozzo, J. W.; Davie, C. P.; Ding, Y.; Franklin, G. J.; Franzen, K. D.; Gefter, M. L.; Hale, S. P.; Hansen, N. J. V.; Israel, D. I.; Jiang, J.; Kavarana, M. J.; Kelley, M. S.; Kollmann, C. S.; Li, F.; Lind, K.; Mataruse, S.; Medeiros, P. F.; Messer, J. A.; Myers, P.; O’Keefe, H.; Oliff, M. C.; Rise, C. E.; Satz, A. L.; Skinner, S. R.; Svendsen, J. L.; Tang, L.; van Vloten, K.; Wagner, R. W.; Yao, G.; Zhao, B.; Morgan, B. A. Design, synthesis and selection of DNA-encoded small-molecule libraries. *Nat. Chem. Biol.* **2009**, *5*, 647–654.

-
- (20) Marone, R.; Cmiljanovic, V.; Giese, B.; Wymann, M. P. Targeting phosphoinositide 3-kinase—Moving towards therapy. *Biochim. Biophys. Acta* **2008**, *1784*, 159–185.
- (21) Kong, D.; Yamori, T. Advances in development of phosphatidylinositol 3-kinase inhibitors. *Curr. Med. Chem.* **2009**, *16*, 2839–2854.
- (22) Wu, P.; Liu, T.; Hu, Y. PI3K inhibitors for cancer therapy: what has been achieved so far? *Curr. Med. Chem.* **2009**, *16*, 916–930.
- (23) Sutherlin, D. P.; Sampath, D.; Berry, M.; Castanedo, G.; Chang, Z.; Chuckowree, I.; Dotson, J.; Folkes, A.; Friedman, L.; Goldsmith, R.; Heffron, T.; Lee, L.; Lesnick, J.; Lewis, C.; Mathieu, S.; Nonomiya, J.; Olivero, A.; Pang, J.; Prior, W. W.; Salphati, L.; Sideris, S.; Tian, Q.; Tsui, V.; Wan, N. C.; Wang, S.; Wiesmann, C.; Wong, S.; Zhu, B.-Y. Discovery of (Thienopyrimidin-2-yl)aminopyrimidines as Potent, Selective, and Orally Available Pan-PI3-Kinase and Dual Pan-PI3-Kinase/mTOR Inhibitors for the Treatment of Cancer. *J. Med. Chem.* **2010**, *53*, 1086–1097.
- (24) Morales, G. A.; Garlich, J. R.; Su, J.; Peng, X.; Newblom, J.; Weber, K.; Durden, D. L. Synthesis and Cancer Stem Cell-Based Activity of Substituted 5-Morpholino-7H-thieno[3,2-b]pyran-7-ones Designed as Next Generation PI3K Inhibitors. *J. Med. Chem.* **2013**, *56*, 1922–1939.
- (25) Scharn, D.; Wenschuh, H.; Reineke, U.; Schneider-Mergener, J.; Germeroth, L. Spatially addressed synthesis of amino- and amino-oxy-substituted 1,3,5-triazine arrays on polymeric membranes. *J. Comb. Chem.* **2000**, *2*, 361–369.
- (26) Chen, Z.; Venkatesan, A. M.; Santos, O. D.; Santos, E. D.; Dehnhardt, C. M.; Ayral-Kaloustian, S.; Ashcroft, J.; McDonalod, L. A.; Mansour, T. S. Stereoselective Synthesis of an Active Metabolite of the Potent PI3 Kinase Inhibitor PKI-179. *J. Org. Chem* **2010**, *75*, 1643–1651.
- (27) Dong, C.-M.; Chen, L.-G.; Duan, X.-M.; Shu, X.-G.; Zeng, T.; Yan, X.-L. 2,4-Dichloro-6-morpholino-1,3,5-triazine. *Acta Crystallogr.* **2005**, *E61*, o1168–o1169.
- (28) Sunduru, N.; Sharma, M.; Srivastava, K.; Rajakumar, S.; Puri, S. K.; Saxena, J. K.; Chauhan, P. M. S. Synthesis of oxalamide and triazine derivatives as a novel class of hybrid 4-aminoquinoline with potent antiplasmodial activity. *Bioorg. Med. Chem.* **2009**, *17*, 6451–6462.
- (29) Haruta, K.; Yaguchi, S.; Matsuno, T.; Tsuchida, Y.; Watanabe, T.; Yoshioka, K.; Yui, R. Immunosuppressive Agent and Anti-Tumor Agent Comprising Heterocyclic Compound as Active Ingredient. WO2006095906 (A1), September 14, 2006.
- (30) Pinson, J.-A.; Zheng, Z.; Miller, M. S.; Chalmers, D. K.; Jennings, I. G.; Thompson, P. E. L-Aminoacyl-triazine Derivatives Are Isoform-Selective PI3K β Inhibitors That Target Nonconserved Asp862 of PI3K β . *ACS Med. Chem. Lett.* **2013**, *4*, 206–210.
- (31) Kong, D.; Yamori, T. ZSTK474 is an ATP-competitive inhibitor of class I phosphatidylinositol 3 kinase isoforms. *Cancer Sci.* **2007**, *98*, 1638–1642.
- (32) Bedford, R. B.; Butts, C. P.; Hurst, T. E.; Lidström, P. The Suzuki Coupling of Aryl Chlorides under Microwave Heating. *Adv. Synth. Catal.* **2004**, *346*, 1627–1630.
- (33) Folkes, A. J.; Ahmadi, K.; Alderton, W. K.; Alix, S.; Baker, S. J.; Box, G.; Chuckowree, I. S.; Clarke, P. A.; Depledge, P.; Eccles, S. A.; Friedman, L. S.; Hayes, A.; Hancox, T. C.;

- Kugendradas, A.; Lensun, L.; Morre, P.; Olivero, A. G.; Pang, J.; Patel, S.; Pergl-Wilson, G. H.; Raynaud, F. L.; Robson, A.; Saghir, N.; Salphati, L.; Sohal, S.; Ultsch, M. H.; Valenti, M.; Wallweber, H. J. A.; Wan, N. C.; Wiesmann, C.; Workman, P.; Zhyvoloup, A.; Zvelebil, M. J.; Shuttleworth, S. J. The identification of 2-(1H-indazol-4-yl)-6-(4-methanesulfonyl-piperazin-1-ylmethyl)-4-morpholin-4-yl-thieno[3,2-d]pyrimidine (GDC-0941) as a potent, selective, orally bioavailable inhibitor of class I PI3 Kinase for the treatment of cancer. *J. Med. Chem.* **2008**, *51*, 5522–5532.
- (34) Friesner, R. A.; Banks, J. L.; Murphy, R. B.; Halgren, T. A.; Klicic, J. J.; Mainz, D. T.; Repasky, M. P.; Knoll, E. H.; Shelley, M.; Perry, J. K.; Shaw, D. E.; Francis, P.; Shenkin, P. S. Glide: A New Approach for Rapid, Accurate Docking and Scoring. 1. Method and Assessment of Docking Accuracy. *J. Med. Chem.* **2004**, *47*, 1739–1749.
- (35) Friesner, R. A.; Murphy, R. B.; Repasky, M. P.; Frye, L. L.; Greenwood, J. R.; Halgren, T. A.; Sanschagrin, P. C.; Mainz, D. T. Extra Precision Glide: Docking and Scoring Incorporating a Model of Hydrophobic Enclosure for Protein-Ligand Complexes. *J. Med. Chem.* **2006**, *49*, 6177–6196.
- (36) Halgren, T. A.; Murphy, R. B.; Friesner, R. A.; Beard, H. S.; Frye, L. L.; Pollard, W. T.; Banks, J. L. Glide: A New Approach for Rapid, Accurate Docking and Scoring. 2. Enrichment Factors in Database Screening. *J. Med. Chem.* **2004**, *47*, 1750–1759.
- (37) Villoutreix, B. O.; Eudes, R.; Miteva, M. A. Structure-based virtual ligand screening: recent success stories. *Comb. Chem. High Throughput Screen.* **2009**, *12*, 1000–1016.
- (38) E. M. Krovat; T. Steindl; T. Langer Recent Advances in Docking and Scoring. *Curr. Comput. Aided Drug Des.* **2005**, *1*, 93–102.
- (39) Sherman, W.; Day, T.; Jacobson, M. P.; Friesner, R. A.; Farid, R. Novel Procedure for Modeling Ligand/Receptor Induced Fit Effects. *J. Med. Chem.* **2006**, *49*, 534–553.
- (40) David, L.; Nielsen, P. A.; Hedstrom, M.; Norden, B. Scope and Limitation of Ligand Docking: Methods, Scoring Functions and Protein Targets. *Curr. Comput. Aided Drug Des.* **2005**, *1*, 275–306.
- (41) Pinson, J.-A.; Schmidt-Kittler, O.; Zhu, J.; Jennings, I. G.; Kinzler, K. W.; Vogelstein, B.; Chalmers, D. K.; Thompson, P. E. Thiazolidinedione-Based PI3K α Inhibitors: An Analysis of Biochemical and Virtual Screening Methods. *ChemMedChem* **2011**, *6*, 514–522.
- (42) Abraham, R. J.; Aboitiz, N.; Merrett, J.; Sherborne, B.; Whitcombe, I. Conformational analysis. Part 34. An NMR investigation of the conformational equilibrium and intramolecular hydrogen bonding in nipecotic acid derivatives. *J. Chem. Soc., Perkin Trans. 2* **2000**, 2382–2392.
- (43) Zheng, Z.; Miller, M. S.; Jennings, I. G.; Thompson, P. E. Mechanisms of PI3K β -Selective Inhibition Revealed by Reciprocal Mutagenesis. *ACS Chem. Biol.* **2013**, *8*, 679–683.

Chapter 4: Dipeptide analogues of ZSTK474 targeting non-conserved region 1 residues

4.1 Introduction

Chapter 3 described the synthesis and evaluation of ZSTK474 analogues, with a focus on replacement of the difluoromethylbenzimidazole moiety. Some of these analogues were found to show improved selectivity for PI3K α , but this was accompanied by a significant loss in potency, highlighting both the sensitivity of the affinity pocket to such changes and the multi-faceted complexities of inhibitor selectivity. Having explored the effect of interactions within the conserved affinity pocket, we wished now to investigate an alternative design approach, namely, targeting the non-conserved residues in Region 1 and specifically p110 α Gln859.

Specific interactions with the non-conserved residue p110 α Gln859, which is an aspartate, lysine and asparagine residue in PI3K β , γ and δ , respectively, have been shown to be important for the PI3K α selectivity of a family of related aminothiazole compounds. Computational models,

confirmed by site-directed mutagenesis, have implicated a specific interaction between the carboxamide group and p110 α Gln859 in the PI3K α selectivity of the Novartis inhibitor, A-66 **15** (Figure 4.1, Figure 4.2a).^{1,2} As discussed in Chapter 3, Bruce *et al.* from Novartis published a report of the optimisation of a non selective aminothiazole lead compound into PI3K α , γ and δ selective inhibitors.³ Their parallel synthesis campaign identified a terminal carboxamide group as being essential for PI3K α selectivity, presumably due to similar interactions with Gln859 as for A-66.³ More recently, a report detailed the medicinal chemistry development of the closely related PI3K α selective inhibitor currently in Phase I/II clinical trials, NVP-BYL719 **6** (Figure 4.1).⁴ An unreleased crystal structure of PI3K α in complex with NVP-BYL719 has confirmed its interaction with Gln859.⁴

The analogous residue in PI3K β , Asp862, has been implicated in the PI3K β selectivity of a novel series of aminoacyl-triazine derivatives based on ZSTK474 described by our group.⁵ In this inhibitor series, one of the morpholine groups of ZSTK474 was replaced by a piperazine ring and coupled to various amino acids, leaving a terminal amino group (Figure 4.1). Interestingly, when a glycine residue was coupled to the piperazine ring (**16a**), the inhibitor displayed dual selectivity for PI3K β and δ . When this was substituted for a L-phenylalanine residue, the selectivity shifted towards PI3K β . Theoretical molecular docking studies of compound **16** suggested the amino group was forming charged interactions with p110 β Asp862 (Figure 4.2b). Site-directed mutagenesis data corroborated this prediction.⁵ These charged interactions cannot be formed in the other isoforms.

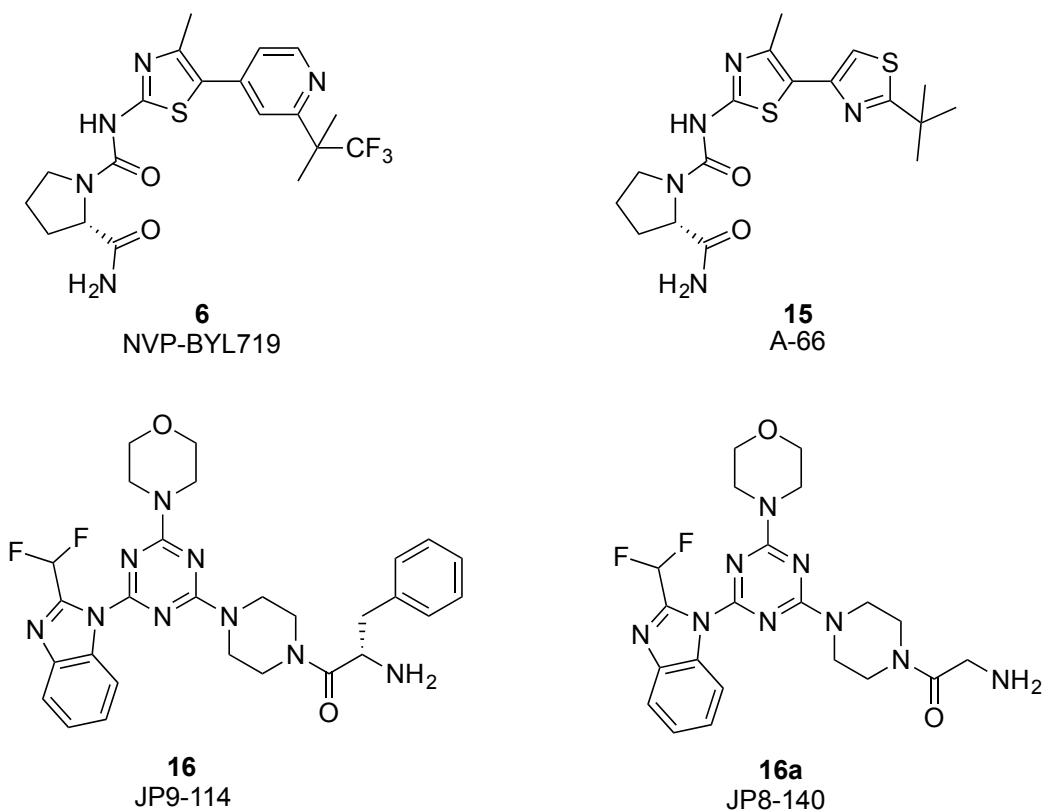


Figure 4.1: Inhibitor structures

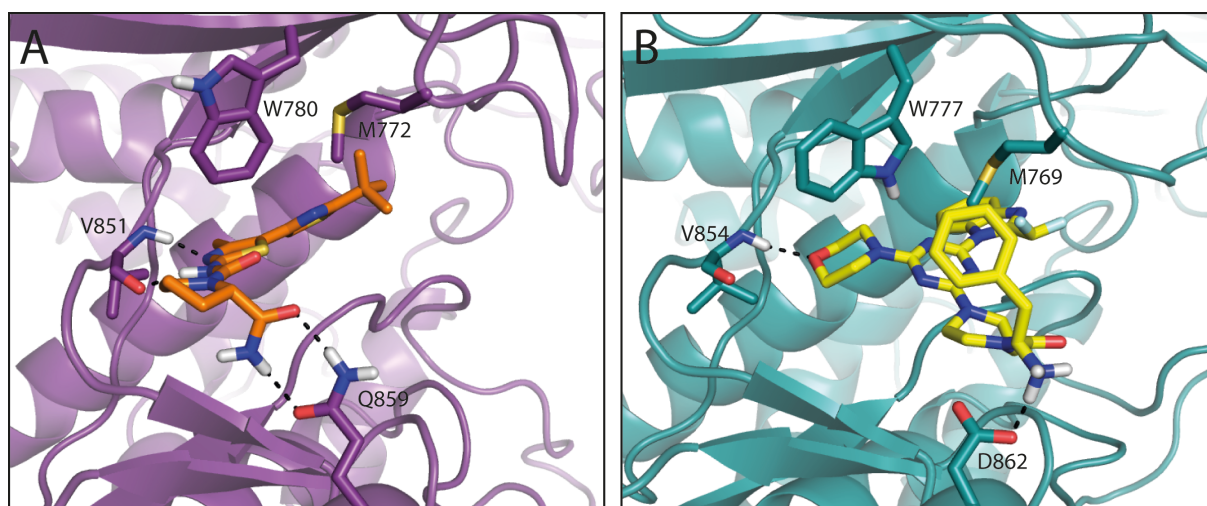


Figure 4.2: A) Homology model of p110 α and docked binding pose of A-66 **15** highlighting the interaction with Gln859¹ B) JP9-114 **16** docked into the crystal structure of p110 β (PDB ID: 2Y3A).⁵

4.1.1 Aims

The reports above have provided rationalisation of both PI3K α and β inhibitor selectivity based on key interactions with non-conserved Region 1 residues. Building on these results, we sought to explore a rational and perhaps general design approach to generate isoform selectivity based on targeting this non-conserved region. In particular, in a similar manner to the aminothiazole inhibitors, we considered that a terminal carboxamide group appended to the ZSTK474 core structure might have the ability to interact selectively with Gln859 of PI3K α or the equivalent non-conserved residue in PI3K δ , Asn836. This chapter describes the synthesis and evaluation of these derivatives.

4.2 Synthesis of dipeptide derivatives

In a similar manner to the aminoacyl-triazine derivatives, we chose to keep the morpholine and 2-difluoromethylbenzimidazole substituents of ZSTK474 constant in this series of PI3K inhibitors.⁵ We replaced the remaining morpholine group with various dipeptide amides. We envisaged that the terminal carboxamide would be able to interact with p110 α Gln859 in a similar manner to the aminothiazoles.¹⁻⁴ The starting point for the conjugation of amino acid amides were the three piperidinylcarboxylic acid analogues described in Chapter 3, **25a**, **25b** and **25f** (Figure 4.3). In the series of aminoacyl-triazine PI3K β inhibitors described above, the most discernible effect in both potency and selectivity was seen with glycinylpiperazine and L-phenylalaninylpiperazine substituents. Analogously, we attached a glycine and L-phenylalanine amides to these three carboxylate linkers to assess the effect of each on potency and selectivity. We later selected the 4-piperidinylcarboxylic acid linker to investigate the effect of other amino acid substitutions on selectivity and potency.

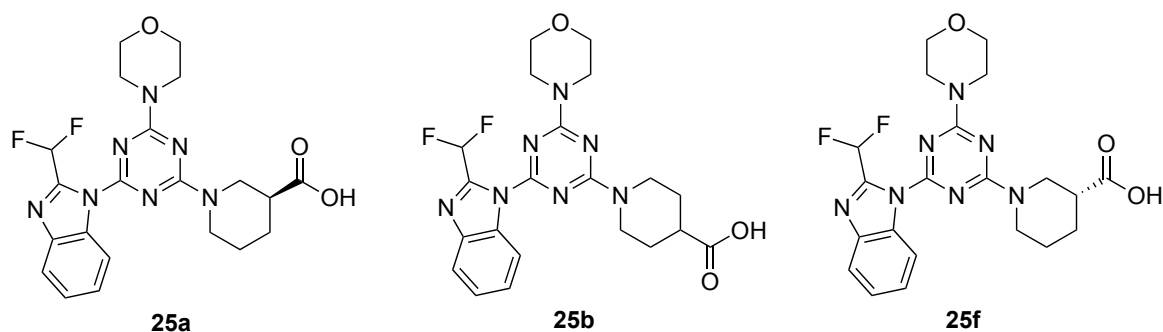
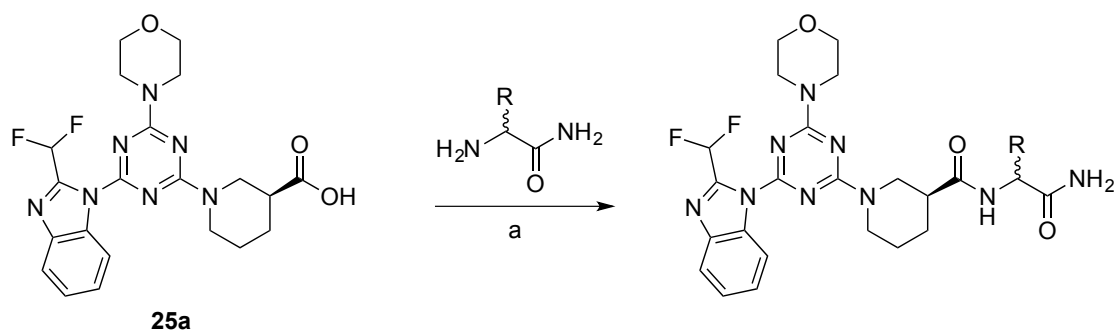
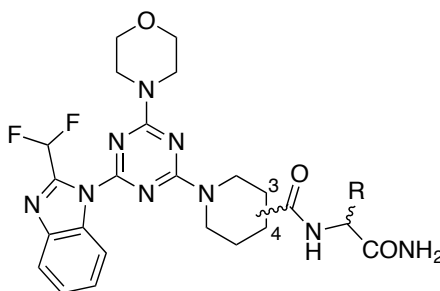


Figure 4.3: Structures of the three piperidinylcarboxyl derivatives used to conjugate to amino acid amides.

The synthesis of these compounds was achieved by the reaction of the key carboxylic acid intermediates described in Chapter 3, **25a**, **25b** or **25f** with amino carboxamides under peptide coupling conditions with HBTU and DIPEA in DMF (Scheme 4.1). Upon addition of water to the reaction mixture, the product precipitated in high purity as determined by LCMS, HPLC and NMR. A total of 10 derivatives were synthesised using this approach (Table 4.1).

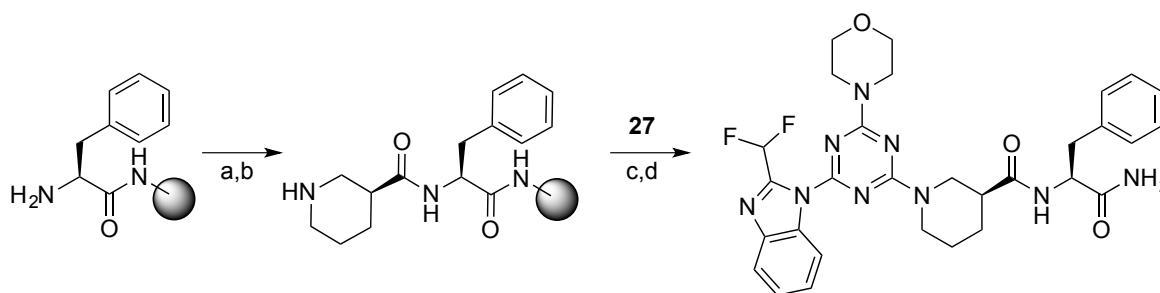


Scheme 4.1: Solution-phase synthesis of ZSTK474 dipeptide analogues. a. HBTU, DIPEA, DMF

Table 4.1: Yields of ZSTK474 dipeptide derivatives

Compound	Linker Position (chirality)	R (chirality)	Yield	HRMS (m/z) [MH] ⁺
43	4	H	67%	Calc'd 516.2278 Found 516.2279
44	4	CH ₂ Ph (S)	63%	Calc'd 606.2747 Found 606.2754
45	3 (S)	H	63%	Calc'd 516.2278 Found 516.2291
46	3 (S)	CH ₂ Ph (S)	68%	Calc'd 606.2747 Found 606.2743
47	3 (R)	H	27%	Calc'd 516.2278 Found 516.2282
48	3 (R)	CH ₂ Ph (S)	88%	Calc'd 606.2747 Found 606.2745
49	4	CH ₃ (S)	28%	Calc'd 530.2434 Found 530.2438
50	4	CH ₃ (R)	35%	Calc'd 530.2434 Found 530.2437
51	4	CH ₂ OH (S)	63%	Calc'd 546.2383 Found 546.2393
52	4	CH(CH ₃) ₂ (S)	44%	Calc'd 558.2747 Found 558.2747

The use of a solid-phase approach amenable to parallel synthesis was also examined using the L-phenylalanine derivative, compound **46**, as an example. The dipeptide units were constructed on Rink Amide resin using standard Fmoc solid-phase peptide synthesis protocols. The dipeptide-resin was then treated with an excess of the key monochloro intermediate **27** with potassium carbonate in DMF at elevated temperatures under microwave heating (Scheme 4.2). Trifluoroacetic acid (TFA) cleavage from the resin yielded the target compound, which could be isolated by semi-preparative HPLC purification. Initial purification was conducted using aqueous acidic HPLC buffers. Unfortunately, it was subsequently found that the difluoromethylbenzimidazole moiety was sensitive to acid-catalysed hydrolysis. Compound **46** was thus purified using TFA-free buffers. However, this limited the efficiency of purification causing low yields and thus limiting the utility of this route.



Scheme 4.2: Solid-phase synthesis of ZSTK474 dipeptide analogues. a. Fmoc-(L)-phenylalanine, HCTU, DIPEA, DMF; b. 20% piperidine in DMF; c. K₂CO₃, DMF, MW, 140°C, 30 minutes; d. 95% aq. trifluoroacetic acid.

As shown in Table 4.1, characterisation by HRMS revealed the correct parent ion for each of the ten compounds. ¹H-NMR and ¹³C-NMR spectra were also consistent with the structures of each of the compounds.

As an example, the ¹H-NMR spectrum of the L-alaninamide derivative, compound **49**, revealed four aromatic resonances at 8.34, 7.93, 7.51 and 7.44 ppm corresponding to the four protons of the benzimidazole group. A ¹H-¹³C HSQC experiment reveals these four signals correspond to the carbon signals at 115.7, 120.7, 125.8 and 124.3 ppm, respectively. The

characteristic triplet signal ($J = 53$ Hz) of the difluoromethine proton was found at 7.73 ppm. The corresponding carbon appeared as a triplet signal at 108.6 ppm ($J = 237$ Hz) in the ^{13}C -NMR. The secondary amide proton appeared as a doublet signal at 7.93 ppm ($J = 7.7$ Hz), split by the adjacent methine proton of the alanine residue. The primary amide protons appeared as two broad singlet resonances at 7.27 and 6.94 ppm. The morpholinyl protons appear as two multiplets at characteristic chemical shifts of 3.86-3.76 and 3.74-3.64 ppm, corresponding to the carbons at 43.6 and 65.9 ppm, respectively. The α -methine proton appears as a multiplet at 4.25-4.15 ppm, corresponding to the carbon at 47.9 ppm. The methyl group is coupled to this methine proton and appears as a doublet at 1.19 ppm ($J = 7.1$ Hz), with the carbon appearing at 18.5 ppm. The piperidinyl methylene protons appear as four signals at 4.64, 3.05, 1.81 and 1.54 ppm, corresponding to carbons at 43.0, 42.8 and 28.1 (2C) ppm. The piperidinyl methine proton appears as a multiplet at 2.57 ppm, and the carbon at 41.4 ppm.

The ^1H and ^{13}C -NMR spectra of the other analogues are comparable with the expected changes associated with the modified dipeptide amides. The glycine analogue compound **43** has a doublet in the ^1H -NMR spectrum at 3.62 ppm ($J = 5.8$ Hz) corresponding to the α -methylene protons. In compounds **45** and **47** the α -protons appear at 3.67 and 3.69 ppm, respectively, overlapping with the multiplet signal from the morpholinyl protons. The phenylalanine analogues, compounds **44**, **46** and **48** have additional aromatic resonances corresponding to the phenyl protons. The L-serine analogue, compound **51**, has a triplet at 4.84 ppm ($J = 5.6$ Hz) from the hydroxyl proton. The methylene protons occur as a triplet at 3.56 ppm ($J = 6.0$ Hz), while the α -methine proton is a doublet of triplets at 4.21 ppm ($J = 8.0$, 5.4 Hz). The L-valine analogue, compound **52**, has a doublet of doublet signal ($J = 9.0$, 6.6 Hz) at 4.12 ppm corresponding to the α -methine proton. The β -methine proton signal appears as a multiplet at 1.96 ppm. The two methyl group protons appear at 0.84 ppm as a triplet ($J = 6.3$ Hz). The methyl protons would be expected to appear as doublet, split by the β -methine proton. In

this case, the protons from each methyl group are presumably non-equivalent and are each represented by a doublet. These two doublets have overlapped to appear as a triplet in the spectrum.

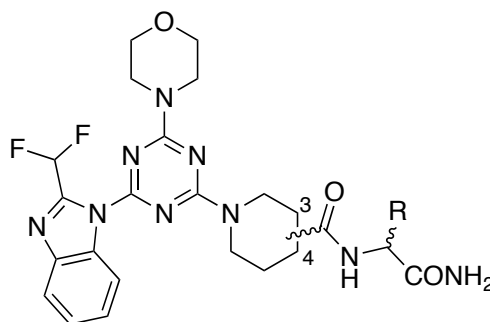
4.3 Evaluation of ZSTK474 dipeptide analogues

The compounds were assayed as inhibitors of each of the Class I PI3Ks with comparison to ZSTK474 to determine the influence of each modification, using the Kinase-Glo® assay described in Chapter 3. Overall, the influence of the substitutions on potency and selectivity were apparent and the compounds showed a range of potencies at each of the four PI3K isoforms (Table 4.2). A general trend was observed indicating selectivity for PI3K δ , or dual PI3K α and δ selectivity. This is in accordance with our hypothesis of using the terminal carboxamide to target the non-conserved residues p110 α Gln859 and p110 δ Asn836.

Firstly, we compared the three piperidinyl linkers coupled to a glycine amide. Compound **43**, with a 4-piperidinyl linker, showed dual selectivity for PI3K α and δ of about 5-7-fold over the other two isoforms. It had IC₅₀ values at PI3K α and δ of 98 and 67 nM, respectively, which is a 3-4-fold decrease compared with ZSTK474. A similar decrease in potency was observed at PI3K γ , with an IC₅₀ of 496 nM. There was a greater decrease at PI3K β of 8-fold, with an IC₅₀ of 329 nM.

Compound **45**, with a 3-(S) substituted piperidinyl linker, was the most potent of the glycine derivatives and mirrored very closely ZSTK474 itself. Compound **45** had an IC₅₀ at PI3K α of 32 nM. It had a slightly improved potency at PI3K β of 24 nM. The potency at PI3K γ and δ were similar to ZSTK474 with IC₅₀ values of 194 nM and 25 nM, respectively.

Table 4.2: Evaluation of ZSTK474 dipeptide analogues. IC₅₀ values are the mean of at least three independent experiments, each conducted in duplicate. Standard errors are all within 20% of the mean (see Appendix 1).



Compound	Linker Position (chirality)	R (chirality)	IC ₅₀ (nM)			
			PI3K α	PI3K β	PI3K γ	PI3K δ
ZSTK474			35	39	166	17
43	4	H	98	329	496	67
44	4	CH ₂ Ph (S)	190	513	708	44
45	3 (S)	H	32	24	194	25
46	3 (S)	CH ₂ Ph (S)	358	342	1983	57
47	3 (R)	H	83	166	445	38
48	3 (R)	CH ₂ Ph (S)	908	1722	1378	263
49	4	CH ₃ (S)	123	207	434	40
50	4	CH ₃ (R)	114	601	536	29
51	4	CH ₂ OH (S)	67	162	521	29
52	4	CH(CH ₃) ₂ (S)	191	602	440	144

Its stereoisomer, compound **47**, with a 3-(R) substituted piperidinyllinker, showed dual selectivity for PI3K α and δ of 4-12-fold. It had an IC₅₀ at PI3K α of 83 nM, a 2-fold decrease compared with ZSTK474. A 2-fold decrease in potency was also seen at PI3K δ , with an IC₅₀ of

38 nM. The decrease in potency was 3-4-fold at PI3K β and γ , with IC₅₀ values of 166 and 445 nM, respectively.

From these results we can see that compound **45** was the most potent of the three linker compounds, being equipotent with ZSTK474, which highlights the ability of the binding site to accommodate large substitutions at this site. As expected, differences in potency and selectivity are observed, presumably because the different linkers alter the binding conformation of the carboxamide. As with ZSTK474, each of the compounds is most potent at PI3K δ , with the exception of **45**, which is equipotent at PI3K β and δ . Little difference is seen in the selectivity between PI3K α and δ in the three derivatives and ZSTK474, however some difference is seen in the selectivity for PI3K δ over PI3K β and γ . The 3-(S)-piperidinyl linker compound **45** has no selectivity between PI3K β and δ . The 4-piperidinyl and 3-(R)-piperidinyl compounds, **43** and **47**, however have 4-5-fold selectivity against PI3K β . In the case of selectivity against PI3K γ , the 4-piperidinyl and 3-(S)-piperidinyl linker compounds **43** and **45** have selectivity of 7-8-fold, while in the 3-(R)-piperidinyl linker this selectivity is increased to 12-fold.

The next series of compounds we investigated was the L-phenylalanine substituted compounds. These compounds showed increased PI3K δ selectivity compared with the glycine analogues with a more marked drop in potency. The compound with the 4-piperidinyl linker, compound **44**, was selective for PI3K δ by 4-16-fold. In addition, it showed an increased PI3K δ potency compared with the glycine analogue, **43**, of 44 nM. This was accompanied by decreases in potency at each of the other isoforms, with IC₅₀ values of 190, 513 and 708 nM at PI3K α , β and γ , respectively.

The compound with the 3-(S) substituted piperidinyl linker, **46**, had 6-35-fold selectivity for PI3K δ , the most PI3K δ selective inhibitor in this series. It showed a 2-fold decrease in potency at PI3K δ compared with the corresponding glycine analogue, **45**, with an IC₅₀ of 57 nM. PI3K δ

selectivity was achieved via a greater drop in potency at each of the other isoforms, with IC₅₀ values of 358, 342 and 1983 nM at PI3K α , β and γ , respectively.

When an L-phenylalanine amide was linked to a 3-(R) substituted piperidinyl linker in **48**, the potency was significantly reduced across all four isoforms. It was most potent at PI3K δ , with an IC₅₀ of 263 nM, a loss of 7-fold compared with the glycine analogue, **47**. Potency losses were also observed at the other isoforms, with IC₅₀ values of 908, 1722 and 1378 nM at PI3K α , β and γ , respectively. This was greater than 10-fold loss in potency at PI3K α and β compared with the glycine analogue, but only 3-fold at PI3K γ .

The switch from the glycine to the L-phenylalanine amide increased the PI3K δ selectivity of these three analogues. Compound **46** has the best PI3K δ selectivity of all the compounds of 6-35-fold, with a reasonable potency of 57 nM. The least selective and the least potent compound was the 3-(R)-piperidinyl linker compound, **48**, with only 3-7-fold selectivity and an IC₅₀ of 263 nM. The compound **44** was most potent at PI3K δ (IC₅₀ of 44 nM), with a slightly lower selectivity over PI3K α of 4-fold. However, the selectivity over PI3K β was greater than for compound **46**, increasing from 6 to 12-fold.

It was a combination of retained potency and emerging selectivity between PI3K β and δ that led us to investigate further amino acid substitutions with the 4-piperidinyl substituted linker. Four amino acids were selected namely, L-alanine, D-alanine, L-serine and L-valine amides. These side-chains allowed us to investigate the effect of stereochemistry, polarity and steric bulk. In the PI3K β selective aminoacyl-triazine derivatives related to **16** discussed earlier, the introduction of L and D amino acids shifted the selectivity between PI3K β and δ , presumably by targeting the terminal amino group towards different non-conserved residues.⁵ We also wanted to see the effect of side-chain chirality on selectivity in this series of analogues.

The change from glycine to the alanine stereoisomers had only a marginal influence, with potency changing less than 2-fold across the board. The D-alanine derivative, **50**, was 4-11-fold selective for PI3K δ , but only the PI3K β potency seemed notably influenced by the chirality, with a decrease by 3-fold for the D-alanine derivative compared to its enantiomer. At each of the other isoforms, the potencies are similar. Such an increase in the PI3K δ selectivity (PI3K β from 5-fold to 21-fold, PI3K γ from 11 to 19-fold) with a simple change in the chirality of the methyl group may appear modest, but could prove significant upon further optimisation.

The substitution with a hydroxymethyl side chain in compound **51** resulted in an overall restoration of potency across the four isoforms. Compound **51** had an IC₅₀ of 29 nM at PI3K δ . The selectivity over PI3K α was decreased to 2-fold, with a PI3K α IC₅₀ of 67 nM. IC₅₀ values at PI3K β and γ were 162 and 521 nM, respectively.

When the L-valine derivative **52** was evaluated, a decrease in potency at the PI3K δ isoform was observed, with an IC₅₀ value of 144 nM. Potency at the PI3K α and β isoforms were similar to the L-phenylalanine derivative, 191 and 602 nM, respectively. PI3K γ potency was increased slightly at 440 nM. Neither of these two analogues showed an increase in PI3K δ selectivity, however they do reveal that the hydroxyl side-chain of **51** is preferred to the isopropyl group of the L-valine derivative, **52**.

4.4 Site-directed mutagenesis

The D-alanine analogue **50** was particularly interesting due to its specifically diminished potency at PI3K β (17-fold drop compared to ZSTK474), while potency at PI3K α and PI3K δ was less influenced. We wished to investigate further to determine whether this selectivity may be a result of disfavoured interaction with p110 β Asp862 or favoured hydrogen bonds to p110 α Gln859 and/or p110 δ Asn836.

Workers in our labs have previously produced a range of site directed mutants of PI3K α and PI3K β . The mutants at this position in PI3K α and PI3K β , p110 α Gln859Asp and p110 β Asp862Gln were selected to study the influence of mutation on the potency of compound **50** and the results compared to the wild-type. When the aspartate residue in PI3K β was mutated to a glutamine (p110 β Asp862Gln), there was a 5-fold improvement in potency compared with the wild-type, essentially restoring the potency seen in PI3K α . However, no difference in inhibition was observed when Gln859 in PI3K α was mutated to an aspartate (Table 4.3).

These results suggest that compound **50** is indeed able to interact with residues in this position. However, there appears to be a degree of flexibility or redundancy in the binding. There is a similar non-conserved residue at a nearby position, p110 α His855 and the analogous PI3K β residue, p110 β Glu858, that these inhibitors could also potentially interact with. When the glutamate is mutated to a histidine in PI3K β , a 2-fold improvement in potency is observed. However, when the histidine in PI3K α is mutated to a glutamate no decrease in potency is observed. It could be that the carboxamide is able to interact with either the histidine or glutamine such that when the residues are mutated in PI3K α no decrease in potency is seen due to redundancy in binding. However, when either of these residues is introduced in PI3K β , an accompanying increase in potency is observed.

Table 4.3: Evaluation of Compound **50** against wild-type PI3K α and β and site-directed isoform mutants. IC₅₀ values are the average of three independent experiments. Standard errors (s.e.) are reported within the table.

PI3K α Mutant	IC ₅₀ \pm S.E. (nM)	PI3K β Mutant	IC ₅₀ \pm S.E. (nM)
PI3K α wild-type	114 \pm 5	PI3K β wild-type	601 \pm 14
p110 α Gln859Asp	100 \pm 8	p110 β Asp862Gln	123 \pm 15
p110 α His855Glu	73 \pm 9	p110 β Glu858His	263 \pm 62

4.5 Conclusions

This chapter has presented the synthesis and evaluation of 10 dipeptide ZSTK474 analogues designed to investigate PI3K α selectivity by targeting interactions with the specific non-conserved residues, α Gln859 and δ Asn836. In line with this intention, a general trend was observed that the compounds tended to show improved PI3K δ selectivity compared to ZSTK474 itself. Compound **46** was the most PI3K δ selective compound, showing selectivity of 6-35-fold. Compound **50** showed the greatest selectivity against PI3K β of 21-fold. Site-directed mutagenesis assay results are consistent with the hypothesis that the interactions dictating selectivity are at the residue p110 α Gln859, or the corresponding residues in other isoforms. The moderate effect on potency upon reciprocal mutagenesis may be a result of redundant alternative binding conformers available to the compounds.

More generally, we have investigated the ability to rationally design isoform selective inhibitors based on the targeting of specific non-conserved interactions. In the introduction to this chapter, literature examples where inhibitor selectivity had been rationalised through specific non-conserved interactions identified via site-directed mutagenesis, computational modelling and crystallography were discussed. However, fewer literature examples exist where these interactions have been targeted as a design strategy towards isoform selective inhibitors. One example is the series of Genentech papers targeting the “tryptophan shelf” as a mechanism to obtain PI3K δ selectivity without inducing specificity pocket formation.⁶⁻⁸ The so-called “tryptophan shelf” is formed by a specific non-conserved residue in Region 2, p110 δ Thr750. The threonine sits parallel to the conserved tryptophan, and its relatively short side-chain allows inhibitors to form hydrophobic interactions with the tryptophan. In the other isoforms, this residue is either an arginine (PI3K α) or lysine (PI3K β and γ), which preclude these interactions. In their series of PI3K δ selective inhibitors, Genentech has successfully designed PI3K δ selective inhibitors by targeting interactions with the “tryptophan shelf”.⁶⁻⁸ Our results have also

demonstrated the applicability of this approach, where we have increased the PI3K δ selectivity of the pan-PI3K inhibitor ZSTK474 from a minimum selectivity of 2 to 6-fold, and a maximum selectivity of 10-fold to 35-fold. Our results can therefore be added to these reports in conveying the general applicability of this approach in the design of isoform selective inhibitors.

Inhibitor flexibility and the resulting redundancy in binding are important considerations when designing inhibitors using this approach. The particular substituents chosen in this case appear too flexible to form selective interactions, with site-directed mutagenesis results suggesting a degree of redundancy in the binding mode. The impact of binding conformation on selectivity is highlighted when the binding modes of two Genentech thienopyrimidine inhibitors are compared (Figure 4.4).⁷ In the non selective inhibitor GDC-0941 (**14**), the 4-methanesulfonylpiperazine group projects towards the P-loop, contacting p110 γ Lys802 and Ala805. When this group is changed to a 4-isopropanolylpiperidine **14d**, these interactions can no longer be formed and so a binding conformation interacting with the tryptophan shelf is preferred, thus increasing PI3K δ selectivity. Incorporation of sterically demanding amines at this position increased PI3K δ selectivity by constraining the inhibitor binding conformation.⁷

Another example of the importance of conformation on binding is in the aminoacyl-triazine series discussed in Section 4.1. The glyciny compound JP8-140 **16a** displayed dual PI3K β and δ selectivity, while the use of L-amino acids shifted selectivity towards PI3K β (as in JP9-114 **16**), and the D-amino acids shifted selectivity towards PI3K δ .⁵ The glyciny compound presumably has a degree of redundancy in binding interactions which can be shifted upon the introduction of chiral amino acids to constrain the binding mode. The series of inhibitors described in this chapter require a similar constraint in order to achieve greater isoform selectivity. Given the good selectivity of the L-phenylalaniny compounds (**44**, **46** and **48**) and the D-alaniny (**50**), a combination of bulky D-amino acids may provide this further constraint on binding mode and result in increased selectivity.

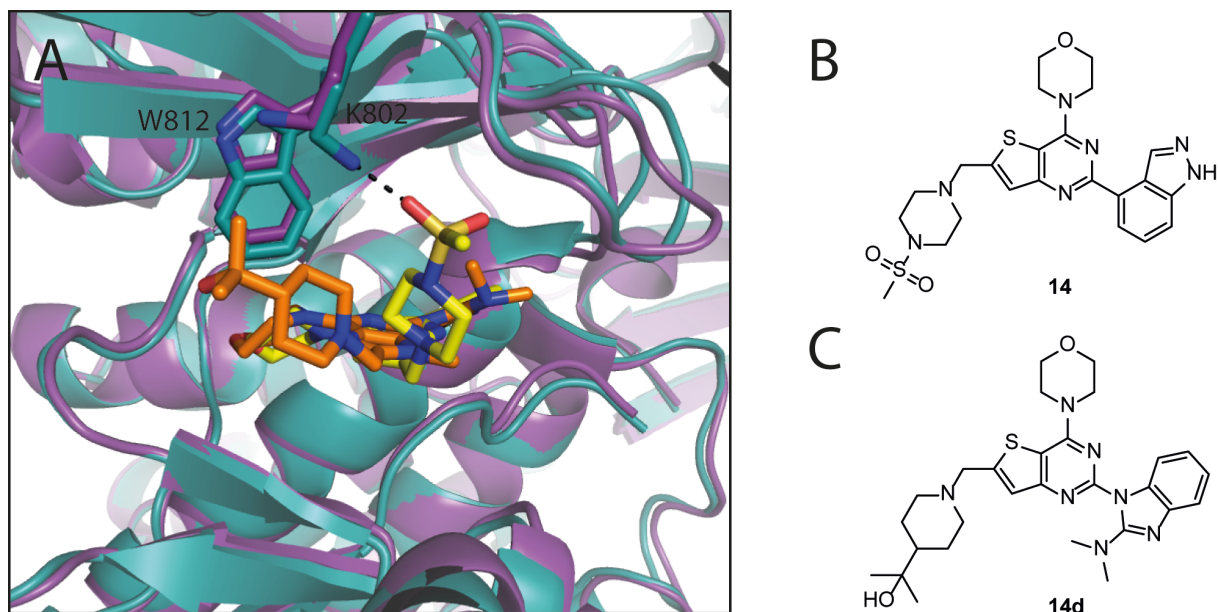


Figure 4.4: a) X-ray crystal structures of GDC-0941 **14** (yellow) bound to p110 γ (PDB ID: 3DBS, teal) and compound **14d** (orange) bound to p110 γ (PDB ID: 4GB9, purple); b) inhibitor structures.

Our results have demonstrated the potential of targeting specific non-conserved residues as a design strategy for isoform selective inhibitors, along with the power of site-directed mutagenesis for increasing understanding of the determinants of isoform selectivity. As our understanding of the mechanisms of isoform selectivity increases, this will greatly aid in the rational design of novel, isoform selective PI3K inhibitors.

4.6 References

- (1) Jamieson, S.; Flanagan, J. U.; Kolekar, S.; Buchanan, C.; Kendall, J. D.; Lee, W.; Rewcastle, G. W.; Denny, W. A.; Singh, R.; Dickson, J.; Baguley, B. C.; Shepherd, P. R. A drug targeting only p110 α can block phosphoinositide 3-kinase signalling and tumour growth in certain cell types. *Biochem. J.* **2011**, *438*, 53–62.
- (2) Zheng, Z.; Amran, S. I.; Zhu, J.; Schmidt-Kittler, O.; Kinzler, K. W.; Vogelstein, B.; Shepherd, P. R.; Thompson, P. E.; Jennings, I. G. Definition of the binding mode of a new class of phosphoinositide 3-kinase α -selective inhibitors using in vitro mutagenesis of non-conserved amino acids and kinetic analysis. *Biochem. J.* **2012**, *444*, 529–535.
- (3) Bruce, I.; Akhlaq, M.; Bloomfield, G. C.; Budd, E.; Cox, B.; Cuenoud, B.; Finan, P.; Gedeck, P.; Hatto, J.; Hayler, J. F.; Head, D.; Keller, T.; Kirman, L.; Leblanc, C.; Grand, D. L.; McCarthy, C.; O'Connor, D.; Owen, C.; Oza, M. S.; Pilgrim, G.; Press, N. E.; Sviridenko, L.; Whitehead, L. Development of isoform selective PI3-kinase inhibitors as pharmacological tools for elucidating the PI3K pathway. *Bioorg. Med. Chem. Lett.* **2012**, *22*, 5445–5450.
- (4) Furet, P.; Guagnano, V.; Fairhurst, R. A.; Imbach-Weese, P.; Bruce, I.; Knapp, M.; Fritsch, C.; Blasco, F.; Blanz, J.; Aichholz, R.; Hamon, J.; Fabbro, D.; Caravatti, G. Discovery of NVP-BYL719 a potent and selective phosphatidylinositol-3 kinase α inhibitor selected for clinical evaluation. *Bioorg. Med. Chem. Lett.* **2013**, *23*, 3741–3748.
- (5) Pinson, J.-A.; Zheng, Z.; Miller, M. S.; Chalmers, D. K.; Jennings, I. G.; Thompson, P. E. L-Aminoacyl-triazine Derivatives Are Isoform-Selective PI3K β Inhibitors That Target Nonconserved Asp862 of PI3K β . *ACS Med. Chem. Lett.* **2013**, *4*, 206–210.
- (6) Sutherlin, D. P.; Baker, S.; Bisconte, A.; Blaney, P. M.; Brown, A.; Chan, B. K.; Chantry, D.; Castanedo, G.; DePledge, P.; Goldsmith, P.; Goldstein, D. M.; Hancox, T.; Kaur, J.; Knowles, D.; Kondru, R.; Lesnick, J.; Lucas, M. C.; Lewis, C.; Murray, J.; Nadin, A. J.; Nonomiya, J.; Pang, J.; Pegg, N.; Price, S.; Reif, K.; Safina, B. S.; Salphati, L.; Staben, S.; Seward, E. M.; Shuttleworth, S.; Sohal, S.; Sweeney, Z. K.; Ultsch, M.; Waszkowycz, B.; Wei, B. Potent and selective inhibitors of PI3K δ : Obtaining isoform selectivity from the affinity pocket and tryptophan shelf. *Bioorg. Med. Chem. Lett.* **2012**, *22*, 4296–4302.
- (7) Murray, J. M.; Sweeney, Z. K.; Chan, B. K.; Balazs, M.; Bradley, E.; Castanedo, G.; Chabot, C.; Chantry, D.; Flagella, M.; Goldstein, D. M.; Kondru, R.; Lesnick, J.; Li, J.; Lucas, M. C.; Nonomiya, J.; Pang, J.; Price, S.; Salphati, L.; Safina, B.; Savy, P. P. A.; Seward, E. M.; Ultsch, M.; Sutherlin, D. P. Potent and Highly Selective Benzimidazole Inhibitors of PI3-Kinase Delta. *J. Med. Chem.* **2012**, *55*, 7686–7695.
- (8) Safina, B. S.; Baker, S.; Baumgardner, M.; Blaney, P. M.; Chan, B. K.; Chen, Y.-H.; Cartwright, M. W.; Castanedo, G.; Chabot, C.; Cheguillaume, A. J.; Goldsmith, P.; Goldstein, D. M.; Goyal, B.; Hancox, T.; Handa, R. K.; Iyer, P. S.; Kaur, J.; Kondru, R. K.; Kenny, J. R.; Krintel, S. L.; Li, J.; Lesnick, J.; Lucas, M. C.; Lewis, C.; Mukadam, S.; Murray, J. M.; Nadin, A. J.; Nonomiya, J.; Padilla, F.; Palmer, W. S.; Pang, J.; Pegg, N.; Price, S.; Reif, K.; Salphati, L.; Savy, P. A.; Seward, E. M.; Shuttleworth, S.; Sohal, S.; Sweeney, Z. K.; Tay, S.; Tivitmahaisoon, P.; Waszkowycz, B.; Wei, B.; Yue, Q.; Zhong, C.; Sutherlin, D. P. Discovery of Novel PI3-Kinase Delta Specific Inhibitors for the Treatment of Rheumatoid Arthritis: Taming CYP3A4 Time-Dependent Inhibition. *J. Med. Chem.* **2012**, *55*, 5887–5900.

Chapter 5: Conclusions and future directions

An increasing number of PI3K inhibitors are entering the clinic for the treatment of cancer. It is still not well established as to whether pan-PI3K or isoform selective inhibitors will be more effective in treating cancer, and which will have a better tolerated side-effect profile. Although isoform selective inhibitors exist for each of the four Class I isoforms, their basis for achieving selectivity is not always well understood. There remains a need to understand the structural basis for inhibitor selectivity to inform future isoform selective inhibitor design. Ideally, efforts should be moving towards the development of oncogenic mutant-specific inhibitors, which would greatly minimise the prospects of clinical side-effects associated with wild-type PI3K inhibitors. In line with this need, this thesis has sought to explore the structural differences that set wild-type PI3K α apart from the other isoforms, and from the His1047Arg oncogenic mutant. Identification of these key differences has the potential to inform future design of PI3K α selective and His1047Arg oncogenic mutant selective inhibitors.

Chapter 2 presented two newly determined X-ray crystal structures of p110 α /nSH2 which yielded some important insights for future drug design. A comparison of the new wild-type structure with that of the oncogenic mutant His1047Arg (PDB ID: 3HHM) has revealed key differences in the interaction of nSH2 with the kinase domain implying a loss of nSH2 regulation in the oncogenic mutant.¹ Dbouk and Backer have recently proposed some novel non-ATP competitive approaches for modulating PI3K β activity, by targeting the binding interface between the cSH2 and kinase domains.² The key interaction differences between the nSH2 domain and the kinase domain of the wild-type and His1047Arg oncogenic mutant that we have identified could potentially be targeted with small molecules to selectively modulate oncogenic PI3K activity. Our crystal structures have also enabled the identification of two lipid-binding sites for PI3K α . Characterisation of the lipid-binding site of PI3K α could provide an alternative to ATP-competitive inhibitors. Lipid-competitive inhibitors would yield improved selectivity over protein kinases. Ongoing work in this area is looking at streamlining the crystallisation of PI3K α , and particularly co-crystallisation with inhibitors. We are currently investigating a novel method to induce crystallisation using molecularly imprinted polymers.³ Most of the inhibitor binding information is from PI3K γ crystal structures, and there are only two inhibitor bound wild-type PI3K α crystal structures available in the PDB at the time of writing.^{4,5} Rational isoform selective inhibitor design ultimately requires a detailed structural understanding of the determinants of selectivity, and we hope that this novel method for crystallisation can contribute to this understanding.

In the following two chapters, we have investigated novel modifications to the pan-PI3K inhibitor ZSTK474 to investigate their effect on isoform selectivity. Chapter 3 has investigated alterations to the aromatic portion of ZSTK474 to probe isoform selective interactions within the affinity pocket of the PI3K ATP-binding site. Benzimidazole substitutions and replacements have revealed the PI3K γ isoform as most sensitive to changes in the affinity pocket binding

moiety of the inhibitor. We have postulated that a key non-conserved residue, p110 γ Tyr787, may contribute to reduced flexibility of the affinity pocket in PI3K γ . These findings advance the understanding of isoform selectivity, and suggest that for inhibitors either targeting or selecting against PI3K γ , careful attention should be paid to the affinity pocket binding portion of the inhibitor.

We have described the development of a novel synthetic approach to regioselectively synthesise 5 or 6-substituted benzimidazole ZSTK474 derivatives. Unfortunately, the methoxy substitutions resulted in a loss in potency, however significant selectivity over PI3K γ was achieved. Future work could investigate alternative 5 or 6 substitutions of the benzimidazole group, including halogens and hydrogen bond donor and acceptor groups. The variations attempted have not been exhaustive, and with this convenient synthetic route an opportunity to develop new analogues has been opened.

Chapter 3 also demonstrated the complexities involved in the rational design of isoform selective inhibitors. The combination of favoured LHS and RHS substituents to form novel ZSTK474 analogues resulted in dramatic losses in potency in most cases. We were able to demonstrate, however, an increase in the PI3K α selectivity compared with the pan-PI3K inhibitor ZSTK474. Compound **39b** showed 4-57-fold selectivity against the other three isoforms. We also sought to utilise computational methods, particularly molecular docking, to investigate how subtle differences in inhibitor structure could markedly influence inhibitor potency. Although providing some possible clues, unfortunately, it was unable to provide definitive answers. Computational methods remain limited in their ability to predict nuances in inhibitor binding modes and protein flexibility. A streamlined approach to obtain X-ray crystal structures of each individual isoform would provide a much more detailed description of inhibitor binding to inform future analogue synthesis.

Chapter 4 investigated the rational design of isoform selective inhibitors by targeting a specific non-conserved residue in the ATP-binding site. Based on two isoform selective inhibitors reported in the literature, A-66 **15** (PI3K α) and JP9-114 **16** (PI3K β), we targeted the residue p110 α Gln859 using a carboxamide group.⁶⁻⁸ The inhibitors demonstrated good potency and selectivity tending towards PI3K δ . The most selective compound was **46**, which demonstrated 6-35-fold selectivity for PI3K δ . When compound **50** was tested against PI3K α and PI3K β site-directed isoform mutants, we were able to demonstrate that this compound was indeed interacting with p110 α Gln859, albeit in a redundant fashion. We have thus demonstrated that the rational design of isoform selectivity is achievable. We identified flexibility or rigidity of the inhibitor as an important consideration in rational isoform selective inhibitor design. The flexibility of our inhibitors limits the degree of isoform selectivity due to redundant interactions with binding-site residues. The constraint of inhibitor binding conformation through the use of chirality and bulky amino acid groups could improve the selectivity of these inhibitors.

The overall aims of this thesis were twofold, firstly to examine the structure and regulation of PI3K α and to investigate structural changes that can influence isoform selectivity. This work has highlighted key differences in the regulation of wild-type PI3K α and the oncogenic mutant His1047Arg. We have demonstrated the power of structural changes in the inhibitor portion targeting the conserved affinity pocket to dramatically affect isoform selectivity, particularly at the PI3K γ isoform. Selectivity achieved for PI3K α against the PI3K γ is greater than the desired 100-fold in three of the compounds tested, **38a**, **38b** and **40a**, however, selectivity against PI3K β and PI3K δ , still require further optimisation. Furthermore, we have demonstrated the applicability of targeting specific non-conserved residues in the PI3K binding site for the rational design of isoform selective inhibitors. A combination of these two approaches, utilising the

information gained in both Chapter 3 and 4 may provide novel routes to the design of PI3K α selective inhibitors.

The future demands an integrated approach to drug discovery combining structural, computational, biochemical and medicinal chemistry perspectives. Structural information of the protein as a whole, works in conjunction with kinetic and biochemical data to help us understand the mechanisms of regulation at a molecular level. As highlighted in Dbouk and Backer, this yields insight into alternative approaches to the modulation of protein activity.² While we await clinical data from the pan and isoform selective PI3K inhibitors currently progressing through the clinic, perhaps the medicinal chemistry efforts should be focused on novel approaches, which may provide better therapeutic options. The challenge is primarily in the discovery of oncogenic mutant specific inhibitors. Because the ATP-binding site of the kinase domain mutant, His1047Arg, does not appear significantly different from that of the wild-type PI3K α , structural information about differences in regulation provides medicinal chemists with alternative options for ways to target this oncogenic mutant.¹ This integrated approach informs the design of future clinical candidates, and will in turn be informed by emerging clinical data as to what is necessary for the effective treatment of cancer.

5.1 References

- (1) Mandelker, D.; Gabelli, S. B.; Schmidt-Kittler, O.; Zhu, J.; Cheong, I.; Huang, C. H.; Kinzler, K. W.; Vogelstein, B.; Amzel, L. M. A frequent kinase domain mutation that changes the interaction between PI3K α and the membrane. *Proc. Natl. Acad. Sci. U.S.A.* **2009**, *106*, 16996–17001.
- (2) Dbouk, H. A.; Backer, J. M. Novel approaches to inhibitor design for the p110 β phosphoinositide 3-kinase. *Trends Pharm. Sci.* **2013**, *34*, 149–153.
- (3) Saridakis, E.; Khurshid, S.; Govada, L.; Phan, Q.; Hawkins, D.; Crichlow, G. V.; Lolis, E.; Reddy, S. M.; Chayen, N. E. Protein Crystallization Facilitated by Molecularly Imprinted Polymers. *Proc. Natl. Acad. Sci. U.S.A.* **2011**, *108*, 11081–11086.
- (4) Hon, W.-C.; Berndt, A.; Williams, R. L. Regulation of lipid binding underlies the activation mechanism of class IA PI3-kinases. *Oncogene* **2012**, *31*, 3655–3666.
- (5) Nacht, M.; Qiao, L.; Sheets, M. P.; St. Martin, T.; Labenski, M.; Mazdiyasni, H.; Karp, R.; Zhu, Z.; Chaturvedi, P.; Bhavsar, D.; Niu, D.; Westlin, W.; Petter, R. C.; Medikonda, A. P.; Singh, J. Discovery of a Potent and Isoform-Selective Targeted Covalent Inhibitor of the Lipid Kinase PI3K α . *J. Med. Chem.* **2013**, *56*, 712–721.
- (6) Jamieson, S.; Flanagan, J. U.; Kolekar, S.; Buchanan, C.; Kendall, J. D.; Lee, W.; Rewcastle, G. W.; Denny, W. A.; Singh, R.; Dickson, J.; Baguley, B. C.; Shepherd, P. R. A drug targeting only p110 α can block phosphoinositide 3-kinase signalling and tumour growth in certain cell types. *Biochem. J.* **2011**, *438*, 53–62.
- (7) Zheng, Z.; Amran, S. I.; Zhu, J.; Schmidt-Kittler, O.; Kinzler, K. W.; Vogelstein, B.; Shepherd, P. R.; Thompson, P. E.; Jennings, I. G. Definition of the binding mode of a new class of phosphoinositide 3-kinase α -selective inhibitors using in vitro mutagenesis of non-conserved amino acids and kinetic analysis. *Biochem. J.* **2012**, *444*, 529–535.
- (8) Pinson, J.-A.; Zheng, Z.; Miller, M. S.; Chalmers, D. K.; Jennings, I. G.; Thompson, P. E. L-Aminoacyl-triazine Derivatives Are Isoform-Selective PI3K β Inhibitors That Target Nonconserved Asp862 of PI3K β . *ACS Med. Chem. Lett.* **2013**, *4*, 206–210.

Chapter 6: Experimental

6.1 Chapter 2 experimental

6.1.1 PI3K protein expression

SF9 cells were grown in suspension culture in SF-900 III Serum Free Media (Invitrogen) supplemented with 0.5% penicillin-streptomycin at 27°C. At a density of 4×10^6 cells per millilitre, cells were infected with wild-type p110 α (or His1047Arg-p110 α , Glu545Lys-p110 α) and p85 α niSH2 (or full length p85 α) viruses at a multiplicity of infection ratio of 3:2. Media was supplemented with a PI3K inhibitor as described in Mandelker *et al.*¹ Cells were harvested 72 hours after infection and the cell pellet collected through centrifugation at 900 x *g*. Protein purification was performed as previously described.^{1,2}

6.1.2 p85 α protein expression and purification

Full length p85 α was expressed heterogeneously in *Escherichia coli* as described previously. Shortly, cells transformed with the pGEX 4T plasmid containing an N-terminal glutathione S-transferase (GST) fusion-p85 α were grown at 37°C in LB medium. Expression was induced with 1 mM isopropyl β -D-1-thiogalactopyranoside (IPTG). Following four hours of induction at 37°C, cells were pelleted and stored at -80°C. Cell pellets were resuspended in PBS, 2mM DTT, Roche complete EDTA-free protease inhibitor cocktail (Roche Diagnostics, Mannheim, Germany), pH 7.4 and lysed using a microfluidiser (Microfluidics, Newton, MA). Clarified lysate was incubated with glutathione sepharose HP resin (GE Healthcare) in binding buffer (PBS, 2mM DTT, pH 7.4) at 4°C for 2 hours with gentle agitation. The GST-tagged p85 α was eluted with 10 volumes of elution buffer (50 mM Tris, 150 mM NaCl, 1 mM EDTA and 10 mM reduced glutathione, pH 8.0). After thrombin cleavage, the p85 α was purified by anion exchange Resource-Q anion exchange column (GE Healthcare). p85 α was eluted using a linear gradient of 0-100% anion exchange buffer B (50 mM Tris, 500 mM NaCl, pH 8.0) over 60 column volumes. p85 α of $\geq 95\%$ homogeneity, as determined by SDS-PAGE were pooled. p85 α was concentrated to 15 mg/mL.

6.1.3 Crystallisation

Crystallisation was performed as previously described and improved with successive rounds of macroseeding.² Crystals were soaked for one hour with 1 mM diC4-phosphatidylinositol-4,5-bisphosphate (Echelon Biosciences).

6.1.4 Data collection

X-ray diffraction data were collected at beamlines X6A and X25 of NSLS at Brookhaven National Laboratory. The crystals diffracted to a resolution of 2.96 Å in the absence of diC4-PIP₂ and 3.37 Å in the presence of diC4-PIP₂. Data were processed with HKL2000.

6.1.5 Structure determination

The free structure was determined by using the coordinates of the previously determined WT p110 α /nSH2 (PDB ID: 2RD0)² as a model. After rigid body and positional refinement, the program Coot³ was used for model building. Initial refinement revealed that the nSH2 domain of p85 α was present and ordered in the structure. Therefore, the nSH2 domain of H1047R p110 α /nSH2 structure (PDB ID: 3HHM)¹ and the p85 α nSH2 crystal structure (PDB ID: 2IUG)⁴ were used as a guide to fit the additional electron density in this region. Iterative rounds of refinement using REFMAC 5.0⁵ yielded a final R_{cryst} of 0.19 and an R_{free} of 0.27 to 2.95 Å in the absence of diC4-PIP₂. The refined coordinates of the free wild type structure were used as an initial model for the determination of the structure in the presence of diC4-PIP₂; refinement yielded an R_{cryst} of 0.24 and an R_{free} of 0.34.

6.1.6 Preparation of BODIPY-FL-PIP₂ vesicles

Unilamellar vesicals containing PC/PE/PS/BODIPY-FL-PIP₂/cholesterol with a molar ratio of 54.9/25/5/0.1/15 were generated as follows: lipids were dried under a stream of nitrogen in a glass test tube then held under vacuum for 24 hours to completely remove organic solvents. Lipids were then heated in the presence of assay buffer (50 mM Tris pH 7.6, 150 mM NaCl, 1mM EDTA, 2mM DTT) at 50°C for 10 minutes. Lipids were resuspended by vortexing, then extruded through a polycarbonate filter with 100 nm pore size to yield unilamellar vesicles with diameter of 100 nm. BODIPY-FL-PIP₂ was purchased from Echelon Biosciences. All other lipids were purchased from Avanti Polar Lipids.

6.1.7 Fluorescence quenching experiments

BODIPY-FL-PIP₂ containing vesicles were diluted to a final concentration of 50 μ M lipid (50 nM BODIPY-FL-PIP₂) in assay buffer (50 mM Tris pH 7.6, 150 mM NaCl, 1 mM EDTA, 2 mM DTT) for all assays. Ovalbumin (0.5 mg/mL) was added to the assay solution to minimise

vesicle binding to glass surfaces during mixing and binding measurements. Fluorescence measurements were taken on a FluoroLog fluorometer from HORIBA Scientific. BODIPY-FL-PIP₂ was excited at 490 nm and emission readings were recorded from 500 to 600 nm. The spectral bandwidths for excitation and emission were 2 and 5 nm, respectively. All binding experiments were conducted at 25°C in a quartz cuvette. Quenching signals were normalised to the fluorescence signal from the vesicle solution alone and adjusted for dilution due to the addition of the corresponding protein.

6.2 Synthetic chemistry

6.2.1 General experimental

All materials were obtained from Sigma-Aldrich, Boron-Molecular, Alfa Aesar, SynChem, Matrix Scientific and Chem Impex and used without further purification.

Thin Layer Chromatography (TLC) was performed using Merck Silica Gel 60 F254 pre-coated plates (0.25 mm) and visualised by ultraviolet light. Flash column chromatography was performed with Silicycle silica gel, 40-63 µm according to the published method.⁶ Crude products were generally pre-adsorbed onto silica prior to column chromatography.

¹H and ¹³C Nuclear Magnetic Resonance (NMR) spectra were recorded at 400.13 MHz and 100.62 MHz, respectively, using a Bruker Avance III Nanobay 400 MHz NMR spectrometer coupled to a BACS 60 automatic sample changer. Chemical shifts (δ) for all ¹H and ¹³C spectra are reported in parts per million (ppm) using deuterated solvent as reference: *d*₁-chloroform (¹H 7.26, ¹³C 77.16 ppm), *d*₄-methanol (¹H 3.31, ¹³C 49.00 ppm), *d*₆-dimethylsulfoxide (¹H 2.50, ¹³C 39.52 ppm). Coupling constants (*J*) are given in hertz (Hz). The ¹H and ¹³C-NMR are reported as follows: chemical shift (δ), multiplicity, coupling constant (*J*) in Hertz (Hz) (quoted to one decimal place), peak integration (or number of carbons) and assignment. For ¹³C-NMR multiplicity is only specified where it is greater than one. The following abbreviations have been

used: s – singlet; d – doublet; t – triplet; q – quartet; br s – broad singlet; dd – doublet of doublets; ddd – doublet of doublet of doublets; m – multiplet.

Liquid chromatography-Mass spectrometry (LCMS) was performed on an Agilent 1220 HPLC coupled to an Agilent 6120 Single Quad Mass Spectrometer, fitted with a 6120 quadrupole detector and a Phenomenex® Luna 5 μm C8(2) 100 Å (50 x 4.6 mm, internal diameter) 5 μm column. Samples were run in a gradient of 5-100% Buffer B (80% acetonitrile, 19.9% water, 0.1% formic acid) in Buffer A (0.1% aqueous formic acid) at 0.5 mL/minute over 4 minutes, maintained as 100% Buffer B for a further 3 minutes, and then gradient of 100-0% Buffer B over 3 minutes. System control and analysis was facilitated with Agilent Chemstation software (version B.04.01) coupled with Easy Access software. Alternatively, an Agilent 1260 UHPLC coupled to an Agilent 6120 Single Quad Mass Spectrometer, fitted with a quadrupole detector and a Poroshell 120 EC-C18 column was used. Samples were run in a gradient of 5-100% Buffer B at 0.5 mL/minute over 2.5 minutes, maintained at 100% Buffer B until 3.8 minutes and then gradient of 100-0% Buffer B to a total of 5 minutes. System control and analysis was facilitated with Agilent Chemstation software (version B.04.03) coupled with Masshunter Easy Access software.

High resolution mass spectrometry (HRMS) were determined as solutions in methanol using a Waters LCT Time of Flight Mass Spectrometer coupled to a 2795 Alliance Separations module. Data were acquired and mass corrected via a dual-spray Leucine Enkephaline reference sample. Mass spectra were created by averaging the scans across each peak and background subtracted of the Total Ion Chromatogram (TIC). Acquisition and analysis were performed with MassLynx v4.1 software. Mass spectrometer conditions: electrospray ionisation (ESI) mode; 550 L/hour desolvation gas flow; 250°C desolvation temperature; 110°C source temperature; 2400 V capillary voltage; 60 V sample cone voltage; 100-1500 m/z scan range; 1 second scan time; internal reference ions – m/z 556.2771. Alternatively, analyses were done on an Agilent 6224

Time of Flight LCMS Mass Spectrometer coupled to an Agilent 1290 Infinity (Agilent, Palo Alto, CA). Chromatographic separation was performed using an Agilent Zorbax SB-C18 Rapid Resolution HT 2.1 x 50 mm, 1.8 μm column (Agilent Technologies, Palo Alto, CA) using an acetonitrile gradient (5-100%) over 3.5 minutes at 0.5 mL/minute. All data were acquired and reference mass corrected via a dual-spray ESI source. Each scan or data point on the TIC is an average of 13,700 transients, producing a spectrum every second. Mass spectra were created by averaging the scans across each peak and background subtracted against the first 10 seconds of the TIC. Acquisition was performed using the Agilent Mass Hunter Data Acquisition software version B.05.00 Build 5.0.5042.2 and analysis was performed using Mass Hunter Qualitative Analysis version B.05.00 Build 5.0.519.13. Mass spectrometer conditions: electrospray ionisation (ESI) mode; 11 L/hour drying gas flow; 45 psi nebuliser; 325°C drying gas temperature; 4000 V capillary voltage; 160 V fragmentor; 65 V skimmer; OCT RFV 750V; 100-1500 m/z scan range; internal reference ions – m/z 121.050873 and 922.009798.

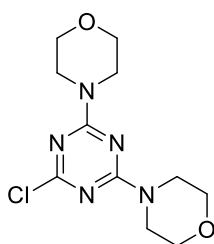
Analytical reverse phase high performance liquid chromatography (RP-HPLC) was conducted on a Waters Millennium 2690 system fitted with a Phenomenex® Luna C8, 100 Å, (50 x 4.6 mm, internal diameter) 5 μm column. Samples were run in a gradient of 0-80% Buffer B (80% acetonitrile, 19.9% water, 0.1% trifluoroacetic acid) in Buffer A (0.1% aqueous trifluoroacetic acid) at a flow rate of 1 mL/minute, with ultraviolet detection at 254 nm.

Semi-preparative RP-HPLC were acquired on a Waters HPLC system (Model 600 controller and Waters 486 Tuneable Absorbance Detector) with a Phenomenex® Luna C8 100 Å, (50 x 21.2 mm, internal diameter) 10 μm column with ultraviolet detection at 254 nm. Samples were run using a gradient elution of 0-80% Buffer B (80% acetonitrile, 19.9% water, 0.1% trifluoroacetic acid) in Buffer A (0.1% aqueous trifluoroacetic acid) over 20 minutes with a flow rate of 10 mL/minute. Where specified, the following acid-free buffers were used: Buffer A (100% water) and Buffer B (80% acetonitrile, 20% water).

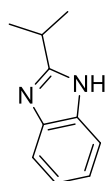
Microwave reactions were performed in a CEM Discover/Explorer automated microwave synthesiser. All tested compounds had greater 95% purity as determined by analytical HPLC.

6.2.2 Regioselective synthesis of 5- and 6-methoxybenzimidazole-1,3,5-triazines as inhibitors of phosphoinositide 3-kinase (published paper)⁷

NOTE: Experimental data taken from Supplementary Information and reformatted. Compounds not discussed in the text of the thesis have been numbered as per the publication, prefixed with a 'P'.



4,4'-(6-chloro-1,3,5-triazine-2,4-diyl)dimorpholine (20). To a stirred solution of cyanuric chloride (6.7 g, 36 mmol) in acetone (60 mL) was added dropwise a solution of morpholine (5.7 g, 66 mmol) and triethylamine (6.6 g, 66 mmol) in acetone (60 mL) at 0°C, and then warmed to room temperature and stirred for 1 hour. The mixture was quenched with water, filtered, washed with water and dried to give **20** as a white powder (6.3 g, 67%). ¹H-NMR (400 MHz, CD₃OD) δ 3.79 (br s, 8H, NCH₂), 3.73-3.68 (m, 8H, OCH₂); LCMS (*m/z*) 286.1 [MH]⁺.

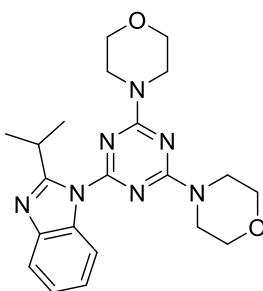


2-isopropyl-1H-benzo[d]imidazole (P10). 1,2-phenylenediamine (0.52 g, 4.8 mmol) and isobutyric acid (0.85 g, 9.6 mmol) were refluxed in 4 M aqueous HCl (2 mL) for 3 hours. The solution was treated with charcoal, filtered, washed with water and neutralised with 23% aqueous NH₃. The precipitate was collected, washed with water and dried to give **P10** as a light

brown powder (0.29 g, 37%). $^1\text{H-NMR}$ (400 MHz, CDCl_3) δ 7.61-7.59 (m, 2H, ArH), 7.25-7.24 (m, 2H, ArH), 3.34-3.27 (m, 1H, CH), 1.47 (d, $J = 7.0$ Hz, 6H, CH_3); LCMS (m/z) 161.2 $[\text{MH}]^+$.

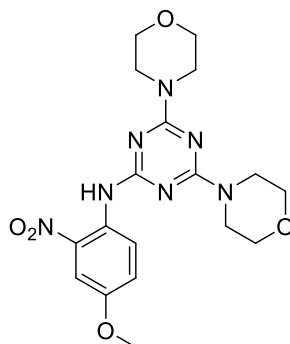
6.2.2.1 General procedure for Buchwald-Hartwig Reactions

To a degassed suspension of **20** (0.50 g, 1.8 mmol), Cs_2CO_3 (0.80 g, 2.5 mmol) and 4- or 5-methoxy-2-nitroaniline (0.35 g, 2.1 mmol) in 1,4-dioxane (15 mL) was added $\text{Pd}(\text{OAc})_2$ (0.004 g, 0.018 mmol, 1 mol%), Xantphos (0.010 g, 0.018 mmol, 1 mol%) and water (1.5 mL). This was exposed to microwave irradiation in a sealed tube at 150°C for 45 minutes, partitioned between water and dichloromethane, extracted a further two times into dichloromethane, dried over Na_2SO_4 and concentrated *in vacuo* to give the crude product. The crude product was then purified via column chromatography using chloroform/ethyl acetate (6:1) as eluent.

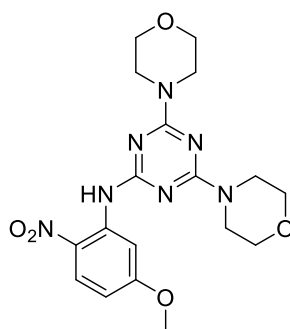


4,4'-(6-(2-isopropyl-1H-benzo[d]imidazol-1-yl)-1,3,5-triazine-2,4-diyl)dimorpholine

(P4c). **20** (0.10 g, 0.35 mmol) and **P10** (0.067 g, 0.42 mmol) gave **P4c** as a light brown powder (0.023 g, 16%). $^1\text{H-NMR}$ (400 MHz, CDCl_3) δ 8.12-8.02 (m, 1H, ArH), 7.79-7.69 (m, 1H, ArH), 7.32-7.22 (m, 2H, ArH), 4.18-4.04 (m, 1H, CH), 3.92-3.85 (m, 8H, NCH_2), 3.79-3.75 (m, 8H, OCH_2), 1.46 (d, $J = 8.6$ Hz, 6H, CH_3); $^{13}\text{C-NMR}$ (101 MHz, CDCl_3) δ 165.5 (C), 163.2 (C), 161.3 (C), 142.8 (C), 134.1 (C), 123.3 (CH), 123.2 (CH), 119.5 (CH), 114.6 (CH), 66.9 (CH_2), 44.1 (CH_2), 28.8 (CH), 22.1 (CH_3); HRMS (ESI+) calcd for $[\text{C}_{21}\text{H}_{27}\text{N}_7\text{O}_2 + \text{H}]^+$ 410.2299, found 410.2311.



N-(4-methoxy-2-nitrophenyl)-4,6-dimorpholino-1,3,5-triazin-2-amine (P6a). **20** (0.50 g, 1.7 mmol) and 4-methoxy-2-nitroaniline (0.35 g, 2.1 mmol) gave **P6a** as an orange powder (0.62 g, 85%). $^1\text{H-NMR}$ (CDCl_3) δ 9.54 (s, 1H, NH), 8.62 (d, J = 9.1 Hz, 1H, ArH), 7.64 (d, J = 2.8 Hz, 1H, ArH), 7.20 (dd, J = 9.4, 3.0 Hz, 1H, ArH), 3.85 (s, 3H, OCH_3), 3.80-3.76 (m, 8H, NCH_2), 3.75-3.71 (m, 8H, OCH_2); LCMS (m/z) 418.1 $[\text{MH}]^+$.

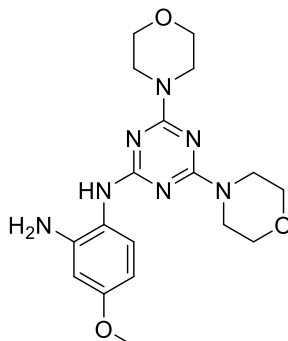


N-(5-methoxy-2-nitrophenyl)-4,6-dimorpholino-1,3,5-triazin-2-amine (P6b). **20** (0.40 g) and 5-methoxy-2-nitroaniline (0.28 g) gave **P6b** as a yellow powder (0.45 g, 77%). $^1\text{H-NMR}$ (CDCl_3) δ 10.35 (s, 1H, NH), 8.47 (s, 1H, ArH), 8.21 (d, J = 9.4 Hz, 1H, ArH), 6.55 (dd, J = 9.4, 2.6 Hz, 1H, ArH), 3.88 (s, 3H, OCH_3), 3.84-3.78 (m, 8H, NCH_2), 3.76-3.72 (m, 8H, OCH_2); LCMS (m/z) 418.1 $[\text{MH}]^+$.

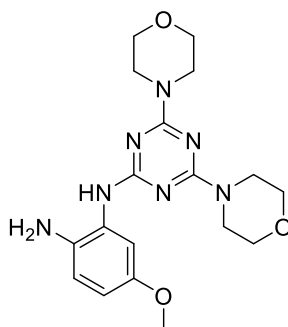
6.2.2.2 General procedure for reduction

Nitroaniline and $\text{SnCl}_2 \cdot 2\text{H}_2\text{O}$ was heated in ethanol or ethyl acetate to 70 °C under nitrogen for 2 hours. The mixture was partitioned between water and ethyl acetate or dichloromethane,

extracted a further two times, dried over Na_2SO_4 and concentrated *in vacuo* to give the crude product. Product was used without further purification.



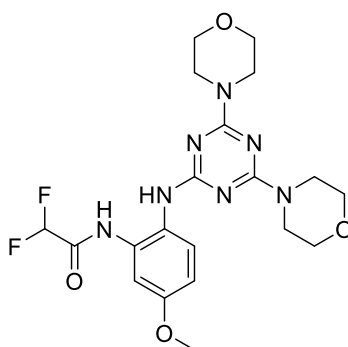
N1-(4,6-dimorpholino-1,3,5-triazin-2-yl)-4-methoxybenzene-1,2-diamine (P7a). **P6a** (0.60 g, 1.4 mmol) and $\text{SnCl}_2 \cdot 2\text{H}_2\text{O}$ (1.6 g, 7.2 mmol) in ethanol (5 mL) gave **P7a** as a light brown powder (0.51 g, 91%). $^1\text{H-NMR}$ (CDCl_3) δ 7.11 (d, $J = 9.2$ Hz, 1H, ArH), 6.35-6.28 (m, 2H, ArH), 6.16 (br s, 1H, NH), 3.94 (br s, 2H, NH_2), 3.77 (s, 3H, OCH_3), 3.75-3.64 (m, 16H, CH_2); LCMS (m/z) 388.1 $[\text{MH}]^+$.



N1-(4,6-dimorpholino-1,3,5-triazin-2-yl)-5-methoxybenzene-1,2-diamine (P7b). **P6b** (0.16 g, 0.38 mmol) and $\text{SnCl}_2 \cdot 2\text{H}_2\text{O}$ (0.42 g, 1.9 mmol) in ethyl acetate (2 mL) gave **P7b** as a light brown powder (0.13 g, 89%). $^1\text{H-NMR}$ (CDCl_3) δ 7.28 (d, $J = 2.8$ Hz, 1H, ArH), 6.74 (d, $J = 8.6$ Hz, 1H, ArH), 6.66 (br s, 1H, NH), 6.57 (dd, $J = 8.6, 2.9$ Hz, 1H, ArH), 3.86 (br s, 2H, NH_2), 3.78-3.74 (m, 8H, NCH_2), 3.74 (s, 3H, OCH_3), 3.72-3.68 (m, 8H, OCH_2); LCMS (m/z) 388.3 $[\text{MH}]^+$.

6.2.2.3 General procedure for acylation

Amine (0.13 mmol) and DIPEA (0.026 g, 0.20 mmol) were dissolved in dichloromethane (2 mL) and acid chloride (0.14 mmol) added. The mixture was stirred at room temperature for 30 minutes, then washed with 1 M HCl, dried over Na₂SO₄ and concentrated *in vacuo* to give the crude product. The crude product was then purified via column chromatography using 1% triethylamine in ethyl acetate as eluent.

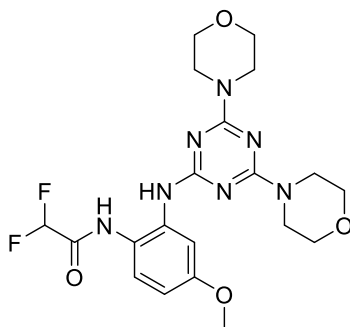


N-(2-((4,6-dimorpholino-1,3,5-triazin-2-yl)amino)-5-methoxyphenyl)-2,2-

difluoroacetamide (P8a). **P7a** (0.10 g, 0.26 mmol), 2,2-difluoroacetyl chloride (0.040 g,

0.34 mmol) and DIPEA (0.044 g, 0.34 mmol) gave **P8a** as a light brown powder (0.059 g, 49%).

¹H-NMR (400 MHz, CDCl₃) δ 10.41 (br s, 1H, NH), 7.51 (d, *J* = 2.8 Hz, 1H, ArH), 7.05 (d, *J* = 8.7 Hz, 1H, ArH), 6.75 (dd, *J* = 8.8, 2.9 Hz, 1H, ArH), 6.44 (s, 1H, NH), 5.95 (t, *J* = 54.4 Hz, 1H, CHF₂), 3.83 (s, 3H, OCH₃), 3.78-3.65 (m, 16H, CH₂); LCMS (*m/z*) 466.3 [MH]⁺.

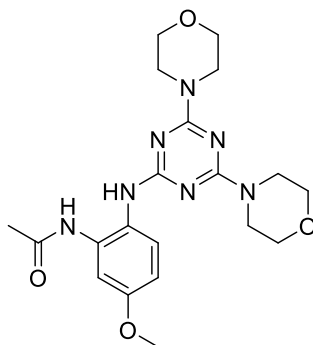


N-(2-((4,6-dimorpholino-1,3,5-triazin-2-yl)amino)-4-methoxyphenyl)-2,2-

difluoroacetamide (P8b). **P7b** (0.10 g, 0.26 mmol), 2,2-difluoroacetyl chloride (0.040 g,

0.34 mmol) and DIPEA (0.044 g, 0.34 mmol) gave **P8b** as a light brown powder (0.074 g, 62%).

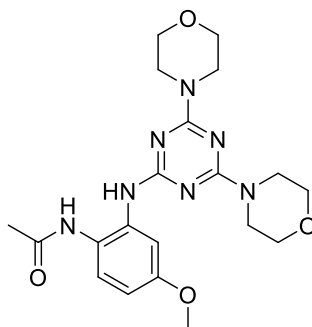
$^1\text{H-NMR}$ (400 MHz, CDCl_3) δ 10.27 (s, 1H, NH), 7.73 (d, $J = 8.9$ Hz, 1H, ArH), 6.83 (dd, $J = 8.9$, 2.8 Hz, 1H, ArH), 6.72 (dd, $J = 1.7$ Hz, 1H, ArH), 6.56 (br s, 1H, NH), 5.94 (t, $J = 54.4$ Hz, 1H, CHF_2), 3.79 (s, 3H, OCH_3), 3.77-3.66 (m, 16H, CH_2); LCMS (m/z) 466.2 $[\text{MH}]^+$.



N-(2-((4,6-dimorpholino-1,3,5-triazin-2-yl)amino)-5-methoxyphenyl)acetamide (P8c).

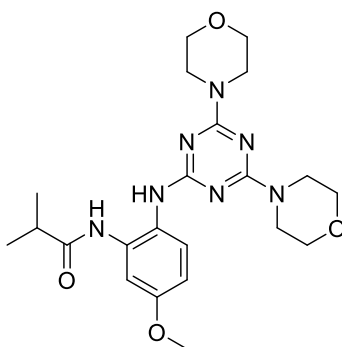
P7a (0.050 g, 0.13 mmol), acetyl chloride (0.011 g, 0.14 mmol) and DIPEA (0.026 g, 0.20 mmol)

gave **P8c** as a light brown powder (0.047 g, 85%). $^1\text{H-NMR}$ (400 MHz, CD_3OD) δ 7.42 (d, $J = 8.9$ Hz, 1H, ArH), 7.12 (d, $J = 2.7$ Hz, 1H, ArH), 6.79 (dd, $J = 8.9$, 2.9 Hz, 1H, ArH), 3.79 (s, 3H, OCH_3), 3.71 (br s, 8H, NCH_2), 3.69-3.65 (m, 8H, OCH_2), 2.13 (s, 3H, CH_3); LCMS (m/z) 430.2 $[\text{MH}]^+$.



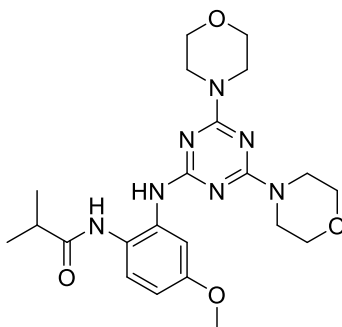
N-(2-((4,6-dimorpholino-1,3,5-triazin-2-yl)amino)-4-methoxyphenyl)acetamide (P8d).

P7b (0.050 g, 0.13 mmol), acetyl chloride (0.011 g, 0.14 mmol) and DIPEA (0.026 g, 0.20 mmol) gave **P8d** as a light brown powder (0.052 g, 94%). $^1\text{H-NMR}$ (400 MHz, CDCl_3) δ 8.21 (br s, 1H, NH), 7.62 (d, J = 8.9 Hz, 1H, ArH), 7.32 (s, 1H, ArH), 6.75 (dd, J = 8.9, 2.9 Hz, 1H, ArH), 3.89-3.71 (m, 19H, CH_2 , OCH_3), 2.24 (s, 3H, CH_3); LCMS (m/z) 430.3 $[\text{MH}]^+$.



N-(2-((4,6-dimorpholino-1,3,5-triazin-2-yl)amino)-5-methoxyphenyl)isobutyramide

(P8e). P7a (0.010 g, 0.26 mmol), isobutyryl chloride (0.031 g, 0.29 mmol) and DIPEA (0.044 g, 0.34 mmol) gave **P8e** as a light brown powder (0.082 g, 72%). $^1\text{H-NMR}$ (400 MHz, CDCl_3) δ 8.60 (br s, 1H, NH), 7.64 (br s, 1H, NH), 7.06 (d, J = 7.8 Hz, 1H, ArH), 6.65 (dd, J = 8.7, 2.9 Hz, 1H, ArH), 6.33 (br s, 1H, ArH), 3.82 (s, 3H, OCH_3), 3.77-3.65 (m, 16H, CH_2), 2.41 (br s, 1H, CH), 1.18 (d, J = 6.9 Hz, 6H, CH_3); LCMS (m/z) 458.3 $[\text{MH}]^+$.

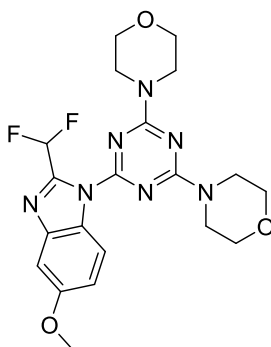


N-(2-((4,6-dimorpholino-1,3,5-triazin-2-yl)amino)-4-methoxyphenyl)isobutyramide

(P8f). P7b (0.010 g, 0.26 mmol), isobutyryl chloride (0.031 g, 0.29 mmol) and DIPEA (0.044 g, 0.34 mmol) gave **P8f** as a light brown powder (0.084 g, 74%). $^1\text{H-NMR}$ (400 MHz, CDCl_3) δ 8.28 (br s, 1H, NH), 7.57 (d, J = 9.0 Hz, 1H, ArH), 6.94 (s, 1H, NH), 6.76 (dd, J = 8.9, 2.8 Hz, 1H, ArH), 6.67 (s, 1H, ArH), 3.83-3.65 (m, 19H, CH_2 , OCH_3), 2.49-2.38 (m, 1H, CH), 1.20 (d, J = 6.9 Hz, 6H, CH_3); LCMS (m/z) 458.3 $[\text{MH}]^+$.

6.2.2.4 General procedure for cyclisation

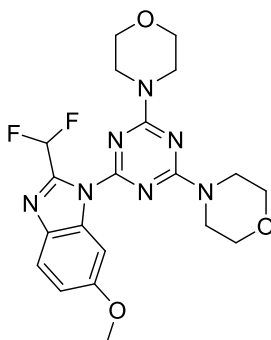
Acylated product (0.11 mmol) was refluxed in xylenes (1 mL) and acetic acid (0.3 mL) overnight. The crude product was concentrated *in vacuo* and purified by column chromatography using 1% triethylamine in ethyl acetate as eluent.



4,4'-(6-(2-(difluoromethyl)-5-methoxy-1H-benzo[d]imidazol-1-yl)-1,3,5-triazine-2,4-diyl)dimorpholine (P9a). P8a (0.032 g, 0.069 mmol) gave **P9a** as a light brown powder

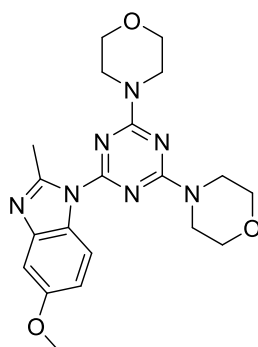
(0.017 g, 55%). $^1\text{H-NMR}$ (400 MHz, CDCl_3) δ 8.21 (d, J = 9.1 Hz, 1H, ArH), 7.55 (t, J = 53.6 Hz, 1H,

CHF₂), 7.33 (d, *J* = 2.5 Hz, 1H, ArH), 7.06 (dd, *J* = 9.1, 2.5 Hz, 1H, ArH), 3.90-3.35 (m, 11H, NCH₂, OCH₃), 3.79 (br s, 8H, OCH₂); ¹³C-NMR (101 MHz, CDCl₃) δ 165.1 (C), 162.0 (C), 157.4 (C), 146.3 (C), 143.0 (C), 128.0 (C), 116.5 (CH), 115.9 (CH), 108.5 (CH), 103.0 (CH), 66.8 (CH₂), 55.8 (CH₃), 44.2 (CH₂); HRMS (ESI+) calcd for [C₂₀H₂₅N₇O₃ + H]⁺ 448.1903, found 448.1918.



4,4'-(6-(2-(difluoromethyl)-6-methoxy-1H-benzo[d]imidazol-1-yl)-1,3,5-triazine-2,4-diyl)dimorpholine (P9b). **P8b** (0.048 g, 0.15 mmol) gave **P9b** as a light brown powder

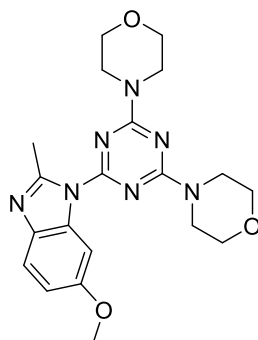
(0.016 g, 35%). ¹H-NMR (400 MHz, CDCl₃) δ 7.90 (d, *J* = 2.5 Hz, 1H, ArH), 7.75 (d, *J* = 8.9 Hz, 1H, ArH), 7.52 (t, *J* = 53.7 Hz, 1H, CHF₂), 7.01 (dd, *J* = 8.9, 2.5 Hz, 1H, ArH), 3.92-3.85 (m, 11H, NCH₂, OCH₃), 3.81-3.76 (m, 8H, OCH₂); ¹³C-NMR (101 MHz, CDCl₃) δ 165.1 (C), 162.2 (C), 158.5 (C), 145.0 (C), 136.5 (C), 134.5 (C), 121.8 (CH), 113.8 (CH), 108.6 (CH), 99.7 (CH), 66.8 (CH₂), 55.7 (CH₃), 44.2 (CH₂); HRMS (ESI+) calcd for [C₂₀H₂₅N₇O₃ + H]⁺ 448.1903, found 448.1918.



4,4'-(6-(5-methoxy-2-methyl-1H-benzo[d]imidazol-1-yl)-1,3,5-triazine-2,4-

diyl)dimorpholine (P9c). **P8c** (0.047 g, 0.11 mmol) gave **P9c** as a light brown powder (0.027 g,

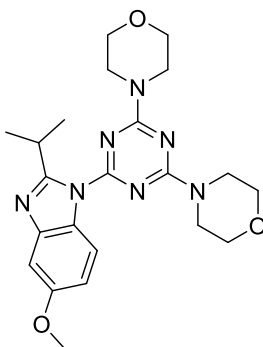
60%). $^1\text{H-NMR}$ (400 MHz, CDCl_3) δ 8.08 (d, J = 8.9 Hz, 1H, ArH), 7.18 (d, J = 2.5 Hz, 1H, ArH), 6.90 (dd, J = 8.9, 2.5 Hz, 1H, ArH), 3.88-3.86 (m, 11H, NCH_2 , OCH_3), 3.79-3.77 (m, 8H, OCH_2), 2.93 (s, 3H, CH_3); $^{13}\text{C-NMR}$ (101 MHz, CDCl_3) δ 165.4 (C), 163.0 (C), 156.8 (C), 153.4 (C), 143.4 (C), 128.3 (C), 115.6 (CH), 112.4 (CH), 101.9 (CH), 66.8 (CH_2), 55.9 (CH_3), 44.1 (CH_2), 19.7 (CH_3); HRMS (ESI+) calcd for $[\text{C}_{20}\text{H}_{25}\text{N}_7\text{O}_3 + \text{H}]^+$ 412.2092, found 412.2108.



4,4'-(6-(6-methoxy-2-methyl-1H-benzo[d]imidazol-1-yl)-1,3,5-triazine-2,4-

diyl)dimorpholine (P9d). **P8d** (0.052 g, 0.12 mmol) gave **P9d** as a light brown powder

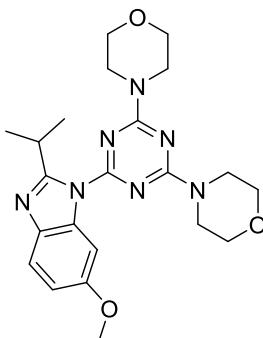
(0.029 g, 58%). $^1\text{H-NMR}$ (400 MHz, CDCl_3) δ 7.80 (d, J = 2.5 Hz, 1H, ArH), 7.58 (d, J = 8.7 Hz, 1H, ArH), 6.93 (dd, J = 8.7, 2.5 Hz, 1H, ArH), 3.89 (br s, 8H, NCH_2), 3.84 (s, 3H, OCH_3), 3.80-3.75 (m, 8H, OCH_2), 2.94 (s, 3H, CH_3); $^{13}\text{C-NMR}$ (101 MHz, CDCl_3) δ 165.3 (C), 163.1 (C), 156.7 (C), 151.9 (C), 137.0 (C), 134.6 (C), 119.3 (CH), 111.8 (CH), 99.9 (CH), 66.8 (CH_2), 55.7 (CH_3), 44.0 (CH_2), 19.5 (CH_3); HRMS (ESI+) calcd for $[\text{C}_{20}\text{H}_{25}\text{N}_7\text{O}_3 + \text{H}]^+$ 412.2092, found 412.2111.



4,4'-(6-(2-isopropyl-5-methoxy-1H-benzo[d]imidazol-1-yl)-1,3,5-triazine-2,4-

diyl)dimorpholine (P9e). **P8e** (0.080 g, 0.17 mmol) gave **P9e** as a light brown powder

(0.050 g, 65%). $^1\text{H-NMR}$ (400 MHz, CDCl_3) δ 7.97 (d, $J = 8.9$ Hz, 1H, ArH), 7.27-7.26 (m, 1H, ArH), 6.88 (dd, $J = 8.9, 2.5$ Hz, 1H, ArH), 4.17-4.04 (m, 1H, CH), 3.90-3.83 (m, 11H, NCH_2 , OCH_3), 3.82-3.73 (m, 8H, OCH_2), 1.45 (d, $J = 6.8$ Hz, 6H, CH_3); $^{13}\text{C-NMR}$ (101 MHz, CDCl_3) δ 165.5 (C), 163.1 (C), 161.8 (C), 156.8 (C), 128.3 (C), 115.3 (CH), 112.7 (CH), 102.0 (CH), 66.8 (CH_2), 55.9 (CH_3), 44.1 (CH_2), 29.0 (CH), 22.1 (CH_3); HRMS (ESI+) calcd for $[\text{C}_{22}\text{H}_{29}\text{N}_7\text{O}_3 + \text{H}]^+$ 440.2405, found 440.2419.

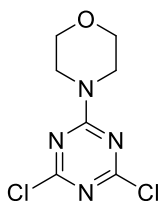


4,4'-(6-(2-isopropyl-6-methoxy-1H-benzo[d]imidazol-1-yl)-1,3,5-triazine-2,4-

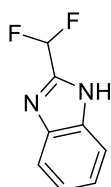
diyl)dimorpholine (P9f). **P8f** (0.084 g, 0.17 mmol) gave **P9f** as a light brown powder (0.061 g, 75%). $^1\text{H-NMR}$ (400 MHz, CDCl_3) δ 7.68 (d, $J = 2.5$ Hz, 1H, ArH), 7.61 (d, $J = 8.7$ Hz, 1H, ArH), 6.89 (dd, $J = 8.7, 2.5$ Hz, 1H, ArH), 4.14-4.02 (m, 1H, CH), 3.92-3.84 (m, 8H, NCH_2), 3.81 (s, 3H, OCH_3), 3.79-3.73 (m, 8H, OCH_2), 1.43 (d, $J = 6.8$ Hz, 6H, CH_3); $^{13}\text{C-NMR}$ (101 MHz, CDCl_3) δ 165.5 (C),

163.2 (C), 160.4 (C), 156.7 (C), 137.0 (C), 134.7 (C), 119.6 (CH), 111.8 (CH), 99.3 (CH), 66.8 (CH₂), 55.8 (CH₃), 44.05 (CH₂), 28.8 (CH), 22.1 (CH₃); HRMS (ESI+) calcd for [C₂₂H₂₉N₇O₃ + H]⁺ 440.2405, found 440.2384.

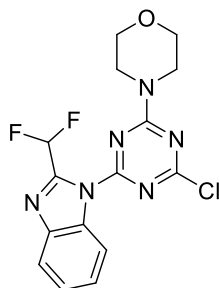
6.2.3 Chapter 3 experimental



4-(4,6-dichloro-1,3,5-triazin-2-yl)morpholine (26). To a stirred solution of cyanuric chloride (5.0 g, 27 mmol) in dry acetone (50 mL) was added dropwise a solution of morpholine (1.7 g, 19 mmol) and triethylamine (1.9 g, 19 mmol) in dry acetone (50 mL) at -20°C. The resulting mixture was quenched with water, filtered, washed with water and cold methanol and dried to give **26** as a white powder (4.3 g, 96%). ¹H-NMR (400 MHz, CD₃OD) δ 3.90-3.88 (m, 4H, NCH₂), 3.77-3.74 (m, 4H, OCH₂); LCMS (*m/z*) 235.1 [MH]⁺.



2-(difluoromethyl)-1H-benzo[d]imidazole (28). 1,2-phenylenediamine (5.4 g, 50 mmol) and difluoroacetic acid (9.6 g, 100 mmol) were refluxed in 4 M aqueous HCl (20 mL) for 3 hours. The solution was treated with charcoal, filtered through Celite, washed with water and neutralised with 23% aqueous NH₃. The precipitate was collected, washed with water and dried to give **28** as an orange powder (7.6 g, 90%). ¹H-NMR (400 MHz, CD₃OD) δ 7.71 (dd, *J* = 6.1, 3.2 Hz, 2H, ArH), 7.38 (dd, *J* = 6.1, 3.1 Hz, 2H, ArH), 6.94 (t, *J* = 53.8 Hz, 1H, CHF₂); LCMS (*m/z*) 169.1 [MH]⁺.

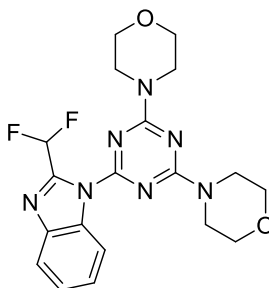


4-(4-chloro-6-(2-(difluoromethyl)-1H-benzo[d]imidazol-1-yl)-1,3,5-triazin-2-

yl)morpholine (27). **26** (6.0 g, 26 mmol), **28** (4.3 g, 26 mmol) and K_2CO_3 (3.6 g, 26 mmol) were suspended in dimethylformamide and stirred at room temperature overnight to give **27** as a white powder (8.6 g, 92%). 1H -NMR (400 MHz, $CDCl_3$) δ 8.45-8.40 (m, 1H, ArH), 7.93-7.88 (m, 1H, ArH), 7.57 (t, $J = 53.5$ Hz, 1H, CHF_2), 7.52-7.41 (m, 2H, ArH), 4.01-3.94 (m, 4H, NCH_2), 3.86-3.79 (m, 4H, OCH_2); LCMS (m/z) 367.1 $[MH]^+$.

6.2.3.1 Preparation of 6-substituted 4-(2-(difluoromethyl)-benzimidazole)-2-morpholino-1,3,5-triazines

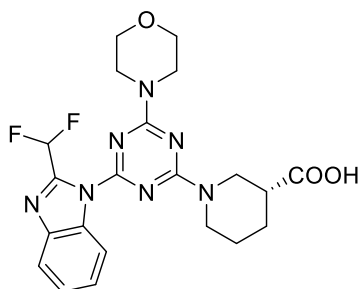
27 (0.20 g, 0.55 mmol), the appropriate amine (1.1 mmol) and K_2CO_3 (0.15 g, 1.1 mmol) were stirred at 50°C under nitrogen overnight. Water was added to quench the reaction and precipitate neutral products. 1 M aqueous HCl was added to adjust the pH to 5 to precipitate compounds **25a-c**. Compounds required no further purification.



4,4'-(6-(2-(difluoromethyl)-1H-benzo[d]imidazol-1-yl)-1,3,5-triazine-2,4-

diyl)dimorpholine (3). **27** (0.10 g, 0.25 mmol), morpholine (0.075 g, 0.50 mmol) and K_2CO_3

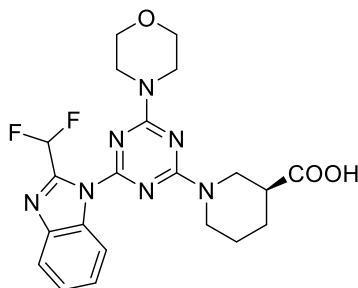
(0.047 g, 0.50 mmol) gave **3** as a white powder (0.086 g, 76%). $^1\text{H-NMR}$ (400 MHz, CDCl_3) δ 8.35-8.32 (m, 1H, ArH), 7.89 (dd, $J = 7.2, 1.4$ Hz, 1H, ArH), 7.63 (t, $J = 53.6$ Hz, 1H, CHF_2), 7.47-7.37 (m, 2H, ArH), 3.88 (br s, 8H, NCH_2), 3.79 (br s, 8H, OCH_2); LCMS (m/z) 418.2 $[\text{MH}]^+$.



(R)-1-(4-(2-(difluoromethyl)-1H-benzo[d]imidazol-1-yl)-6-morpholino-1,3,5-triazin-2-yl)piperidine-3-carboxylic acid (25a). **27** (0.20 g, 0.55 mmol), (R)-nipecotic acid (0.14 g,

1.1 mmol) and K_2CO_3 (0.15 g, 1.1 mmol) gave **25a** as a white powder (0.21 g, 79%). The spectra were consistent with conformational isomers giving rise to two sets of signals in 1:1 ratio.

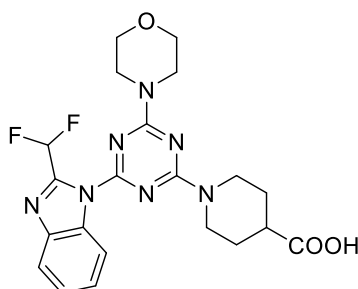
$^1\text{H-NMR}$ (400 MHz, $(\text{CD}_3)_2\text{SO}$) δ 8.39 (d, $J = 7.7$ Hz, 1H, ArH), 8.32 (d, $J = 8.2$ Hz, 1H, ArH), 7.84 (d, $J = 7.5$ Hz, 2H, ArH), 7.75 (t, $J = 52.7$ Hz, 1H, CHF_2), 7.72 (t, $J = 52.9$ Hz, 1H, CHF_2), 7.52-7.39 (m, 4H, ArH), 4.64 (dd, $J = 12.5, 2.5$ Hz, 1H, CH_2), 4.46 (dd, $J = 12.8, 2.6$ Hz, 1H, CH_2), 4.42-4.34 (m, 1H, CH_2), 4.30-4.21 (m, 1H, CH_2), 3.83-3.75 (m, 8H, NCH_2 (morpholine)), 3.72-3.65 (m, 8H, OCH_2), 3.52-3.43 (m, 2H, CH_2), 3.33-3.13 (m, 2H, CH_2), 2.58-2.40 (m, 2H, CH), 2.07-1.93 (m, 2H, CH_2), 1.82-1.63 (m, 4H, CH_2), 1.54-1.42 (m, 2H, CH_2); $^{13}\text{C-NMR}$ (101 MHz, $(\text{CD}_3)_2\text{SO}$) δ 174.5 (C), 174.3 (C), 164.5 (C), 164.1 (C), 161.3 (C), 145.9 (t, $J = 26.4$ Hz, C), 141.4 (C), 132.9 (C), 125.8 (CH), 125.7 (CH), 124.3 (CH), 120.7 (CH), 115.9 (CH), 115.7 (CH), 108.5 (t, $J = 237.3$ Hz, CH), 65.9 (CH_2), 45.4 (CH_2), 45.0 (CH_2), 43.6 (CH_2), 43.5 (CH_2), 40.6 (CH), 40.5 (CH), 27.0 (CH_2), 26.7 (CH_2), 23.9 (CH_2), 23.6 (CH_2); HRMS (ESI+) calcd for $[\text{C}_{21}\text{H}_{23}\text{F}_2\text{N}_7\text{O}_3 + \text{H}]^+$ 460.1903, found 460.1897.



(S)-1-(4-(2-(difluoromethyl)-1H-benzo[d]imidazol-1-yl)-6-morpholino-1,3,5-triazin-2-yl)piperidine-3-carboxylic acid (25b)⁸. **27** (0.20 g, 0.55 mmol), (S)-nipecotic acid (0.14 g,

1.1 mmol) and K₂CO₃ (0.15 g, 1.1 mmol) gave **25b** as a white powder (0.18 g, 71%). The spectra were consistent with conformational isomers giving rise to two sets of signals in 1:1 ratio.

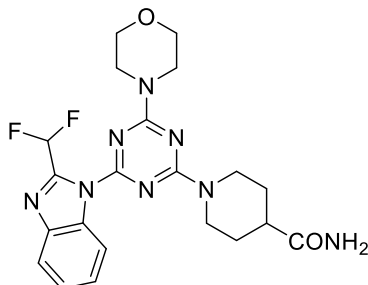
¹H-NMR (400 MHz, (CD₃)₂SO) δ 8.40 (d, *J* = 7.7 Hz, 1H, ArH), 8.33 (d, *J* = 8.2 Hz, 1H, ArH), 7.85 (d, *J* = 7.4 Hz, 2H, ArH), 7.76 (t, *J* = 52.2 Hz, 1H, CHF₂), 7.73 (t, *J* = 53.4 Hz, 1H, CHF₂), 7.54-7.40 (m, 4H, ArH), 4.65 (dd, *J* = 13.0, 2.6 Hz, 1H, CH₂), 4.47 (dd, *J* = 13.0, 2.9 Hz, 1H, CH₂), 4.44-4.36 (m, 1H, CH₂), 4.31-4.23 (m, 1H, CH₂), 3.86-3.76 (m, 8H, NCH₂ (morpholine)), 3.74-3.64 (m, 8H, OCH₂), 3.53-3.44 (m, 1H, CH₂), 3.30-3.13 (m, 2H, CH₂), 2.59-2.42 (m, 2H, CH), 2.07-1.94 (m, 2H, CH₂), 1.85-1.62 (m, 2H, CH₂), 1.57 (m, 2H, CH₂); LCMS (*m/z*) 460.3 [MH]⁺.



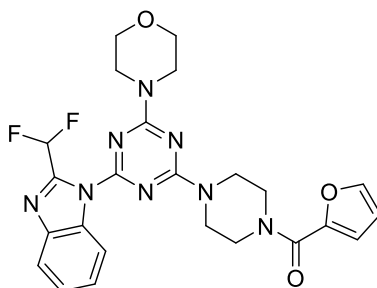
1-(4-(2-(difluoromethyl)-1H-benzo[d]imidazol-1-yl)-6-morpholino-1,3,5-triazin-2-yl)piperidine-4-carboxylic acid (25c)⁸. **27** (0.20 g, 0.55 mmol) and isonipecotic acid (0.14 g,

1.1 mmol) and K₂CO₃ (0.15 g, 1.1 mmol) gave **25c** as a white powder (0.17 g, 67%). ¹H-NMR (400 MHz, CDCl₃) δ 8.35-8.31 (m, 1H, ArH), 7.92-7.88 (m, 1H, ArH), 7.58 (t, *J* = 53.6 Hz, 1H, CHF₂), 7.46-7.37 (m, 2H, ArH), 4.61 (d, *J* = 11.9 Hz, 2H, CH₂), 3.91-3.85 (m, 4H, NCH₂ (morpholine)),

3.82-3.77 (m, 4H, OCH₂), 3.29-3.13 (m, 2H, CH₂), 2.74-2.65 (m, 1H, CH), 2.15-2.01 (m, 2H, CH₂), 1.85-1.73 (m, 2H, CH₂); LCMS (*m/z*) 460.3 [MH]⁺.



1-(4-(2-(difluoromethyl)-1H-benzo[d]imidazol-1-yl)-6-morpholino-1,3,5-triazin-2-yl)piperidine-4-carboxamide (25d)⁸. **27** (0.10 g, 0.27 mmol), isonipecotamide (0.070 g, 0.55 mmol) and K₂CO₃ (0.075 g, 0.55 mmol) gave **25d** as a white powder (0.11 g, 86%). ¹H-NMR (400 MHz, CDCl₃) δ 8.36-8.31 (m, 1H, ArH), 7.91-7.87 (m, 1H, ArH), 7.58 (t, *J* = 51.4 Hz, 1H, CHF₂), 7.44-7.37 (m, 2H, ArH), 5.57 (s, 1H, NH₂), 5.51 (s, 1H, NH₂), 4.76 (br s, 2H, CH₂), 3.94-3.84 (m, 4H, NCH₂ (morpholine)), 3.83-3.73 (m, 4H, OCH₂), 3.16-2.98 (m, 2H, CH₂), 2.55-2.46 (m, 1H, CH), 2.00 (br s, 2H, CH₂), 1.87-1.71 (m, 2H, CH₂); LCMS (*m/z*) 459.3 [MH]⁺.

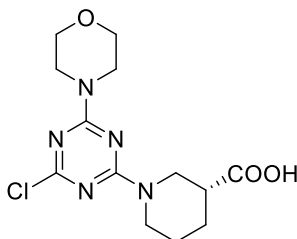


(4-(4-(2-(difluoromethyl)-1H-benzo[d]imidazol-1-yl)-6-morpholino-1,3,5-triazin-2-yl)piperazin-1-yl)(furan-2-yl)methanone (25f)⁸. **27** (0.10 g, 0.27 mmol), 1-(2-furoyl)piperazine (0.10 g, 0.55 mmol) and K₂CO₃ (0.075 g, 0.55 mmol) gave **25f** as a white powder (0.11 g, 79%). ¹H-NMR (400 MHz, CDCl₃) δ 8.34 (d, *J* = 7.6 Hz, 1H, ArH), 7.90 (d, *J* = 7.4 Hz, 1H, ArH), 7.56 (t, *J* = 53.6 Hz, 1H, CHF₂), 7.53 (s, 1H, ArH), 7.48-7.37 (m, 2H, ArH), 7.10

(d, $J = 3.0$ Hz, 1H, ArH), 6.53 (dd, $J = 3.4, 1.8$ Hz, 1H, ArH), 4.02-3.87 (m, 12H, NCH₂), 3.83-3.75 (m, 4H, OCH₂); LCMS (m/z) 511.3 [MH]⁺.

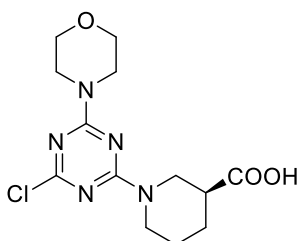
6.2.3.2 Preparation of 4-substituted 6-chloro-2-morpholino-1,3,5-triazines

A mixture of **26** (0.24 g, 1 mmol), the appropriate amine (1 mmol) and K₂CO₃ (0.14 g, 1 mmol) were suspended in dimethylformamide and stirred at room temperature for 4 hours under nitrogen. The reaction was quenched with water (for **32-34**) or 1 M HCl (for **29-31**) and the resultant precipitate filtered and dried *in vacuo* to yield the desired product.



(R)-1-(4-chloro-6-morpholino-1,3,5-triazin-2-yl)piperidine-3-carboxylic acid (**29**). **26**

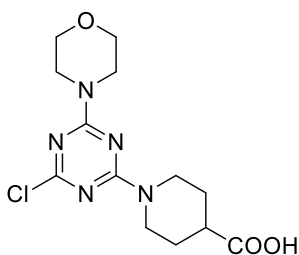
(0.25 g, 1.1 mmol) and (R)-nipecotic acid (0.14 g, 1.1 mmol) gave **29** as a white powder (0.26 g, 76%). ¹H-NMR (400 MHz, CDCl₃) δ 4.71 (br s, 1H, CH₂), 4.48 (d, $J = 12.6$ Hz, 1H, CH₂), 3.82-3.76 (m, 4H, NCH₂ (morpholine)), 3.74-3.68 (m, 4H, OCH₂), 3.23-3.17 (m, 1H, CH₂), 3.02 (t, $J = 12.7$ Hz, 1H, CH₂), 2.59-2.51 (m, 1H, CH), 2.18-2.14 (m, 1H, CH₂), 1.84-1.74 (m, 2H, CH₂), 1.58-1.48 (m, 1H, CH₂); LCMS (m/z) 328.1 [MH]⁺.



(S)-1-(4-chloro-6-morpholino-1,3,5-triazin-2-yl)piperidine-3-carboxylic acid (**30**). **26**

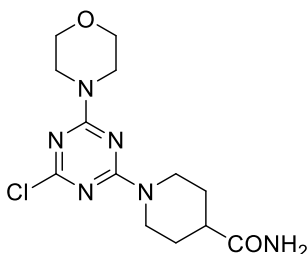
(0.50 g, 2.2 mmol) and (S)-nipecotic acid (0.28 g, 2.2 mmol) gave **30** as a white powder (0.65 g,

99%). $^1\text{H-NMR}$ (400 MHz, CDCl_3) δ 4.71 (br s, 1H, CH_2), 4.49-4.46 (m, 1H, CH_2), 3.79 (br s, 4H, NCH_2 (morpholine)), 3.72-3.70 (m, 4H, OCH_2), 3.24-3.18 (m, 1H, CH_2), 3.02 (t, $J = 11.5$ Hz, 1H, CH_2), 2.58-2.53 (m, 1H, CH), 2.18-2.14 (m, 1H, CH_2), 1.83-1.74 (m, 2H, CH_2), 1.58-1.49 (m, 1H, CH_2); LCMS (m/z) 328.1 $[\text{MH}]^+$.



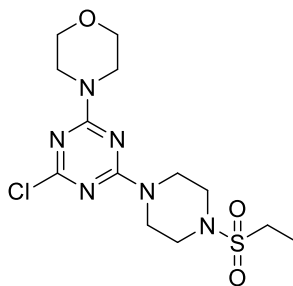
1-(4-chloro-6-morpholino-1,3,5-triazin-2-yl)piperidine-4-carboxylic acid (31). **26** (0.50 g, 2.1 mmol) and isonipecotic acid (0.28 g, 2.1 mmol) gave **31** as a white powder (0.51 g, 78%).

$^1\text{H-NMR}$ (400 MHz, CDCl_3) δ 4.57 (br s, 2H, CH_2), 3.79 (br s, 4H, NCH_2 (morpholine)), 3.74-3.69 (m, 4H, OCH_2), 3.11 (t, $J = 11.3$ Hz, 2H, CH_2), 2.70-2.62 (m, 1H, CH), 2.04-2.01 (m, 2H, CH_2), 1.79-1.69 (m, 2H, CH_2); LCMS (m/z) 328.2 $[\text{MH}]^+$.



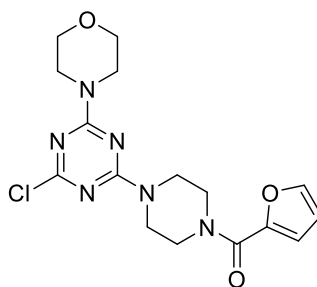
1-(4-chloro-6-morpholino-1,3,5-triazin-2-yl)piperidine-4-carboxamide (32). **26** (0.25 g, 1.1 mmol) and isonipecotamide (0.14 g, 1.1 mmol) gave **32** as a white powder (0.31 g, 95%).

$^1\text{H-NMR}$ (400 MHz, CDCl_3) δ 5.44 (s, 1H, NH_2), 5.29 (s, 1H, NH_2), 4.71 (br s, 2H, CH_2), 3.79 (br s, 4H, NCH_2 (morpholine)), 3.72-3.70 (m, 4H, OCH_2), 2.98-2.92 (m, 2H, CH_2), 2.46-2.39 (m, 1H, CH), 1.96-1.92 (m, 2H, CH_2), 1.73-1.65 (m, 2H, CH_2); LCMS (m/z) 327.2 $[\text{MH}]^+$.



4-(4-chloro-6-(4-(ethylsulfonyl)piperazin-1-yl)-1,3,5-triazin-2-yl)morpholine (33). 26

(0.25 g, 1.1 mmol) and 1-(ethylsulfonyl)piperazine (0.19 g, 1.1 mmol) gave **33** as a white powder (0.31 g, 78%). $^1\text{H-NMR}$ (400 MHz, CDCl_3) δ 3.90-3.68 (m, 12H, NCH_2), 3.33 (m, 4H, OCH_2), 2.97 (q, $J = 7.4$ Hz, 2H, CH_2CH_3), 1.38 (t, $J = 7.4$ Hz, 3H, CH_2CH_3); LCMS (m/z) 377.1 $[\text{MH}]^+$.



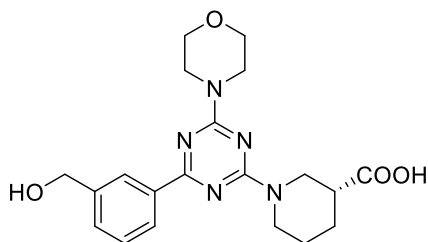
(4-(4-chloro-6-morpholino-1,3,5-triazin-2-yl)piperazin-1-yl)(furan-2-yl)methanone (34). 26

(0.25 g, 1.1 mmol) and 1-(2-furoyl)piperazine (0.20 g, 1.1 mmol) with extraction with ethyl acetate after addition of water, dried over Na_2SO_4 and concentrated *in vacuo* to give **34** as a light brown foam (0.36 g, 96%). $^1\text{H-NMR}$ (400 MHz, CDCl_3) δ 7.50 (dd, $J = 1.8, 0.8$ Hz, 1H, ArH), 7.07 (dd, $J = 3.5, 0.8$ Hz, 1H, ArH), 6.51 (dd, $J = 3.5, 1.8$ Hz, 1H, ArH), 3.93-3.77 (m, 14H, NCH_2), 3.74-3.69 (m, 4H, OCH_2); LCMS (m/z) 379.2 $[\text{MH}]^+$.

6.2.3.3 Preparation of Suzuki coupled products

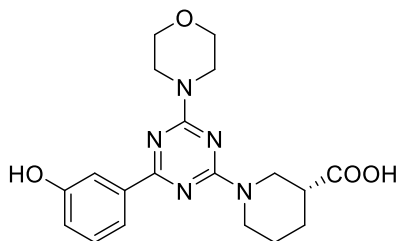
To a degassed suspension of 6-chloro-1,3,5-triazine (0.31 mmol), Cs_2CO_3 (0.20 g, 0.61 mmol) and boronic acid (0.40 mmol) in dimethylformamide or 1,4-dioxane was added $\text{Pd}(\text{OAc})_2$ (0.0007 g, 0.003 mmol, 1 mol%), PCy_3 (0.001 g, 0.003 mmol, 1 mol%), TBAB (0.001 g, 0.003 mmol,

1 mol%) and water (0.5 mL). This was exposed to microwave irradiation at 150°C for 30 minutes, partitioned between water and ethyl acetate, extracted a further two times into ethyl acetate, dried over Na₂SO₄ and concentrated *in vacuo* to give the crude product. The crude product was then purified via column chromatography and semi-preparative reverse-phase HPLC where necessary.



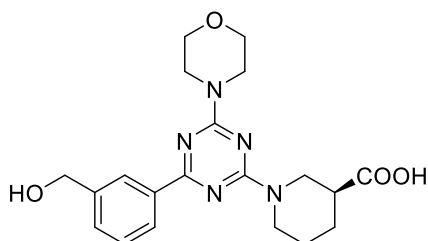
(R)-1-(4-(3-(hydroxymethyl)phenyl)-6-morpholino-1,3,5-triazin-2-yl)piperidine-3-carboxylic acid (37a). **29** (0.10 g, 0.31 mmol) and 3-(hydroxymethyl)phenylboronic acid

(0.060 g, 0.40 mmol) gave **37a** as a white powder (0.091 g, 72%). ¹H-NMR (400 MHz, CD₃OD) δ 8.38 (s, 1H, ArH), 8.28 (d, *J* = 7.7 Hz, 1H, ArH), 7.51-7.47 (m, 1H, ArH), 7.41 (t, *J* = 7.6 Hz, 1H, ArH), 4.67 (s, 2H, CH₂OH), 3.90 (br s, 4H, NCH₂ (morpholine)), 3.74 -3.71 (m, 4H, OCH₂), 3.21-3.13 (m, 1H, CH₂), 3.07-3.01 (m, 1H, CH₂), 2.50-2.41 (m, 1H, CH), 2.15-2.11 (m, 1H, CH₂), 1.84-1.79 (m, 1H, CH₂), 1.77-1.70 (m, 1H, CH₂), 1.59-1.52 (m, 1H, CH₂), extra resonances equating to 2H are expected, these appear to be obscured by the water signal; ¹³C-NMR (101 MHz, (CD₃)SO) δ 174.7 (C), 169.5 (C), 164.7 (C), 164.5 (C), 142.6 (C), 136.7 (C), 129.7 (CH), 128.0 (CH), 126.5 (CH), 126.0 (CH), 66.0 (CH₂), 62.9 (CH₂), 44.6 (CH₂), 43.3 (CH₂), 40.7 (CH), 27.2 (CH₂), 24.0 (CH₂); LCMS (*m/z*) 400.1 [MH]⁺; HRMS (ESI⁺) calcd for [C₂₀H₂₅N₅O₄ + H]⁺ 400.1979, found 400.1975.



(R)-1-(4-(3-hydroxyphenyl)-6-morpholino-1,3,5-triazin-2-yl)piperidine-3-carboxylic acid

(37b). **29** (0.10 g, 0.31 mmol) and 3-hydroxyphenylboronic acid (0.055 g, 0.40 mmol) gave **37b** as a white powder (0.019 g, 16%). $^1\text{H-NMR}$ (400 MHz, CD_3OD) δ 7.85-7.81 (m, 2H, ArH), 7.24 (t, $J = 7.9$ Hz, 1H, ArH), 6.91 (ddd, $J = 8.0, 2.6, 1.0$ Hz, 1H, ArH), 3.89 (br s, 4H, NCH_2 (morpholine)), 3.74 (m, 4H, OCH_2), 3.24-3.17 (m, 1H, CH_2), 3.07 (br s, 1H, CH_2), 2.51-2.45 (m, 1H, CH), 2.16-2.11 (m, 1H, CH_2), 1.84-1.70 (m, 2H, CH_2), 1.58-1.51 (m, 1H, CH_2), extra resonances equating to 2H are expected, these appear to be obscured by the water signal; $^{13}\text{C-NMR}$ (101 MHz, CD_3OD) δ 178.8 (C), 170.2 (C), 165.3 (C), 165.1 (C), 164.5 (C), 129.5 (CH), 120.9 (CH), 118.6 (CH), 115.2 (CH), 67.0 (CH_2), 45.2 (CH_2), 44.0 (CH_2), 43.8 (CH_2), 41.2 (CH), 27.6 (CH_2), 24.3 (CH_2); LCMS (m/z) 386.1 [MH] $^+$; HRMS (ESI $^+$) calcd for $[\text{C}_{19}\text{H}_{22}\text{N}_5\text{O}_4 + \text{H}]^+$ 386.1823, found 386.1832.

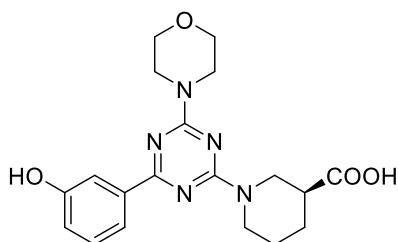


(S)-1-(4-(3-(hydroxymethyl)phenyl)-6-morpholino-1,3,5-triazin-2-yl)piperidine-3-

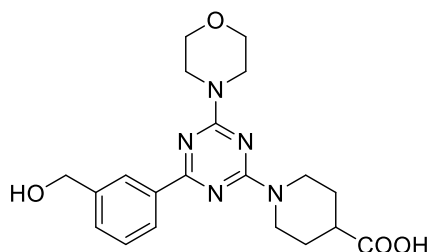
carboxylic acid (38a). **30** (0.050 g, 0.15 mmol) and 3-(hydroxymethyl)phenylboronic acid

(0.060 g, 0.39 mmol) gave **38a** as a white powder (0.042 g, 70%). $^1\text{H-NMR}$ (400 MHz, CD_3OD) δ 8.39 (s, 1H, ArH), 8.29 (d, $J = 7.5$ Hz, 1H, ArH), 7.53-7.46 (m, 1H, ArH), 7.41 (dd, $J = 7.6, 7.6$ Hz, 1H, ArH), 5.20-4.87 (m, 2H, CH_2), 4.67 (s, 2H, CH_2OH), 3.91 (br s, 4H, NCH_2 (morpholine)), 3.79-3.68 (m, 4H, OCH_2), 3.01-2.91 (m, 1H, CH_2), 2.85 (t, $J = 11.4$ Hz, 1H, CH_2), 2.35-2.26 (m, 1H, CH),

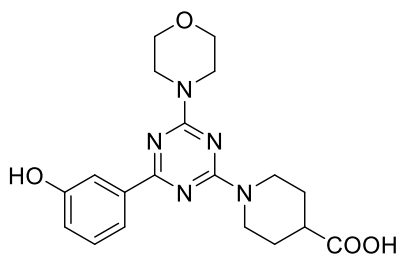
2.14 (d, $J = 12.4$ Hz, 1H, CH₂), 1.80 (d, $J = 12.9$ Hz, 1H, CH₂), 1.75-1.64 (m, 1H, CH₂), 1.59-1.43 (m, 1H, CH₂); ¹³C-NMR (101 MHz, CD₃OD) δ 182.5 (C), 171.6 (C), 166.7 (C), 166.2 (C), 142.6 (C), 139.0 (C), 130.9 (CH), 129.1 (CH), 128.4 (CH), 128.0 (CH), 67.9 (CH₂), 65.2 (CH₂), 47.8 (CH₂), 46.8 (CH), 44.9 (CH₂), 30.3 (CH₂), 26.4 (CH₂); LCMS (m/z) 400.2 [MH]⁺; HRMS (ESI⁺) calcd for [C₂₀H₂₄N₅O₄ + H]⁺ 400.1979, found 400.1984.



(S)-1-(4-(3-hydroxyphenyl)-6-morpholino-1,3,5-triazin-2-yl)piperidine-3-carboxylic acid (38b). **30** (0.10 g, 0.31 mmol) and 3-hydroxyphenylboronic acid (0.055 g, 0.40 mmol) gave **38b** as a white powder (0.039 g, 21% [as doubly protonated TFA salt]). ¹H-NMR (400 MHz, CD₃OD) δ 7.75-7.71 (m, 1H, ArH), 7.71-7.69 (m, 1H, ArH), 7.30 (t, $J = 7.9$ Hz, 1H, ArH), 6.99 (ddd, $J = 8.1, 2.5, 0.9$ Hz, 1H, ArH), 4.69 (dd, $J = 13.4, 3.8$ Hz, 1H, CH₂), 4.46 (br s, 1H, CH₂), 3.97-3.88 (m, 4H, NCH₂ (morpholine)), 3.81-3.72 (m, 4H, OCH₂), 3.56-3.37 (m, 2H, CH₂), 2.58 (br s, 1H, CH), 2.18-2.08 (m, 1H, CH₂), 1.88-1.75 (m, 2H, CH₂), 1.67-1.52 (m, 1H, CH₂); ¹³C-NMR (101 MHz, CD₃OD) δ 176.9 (C), 175.4 (C), 164.6 (C), 164.2 (C), 158.7 (C), 158.6 (C), 130.6 (CH), 120.9 (CH), 120.6 (CH), 116.3 (CH), 67.9 (CH₂), 46.9 (CH₂), 45.4 (CH₂), 42.3 (CH), 28.5 (CH₂), 28.4 (CH₂), 25.2 (CH₂); LCMS (m/z) 386.2 [MH]⁺; HRMS (ESI⁺) calcd for [C₁₉H₂₂N₅O₄ + H]⁺ 386.1823, found 386.1834.

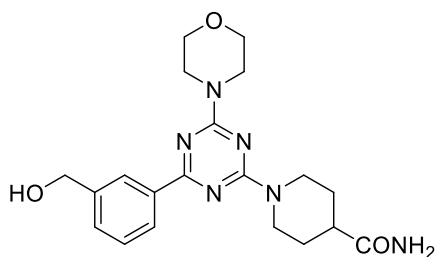


1-(4-(3-(hydroxymethyl)phenyl)-6-morpholino-1,3,5-triazin-2-yl)piperidine-4-carboxylic acid (39a). **31** (0.10 g, 0.31 mmol) and 3-(hydroxymethyl)phenylboronic acid (0.060 g, 0.40 mmol) gave **39a** as a white powder (0.011 g, 9%). $^1\text{H-NMR}$ (400 MHz, CD_3OD) δ 8.38 (s, 1H, ArH), 8.28 (dt, J = 7.7, 1.5 Hz, 1H, ArH), 7.49 (dt, J = 7.9, 1.5 Hz, 1H, ArH), 7.42 (t, J = 7.6 Hz, 1H, ArH), 4.86-4.73 (m, 2H, CH_2), 4.68 (s, 2H, CH_2OH), 3.91 (br s, 4H, NCH_2 (morpholine)), 3.79-3.69 (m, 4H, OCH_2), 3.18-3.06 (m, 2H, CH_2), 2.64-2.55 (m, 1H, CH), 2.05-1.95 (m, 2H, CH_2), 1.70-1.59 (m, 2H, CH_2); $^{13}\text{C-NMR}$ (101 MHz, CD_3OD) δ 178.5 (C), 171.7 (C), 166.7 (C), 166.3 (C), 142.7 (C), 138.9 (C), 131.0 (CH), 129.1 (CH), 128.4 (CH), 127.9 (CH), 67.9 (CH_2), 65.2 (CH_2), 44.9 (CH_2), 43.7 (CH_2), 42.4 (CH), 29.3 (CH_2); LCMS (m/z) 400.1 [MH] $^+$; HRMS (ESI $^+$) calcd for [$\text{C}_{20}\text{H}_{24}\text{N}_5\text{O}_4 + \text{H}$] $^+$ 400.1979, found 400.1983.

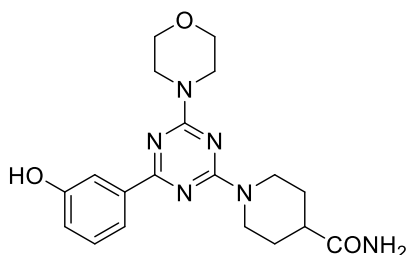


1-(4-(3-hydroxyphenyl)-6-morpholino-1,3,5-triazin-2-yl)piperidine-4-carboxylic acid (39b). **31** (0.10 g, 0.31 mmol) and 3-hydroxyphenylboronic acid (0.055 g, 0.40 mmol) gave **39b** as a white powder (0.021 g, 15% [as doubly protonated TFA salt]). $^1\text{H-NMR}$ (400 MHz, CD_3OD) δ 7.71-7.68 (m, 1H, ArH), 7.68-7.66 (m, 1H, ArH), 7.32 (t, J = 7.9 Hz, 1H, ArH), 7.02 (ddd, J = 8.1, 2.6, 0.9 Hz, 1H, ArH), 4.67 (d, J = 13.4 Hz, 2H, CH_2), 3.97-3.87 (m, 4H, NCH_2 (morpholine)), 3.79-3.71 (m, 4H, OCH_2), 3.24 (t, J = 11.6 Hz, 2H, CH_2), 2.72-2.63 (m, 1H, CH), 2.09-1.98 (m, 2H, CH_2), 1.77-

1.64 (m, 2H, CH₂); ¹³C-NMR (101 MHz, CD₃OD) δ 178.1 (C), 168.8 (C), 163.4 (C), 162.8 (C), 158.8 (C), 137.1 (C), 130.6 (CH), 120.9 (CH), 120.6 (CH), 116.4 (CH), 67.6 (CH₂), 45.6 (CH₂), 44.5 (CH₂), 41.9 (CH), 29.1 (CH₂); LCMS (*m/z*) 386.1 [MH]⁺; HRMS (ESI⁺) calcd for [C₁₉H₂₂N₅O₄ + H]⁺ 386.1823, found 386.1834.

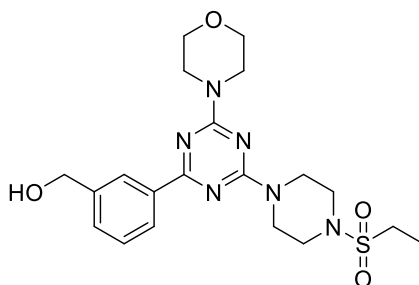


1-(4-(3-(hydroxymethyl)phenyl)-6-morpholino-1,3,5-triazin-2-yl)piperidine-4-carboxamide (40a). **32** (0.050 g, 0.15 mmol) and 3-(hydroxymethyl)phenylboronic acid (0.060 g, 0.39 mmol) gave **40a** as a white powder (0.035 g, 58%). ¹H-NMR (400 MHz, (CD₃)₂SO) δ 8.29 (s, 1H, ArH), 8.21 (d, *J* = 7.6 Hz, 1H, ArH), 7.49-7.45 (m, 1H, ArH), 7.42 (t, *J* = 7.5 Hz, 1H, ArH), 7.31 (s, 1H, NH₂), 6.80 (s, 1H, NH₂), 5.28 (t, *J* = 5.8 Hz, 1H, OH), 4.95-4.63 (m, 2H, CH₂), 4.56 (d, *J* = 5.8 Hz, 2H, CH₂OH), 3.81 (br s, 4H, NCH₂ (morpholine)), 3.70-3.61 (m, 4H, OCH₂), 2.94 (br s, 2H, CH₂), 2.44-2.34 (m, 1H, CH), 1.85-1.75 (m, 2H, CH₂), 1.53-1.41 (m, 2H, CH₂); ¹³C-NMR (101 MHz, (CD₃)₂SO) δ 176.2 (C), 169.5 (C), 164.8 (C), 164.4 (C), 142.6 (C), 136.8 (C), 129.7 (CH), 128.0 (CH), 126.6 (CH), 126.1 (CH), 66.1 (CH₂), 62.3 (CH₂), 43.3 (CH₂), 42.5 (CH₂), 41.9 (CH), 28.3 (CH₂); LCMS (*m/z*) 399.3 [MH]⁺; HRMS (ESI⁺) calcd for [C₂₀H₂₅N₆O₃ + H]⁺ 399.2139, found 399.2129.



1-(4-(3-hydroxyphenyl)-6-morpholino-1,3,5-triazin-2-yl)piperidine-4-carboxamide

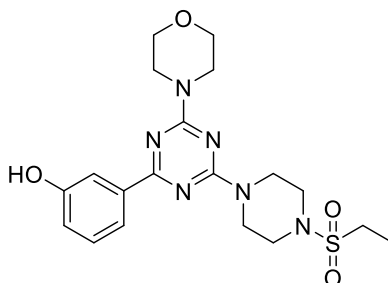
(40b). 32 (0.10 g, 0.31 mmol) and 3-hydroxyphenylboronic acid (0.060 g, 0.40 mmol) gave **40b** as a white powder (0.019 g, 12% [as doubly protonated TFA salt]). $^1\text{H-NMR}$ (400 MHz, CD_3OD) δ 7.75-7.72 (m, 1H, ArH), 7.72-7.70 (m, 1H, ArH), 7.30 (t, $J = 7.9$ Hz, 1H, ArH), 6.99 (ddd, $J = 8.1, 2.6, 1.0$ Hz, 1H, ArH), 4.92-4.79 (m, 2H, CH_2) 3.94-3.88 (m, 4H, NCH_2 (morpholine)), 3.78-3.72 (m, 4H, OCH_2), 3.06 (t, $J = 12.4$ Hz, 2H, CH_2), 2.63-2.53 (m, 1H, CH), 1.92 (dd, $J = 13.0, 2.5$ Hz, 2H, CH_2), 1.76-1.63 (m, 2H, CH_2); $^{13}\text{C-NMR}$ (101 MHz, CD_3OD) δ 180.1 (C), 158.9 (C), 130.6 (CH), 120.9 (CH), 120.7 (CH), 116.4 (CH), 67.6 (CH_2), 45.7 (CH_2), 44.8 (CH_2), 43.4 (CH), 29.6 (CH_2); LCMS (m/z) 385.1 $[\text{MH}]^+$; HRMS (ESI+) calcd for $[\text{C}_{19}\text{H}_{23}\text{N}_6\text{O}_3 + \text{H}]^+$ 385.1983, found 385.1979.



(3-(4-(4-(ethylsulfonyl)piperazin-1-yl)-6-morpholino-1,3,5-triazin-2-yl)phenyl)methanol

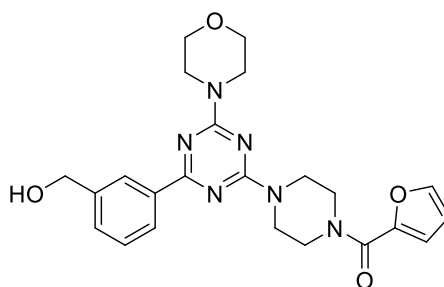
(41a). 33 (0.097 g, 0.27 mmol) and 3-(hydroxymethyl)phenylboronic acid (0.052 g, 0.35 mmol) gave **41a** as a white powder (0.089 g, 74%). $^1\text{H-NMR}$ (400 MHz, CDCl_3) δ 8.36 (s, 1H, ArH), 8.31 (d, $J = 7.7$ Hz, 1H, ArH), 7.53-7.48 (m, 1H, ArH), 7.44 (t, $J = 7.6$ Hz, 1H, ArH), 4.78 (s, 2H, CH_2), 4.11-3.85 (m, 8H, CH_2 (morpholine)), 3.79-3.74 (m, 4H, CH_2), 3.40-3.34 (m, 4H, CH_2), 2.98 (q, $J = 7.4$ Hz, 2H, CH_2CH_3), 1.39 (t, $J = 7.4$ Hz, 3H, CH_2CH_3); $^{13}\text{C-NMR}$ (101 MHz, CDCl_3) δ 170.4 (C),

165.2 (C), 165.1 (C), 141.0 (C), 137.5 (C), 130.3 (CH), 128.6 (CH), 128.0 (CH), 127.1 (CH), 67.0 (CH₂), 65.5 (CH₂), 45.9 (CH₂), 44.1 (CH₂), 43.9 (CH₂), 43.4 (CH₂), 7.9 (CH₃); LCMS (*m/z*) 449.1 [MH]⁺; HRMS (ESI⁺) calcd for [C₂₀H₂₈N₆O₄S + H]⁺ 449.1966, found 449.1977.



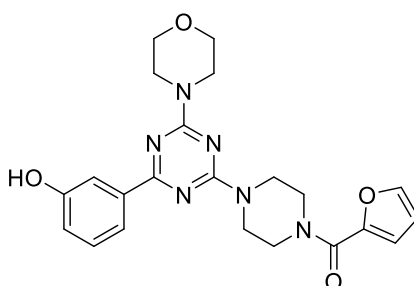
3-(4-(4-(ethylsulfonyl)piperazin-1-yl)-6-morpholino-1,3,5-triazin-2-yl)phenol (41b). 33

(0.10 g, 0.27 mmol) and 3-hydroxyphenylboronic acid (0.052 g, 0.038 mmol) gave **41b** as a white powder (0.018 g, 16%). ¹H-NMR (400 MHz, CDCl₃) δ 7.97-7.93 (m, 1H, ArH), 7.86-7.83 (m, 1H, ArH), 7.32 (t, *J* = 7.9 Hz, 1H, ArH), 6.98 (ddd, *J* = 8.0, 2.7, 0.9 Hz, 1H, ArH), 5.02 (br s, 1H, OH), 4.08-3.83 (m, 8H, CH₂ (morpholine)), 3.79-3.74 (m, 4H, CH₂), 3.40-3.32 (m, 4H, CH₂), 2.98 (q, *J* = 7.4 Hz, 2H, CH₂CH₃), 1.39 (t, *J* = 7.4 Hz, 3H, CH₂CH₃); ¹³C-NMR (101 MHz, CDCl₃) δ 129.6 (CH), 121.1 (CH), 118.8 (CH), 115.2 (CH), 67.0 (CH₂), 45.9 (CH₂), 44.1 (CH₂), 7.9 (CH₃) (insufficient sample was obtained to see quaternary carbon signals); LCMS (*m/z*) 435.1 [MH]⁺; HRMS (ESI⁺) calcd for [C₁₉H₂₆N₆O₄S + H]⁺ 435.1809, found 435.1830.



Furan-2-yl(4-(4-(3-(hydroxymethyl)phenyl)-6-morpholino-1,3,5-triazin-2-yl)piperazin-1-yl)methanone (42a). 34 (0.050 g, 0.13 mmol) and 3-(hydroxymethyl)phenylboronic acid (0.026 g, 0.17 mmol) gave **42a** as a white powder (0.037 g, 47% [as triply protonated TFA salt]).

^1H -NMR (400 MHz, CDCl_3) δ 8.30 (s, 1H, ArH), 8.15 (d, $J = 7.7$ Hz, 1H, ArH), 7.54-7.51 (m, 2H, ArH), 7.45 (t, $J = 7.7$ Hz, 1H, ArH), 7.11 (dd, $J = 3.5, 0.8$ Hz, 1H, ArH), 6.53 (dd, $J = 3.5, 1.8$ Hz, 1H, ArH), 6.46 (br s, 3H, NH), 4.78 (s, 2H, CH_2OH), 4.14-3.86 (m, 12H, CH_2), 3.83-3.76 (m, 4H, CH_2); ^{13}C -NMR (101 MHz, CD_3OD) δ 169.7 (C), 164.3 (C), 159.5 (C), 147.8 (C), 144.2 (CH), 141.2 (C), 136.6 (C), 130.6 (CH), 128.7 (CH), 128.0 (CH), 127.1 (CH), 117.4 (CH), 111.7 (CH), 66.7 (CH_2), 64.7 (CH_2); LCMS (m/z) 451.2 [MH] $^+$; HRMS (ESI $^+$) calcd for $[\text{C}_{23}\text{H}_{25}\text{N}_6\text{O}_4 + \text{H}]^+$ 451.2088, found 451.2086.



furan-2-yl(4-(4-(3-hydroxyphenyl)-6-morpholino-1,3,5-triazin-2-yl)piperazin-1-

yl)methanone (42b). **34** (0.10 g, 0.26 mmol) and 3-hydroxyphenylboronic acid (0.047 g,

0.34 mmol) gave **42b** as a white powder (0.011 g, 5% [as triply protonated TFA salt]); ^1H -NMR

(400 MHz, CD_3OD) δ 7.83-7.80 (m, 1H, ArH), 7.79-7.77 (m, 1H, ArH), 7.72 (dd, $J = 1.8, 0.8$ Hz),

7.28 (t, $J = 7.9$ Hz, 1H, ArH), 7.10 (dd, $J = 3.5, 0.8$ Hz, 1H, ArH), 6.96 (ddd, $J = 8.1, 2.6, 1.0$ Hz, 1H,

ArH), 6.61 (dd, $J = 3.5, 1.8$ Hz, 1H, ArH), 4.06-3.87 (m, 12H, CH_2), 3.77-3.73 (m, 4H, CH_2); ^{13}C -NMR

(101 MHz, CD_3OD) δ 159.5 (C), 156.7 (C), 147.7 (C), 144.2 (CH), 129.6 (CH), 120.7 (CH), 119.9

(CH), 117.5 (CH), 115.6 (CH), 111.7 (CH), 66.8 (CH_2), 44.4 (CH_2), 44.0 (CH_2) (an additional four

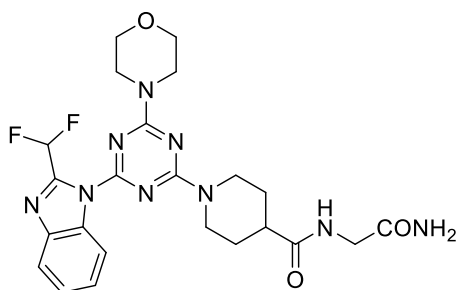
quaternary C resonances are expected, insufficient material was obtained to see these signals);

LCMS (m/z) 437.1 [MH] $^+$; HRMS (ESI $^+$) calcd for $[\text{C}_{22}\text{H}_{24}\text{N}_6\text{O}_4 + \text{H}]^+$ 437.1932, found 437.1942.

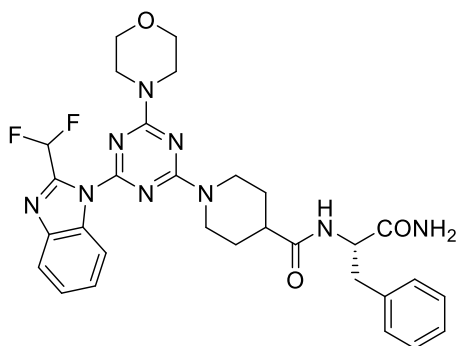
6.2.4 Chapter 4 experimental

6.2.4.1 General Method for Peptide Coupling

To a stirring solution of **25a**, **25b** or **25f** (0.10 g, 0.23 mmol), amino carboxamide hydrochloride salt (0.24 mmol) and HBTU (0.091 g, 0.24 mmol) in dimethylformamide (5 mL) was added DIPEA (0.056 g, 0.44 mmol) and stirred under nitrogen until reaction was completed as monitored by LCMS. Water was added and precipitate was collected and washed with water and methanol.

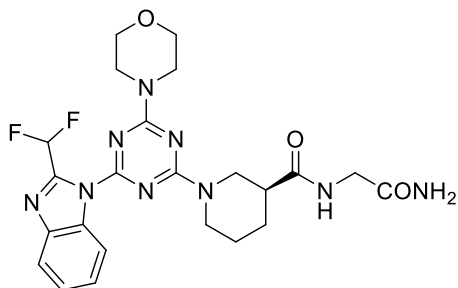


N-(2-amino-2-oxoethyl)-1-(4-(2-(difluoromethyl)-1H-benzo[d]imidazol-1-yl)-6-morpholino-1,3,5-triazin-2-yl)piperidine-4-carboxamide (43**).** **25b** (0.10 g, 0.23 mmol) and glycineamide.HCl (0.026 g, 0.24 mmol) gave **43** as a white powder (0.075 g, 67%). ¹H-NMR (400 MHz, (CD₃)₂SO) δ 8.34 (d, *J* = 8.2 Hz, 1H, ArH), 8.02 (t, *J* = 5.7 Hz, 1H, NH), 7.88-7.83 (m, 1H, ArH), 7.73 (t, *J* = 52.8 Hz, 1H, CHF₂), 7.54-7.48 (m, 1H, ArH), 7.46-7.40 (m, 1H, ArH), 7.26 (br s, 1H, NH), 7.00 (br s, 1H, NH), 4.71-4.56 (m, 2H, CH₂), 3.83-3.77 (m, 4H, NCH₂ (morpholine)), 3.73-3.66 (m, 4H, OCH₂), 3.62 (d, *J* = 5.8 Hz, 2H, NHCH₂), 3.15-2.98 (m, 2H, CH₂), 2.63-2.53 (m, 1H, CH), 1.90-1.80 (m, 2H, CH₂), 1.63-1.48 (m, 2H, CH₂); ¹³C-NMR (101 MHz, (CD₃)₂SO) δ 174.1 (C), 171.0 (C), 164.6 (C), 164.0 (C), 161.4 (C), 145.9 (C), 141.3 (C), 132.9 (C), 125.9 (CH), 124.3 (CH), 120.7 (CH), 115.7 (CH), 108.6 (t, *J* = 237.0 Hz, CHF₂), 65.9 (CH₂), 43.7 (CH₂), 43.0 (CH₂), 42.8 (CH₂), 41.7 (CH₂), 41.5 (CH), 28.2 (CH₂), 28.0 (CH₂); HRMS (ESI+) calcd for [C₂₃H₂₇F₂N₉O₃ + H]⁺ 516.2278, found 516.2279.



(S)-N-(1-amino-1-oxo-3-phenylpropan-2-yl)-1-(4-(2-(difluoromethyl)-1H-benzo[d]imidazol-1-yl)-6-morpholino-1,3,5-triazin-2-yl)piperidine-4-carboxamide (44**).**

25b (0.10 g, 0.23 mmol) and L-phenylalanine amide.HCl (0.048 g, 0.24 mmol) gave **44** as a white powder (0.083 g, 63%). $^1\text{H-NMR}$ (400 MHz, $(\text{CD}_3)_2\text{SO}$) δ 8.32 (d, $J = 8.2$ Hz, 1H, ArH), 7.99 (d, $J = 8.7$ Hz, 1H, ArH), 7.85 (d, $J = 7.8$ Hz, 1H, ArH), 7.65 (t, $J = 52.8$ Hz, 1H, CHF_2), 7.51 (t, $J = 7.7$ Hz, 1H, ArH), 7.46-7.40 (m, 2H, ArH, NH), 7.28-7.21 (m, 4H, ArH), 7.17 (s, 1H, NH), 7.05 (s, 1H, NH), 4.63-4.39 (m, 3H, CH_2), 3.83-3.76 (m, 4H, NCH_2 (morpholine)), 3.69 (br s, 4H, OCH_2), 3.10-2.95 (m, 3H, CH_2), 2.80-2.71 (m, 1H, CH_2), 2.55-2.45 (m, 1H, CH), 1.74 (t, $J = 13.8$ Hz, 1H, CH_2), 1.65-1.56 (m, 1H, CH_2), 1.54-1.42 (m, 1H, CH_2), 1.38-1.26 (m, 1H, CH_2); $^{13}\text{C-NMR}$ (101 MHz, $(\text{CD}_3)_2\text{SO}$) δ 173.5 (C), 173.3 (C), 164.5 (C), 164.0 (C), 161.3 (C), 145.9 (C), 141.3 (C), 138.2 (C), 132.9 (C), 129.2 (CH), 127.9 (CH), 126.2 (CH), 125.8 (CH), 124.3 (CH), 120.7 (CH), 115.7 (CH), 108.6 (t, $J = 237.0$ Hz, CHF_2), 65.9 (CH_2), 53.4 (CH), 43.6 (CH_2), 42.9 (CH_2), 42.6 (CH_2), 41.4 (CH), 37.7 (CH_2); HRMS (ESI+) calcd for $[\text{C}_{30}\text{H}_{34}\text{F}_2\text{N}_9\text{O}_3 + \text{H}]^+$ 606.2747, found 606.2754.

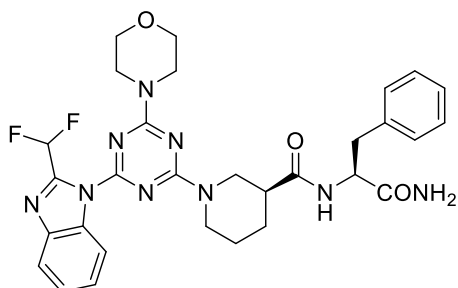


(S)-N-(2-amino-2-oxoethyl)-1-(4-(2-(difluoromethyl)-1H-benzo[d]imidazol-1-yl)-6-

morpholino-1,3,5-triazin-2-yl)piperidine-3-carboxamide (45). **25a** (0.10 g, 0.23 mmol) and

glycinamide.HCl (0.026 g, 0.25 mmol) gave **45** as a white powder (0.071 g, 63%). $^1\text{H-NMR}$

(400 MHz, $(\text{CD}_3)_2\text{SO}$) δ 8.34 (dd, $J = 7.9, 4.7$ Hz, 1H, ArH), 8.10 (t, $J = 5.4$ Hz, 1H, NH), 7.84 (d, $J = 8.2$ Hz, 1H, ArH), 7.73 (t, $J = 52.8$ Hz, 1H, CHF_2), 7.55-7.47 (m, 1H, ArH), 7.42 (td, $J = 7.6, 2.6$ Hz, 1H, ArH), 7.28 (d, $J = 15.9$ Hz, 1H, NH), 7.03 (br s, 1H, NH), 4.70-4.48 (m, 2H, CH_2), 3.86-3.75 (m, 4H, NCH_2 (morpholine)), 3.73-3.62 (m, 6H, OCH_2 , NHCH_2), 3.27-3.01 (m, 2H, CH_2), 2.48-2.39 (m, 1H, CH), 2.02-1.90 (m, 1H, CH_2), 1.88-1.75 (m, 1H, CH_2), 1.74-1.69 (m, 1H, CH_2), 1.52-1.38 (m, 1H, CH_2); $^{13}\text{C-NMR}$ (101 MHz, $(\text{CD}_3)_2\text{SO}$) δ 172.9 (C), 170.8 (C), 164.5 (C), 164.1 (C), 161.3 (C), 145.9 (t, $J = 27.3$ Hz, C), 141.3 (C), 132.9 (C), 125.9 (CH), 124.3 (CH), 120.6 (CH), 115.8 (CH), 108.54 (t, $J = 236.8$ Hz, CHF_2), 65.8 (CH_2), 45.6 (CH_2), 43.6 (CH_2), 43.4 (CH_2), 41.9 (CH), 41.6 (CH_2), 27.8 (CH_2), 24.0 (CH_2); HRMS (ESI+) calcd for $[\text{C}_{23}\text{H}_{27}\text{F}_2\text{N}_9\text{O}_3 + \text{H}]^+$ 516.2278, found 516.2291.

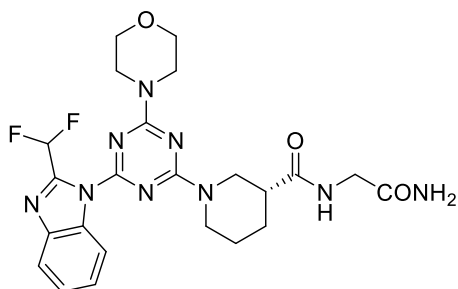


(S)-N-((S)-1-amino-1-oxo-3-phenylpropan-2-yl)-1-(4-(2-(difluoromethyl)-1H-

benzo[d]imidazol-1-yl)-6-morpholino-1,3,5-triazin-2-yl)piperidine-3-carboxamide (46).

25b (0.057 g, 0.12 mmol) and L-phenylalanine.HCl (0.048 g, 0.14 mmol) gave **46** as a white

powder (0.051 g, 68%). $^1\text{H-NMR}$ (400 MHz, $(\text{CD}_3)_2\text{SO}$) δ 8.32 (d, $J = 8.2$ Hz, 1H, ArH), 8.07 (t, $J = 9.2$ Hz, 1H, NH) 7.87-7.81 (m, 1H, ArH), 7.71 (t, $J = 52.8$ Hz, 1H, CHF_2), 7.56-7.39 (m, 3H, ArH), 7.29-7.15 (m, 5H, ArH, NH), 7.11 (s, 1H, NH), 4.60-4.46 (m, 3H), 3.86-3.65 (m, 8H, CH_2 (morpholine)), 3.07-2.91 (m, 3H), 2.79-2.70 (m, 1H), 2.46-2.32 (m, 1H), 1.76-1.60 (m, 2H), 1.51-1.30 (m, 2H); $^{13}\text{C-NMR}$ (101 MHz, $(\text{CD}_3)_2\text{SO}$) δ 173.2 (C), 172.5 (C), 164.5 (C), 164.1 (C), 161.3 (C), 145.9 (C), 141.3 (C), 138.1 (C), 132.9 (C), 129.2 (CH), 129.0 (CH), 127.9 (CH), 126.2 (CH), 126.0 (CH), 125.9 (CH), 124.3 (CH), 120.7 (CH), 115.8 (CH), 108.6 (t, $J = 240.9$ Hz, CHF_2), 65.9 (CH_2), 53.4 (CH), 45.5 (CH_2), 43.6 (CH_2), 43.4 (CH_2), 41.7 (CH), 37.8 (CH_2), 28.2 (CH_2), 24.0 (CH_2); HRMS (ESI+) calcd for $[\text{C}_{30}\text{H}_{34}\text{F}_2\text{N}_9\text{O}_3 + \text{H}]^+$ 606.2747, found 606.2743.

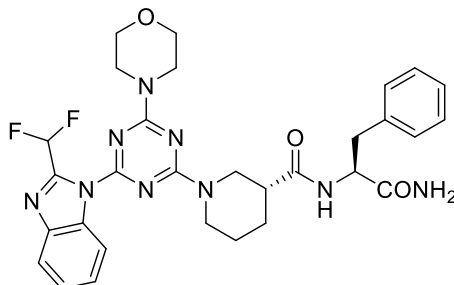


(R)-N-(2-amino-2-oxoethyl)-1-(4-(2-(difluoromethyl)-1H-benzo[d]imidazol-1-yl)-6-

morpholino-1,3,5-triazin-2-yl)piperidine-3-carboxamide (47). 25f (0.087 g, 0.19 mmol)

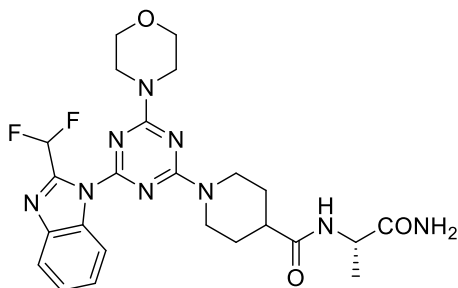
and glycineamide.HCl (0.023 g, 0.21 mmol) gave **47** as a yellow powder (0.026 g, 27%). $^1\text{H-NMR}$ (400 MHz, $(\text{CD}_3)_2\text{SO}$) δ 8.34 (dd, $J = 8.1, 3.3$ Hz, 1H, ArH), 8.10 (t, $J = 5.4$ Hz, 1H, NH), 7.88-7.82 (m, 1H, ArH), 7.73 (t, $J = 52.8$ Hz, 1H, CHF_2), 7.55-7.48 (m, 1H, ArH), 7.45-7.39 (m, 1H, ArH), 7.28 (d, $J = 15.5$ Hz, 1H, NH_2), 7.03 (s, 1H, NH_2), 4.69-4.51 (m, 2H, CH_2), 3.86-3.75 (m, 4H, CH_2 , NCH_2 (morpholine)), 3.75-3.62 (m, 6H, OCH_2 , NHCH_2), 3.26-3.01 (m, 2H, CH_2), 2.52-2.40 (m, 1H, CH), 2.01-1.90 (m, 1H, CH_2), 1.87-1.75 (m, 1H, CH_2), 1.74-1.62 (m, 1H, CH_2), 1.52-1.38 (m, 1H, CH_2); $^{13}\text{C-NMR}$ (101 MHz, $(\text{CD}_3)_2\text{SO}$) δ 173.0 (C), 170.9 (C), 164.5 (C), 164.1 (C), 161.3 (C), 145.9 (t, $J = 27.0$ Hz, C), 141.3 (C), 132.9 (C), 125.9 (CH), 124.3 (CH), 120.7 (CH), 115.8 (CH), 108.6 (t,

$J = 238.4$ Hz, CHF_2), 65.9 (CH_2), 45.7 (CH_2), 43.6 (CH_2), 43.5 (CH_2), 42.0 (CH), 41.7 (CH_2), 27.8 (CH_2), 24.1 (CH_2); HRMS (ESI+) calcd for $[\text{C}_{23}\text{H}_{27}\text{F}_2\text{N}_9\text{O}_3 + \text{H}]^+$ 516.2278, found 516.2282.

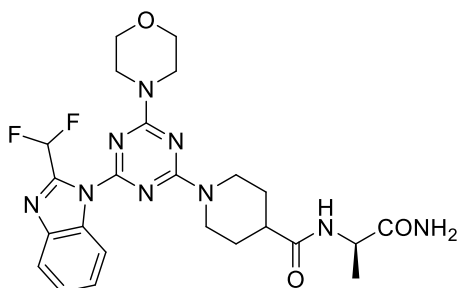


(R)-N-((S)-1-amino-1-oxo-3-phenylpropan-2-yl)-1-(4-(2-(difluoromethyl)-1H-benzo[d]imidazol-1-yl)-6-morpholino-1,3,5-triazin-2-yl)piperidine-3-carboxamide (48).

25f (0.10 g, 0.22 mmol) and L-phenylalanine amide.HCl (0.048 g, 0.24 mmol) gave **48** as a white powder (0.116 g, 88%). $^1\text{H-NMR}$ (400 MHz, $(\text{CD}_3)_2\text{SO}$) δ 8.34-8.29 (m, 1H, ArH), 8.08 (t, $J = 9.4$ Hz, 1H, NH), 7.87-7.83 (m, 1H, ArH), 7.71 (t, $J = 52.7$ Hz, 1H, CHF_2), 7.54-7.48 (m, 1H, ArH), 7.46-7.40 (m, 2H, ArH), 7.25-7.21 (m, 3H, ArH), 7.20-7.15 (m, 1H, NH), 7.13-7.02 (m, 2H, NH), 4.58-4.36 (m, 3H), 3.86-3.75 (m, 4H, CH_2 , NCH_2 (morpholine)), 3.75-3.65 (m, 4H, OCH_2), 3.09-2.93 (m, 3H), 2.80-2.72 (m, 1H), 2.47-2.31 (m, 1H, CH), 1.90-1.83 (m, 1H, CH_2), 1.78-1.69 (m, 1H, CH_2), 1.69-1.58 (m, 1H, CH_2), 1.47-1.34 (m, 1H, CH_2); $^{13}\text{C-NMR}$ (101 MHz, $(\text{CD}_3)_2\text{SO}$) δ 173.2 (C), 172.9 (C), 172.2 (C), 164.5 (C), 164.0 (C), 161.3 (C), 141.3 (C), 138.1 (C), 132.9 (C), 129.0 (CH), 127.9 (CH), 126.1 (CH), 125.9 (CH), 124.33 (CH), 120.7 (CH), 115.7 (CH), 108.6 (CH), 65.9 (CH_2), 53.6 (CH), 45.6 (CH_2), 45.4 (CH_2), 43.6 (CH_2), 43.4 (CH_2), 41.9 (CH), 27.6 (CH_2), 24.0 (CH_2); HRMS (ESI+) calcd for $[\text{C}_{23}\text{H}_{27}\text{F}_2\text{N}_9\text{O}_3 + \text{H}]^+$ 606.2747, found 606.2745.

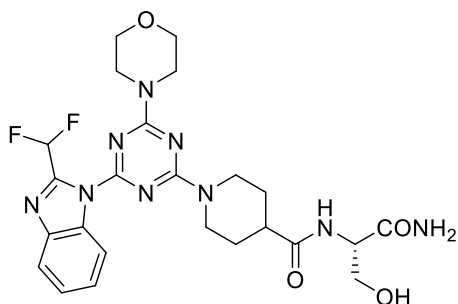


(S)-N-(1-amino-1-oxopropan-2-yl)-1-(4-(2-(difluoromethyl)-1H-benzo[d]imidazol-1-yl)-6-morpholino-1,3,5-triazin-2-yl)piperidine-4-carboxamide (49). **25b** (0.10 g, 0.23 mmol) and L-alaninamide.HCl (0.032 g, 0.24 mmol) gave **49** as a white powder (0.035, 28%). $^1\text{H-NMR}$ (400 MHz, $(\text{CD}_3)_2\text{SO}$) δ 8.34 (d, $J = 8.2$ Hz, 1H, ArH), 7.93 (d, $J = 7.7$ Hz, 1H, NH), 7.88-7.83 (m, 1H, ArH), 7.73 (t, $J = 52.8$ Hz, 1H, CHF_2), 7.53-7.48 (m, 1H, ArH), 7.45-7.40 (m, 1H, ArH), 7.27 (s, 1H, NH_2), 6.94 (s, 1H, NH_2), 4.72-4.57 (m, 2H, CH_2), 4.20 (p, $J = 7.1$ Hz, 1H, CHCH_3), 3.86-3.76 (m, 4H, NCH_2 (morpholine)), 3.69 (br s, 4H, OCH_2), 3.14-2.96 (m, 2H, CH_2), 2.63-2.53 (m, 1H, CH), 1.90-1.76 (m, 2H, CH_2), 1.62-1.46 (m, 2H, CH_2), 1.19 (d, $J = 7.1$ Hz, 3H, CH_3); $^{13}\text{C-NMR}$ (101 MHz, $(\text{CD}_3)_2\text{SO}$) δ 174.4 (C), 173.5 (C), 164.5 (C), 164.0 (C), 161.4 (C), 145.9 (C), 141.3 (C), 132.9 (C), 125.8 (CH), 124.3 (CH), 120.7 (CH), 115.7 (CH), 108.6 (t, $J = 237.0$ Hz, CHF_2), 65.9 (CH_2), 47.8 (CH), 43.6 (CH_2), 43.0 (CH_2), 42.8 (CH_2), 41.4 (CH), 28.1 (CH_2), 18.3 (CH_3); HRMS (ESI+) calcd for $[\text{C}_{24}\text{H}_{29}\text{F}_2\text{N}_9\text{O}_3 + \text{H}]^+$ 530.2434, found 530.2438.



(R)-N-(1-amino-1-oxopropan-2-yl)-1-(4-(2-(difluoromethyl)-1H-benzo[d]imidazol-1-yl)-6-morpholino-1,3,5-triazin-2-yl)piperidine-4-carboxamide (50). **25b** (0.10 g, 0.23 mmol) and D-alaninamide.HCl (0.032 g, 0.24 mmol) gave **50** as a white powder (0.040, 35%). $^1\text{H-NMR}$

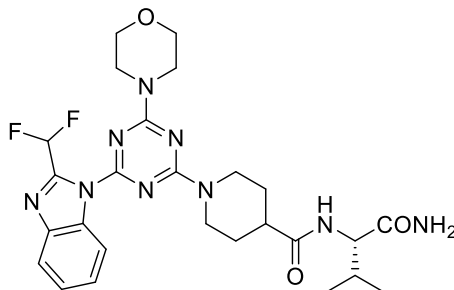
(400 MHz, (CD₃)₂SO) δ 8.34 (d, J = 8.2 Hz, 1H, ArH), 7.93 (d, J = 7.7 Hz, 1H, NH), 7.88-7.83 (m, 1H, ArH), 7.73 (t, J = 52.8 Hz, 1H, CHF₂), 7.54-7.47 (m, 1H, ArH), 7.46-7.40 (m, 1H, ArH), 7.28 (s, 1H, NH₂), 6.94 (s, 1H, NH₂), 4.73-4.56 (m, 2H, CH₂), 4.20 (p, J = 7.2 Hz, 1H, CHCH₃), 3.86-3.76 (m, 4H, NCH₂ (morpholine)), 3.69 (br s, 4H, OCH₂), 3.12-2.96 (m, 2H, CH₂), 2.62-2.53 (m, 1H, CH), 1.88-1.76 (m, 2H, CH₂), 1.61-1.48 (m, 2H, CH₂), 1.19 (d, J = 7.1 Hz, 3H, CH₃); ¹³C-NMR (101 MHz, (CD₃)₂SO) δ 174.4 (C), 173.5 (C), 164.5 (C), 164.0 (C), 161.4 (C), 145.9 (t, J = 26.6 Hz, C), 141.3 (C), 132.9 (C), 125.8 (CH), 124.3 (CH), 120.7 (CH), 115.7 (CH), 108.6 (t, J = 237.0 Hz, CHF₂), 65.9 (CH₂), 47.8 (CH), 43.6 (CH₂), 43.0 (CH₂), 42.8 (CH₂), 41.4 (CH), 28.1 (CH₂), 18.3 (CH₃); HRMS (ESI⁺) calcd for [C₂₄H₂₉F₂N₉O₃ + H]⁺ 530.2434, found 530.2437.



(S)-N-(1-amino-3-hydroxy-1-oxopropan-2-yl)-1-(4-(2-(difluoromethyl)-1H-benzo[d]imidazol-1-yl)-6-morpholino-1,3,5-triazin-2-yl)piperidine-4-carboxamide (51).

25b (0.10 g, 0.23 mmol) and L-serine amide.HCl (0.034 g, 0.24 mmol) gave **51** as a white powder (0.077 g, 63%). ¹H-NMR (400 MHz, (CD₃)₂SO) δ 8.34 (d, J = 8.2 Hz, 1H, ArH), 7.85 (d, J = 7.9 Hz, 1H, NH), 7.77 (d, J = 8.2 Hz, 1H, ArH), 7.73 (t, J = 52.8 Hz, 1H, CHF₂), 7.53-7.48 (m, 1H, ArH), 7.45-7.40 (m, 1H, ArH), 7.26 (br s, 1H, NH₂), 7.05 (s, 1H, NH₂), 4.84 (t, J = 5.6 Hz, 1H, OH), 4.72-4.57 (m, 2H, CH₂), 4.21 (dt, J = 8.0, 5.4 Hz, 1H, CHCH₂OH), 3.86-3.76 (m, 4H, NCH₂ (morpholine)), 3.75-3.65 (m, 4H, OCH₂), 3.56 (t, J = 6.0 Hz, 2H, CH₂OH), 3.14-2.97 (m, 2H, CH₂), 2.68-2.58 (m, 1H, CH), 1.92-1.78 (m, 2H, CH₂), 1.61-1.47 (m, 2H, CH₂); ¹³C-NMR (101 MHz, (CD₃)₂SO) δ 174.9 (C), 172.2 (C), 164.5 (C), 164.0 (C), 161.4 (C), 145.9 (t, J = 26.6 Hz, C), 141.3 (C), 132.9 (C), 125.8 (CH), 124.3 (CH), 120.7 (CH), 115.7 (CH), 108.6 (t, J = 237.2 Hz, CHF₂), 65.9 (CH₂), 61.8 (CH₂), 54.9

(CH), 43.6 (CH₂), 43.0 (d, J = 20.5 Hz, CH₂), 41.5 (CH), 28.2 (t, J = 22.0 Hz, CH₂); HRMS (ESI+) calcd for [C₂₄H₃₀F₂N₉O₄ + H]⁺ 546.2383, found 546.2393.



(S)-N-(1-amino-3-methyl-1-oxobutan-2-yl)-1-(4-(2-(difluoromethyl)-1H-benzo[d]imidazol-1-yl)-6-morpholino-1,3,5-triazin-2-yl)piperidine-4-carboxamide (52).

25b (0.10 g, 0.23 mmol) and L-valine amide.HCl (0.037 g, 0.24 mmol) gave **52** as a white powder (0.054 g, 44%). ¹H-NMR (400 MHz, (CD₃)₂SO) δ 8.34 (d, J = 8.2 Hz, 1H, ArH), 7.85 (d, J = 7.9 Hz, 1H, ArH), 7.78 (d, J = 9.1 Hz, 1H, NH), 7.67 (t, J = 52.8 Hz, 1H, CHF₂), 7.53-7.48 (m, 1H, ArH), 7.45-7.40 (m, 1H, ArH), 7.36 (s, 1H, NH₂), 6.99 (s, 1H, NH₂), 4.73-4.59 (m, 2H, CH₂), 4.12 (dd, J = 9.0, 6.6 Hz, 1H, CHCH(CH₃)₂), 3.80 (br s, 4H, NCH₂ (morpholine)), 3.69 (br s, 4H, OCH₂), 3.12-2.95 (m, 2H, CH₂), 2.73-2.62 (m, 1H, CH₂), 2.01-1.91 (m, 1H, CH(CH₃)₂), 1.88-1.74 (m, 2H, CH₂), 1.60-1.47 (m, 2H, CH₂), 0.84 (t, J = 6.3 Hz, 6H, CH₃); ¹³C-NMR (101 MHz, (CD₃)₂SO) δ 173.9 (C), 173.1 (C), 164.5 (C), 164.0 (C), 161.4 (C), 141.3 (C), 132.9 (C), 125.9 (CH), 124.3 (CH), 120.7 (CH), 115.7 (CH), 108.6 (t, J = 237.0 Hz, CHF₂), 65.9 (CH₂), 57.1 (CH), 43.7 (CH₂), 43.0 (CH₂), 41.4 (CH), 30.4 (CH), 19.4 (CH), 18.0 (CH); HRMS (ESI+) calcd for [C₂₆H₃₄F₂N₉O₃ + H]⁺ 558.2747, found 558.2747.

6.3 Enzyme assays

Inhibitors were dissolved in dimethylsulfoxide at 10 mM concentration. PI3K enzyme activity was determined using a luminescent assay measuring ATP consumption. PI3K enzyme activity was determined in 50 μL of 20 mM HEPES (pH 7.5) and 0.5 mM MgCl₂ with 200 μM

phosphatidylinositol and 10 μ M ATP. After a 60 minute incubation at room temperature (22°C), the reaction was stopped by the addition of 50 μ L of Kinase-Glo® (Promega) followed by a further 30 minute incubation. Luminescence was then read using a Fluostar plate reader (BMG Labtech). Inhibitors were diluted in 20% (v/v) DMSO at decreasing concentrations in order to generate a concentration versus inhibition of enzyme activity curve which was then analysed using GraphPad Prism version 5.00 for Windows to calculate the IC₅₀.

6.4 Docking

Molecular modelling studies were performed using the Schrödinger software suite. The protein structure was prepared using the Protein Preparation Wizard in Maestro, which included adding hydrogens and removing all water molecules. Ligands were prepared using LigPrep within Maestro. Docking studies were performed on p110 γ (PDB ID: 3DBS) and p110 δ (PDB ID: 2WXL) using Glide v5.8023 (Schrödinger) extra-precision (XP) mode using default settings.⁹ The ATP binding site was identified by the centroid of the co-crystallised ligand as a defined box of 20 x 20 x 20 Å.

6.5 References

- (1) Mandelker, D.; Gabelli, S. B.; Schmidt-Kittler, O.; Zhu, J.; Cheong, I.; Huang, C. H.; Kinzler, K. W.; Vogelstein, B.; Amzel, L. M. A frequent kinase domain mutation that changes the interaction between PI3K α and the membrane. *Proc. Natl. Acad. Sci. U.S.A.* **2009**, *106*, 16996–17001.
- (2) Huang, C. H.; Mandelker, D.; Schmidt-Kittler, O.; Samuels, Y.; Velculescu, V. E.; Kinzler, K. W.; Vogelstein, B.; Gabelli, S. B.; Amzel, L. M. The structure of a human p110 α /p85 α complex elucidates the effects of oncogenic PI3K α mutations. *Science* **2007**, *318*, 1744–1748.
- (3) Emsley, P.; Cowtan, K. Coot: model-building tools for molecular graphics. *Acta Crystallogr. D Biol. Crystallogr.* **2004**, *60*, 2126–2132.
- (4) Nolte, R. T.; Eck, M. J.; Schlessinger, J.; Shoelson, S. E.; Harrison, S. C. Crystal structure of the PI 3-kinase p85 amino-terminal SH2 domain and its phosphopeptide complexes. *Nat. Struct. Biol.* **1996**, *3*, 364–374.
- (5) Vagin, A. A.; Steiner, R. A.; Lebedev, A. A.; Potterton, L.; McNicholas, S.; Long, F.; Murshudov, G. N. REFMAC5 dictionary: organization of prior chemical knowledge and guidelines for its use. *Acta Crystallogr. D Biol. Crystallogr.* **2004**, *60*, 2184–2195.
- (6) Still, W. C.; Kahn, M.; Mitra, A. Rapid Chromatographic Technique for Preparative Separations with Moderate Resolution. *J. Org. Chem* **1978**, *43*, 2923–2925.
- (7) Miller, M. S.; Pinson, J.-A.; Zheng, Z.; Jennings, I. G.; Thompson, P. E. Regioselective synthesis of 5- and 6-methoxybenzimidazole-1,3,5-triazines as inhibitors of phosphoinositide 3-kinase. *Bioorg. Med. Chem. Lett.* **2013**, *23*, 802–805.
- (8) Pinson, J. A. PI3 Kinase and inhibitors: Targeting isoform selectivity. PhD Dissertation, Monash University, 2011.
- (9) Friesner, R. A.; Murphy, R. B.; Repasky, M. P.; Frye, L. L.; Greenwood, J. R.; Halgren, T. A.; Sanschagrin, P. C.; Mainz, D. T. Extra Precision Glide: Docking and Scoring Incorporating a Model of Hydrophobic Enclosure for Protein-Ligand Complexes. *J. Med. Chem.* **2006**, *49*, 6177–6196.

Appendices

Appendix 1: Assay results

Table A1: Summary of the assay results. Each compound was tested against recombinant PI3K α , β , γ and δ using the Kinase-Glo® assay. The IC₅₀ values quoted are the mean of at least three independent experiments with the standard errors quoted.

Compound	IC ₅₀ \pm S.E. (nM)			
	PI3K α	PI3K β	PI3K γ	PI3K δ
3	35 \pm 6	39 \pm 4	166 \pm 25	17 \pm 2
P9a	>5000	>10000	>10000	>1000
P9b	375 \pm 116	214 \pm 40	>10000	110 \pm 31
P4b	290 \pm 50	523 \pm 10	1860 \pm 330	187 \pm 26
P9c	9200 \pm 1500	>10000	>10000	2770 \pm 55
P9d	823 \pm 86	1790 \pm 230	>10000	458 \pm 11
P4c	431 \pm 14	419 \pm 41	2530 \pm 140	128 \pm 19
P9e	>10000	>10000	>10000	>1000
P9f	1050 \pm 280	726 \pm 150	>10000	423 \pm 55
24a	41 \pm 3	56 \pm 4	625 \pm 32	45 \pm 11
24b	59 \pm 5	124 \pm 28	1293 \pm 175	106 \pm 12
25a	40 \pm 5	215 \pm 28	231 \pm 28	42 \pm 3
25b	75.6 \pm 0.3	217 \pm 23	64 \pm 8	38 \pm 7
25c	65 \pm 4	165 \pm 37	304 \pm 6	35 \pm 3
25d	100 \pm 13	428 \pm 67	247 \pm 48	163 \pm 33
25e	112 \pm 10	134 \pm 31	626 \pm 125	33 \pm 2
25f	183 \pm 39	428 \pm 67	247 \pm 48	163 \pm 33
37a	411 \pm 100	1180 \pm 96	2460 \pm 510	433 \pm 86
37b	567 \pm 110	2810 \pm 601	4950 \pm 1410	1290 \pm 297
38a	811 \pm 23	3050 \pm 619	>100000	1820 \pm 343
38b	477 \pm 47	166 \pm 280	>50000	800 \pm 39

39a	350 ± 73	2020 ± 505	>10000	786 ± 142
39b	614 ± 14	640 ± 875	35000 ± 3300	2410 ± 66
40a	249 ± 30	939 ± 180	>50000	563 ± 33
40b	292 ± 72	1220 ± 46	>10000	454 ± 14
41a	128 ± 15	552 ± 41	1880 ± 190	201 ± 22
41b	252 ± 49	1950 ± 381	>10000	566 ± 63
42a	51 ± 11	70 ± 13	4920 ± 330	32 ± 1
42b	74 ± 17	71 ± 4	2880 ± 360	80 ± 23
43	98 ± 19	329 ± 24	496 ± 69	67 ± 8
44	190 ± 14	513 ± 29	708 ± 129	44 ± 1
45	32 ± 4	24 ± 3	194 ± 29	25 ± 2
46	358 ± 28	342 ± 59	1983 ± 399	57 ± 5
47	83 ± 4	166 ± 34	445 ± 104	38 ± 7
48	908 ± 89	1722 ± 202	1378 ± 63	263 ± 41
49	123 ± 13	207 ± 31	434 ± 41	40 ± 5
50	114 ± 5	601 ± 14	536 ± 69	29 ± 2
51	67 ± 6	162 ± 20	521 ± 34	29 ± 7
52	191 ± 43	602 ± 15	440 ± 2	144 ± 13

Appendix 2: Docking results for p110 γ

Table A2: Compounds were docked into the p110 γ crystal structure (PDB ID: 3DBS) using Glide. The Gscore is tabulated alongside the $\log_{10}(\text{IC}_{50})$ for comparison. The compound ranks according to both the Gscore and IC_{50} are provided, where 1 represents the 'best' compound.

Compound	Gscore	$\log_{10}(\text{IC}_{50})$	Rank (Gscore)	Rank (IC_{50})
3	-6.79	-6.78	13	2
24a	-6.74	-6.20	14	7
24b	-6.89	-5.89	9	9
25a	-7.31	-6.64	5	3
25b	-6.87	-7.19	10	1
25c	-7.69	-6.52	3	5
25d	-6.27	-6.33	19	6
25e	-6.45	-6.20	16	8
25f	-7.26	-6.61	6	4
37a	-5.38	-5.61	21	11
37b	-7.14	-5.31	8	14
38a	-9.87	> -4.00	1	>15
38b	-8.74	> -4.30	2	>15
39a	-7.24	> -5.00	7	>15
39b	-6.83	-4.46	12	>15
40a	-7.58	> -4.30	4	>15
40b	-6.78	> -5.00	11	>15
41a	-6.28	-5.73	18	10
41b	-6.08	> -5.00	20	>15
42a	-6.67	-5.31	15	13
42b	-6.41	-5.54	17	12

Appendix 3: Docking results for p110 δ

Table A3: Compounds were docked into the p110 δ crystal structure (PDB ID: 2WXL) using Glide. The Gscore is tabulated alongside the $\log_{10}(\text{IC}_{50})$ for comparison. The compound ranks according to both the Gscore and IC_{50} are provided, where 1 represents the 'best' compound.

Compound	Gscore	$\log_{10}(\text{IC}_{50})$	Rank (docking)	Rank (IC_{50})
3	-9.81	-7.77	9	1
24a	-8.75	-7.35	20	7
24b	-9.63	-6.97	14	10
25a	-9.47	-7.38	17	6
25b	-9.78	-7.42	11	5
25c	-9.83	-7.46	8	4
25d	-9.86	-7.16	5	8
25e	-9.83	-7.43	7	3
25f	-9.75	-6.79	12	11
37a	-9.78	-6.36	10	13
37b	-9.63	-5.89	15	19
38a	-9.50	-5.74	16	20
38b	-7.77	-6.10	21	18
39a	-9.84	-6.10	6	17
39b	-10.47	-5.62	1	21
40a	-9.93	-6.25	3	15
40b	-10.20	-6.34	2	14
41a	-9.93	-6.70	4	12
41b	-9.17	-6.25	19	16
42a	-9.70	-7.49	13	2
42b	-9.37	-7.10	18	9

Appendix 4: Publication

Pinson, J.-A.; Zheng, Z.; **Miller, M. S.**; Chalmers, D. K.; Jennings, I. G.; Thompson, P. E.
L-Aminoacyl-triazine Derivatives Are Isoform-Selective PI3K β Inhibitors That Target
Nonconserved Asp862 of PI3K β . *ACS Med. Chem. Lett.* **2013**, 4, 206–210.

Candidate conducted molecular docking studies and prepared appropriate figures.

L-Aminoacyl-triazine Derivatives Are Isoform-Selective PI3K β Inhibitors That Target Nonconserved Asp862 of PI3K β

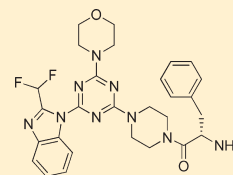
Jo-Anne Pinson, Zhaohua Zheng, Michelle S. Miller, David K. Chalmers, Ian G. Jennings, and Philip E. Thompson*

Medicinal Chemistry, Monash Institute of Pharmaceutical Sciences, Monash University, 381 Royal Parade, Parkville 3052 Australia.

S Supporting Information

ABSTRACT: A series of aminoacyl-triazine derivatives based upon the pan-PI3K inhibitor ZSTK474 were identified as potent and isoform-selective inhibitors of PI3K β . The compounds showed selectivity based upon stereochemistry with L-amino acyl derivatives preferring PI3K β , while their D-congeners favored PI3K δ . The mechanistic basis of this inhibition was studied using site-directed mutants. One Asp residue, D862, was identified as a critical participant in binding to the PI3K β -selective inhibitors, distinguishing this class from other reported PI3K β -selective inhibitors. The compounds show strong inhibition of cellular Akt phosphorylation and growth of PTEN-deficient MD-MBA-468 cells.

KEYWORDS: PI3 kinase, p110 β , ZSTK474, cancer



The phosphatidylinositol 3-kinases (PI3K) are a family of lipid kinases that regulate intracellular signaling for numerous cellular events such as cell migration, growth, and survival.¹ Because of their important roles in signal transduction, dysregulation in the PI3K pathway could lead to various diseases including cancer.² Two of the key genetic alterations identified for this pathway in cancer are mutation in the PIK3CA gene, which encodes p110 α (PI3K α catalytic subunit),³ and the loss of the tumor suppressor, phosphatase and tensin homologue (PTEN).⁴ Recently, there has been accumulating evidence showing that PI3K β plays a key role in tumorigenesis driven by PTEN loss.⁵ It was found that down-regulation of the PIK3CB gene, which encodes p110 β (PI3K β catalytic subunit), inhibited PI3K signaling as well as growth both in vitro and in vivo. In an animal prostate cancer model, the ablation of p110 β blocked tumorigenesis and decreased Akt phosphorylation, but the same results were not observed by p110 α ablation.⁶

The majority of inhibitors currently in clinical trials are class I pan-PI3K inhibitors.⁷ Because each of the PI3K isoforms has their own although overlapping physiological roles, isoform-selective PI3K inhibitors may hold some therapeutic advantages with respect to reducing off-target effects. In recent years, isoform-selective inhibitors have emerged, and compounds such as BYL719, a PI3K α selective inhibitor, and CAL-101,^{8,9} a PI3K δ -specific inhibitor, are now in phase I/II clinical trials. While these and other isoform-selective inhibitors have been reported, there is still relatively scant understanding of the mechanisms underpinning selectivity. From the structure of the adenosine triphosphate (ATP)-bound state of the enzyme (PDB: 1E8X), it is apparent that much of the inner core of the binding site is highly conserved across the class I isoforms.¹⁰ However, two nonconserved regions of the binding site have also been identified as capable of executing selective interactions with inhibitors (Figure 1). Region 1 from PI3K β

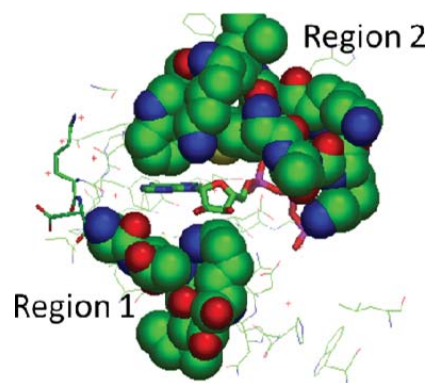


Figure 1. Nonconserved regions 1 and 2 of the PI3K γ binding site (shown in space-filling representations). PDB code: 1E8X.

855 to 862 encompasses a loop that sits under the ribose pocket and influences the binding of PI3K α selective inhibitor A-66 (a BYL719 analogue).¹¹ Region 2 from PI3K β 772–788 corresponds to the protein kinase “P-loop”.¹¹ This region has been shown to dictate selective inhibitor binding in a number of ways—first, a conserved methionine residue can shift to expose a cryptic binding pocket, as in the so-called “propeller-shaped” mode of binding of PI3K δ -selective compounds like PIK-39 (a CAL-101 analogue).¹² Other PI3K δ -selective inhibitors have been shown to access a “tryptophan shelf” adjacent to a nonconserved threonine. Also, the PI3K α -selective inhibitors PIK75 and J-32 have been shown to be

Received: October 14, 2012

Accepted: December 20, 2012

Published: December 20, 2012



ACS Publications

© 2012 American Chemical Society

206

dx.doi.org/10.1021/ml300336j | ACS Med. Chem. Lett. 2013, 4, 206–210

sensitive to mutation at nonconserved residues of region 2.¹¹ There are clearly other mechanisms by which inhibitors exhibit isoform selectivity. This is especially apparent in PI3K γ -selective inhibitors that show interaction only with conserved residues of the binding site and induce little conformational change from the ATP-bound state.¹³

Until recently, the pharmacological evaluation of PI3K β inhibition has rested upon a series of compounds described by Thrombogenix/Kinacia.^{14,15} These included TGX221 and KN309 (Figure 2). Astra-Zeneca has subsequently progressed

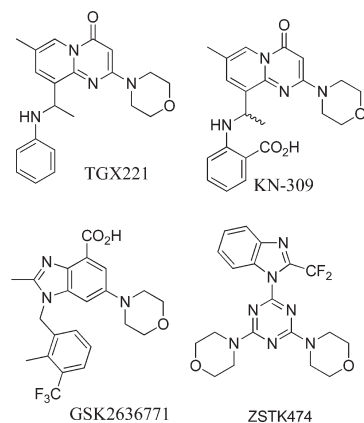


Figure 2. Structures of PI3K inhibitors.

the optically pure R-enantiomer of KN309 into human trials as AZD6482 (aka KIN193).¹⁶ The molecular basis for the observed selectivity has not yet been established, although Knight et al. proposed that TGX280 (PIK108) could be

accommodated in region 2, via the “propeller-shaped” mode described above. We had previously ruled out an interaction with the region 1 residues as the basis for selectivity.¹⁷

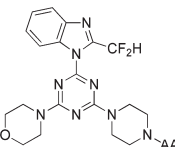
Recently, new PI3K β -selective compounds reminiscent of TGX221 have been reported. GSK2636771 has progressed to phase I/IIa clinical trials to treat advanced solid tumors with PTEN deficiency. Other analogous series have been described,^{18–23} and cocrystals of compounds with PI3K γ (PDB: 4FJY, 4FJZ, and 4G11) and PI3K δ (4AJW) support the analogy between these and the “propeller-shaped” compounds. The only reported X-ray structure of PI3K β in complex with the pan-PI3K inhibitor GDC9041 (PDB: 2Y3A) displays a conventional “flat” binding pose.²⁴

Our hypothesis was that isoform-selective inhibition of PI3K β should be achievable by targeting the nonconserved residues of region 1. In particular, the acidic Asp862 residue at PI3K β is exchanged for Gln, Lys, and Asn in PI3K α , γ , and δ , respectively. Adaptation of the pan-PI3K inhibitor ZSTK474 (Figure 2),²⁵ which projects one morpholinyl ring toward this region, was considered the logical template compound.¹² We have identified compounds that selectively inhibit PI3K β and moreover have demonstrated the role of D862 by showing that mutagenesis of that residue prevents inhibition by these compounds.

The synthesis of the substituted triazines was performed largely as previously reported (see the Supporting Information).^{26–28} Condensation of protected amino acid derivatives to piperazinyl analogues of ZSTK474 yielded the N-protected derivatives, which could be deprotected to give the free aminoacyl compounds 17 and 19–28. Alternatively condensation with N-acetylglycine or N,N-dimethylglycine gave the products 18 and 29, respectively.

The PI3K assay data are summarized in Table 1 and identify that the substituent has a significant influence upon isoform selectivity, consistent with our hypothesis. Compound 17

Table 1. Structure and Inhibition of PI3K Isoforms by ZSTK474 Analogues



compd	AA residue	PI3K isoform IC ₅₀ (nM) ^a				β/δ selectivity ratio
		α	β	γ	δ	
ZSTK474		6	6	38	3	0.5
17	Gly	1500	35	9900	110	3.0
18	Ac-Gly	42	54	380	26	0.48
19	L-Ala	3500	31	3600	490	15.7
20	D-Ala	3700	1000	2000	70	0.070
21	L-Phe	4700	63	>100 μ M	2200	34.8
22	D-Phe	>10 μ M	>10 μ M	>10 μ M	3600	<0.36
23	L-Ile	6300	67	>10 μ M	1000	15.6
24	L-Tyr	3300	220	>10 μ M	1200	5.4
25	L-Pro	2200	26	>10 μ M	390	15.1
26	L-Lys	2300	50	>10 μ M	670	13.4
27	β -Ala	720	98	3900	58	0.6
28	N-Me-L-Ala	1500	260	8000	290	1.1
29	N,N-diMeGly	1600	2400	>10 μ M	330	0.14

^aIC₅₀ values are means of at least two duplicate experiments (Kinase-Glo). Standard errors were all within 25% of the mean. Assays were performed using 10 μ M ATP.

ACS Medicinal Chemistry Letters

Letter

showed potent dual inhibition of PI3K β and PI3K δ with very poor inhibition of the PI3K α and PI3K γ isoforms. Incorporation of an *N*-acetylglutamine residue **18** resulted in pan-PI3K potency, suggesting the importance of the amino function to the observed selectivity.

Compounds **19**–**29** were all PI3K β and/or PI3K δ preferring ligands. Strikingly, the introduction of an *L*-alanine substituent resulted in a compound **19** with 15-fold selectivity for PI3K β over PI3K δ , while the opposite stereoisomer with a *D*-alanine substituent **21** showed 15-fold selectivity for PI3K δ over PI3K β . Pursuing the potential for *L*-amino acids providing for PI3K β selectivity in general held true. Most selective was *L*-Phe (**21**), which showed 35-fold selectivity for PI3K β over PI3K δ with the *L*-Ile (**23**), *L*-Tyr (**24**), *L*-Pro (**25**), and *L*-Lys (**26**) derivatives showing 6–16-fold selectivity. Homologation to β -Ala (**27**) and further substitution on the amino group as in **28** and **29** dropped the preference for PI3K β significantly.

To test the premise that the observed PI3K β selectivity was due to the interaction between the primary amino group of inhibitors and the nonconserved residues of the binding site, compounds were tested against a variety of mutant forms of PI3K β where the nonconserved residues were exchanged for their equivalent residues in PI3K α .

The PI3K β -selective compounds were very sensitive to mutation at region 1 residue D862Q (see Supplementary Figure 1 in the Supporting Information). The IC₅₀ values were determined for **19**, **21**, and **23** against the WT and mutant D862Q form as well as the WT and reciprocal mutant in PI3K α (Table 2). Note that the mutations do not hinder the catalytic

Table 2. Inhibition of PI3K Isoforms and in Vitro Mutants by ZSTK474 Analogues

compd	PI3K isoform IC ₅₀ (nM) ^a					fold change α WT \rightarrow α Q859D	fold change β WT \rightarrow β D862Q
	PI3K α WT	PI3K α Q859D	PI3K β WT	PI3K β D862Q			
19	8200	2300	62	890	↓3.5		↑14
21	12000	8100	74	6000	↓1.4		↑82
23	9200	2800	140	1400	↓3.3		↑10

^aIC₅₀ values are means of at least two duplicate experiments (Kinase-Glo). Assays were performed using 100 μ M ATP. A full table including standard errors is provided as Supplementary Table 2 in the Supporting Information.

properties of the mutant enzymes (Supplementary Table 1 in the Supporting Information). Each of the compounds shows a greater than 10-fold change in IC₅₀ against the mutant form of PI3K β . The IC₅₀ of **21** drops 82-fold as compared to the wild-type isoform upon introduction of the D862Q mutation. The reciprocal mutation in PI3K α D859Q does not restore inhibitory potency of **21** at PI3K α , although some enhancement in potency is observed for compounds **19** and **23**. These data clearly distinguish the mechanism of selectivity of these compounds from that of TGX221 and TGX286, which are unaffected by the mutation D862Q in PI3K β .¹⁷

The data from these studies suggest a clear and dramatic influence of aminoacyl substitution upon PI3K binding as compared to ZSTK474. It should be noted that in all cases, the inhibitory potency is poorer against every isoform, but the loss of affinity is more modest at PI3K β . The presence of the acidic group D862 in PI3K β is effectively rescuing binding. The conformational restriction engendered by the *L*- α -substituent

restricts the interaction to D862 alone and blocks possible interaction with E858, which is also an acidic residue in PI3K δ (D831). This may also explain the potency of **17** and **20** at PI3K δ .

Docking simulations support this model. In the wild-type enzyme, **21** adopted the anticipated pose closely overlaying the reported pose of ZSTK474 in PI3K δ ¹² and making a specific interaction of the free amine with D862 (Figure 3). In the

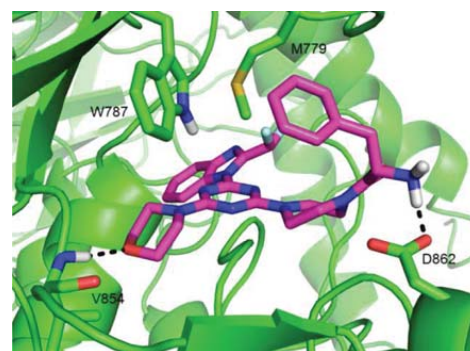


Figure 3. Docking solution for compound **21** into a model of PI3K β derived from crystal structure PDB: 2Y3A.

D862Q mutant form, not only is this specific interaction lost, but the compound can no longer adopt this pose, suggesting that the aspartyl residue acts to compensate for other unfavorable interactions associated with the inclusion of a phenylalanine substituent.

Finally, we assessed whether these compounds exhibited cell-based activity that might make them worthy of further pharmacological study and comparison to other recently reported PI3K β inhibitors.¹⁹ The PTEN-deficient cell line MDA-MB-468 was used to measure inhibition of Akt phosphorylation and inhibition of cell growth. Dose-dependent inhibition of both activities was observed with each of the inhibitors tested. Compound **21** showed strong cellular inhibition of Akt phosphorylation relative to the direct enzyme assay with IC₅₀ values <10 nM (Supplementary Figure 2 in the Supporting Information). Compound **21** showed comparable potency to ZSTK474 in cell growth despite both lower potency at PI3K β and poor potency at the other isoforms (Table 3).

Table 3. Inhibition of Cell Growth in Breast Cancer Cell Line by ZSTK474 Analogues

	MDA-MB-468 growth EC ₅₀ (μ M)
ZSTK474	3.2 \pm 1.4
17	15 \pm 5.3
19	13 \pm 1.2
21	4.6 \pm 1.1
23	11 \pm 1.1

While improved cell permeability relative to ZSTK474 may provide one explanation for this efficacy, other factors may be contributing such as cellular metabolism or activity at other PI3K pathway enzymes. In a screen (KinomeScan) of **21** versus another 96 kinases, only the class II PI3K PI3KC2 β showed binding affinity comparable to that seen for PI3K β . The results

generally mirror that seen for ZSTK474 itself²⁹ (Supplementary Table 3 in the Supporting Information).

In summary, on the basis of the observed X-ray structure of ZSTK474 in PI3K δ , a series of 1-aminoacylpiperazine-substituted analogues have been prepared that exhibit excellent potency and selectivity for PI3K β isoforms. The configuration of the amino acids is pivotal to the selectivity, underpinning a well-defined interaction with the nonconserved binding site residue D862. The inhibitors show an alternate mechanistic basis for selectivity in comparison to other recently reported selective inhibitors. The compounds show inhibition of PI3K β -dependent function in PTEN-deficient cancer cells and effectively inhibit growth of the cell line. The compounds provide a basis for the further study of PI3K β function in a number of disease contexts.

■ ASSOCIATED CONTENT

Supporting Information

Full experimental details relating to the synthesis of compounds and methods for biochemical and cellular assays. This material is available free of charge via the Internet at <http://pubs.acs.org>.

■ AUTHOR INFORMATION

Corresponding Author

*Corresponding Author Philip Thompson; Tel: [REDACTED]

Funding

J.-A.P. and M.S.M. are recipients of Australian Postgraduate Award (APA) Scholarships. M.S.M. was the recipient of a top-up scholarship from the CRC for Cancer Therapeutics. This work was funded through the National Institutes of Health Grants CA43460 and CA62924, the Virginia and D.K. Ludwig Fund for Cancer Research (USA), the Cancer Council Victoria No. 436708, and a National Health and Medical Research Council Grant No. 545943 (Australia).

Notes

The authors declare no competing financial interest.

■ ABBREVIATIONS

ATP, adenosine triphosphate; Fmo, fluorenylmethyloxycarbonyl; PI3K, phosphoinositide 3-kinase; PTEN, phosphatase and tensin homologue

■ REFERENCES

- (1) Vanhaesebroeck, B.; Stephens, L.; Hawkins, P. PI3K signalling: the path to discovery and understanding. *Nat. Rev. Mol. Cell. Biol.* **2012**, *13*, 195–203.
- (2) Courtney, K. D.; Corcoran, R. B.; Engelman, J. A. The PI3K Pathway As Drug Target in Human Cancer. *J. Clin. Oncol.* **2010**, *28*, 1075–1083.
- (3) Samuels, Y.; Wang, Z. H.; Bardelli, A.; Silliman, N.; Ptak, J.; Szabo, S.; Yan, H.; Gazdar, A.; Powell, D. M.; Riggins, G. J.; Willson, J. K. V.; Markowitz, S.; Kinzler, K. W.; Vogelstein, B.; Velculescu, V. E. High frequency of mutations of the PIK3CA gene in human cancers. *Science* **2004**, *304*, 554–554.
- (4) Li, J.; Yen, C.; Liaw, D.; Podsypanina, K.; Bose, S.; Wang, S. I.; Puc, J.; Miliaresis, C.; Rodgers, L.; McCombie, R.; Bigner, S. H.; Giovannella, B. C.; Ittmann, M.; Tycko, B.; Hibshoosh, H.; Wigler, M. H.; Parsons, R. PTEN, a putative protein tyrosine phosphatase gene mutated in human brain, breast, and prostate cancer. *Science* **1997**, *275*, 1943–1947.
- (5) Wee, S.; Wiederschain, D.; Maira, S. M.; Loo, A.; Miller, C.; deBeaumont, R.; Stegmeier, F.; Yao, Y. M.; Lengauer, C. PTEN-

deficient cancers depend on PIK3CB. *Proc. Natl. Acad. Sci. U.S.A.* **2008**, *105*, 13057–13062.

(6) Jia, S.; Liu, Z.; Zhang, S.; Liu, P.; Zhang, L.; Lee, S. H.; Zhang, J.; Signoretti, S.; Loda, M.; Roberts, T. M.; Zhao, J. J. Essential roles of PI(3)K-p110beta in cell growth, metabolism and tumorigenesis. *Nature* **2008**, *454*, 776–779.

(7) Shuttleworth, S. J.; Silva, F. A.; Cecil, A. R. L.; Tomassi, C. D.; Hill, T. J.; Raynaud, F. I.; Clarke, P. A.; Workman, P. Progress in the Preclinical Discovery and Clinical Development of Class I and Dual Class I/IV Phosphoinositide 3-Kinase (PI3K) Inhibitors. *Curr. Med. Chem.* **2011**, *18*, 2686–2714.

(8) Castillo, J. J.; Furman, M.; Winer, E. S. CAL-101: A phosphatidylinositol-3-kinase p110-delta inhibitor for the treatment of lymphoid malignancies. *Expert Opin. Invest. Drugs* **2012**, *21*, 15–22.

(9) Meadows, S. A.; Vega, F.; Kashishian, A.; Johnson, D.; Diehl, V.; Miller, L. L.; Younes, A.; Lannutti, B. J. PI3Kdelta inhibitor, GS-1101 (CAL-101), attenuates pathway signaling, induces apoptosis, and overcomes signals from the microenvironment in cellular models of Hodgkin lymphoma. *Blood* **2012**, *119*, 1897–1900.

(10) Walker, E. H.; Perisic, O.; Ried, C.; Stephens, L.; Williams, R. L. Structural insights into phosphoinositide 3-kinase catalysis and signalling. *Nature* **1999**, *402*, 313–320.

(11) Zheng, Z. H.; Amran, S. I.; Zhu, J. X.; Schmidt-Kittler, O.; Kinzler, K. W.; Vogelstein, B.; Shepherd, P. R.; Thompson, P. E.; Jennings, I. G. Definition of the binding mode of a new class of phosphoinositide 3-kinase alpha-selective inhibitors using in vitro mutagenesis of non-conserved amino acids and kinetic analysis. *Biochem. J.* **2012**, *444*, 529–535.

(12) Berndt, A.; Miller, S.; Williams, O.; Le, D. D.; Houseman, B. T.; Pacold, J. I.; Gorrec, F.; Hon, W. C.; Liu, Y.; Rommel, C.; Gaillard, P.; Ruckle, T.; Schwarz, M. K.; Shokat, K. M.; Shaw, J. P.; Williams, R. L. The p110 delta structure: mechanisms for selectivity and potency of new PI(3)K inhibitors. *Nat. Chem. Biol.* **2010**, *6*, 117–124.

(13) Camps, M.; Ruckle, T.; Ji, H.; Ardisson, V.; Rintelen, F.; Shaw, J.; Ferrandi, C.; Chabert, C.; Gillieron, C.; Francon, B.; Martin, T.; Gretener, D.; Perrin, D.; Leroy, D.; Vitte, P. A.; Hirsch, E.; Wymann, M. P.; Cirillo, R.; Schwarz, M. K.; Rommel, C. Blockade of PI3Kgamma suppresses joint inflammation and damage in mouse models of rheumatoid arthritis. *Nat. Med.* **2005**, *11*, 936–943.

(14) Jackson, S. P.; Schoenwaelder, S. M.; Goncalves, L.; Nesbitt, W. S.; Yap, C. L.; Wright, C. E.; Kenche, V.; Anderson, K. E.; Doppeide, S. M.; Yuan, Y.; Sturgeon, S. A.; Prabakaran, H.; Thompson, P. E.; Smith, G. D.; Shepherd, P. R.; Daniele, N.; Kulkarni, S.; Abbott, B.; Saylik, D.; Jones, C.; Lu, L.; Giuliano, S.; Hughan, S. C.; Angus, J. A.; Robertson, A. D.; Salem, H. H. PI 3-kinase p110beta: a new target for antithrombotic therapy. *Nat. Med.* **2005**, *11*, 507–514.

(15) Knight, Z. A.; Gonzalez, B.; Feldman, M. E.; Zunder, E. R.; Goldenberg, D. D.; Williams, O.; Loewith, R.; Stokoe, D.; Balla, A.; Toth, B.; Balla, T.; Weiss, W. A.; Williams, R. L.; Shokat, K. M. A pharmacological map of the PI3-K family defines a role for p110alpha in insulin signaling. *Cell* **2006**, *125*, 733–747.

(16) Nylander, S.; Kull, B.; Bjorkman, J.; Ulvinge, J. C.; Oakes, N.; Emanuelsson, B.; Andersson, M.; Skarby, T.; Inghardt, T.; Fjellstrom, O.; Gustafsson, D. Human target validation of phosphoinositide 3-kinase (PI3K)beta; effects on platelets and insulin sensitivity, using AZD6482 a novel PI3Kbeta inhibitor. *J. Thromb. Haemostasis* **2012**, *10*, 2127–2136.

(17) Frazzetto, M.; Suphioglu, C.; Zhu, J.; Schmidt-Kittler, O.; Jennings, I. G.; Cranmer, S. L.; Jackson, S. P.; Kinzler, K. W.; Vogelstein, B.; Thompson, P. E. Dissecting isoform selectivity of PI3K inhibitors: The role of non-conserved residues in the catalytic pocket. *Biochem. J.* **2008**, *414*, 383–390.

(18) Lin, H.; Schulz, M. J.; Xie, R.; Zeng, J.; Luengo, J. I.; Squire, M. D.; Tedesco, R.; Qu, J.; Erhard, K.; Mack, J. F.; Raha, K.; Plant, R.; Rominger, C. M.; Ariazi, J. L.; Sher, C. S.; Schaber, M. D.; McCurdy-Freed, J.; Spengler, M. D.; Davis, C. B.; Hardwicke, M. A.; Rivero, R. A. Rational Design, Synthesis, and SAR of a Novel Thiazolopyrimidinone Series of Selective PI3K-beta Inhibitors. *ACS Med. Chem. Lett.* **2012**, *3*, 524–529.

- (19) Lin, H.; Erhard, K.; Hardwicke, M. A.; Luengo, J. I.; Mack, J. F.; McSurdy-Freed, J.; Plant, R.; Raha, K.; Rominger, C. M.; Sanchez, R. M.; Schaber, M. D.; Schulz, M. J.; Spengler, M. D.; Tedesco, R.; Xie, R.; Zeng, J. J.; Rivero, R. A. Synthesis and structure-activity relationships of imidazo[1,2-a]pyrimidin-5(1H)-ones as a novel series of beta isoform selective phosphatidylinositol 3-kinase inhibitors. *Bioorg. Med. Chem. Lett.* **2012**, *22*, 2230–2234.
- (20) Sanchez, R. M.; Erhard, K.; Hardwicke, M. A.; Lin, H.; McSurdy-Freed, J.; Plant, R.; Raha, K.; Rominger, C. M.; Schaber, M. D.; Spengler, M. D.; Moore, M. L.; Yu, H. Y.; Luengo, J. I.; Tedesco, R.; Rivero, R. A. Synthesis and structure-activity relationships of 1,2,4-triazolo[1,5-a]pyrimidin-7(3H)-ones as novel series of potent beta isoform selective phosphatidylinositol 3-kinase inhibitors. *Bioorg. Med. Chem. Lett.* **2012**, *22*, 3198–3202.
- (21) Certal, V.; Halley, F.; Virone-Oddos, A.; Delorme, C.; Karlsson, A.; Rak, A.; Thompson, F.; Filoche-Romme, B.; El-Ahmad, Y.; Carry, J. C.; Abecassis, P. Y.; Lejeune, P.; Vincent, L.; Bonnevaux, H.; Nicolas, J. P.; Bertrand, T.; Marquette, J. P.; Michot, N.; Benard, T.; Below, P.; Vade, I.; Chatreaux, F.; Lebourg, G.; Pilorge, F.; Angouillan-Boniface, O.; Louboutin, A.; Lengauer, C.; Schio, L. Discovery and optimization of new benzimidazole- and benzoxazole-pyrimidone selective PI3Kbeta inhibitors for the treatment of phosphatase and TENSin homologue (PTEN)-deficient cancers. *J. Med. Chem.* **2012**, *55*, 4788–4805.
- (22) Certal, V.; Halley, F.; Virone-Oddos, A.; Thompson, F.; Filoche-Romme, B.; El-Ahmad, Y.; Carry, J.-C.; Delorme, C.; Karlsson, A.; Abecassis, P.-Y.; Vincent, L.; Bonnevaux, H.; Nicolas, J.-P.; Morales, R.; Michot, N.; Vade, I.; Louboutin, A.; Perron, S.; Doerflinger, G.; Tric, B.; Monget, S.; Lengauer, C.; Schio, L. Preparation and optimization of new 4-(morpholin-4-yl)-(6-oxo-1,6-dihydropyrimidin-2-yl)amide derivatives as PI3K β inhibitors. *Bioorg. Med. Chem. Lett.* **2012**, *22*, 6381–6384.
- (23) Gonzalez-Lopez de Turiso, F.; Shin, Y.; Brown, M.; Cardozo, M.; Chen, Y.; Fong, D.; Hao, X.; He, X.; Henne, K.; Hu, Y.-L.; Johnson, M. G.; Kohn, T.; Lohman, J.; McBride, H. J.; McGee, L. R.; Medina, J. C.; Metz, D.; Miner, K.; Mohn, D.; Pattaropong, V.; Seganish, J.; Simard, J. L.; Wannberg, S.; Whittington, D. A.; Yu, G.; Cushing, T. D. Discovery and in Vivo Evaluation of Dual PI3K β / δ Inhibitors. *J. Med. Chem.* **2012**, *55*, 7667–7685.
- (24) Zhang, X. X.; Vadas, O.; Perisic, O.; Anderson, K. E.; Clark, J.; Hawkins, P. T.; Stephens, L. R.; Williams, R. L. Structure of Lipid Kinase p110 beta/p85 beta Elucidates an Unusual SH2-Domain-Mediated Inhibitory Mechanism. *Mol. Cell* **2011**, *41*, S67–S78.
- (25) Yaguchi, S.; Fukui, Y.; Koshimizu, I.; Yoshimi, H.; Matsuno, T.; Gouda, H.; Hirono, S.; Yamazaki, K.; Yamori, T. Antitumor activity of ZSTK474, a new phosphatidylinositol 3-kinase inhibitor. *J. Natl. Cancer Inst.* **2006**, *98*, 545–556.
- (26) Matsuno, T.; Kato, M.; Tsuchida, Y.; Takahashi, M.; Yaguchi, S.; Terada, S. Synthesis and aromatase-inhibitory activity of imidazolyl-1,3,5-triazine derivatives. *Chem. Pharm. Bull.* **1997**, *45*, 291–296.
- (27) Matsuno, T.; Kato, M.; Sasahara, H.; Watanabe, T.; Inaba, M.; Takahashi, M.; Yaguchi, S.; Yoshioka, K.; Sakato, M.; Kawashima, S. Synthesis and antitumor activity of benzimidazolyl-1,3,5-triazine and benzimidazolylpyrimidine derivatives. *Chem. Pharm. Bull.* **2000**, *48*, 1778–1781.
- (28) Rewcastle, G. W.; Gamage, S. A.; Flanagan, J. U.; Frederick, R.; Denny, W. A.; Baguley, B. C.; Kestell, P.; Singh, R.; Kendall, J. D.; Marshall, E. S.; Lill, C. L.; Lee, W. J.; Kolekar, S.; Buchanan, C. M.; Jamieson, S. M. F.; Shepherd, P. R. Synthesis and Biological Evaluation of Novel Analogues of the Pan Class I Phosphatidylinositol 3-Kinase (PI3K) Inhibitor 2-(Difluoromethyl)-1-[4,6-di(4-morpholinyl)-1,3,5-triazin-2-yl]-1H-benzimidazole (ZSTK474). *J. Med. Chem.* **2011**, *54*, 7105–7126.
- (29) Kong, D. X.; Dan, S. G.; Yamazaki, K.; Yamori, T. Inhibition profiles of phosphatidylinositol 3-kinase inhibitors against PI3K superfamily and human cancer cell line panel JFCR39. *Eur. J. Cancer* **2010**, *46*, 1111–1121.

Appendix 5: Publication

Zheng, Z.; **Miller, M. S.**; Jennings, I. G.; Thompson, P. E. Mechanisms of PI3K β -Selective Inhibition Revealed by Reciprocal Mutagenesis. *ACS Chem. Biol.* **2013**, *8*, 679–683.

Candidate performed docking of (R)-TGX221 and prepared images for Figure 1.

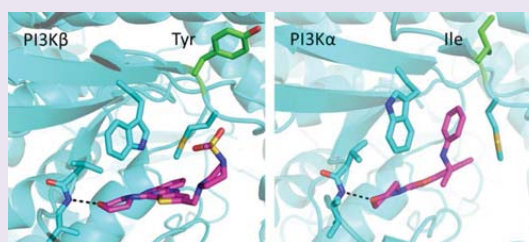
Mechanisms of PI3K β -Selective Inhibition Revealed by Reciprocal Mutagenesis

Zhaohua Zheng, Michelle S. Miller, Ian G. Jennings,* and Philip E. Thompson*

Medicinal Chemistry, Monash Institute of Pharmaceutical Sciences, Monash University, 381 Royal Parade, Parkville 3052, Australia

S Supporting Information

ABSTRACT: The p110 β isoform of PI3 kinase (PI3K β) has been implicated in pathological disorders such as thrombosis and cancer and a number of PI3K β -selective inhibitors have recently progressed into clinical studies. Although crystallography studies identify a binding site conformation favored by the inhibitors, no specific interaction explains the observed selectivity. Using site-directed mutagenesis we have identified a specific tyrosine residue of the binding site Y778 that dictates the ability of the PI3K β isoform to bind these inhibitors. When mutated to isoleucine, PI3K β has reduced ability to present a specific cryptic binding site into which a range of reported PI3K β inhibitors can bind, and conversely when tyrosine is introduced into the same position in PI3K α , the same inhibitors gain potency. The results provide a cogent explanation for the selectivity profiles displayed by these PI3K inhibitors and maybe others as well.



The phosphatidylinositol 3-kinases (PI3K) are a family of lipid kinases that regulate intracellular signaling for numerous cellular events such as cell migration, growth, and survival.¹ PI3K β was first identified as a potential therapeutic target in thrombosis, and more recently, there has been accumulating evidence showing that PI3K β plays a key role in certain cancers accompanied by the loss of the tumor suppressor PTEN.^{2,3} Because each of the PI3K isoforms has their own, although overlapping, physiological roles, isoform-selective PI3K inhibitors may hold some therapeutic advantages with respect to reducing off-target effects. While the majority of PI3K inhibitors currently in clinical trials are Class I pan-PI3K inhibitors,⁴ some PI3K β isoform-selective inhibitors have emerged. These include TGX221, TGX286, and AZD6482 (aka KIN193).^{5–7} Recently, a number of new PI3K β -selective compounds have been reported. GSK2636771 has progressed to phase I/IIa clinical trial to treat advanced solid tumors with PTEN deficiency, and other analogous series have been described by GSK.^{8–10} Other compounds have also been described by Sanofi and Amgen.^{11–13}

While these and other isoform selective inhibitors have been reported, the mechanistic details underpinning selectivity are poorly understood. Since the first X-ray structures of PI3K were reported, it has been apparent that much of the inner core of the binding site is highly conserved across the class I isoforms.¹⁴ Two nonconserved regions of the binding site have been identified as capable of executing selective interactions with inhibitors (Supplementary Figure S1). One region encompasses a loop, which sits under the ribose pocket that is relatively large in the PI3 kinases (from PI3K β 855 to 862).¹⁵ A second region encompasses PI3K β 772–788 and corresponds to the protein kinase P-loop that is a key

contributor to substrate binding.^{16,17} Here, a cryptic binding pocket has been identified, whereby a conserved methionine residue (M779 of PI3K β) can shift to facilitate binding by the so-called “propeller-shaped” inhibitors. This has been observed for PI3K δ -selective compounds like PIK-39 and IC87114.^{6,18} A methionine shifted conformer of PI3K β appears also to be accessed by PI3K β selective inhibitors although there is no direct evidence for this. PI3K β -selective inhibitors have been cocrystallized in this conformation with PI3K α , δ (Figure 1b,c) and γ , but the only reported X-ray structure of PI3K β displays a conventional flat conformer (Figure 1a).^{18,19}

While the conformer has been identified and can be associated with binding of PI3K β and PI3K δ inhibitors, the finer details that dictate the propensity to form this pocket remain unclear. It has been speculated that the multiple differences in the P-loop sequence (Supplementary Figure S1) contribute to isoform-specific conformational behavior.¹⁶

Reciprocal mutation has been a useful technique to unravel the various mechanisms that underpin PI3K inhibitor selectivity. In this approach, nonconserved residues of the binding site are swapped between the isoforms of interest to determine what influence if any that residue has on inhibitor binding.¹⁵ Recently we showed that the binding of PI3K α selective inhibitors such as A-66, PIK75, and J-32 have been shown to be sensitive to mutation at nonconserved residues.¹⁷ Our earlier work with TGX221 and TGX286 showed them to be insensitive to mutations in the region PI3K β 855 to 862.¹⁵

Received: December 5, 2012

Accepted: January 29, 2013

Published: January 29, 2013



ACS Publications

© 2013 American Chemical Society

679

dx.doi.org/10.1021/cb300666s | ACS Chem. Biol. 2013, 8, 679–683

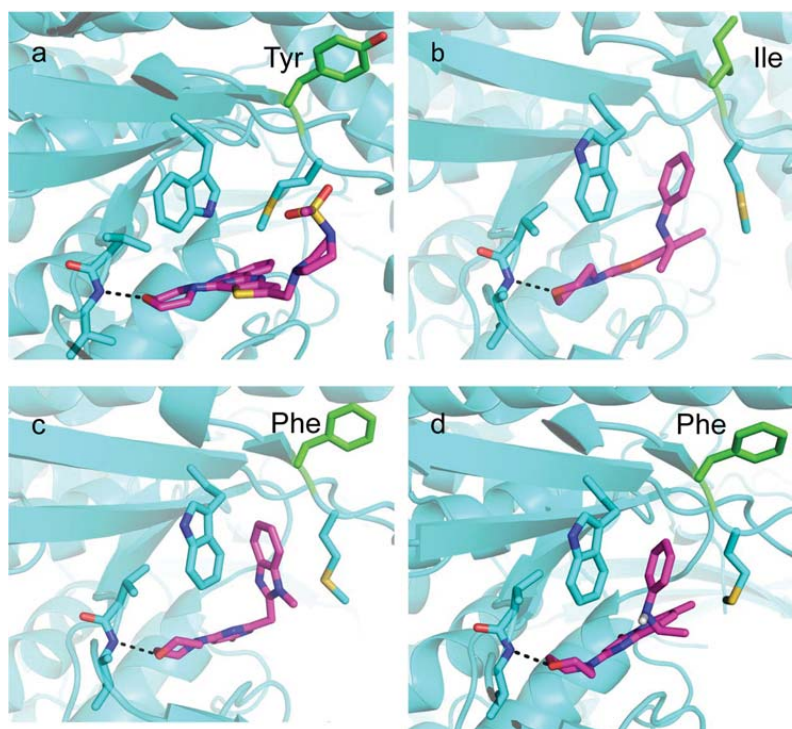


Figure 1. Structures of PI3K isoforms highlighting the active site nonconserved residues corresponding to Y778 of PI3K β and the conformation of the adjacent conserved methionine: (a) GDC0941 in PI3K β (2Y3A); (b) PIK108 in PI3K α (4A55); (c) compound VWN in PI3K δ (4AJW); (d) model of (R)-TGX221 in PI3K δ . Note that the side chain projects away from the active site and is not predicted to participate directly in binding.

Here, we report on the dramatic influence of a single tyrosine residue Y778 and equally its counterpart in PI3K α I771 in determining the potency of four chemically distinct PI3K β -selective inhibitors at each isoform. On the basis of crystallographic evidence, these residues play no direct part in the binding of the inhibitor, nor do they appear to change conformation (Figure 1). Critically though, the side chains appear to influence the conformers available to the loop formed by the adjacent residues of PI3K β 779–788. In doing so, they dictate the ability of the PI3K β isoform to adopt the methionine shifted conformation and thus the selectivity of these four inhibitors for PI3K β over PI3K α .

Our approach exemplified in earlier work has been to screen PI3K inhibitors of interest against a range of point mutant forms of the target enzyme. In this case, we screened four PI3K β inhibitors TGX221, TGX286, GSK2636771, and SAN7¹¹ (compound 7 of Certal et al.¹¹) against mutant forms of PI3K β where the nonconserved residues of the binding site were present as their non-equivalent form in PI3K α . We screened the four compounds at or near their IC_{50} value against WT PI3K β (Figure 2). The results clearly show that, in each case, Y778I–PI3K was poorly inhibited by the compounds. Only modest effects were seen against PI3K β mutated at the other nonconserved residues.

On the basis of the screening data shown above, the IC_{50} values of the compounds were determined for both the Y778I–PI3K β mutant and the reciprocal mutant I771Y in PI3K α (Table 1 and Supplementary Table 1). Each of the compounds

shows a shift in IC_{50} associated with the Y778I–PI3K β and the reciprocal mutant I771Y–PI3K α as compared to the corresponding wild-type isoform. Most dramatically, the IC_{50} for GSK2636771 versus PI3K β changes by 150-fold upon mutation. The reciprocal mutation in PI3K α changes it from inactive to an IC_{50} of 1.6 μ M, at least a 60-fold change. TGX221 and SAN7 show lesser but still striking changes in activity. Essentially, each compound prefers to inhibit a form of each enzyme where the tyrosine residue rather than an isoleucine residue is present. Note that the mutations have no substantial effect on the catalytic properties of the enzyme (Supplementary Table 2).

The results described above clearly identify the tyrosine residue Y778 as a pivotal regulator of PI3K β -isoform selectivity with respect to PI3K α , and this may extend to the relative selectivity versus the PI3K γ and PI3K δ isoforms where the residue at this position also differs. Inspection of the collected crystallographic data for PI3K inhibitors provides a mechanistic rationale to explain the data. First, sequence alignment shows a pivotal distinction between the four class I PI3K isoforms. At PI3K α , β , γ , and δ , the residue at this position is isoleucine, tyrosine, valine, or phenylalanine, respectively (Supplementary Figure 1). This provides a clear distinction between the two isoforms bearing an aromatic residue (PI3K β and PI3K δ) and those containing an aliphatic residue (PI3K α and PI3K γ). Noting that TGX221, TGX286, GSK2636771, and SAN7 all show less selectivity for PI3K δ and the propeller-style inhibitors all prefer PI3K β and/or PI3K δ , this implies that the aromatic

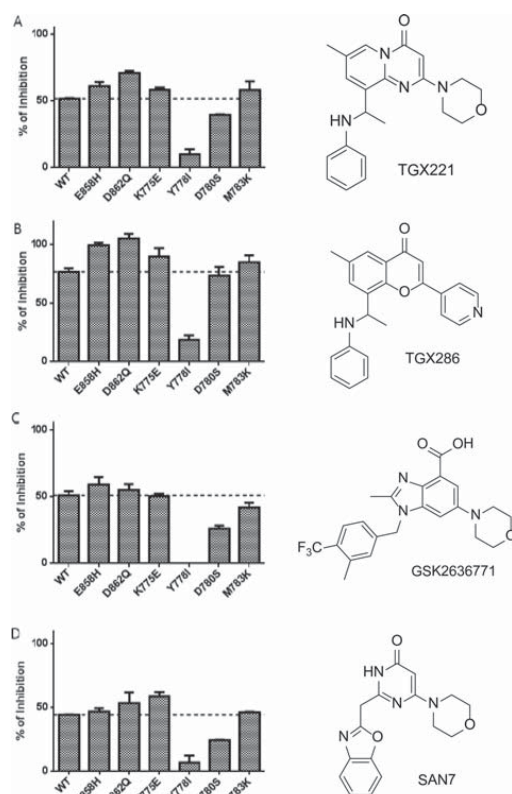


Figure 2. Effect of PI3K β isoform mutations on compound inhibition profiles at selected concentrations: (A) TGX221, 100 nM; (B) TGX286, 120 nM; (C) GSK2636771, 50 nM; (D) SAN7, 200 nM. Purified p110 β WT and mutant enzymes were prepared as described in the Supplementary Methods section. Reciprocal mutants have the WT amino acid replaced by the equivalent amino acid in p110 α . The PI3K activity assay was carried out as described in the Supplementary Methods section. Error bars represent standard deviation from two independent experiments.

residues in some way facilitate formation of the methionine-open conformer of PI3K. In addition to the striking loss of affinity resulting from the replacement of the tyrosine by isoleucine in PI3K β , the increase in potency when tyrosine replaces I771 in PI3K α is also important as it shows that the tyrosine residue enables formation of an otherwise poorly accessed conformer.

So how does the residue at this position actually influence ligand binding? Two features stand out when the available crystallographic data relating to PI3K is assessed. First, in superposition of all the PI3K structures, the residue at this position is effectively fixed, irrespective of isoform or ligand binding mode, and the backbone and C α –C β across all these structures basically superimpose (Figure 1). Second, this residue does not participate directly in ligand binding in any cocrystal; the side chain points away from the catalytic site. Taken together, this suggests that the residue at this position acts as a pivot point for the residues around it, directing the conformational outcomes of the solvent exposed P-loop residues to ultimately favor or disfavor the two identified conformers of the adjacent methionine. How the nature of the amino acid actually drives those conformational choices is still a challenging question to answer, particularly as the crystal structures for PI3K β and PI3K α have only been solved to moderate resolution.

Another feature to be drawn from the data is the relative change in selectivity with each of the inhibitors. While the selectivity of GSK2636771 changes over 9000-fold upon reciprocal mutation, SAN7 and TGX221 show a more modest change. The likely explanation is that SAN7 and probably TGX221 can be accommodated in different binding modes, probably in the flat pose adopted by compounds such as GDC0941, while GSK2636771 cannot be.

We believe these results have multiple levels of significance for the study of PI3K inhibition. In the first instance, it provides a straightforward model for understanding inhibitor binding that can be tested experimentally, which is always of great use in ligand design. The reciprocal mutant system can also be used to identify mechanistic differences underpinning selectivity in other compound classes or other isoforms. We have recently described a novel class of PI3K β selective inhibitors that achieve selectivity through a distinct mechanism.²⁰ These compounds are unaffected by the Y778I mutation, but another residue, D862, selects for PI3K β via a direct interaction with an amino-acyl functional group on the inhibitor.

Second, identifying single-point changes that render the enzyme opaque to pharmacological inhibitors without an effect on catalytic activity provides for the development of exquisite systems for studying the cell based functions of PI3K β . As Y778I–PI3K β is insensitive to GSK2636771, it might be included in isogene replacement studies to characterize the specific effects of that isoform, particularly in models of cancer. The mutation has only a small influence on the catalytic activity of the enzymes (see Supplementary Table 2). It also presages a simple pathway by which a cancer cell might generate resistance to GSK2636771 or other propeller-shaped inhibitors.

Table 1. Inhibition of PI3K Isoforms and in Vitro Mutants

compound	PI3K isoform IC ₅₀ (nM) ^a						reciprocal change ^b Y \leftrightarrow I
	PI3K α WT	PI3K α I771Y	fold change α WT \rightarrow α I771Y	PI3K β WT	PI3K β Y778I	fold change β WT \rightarrow β Y778I	
TGX221	4040	280	↓14.5	65	1000	↑16	230
TGX286	>100000	1100	↓>90	130	2600	↑20	>1800
GSK2636771	>100000	1600	↓>60	61	9400	↑150	>9200
SAN7	9600	2200	↓4.4	240	2300	↑9.6	42

^aIC₅₀ values are means of at least three duplicate experiments (see Supplementary Table 1 for standard deviations of mean data). Assays were performed using 10 μ M ATP as described in the Methods section. ^bReciprocal change refers to the change in selectivity of inhibitor due to reciprocal mutation.

Finally, these results show the subtlety that underpins conformational plasticity in the binding site. In the design of anticancer drugs, the concept of selectively inhibiting one of the oncogenic mutants of PI3K α is an attractive but seemingly intractable task. We have shown in our results here that that allosteric effects can result in binding site differences between wild-type and mutant forms of PI3K. The corollary is that there might be active site conformers that are available to oncogenic PI3K α that are not available to the wild-type enzyme. The challenge will be to find the inhibitors that can exploit those forms.

METHODS

Generation of PI3K, p110 Mutant Baculovirus. The methods used to generate the PI3K p110 mutants have been described previously.¹⁷ Briefly, the mutant DNA was produced using a pair of oligos incorporating the appropriate mutation and PCR using Pfu DNA polymerase (Promega) with the appropriate wild-type p110 pFastBac (Life Technologies) plasmid as the DNA template. The DNA sequence was then confirmed as containing the correct mutation with the remaining DNA sequence found to be identical to the WT sequence. Mutant pFastBac plasmids were then transformed into DH10Bac *E. coli* (Life Technologies) with bacmid DNA purified and confirmed as recombinant using PCR.

Recombinant bacmid DNA was then transfected, using lipofectin (Life Technologies), into Sf21 insect cells with the medium containing recombinant virus collected after 3–5 days incubation at 27 °C. High titer virus stock was then produced by amplification through two cycles of infection. Production of p110 protein was confirmed by Western blotting of cell extracts separated by SDS-PAGE using a p110 α or β specific antibody.

Protein Expression and Purification. Sf21 cells (2×10^6 cells/mL, 200 mL total volume) were cotransfected with p110 and p85 recombinant baculovirus and incubated shaking at 140 rpm for 48 h at 27 °C. Following this, cells were collected by centrifugation and stored at –80 °C until ready for extraction. The p110/p85 PI3K protein complex was extracted from the cells and purified using Ni-agarose chromatography as previously described.¹⁶ Fractions containing the PI3K protein were pooled and dialyzed against 50 mM Tris HCl, pH 7.5, 300 mM NaCl, at 4 °C. PI3K protein was then stored in 20% (v/v) glycerol and 2 mM dithiothreitol at –80 °C. Each mutant was characterized by measuring the kinetic parameters (K_m ATP, and K_m PI phosphatidyl inositol) of the PI3K enzyme reaction, and in each case, it was shown that there was no difference between the WT enzyme and the mutants.

Inhibitors. TGX221 (7-methyl-2-morpholino-9-(1-(phenylamino)-ethyl)-4H-pyrido[1,2-a]pyrimidin-4-one) was a generous gift of Prof. Shaun Jackson, Australian Centre for Blood Diseases, Victoria, Australia. TGX286 (6-methyl-8-(1-(phenylamino)ethyl)-2-(pyridin-4-yl)-4H-chromen-4-one) was synthesized according to Knight et al.⁶ GSK2636771 (2-methyl-1-(3-methyl-4-(trifluoromethyl)benzyl)-6-morpholino-1H-benzo[d]imidazole-4-carboxylic acid) was obtained from Active Biochem (New Jersey, U.S.A.). SAN7 (2-(benzo[d]-oxazol-2-ylmethyl)-6-morpholinopyrimidin-4(3H)-one) was synthesized according to the method described in Certal et al.¹¹

Inhibition Assays. The PI3K inhibitors were dissolved at 10 mM in dimethyl sulphoxide (DMSO) and stored at –20 °C until use. PI3K enzyme activity was determined using a luminescence assay measuring ATP consumption. PI3K enzyme activity was determined in 50 μ L of 20 mM Hepes, pH 7.5, 5 mM MgCl₂ with PI and ATP at the indicated concentrations.¹⁷ After a 60 min incubation at RT, the reaction was stopped by the addition of 50 μ L of Kinase-Glo (Promega) followed by a further 15 min incubation. Luminescence was then read using a Fluostar plate reader (BMG Labtech). Inhibitors were diluted in 20% (v/v) DMSO at the indicated concentrations in order to generate a concentration versus inhibition of enzyme activity curve, which was then analyzed using GraphPad Prism (version 6.00 for Windows) in order to calculate the IC₅₀.

ASSOCIATED CONTENT

Supporting Information

Sequence alignment of region 1 and region 2 of nonconserved amino acids; IC₅₀ determinations including standard deviations of the mean for data presented in Table 1; biochemical characterisation of WT and selected mutant recombinant isoforms. This material is available free of charge via the Internet at <http://pubs.acs.org>.

AUTHOR INFORMATION

Corresponding Author

* [Redacted]

Author Contributions

Z.Z. performed the biochemical experiments; M.S.M. performed the structural analyses and performed docking experiments; P.E.T. performed the chemical syntheses. I.G.J. and P.E.T. designed the experiments and wrote the manuscript.

Notes

The authors declare no competing financial interest.

ACKNOWLEDGMENTS

M.S.M. is a recipient of an Australian Postgraduate Award (APA) Scholarship. M.S.M. was a recipient of a top-up scholarship from the CRC for Cancer Therapeutics. This work was funded through grants from the Cancer Council Victoria no. 436708 and the National Health and Medical Research Council no. 545943 (Australia).

ABBREVIATIONS

ATP, adenosine triphosphate; PI3K, phosphoinositide 3-kinase; PTEN, phosphatase and tensin homologue

REFERENCES

- (1) Vanhaesebroeck, B.; Stephens, L.; and Hawkins, P. (2012) PI3K signalling: the path to discovery and understanding. *Nat. Rev. Mol. Cell Biol.* 13, 195–203.
- (2) Wee, S.; Wiederschain, D.; Maira, S. M.; Loo, A.; Miller, C.; deBeaumont, R.; Stegmeier, F.; Yao, Y. M.; and Lengauer, C. (2008) PTEN-deficient cancers depend on PIK3CB. *Proc. Natl. Acad. Sci. U.S.A.* 105, 13057–13062.
- (3) Jia, S.; Liu, Z.; Zhang, S.; Liu, P.; Zhang, L.; Lee, S. H.; Zhang, J.; Signoretti, S.; Loda, M.; Roberts, T. M.; and Zhao, J. J. (2008) Essential roles of PI(3)K-p110[bgr] in cell growth, metabolism and tumorigenesis. *Nature* 454, 776–779.
- (4) Shuttleworth, S. J.; Silva, F. A.; Cecil, A. R. L.; Tomassi, C. D.; Hill, T. J.; Raynaud, F. I.; Clarke, P. A.; and Workman, P. (2011) Progress in the preclinical discovery and clinical development of Class I and Dual Class I/IV phosphoinositide 3-kinase (PI3K) inhibitors. *Curr. Med. Chem.* 18, 2686–2714.
- (5) Jackson, S. P.; Schoenwaelder, S. M.; Goncalves, I.; Nesbitt, W. S.; Yap, C. L.; Wright, C. E.; Kenche, V.; Anderson, K. E.; Doppeide, S. M.; Yuan, Y.; Sturgeon, S. A.; Prabakaran, H.; Thompson, P. E.; Smith, G. D.; Shepherd, P. R.; Daniele, N.; Kulkarni, S.; Abbott, B.; Saylik, D.; Jones, C.; Lu, L.; Giuliano, S.; Hugan, S. C.; Angus, J. A.; Robertson, A. D.; and Salem, H. H. (2005) PI 3-kinase p110beta: a new target for antithrombotic therapy. *Nat. Med.* 11, 507–514.
- (6) Knight, Z. A.; Gonzalez, B.; Feldman, M. E.; Zunder, E. R.; Goldenberg, D. D.; Williams, O.; Loewith, R.; Stokoe, D.; Balla, A.; Toth, B.; Balla, T.; Weiss, W. A.; Williams, R. L.; and Shokat, K. M. (2006) A pharmacological map of the PI3-K family defines a role for p110alpha in insulin signaling. *Cell* 125, 733–747.

- (7) Nylander, S., Kull, B., Bjorkman, J. A., Ulvinge, J. C., Oakes, N., Emanuelsson, B. M., Andersson, M., Skarby, T., Inghardt, T., Fjellstrom, O., and Gustafsson, D. (2012) Human target validation of phosphoinositide 3-kinase (PI3K)β: effects on platelets and insulin sensitivity, using AZD6482 a novel PI3K beta inhibitor. *J. Thromb. Haemostasis* 10, 2127–2136.
- (8) Lin, H., Schulz, M. J., Xie, R., Zeng, J., Luengo, J. I., Squire, M. D., Tedesco, R., Qu, J., Erhard, K., Mack, J. F., Raha, K., Plant, R., Rominger, C. M., Ariazi, J. L., Sher, C. S., Schaber, M. D., McSurdy-Freed, J., Spengler, M. D., Davis, C. B., Hardwicke, M. A., and Rivero, R. A. (2012) Rational design, synthesis, and SAR of a novel thiazolopyrimidinone series of selective PI3K-beta inhibitors. *ACS Med. Chem. Lett.* 3, 524–529.
- (9) Lin, H., Erhard, K., Hardwicke, M. A., Luengo, J. I., Mack, J. F., McSurdy-Freed, J., Plant, R., Raha, K., Rominger, C. M., Sanchez, R. M., Schaber, M. D., Schulz, M. J., Spengler, M. D., Tedesco, R., Xie, R., Zeng, J. J., and Rivero, R. A. (2012) Synthesis and structure–activity relationships of imidazo[1,2-a]pyrimidin-5(1H)-ones as a novel series of beta isoform selective phosphatidylinositol 3-kinase inhibitors. *Bioorg. Med. Chem. Lett.* 22, 2230–2234.
- (10) Sanchez, R. M., Erhard, K., Hardwicke, M. A., Lin, H., McSurdy-Freed, J., Plant, R., Raha, K., Rominger, C. M., Schaber, M. D., Spengler, M. D., Moore, M. L., Yu, H. Y., Luengo, J. I., Tedesco, R., and Rivero, R. A. (2012) Synthesis and structure–activity relationships of 1,2,4-triazolo[1,5-a]pyrimidin-7(3H)-ones as novel series of potent beta isoform selective phosphatidylinositol 3-kinase inhibitors. *Bioorg. Med. Chem. Lett.* 22, 3198–3202.
- (11) Certal, V., Halley, F., Virone-Oddos, A., Delorme, C., Karlsson, A., Rak, A., Thompson, F., Filoche-Romme, B., El-Ahmad, Y., Carry, J. C., Abecassis, P. Y., Lejeune, P., Vincent, L., Bonnevaux, H., Nicolas, J. P., Bertrand, T., Marquette, J. P., Michot, N., Benard, T., Below, P., Vade, I., Chatreaux, F., Lebourg, G., Pilorge, F., Angouillant-Boniface, O., Louboutin, A., Lengauer, C., and Schio, L. (2012) Discovery and optimization of new benzimidazole- and benzoxazole-pyrimidone selective PI3Kβ inhibitors for the treatment of phosphatase and PTEN homologous (PTEN)-deficient cancers. *J. Med. Chem.* 55, 4788–4805.
- (12) Certal, V., Halley, F., Virone-Oddos, A., Thompson, F., Filoche-Romme, B., El-Ahmad, Y., Carry, J.-C., Delorme, C., Karlsson, A., Abecassis, P.-Y., Vincent, L., Bonnevaux, H., Nicolas, J.-P., Morales, R., Michot, N., Vade, I., Louboutin, A., Perron, S., Doerflinger, G., Tric, B., Monget, S., Lengauer, C., and Schio, L. (2012) Preparation and optimization of new 4-(morpholin-4-yl)-(6-oxo-1,6-dihydropyrimidin-2-yl)amide derivatives as PI3Kβ inhibitors. *Bioorg. Med. Chem. Lett.* 22, 6381–6384.
- (13) Gonzalez-Lopez de Turiso, F., Shin, Y., Brown, M., Cardozo, M., Chen, Y., Fong, D., Hao, X., He, X., Henne, K., Hu, Y.-L., Johnson, M. G., Kohn, T., Lohman, J., McBride, H. J., McGee, L. R., Medina, J. C., Metz, D., Miner, K., Mohn, D., Pattaropong, V., Segamish, J., Simard, J. L., Wannberg, S., Whittington, D. A., Yu, G., and Cushing, T. D. (2012) Discovery and in vivo evaluation of dual PI3Kβ/δ inhibitors. *J. Med. Chem.* 55, 7667–7685.
- (14) Walker, E. H., Perisic, O., Ried, C., Stephens, L., and Williams, R. L. (1999) Structural insights into phosphoinositide 3-kinase catalysis and signalling. *Nature* 402, 313–320.
- (15) Frazzetto, M., Suphioglu, C., Zhu, J., Schmidt-Kittler, O., Jennings, I. G., Cranmer, S. L., Jackson, S. P., Kinzler, K. W., Vogelstein, B., and Thompson, P. E. (2008) Dissecting isoform selectivity of PI3K inhibitors: the role of non-conserved residues in the catalytic pocket. *Biochem. J.* 414, 383–390.
- (16) Zheng, Z. H., Amran, S. I., Thompson, P. E., and Jennings, I. G. (2011) Isoform-selective inhibition of phosphoinositide 3-kinase: Identification of a new region of nonconserved amino acids critical for p110 alpha inhibition. *Mol. Pharmacol.* 80, 657–664.
- (17) Zheng, Z. H., Amran, S. I., Zhu, J. X., Schmidt-Kittler, O., Kinzler, K. W., Vogelstein, B., Shepherd, P. R., Thompson, P. E., and Jennings, I. G. (2012) Definition of the binding mode of a new class of phosphoinositide 3-kinase alpha-selective inhibitors using in vitro mutagenesis of non-conserved amino acids and kinetic analysis. *Biochem. J.* 444, 529–535.
- (18) Berndt, A., Miller, S., Williams, O., Le, D. D., Houseman, B. T., Pacold, J. I., Gorrec, F., Hon, W. C., Liu, Y., Rommel, C., Gaillard, P., Ruckle, T., Schwarz, M. K., Shokat, K. M., Shaw, J. P., and Williams, R. L. (2010) The p110 delta structure: mechanisms for selectivity and potency of new PI(3)K inhibitors. *Nat. Chem. Biol.* 6, 117–124.
- (19) Zhang, X. X., Vadas, O., Perisic, O., Anderson, K. E., Clark, J., Hawkins, P. T., Stephens, L. R., and Williams, R. L. (2011) Structure of lipid kinase p110 beta/p85 beta elucidates an unusual SH2-domain-mediated inhibitory mechanism. *Mol. Cell* 41, 567–578.
- (20) Pinson, J.-A., Zheng, Z., Miller, M. S., Chalmers, D. K., Jennings, I. G., and Thompson, P. E. (2012) 1-Aminoacyl-triazine derivatives are isoform-selective PI3Kβ inhibitors that target non-conserved Asp862 of PI3Kβ. *ACS Med. Chem. Lett.*, DOI: <http://dx.doi.org/10.1021/ml300336j>.

